Hydrogen-bonded layer structures based on guanidinium sulfonates

Burke, Nichola Jayne

Award date:
2005

Awarding institution:
University of Bath

Hydrogen-Bonded Layer Structures based on Guanidinium Sulfonates

Submitted by
Nichola Jayne Burke
For the degree of Doctor of Philosophy

University of Bath
Department of Chemistry
May 2005

ProQuest LLC
789 East Eisenhower Parkway
P.O. Box 1346
Ann Arbor, MI 48106-1346

Abstract

This thesis discusses the synthesis and characterisation of hydrogen-bonded materials based on the guanidinium sulfonate motif, and the robustness of the hexagonal GS array. The salts guanidinium chloride, methylguanidinium chloride, ethylguanidinium sulfate and dimethylguanidinium sulfate have been crystallised with a variety of sodium mono- and disulfonates. This led to the formation of 35 novel crystalline materials that have been structurally characterised.

Chapter 1 provides an introduction to crystal engineering. It includes a discussion on hydrogen bonding in addition to other supramolecular interactions that are observed between molecules in the crystalline state.

Chapter 2 discusses the products formed when the guanidinium salts mentioned are crystallised with the phosphine sulfonate compounds $Na[PPh_2(C_6H_4SO_3\text{-}3)]$, $Na[O{=}PPh_2(C_6H_4SO_3\text{-}3)]$ and the metal containing disulfonate $Na_2[IrCl(CO)\{PPh_2(C_6H_4SO_3\text{-}3)\}_2]$. The hydrogen bonding in the resulting structures is discussed, and the structural effects of varying substitution in the guanidinium cation are analysed for each sulfonate system.

The products formed when substituted guanidinium salts are crystallised with a range of organic mono- and disulfonates, and the hydrogen-bonded structures observed are presented and discussed in Chapter 3. These compounds are also compared to the analogous structures containing the unsubstituted guanidinium cation, which have been previously reported.

Chapter 4 focuses on incorporating sulfonate dyes into the guanidinium sulfonate network using methyl orange, ethyl orange and 4-aminoazobenzene-4'-sulfonate sodium salts. The GS compounds incorporating each of these dyes and the guanidinium and substituted guanidinium cations have been structurally characterised using X-ray crystallography. The reactions of these hydrogen-bonded arrays with HCl and NH_3 gases are examined using X-ray powder diffraction, UV-visible and infrared spectroscopic techniques.

Acknowledgements

Firstly, I would like to thank my supervisors Dr. Andrew Burrows and Dr. Mary Mahon for their guidance, support and endless patience throughout my PhD at Bath.

I would also like to thank the academic lecturers, especially Prof. Paul Raithby, and the administrative and technical staff for all their help during my time at Bath.

Special thanks must go to David Smith, for keeping me sane and giving me much of his time and company, Piers Taylor for keeping me entertained, Teresa Savarese for allowing me to offload my troubles and keeping me smiling and to both Kevin Cassar and Andrew Kirk for their help and for putting up with my varied mood swings while writing my thesis.

I would like to thank those involved in giving me the opportunity to work at the synchrotron radiation source in Daresbury. Many thanks must go to Dr. Simon Teat, Dr. John Warren and especially Dr Mary Mahon, for all their time and effort that was devoted to my work at station 9.8.

The EPSRC is gratefully acknowledged for providing financial support, both for the funding of my PhD and for providing beam time at the SRS.

I would like to thank my close friends, Shayna Suleyman and James Cooper who both helped me through so many experiences I could not have managed alone, and the many friends I have made during my time in Bath.

Special thanks go to my wonderful partner Martin Jensen for his love and to his parents and family for their support.

Last but not least, I would like to thank my family who have always believed in my ability; my brother David and especially my Mum and Dad for all their love and support throughout my years at Bath, and the many years of my education. They sacrificed so much to give me the best opportunities available, and have always encouraged me to fulfil my ambitious dreams.

List of Publications

The following publications were reported as a direct result of the research described within this thesis, along with those reported by the group that I was also involved in:

1. Incorporation of sulfonate dyes into hydrogen-bonded networks.
   CrystEngComm 6: 429-436 Sep 17 2004, Burke NJ, Burrows AD, Mahon MF, Teat SJ

2. Zinc dicarboxylate polymers and dimers: thiourea substitution as a tool in supramolecular synthesis.
   Dalton Trans (20): 3840-3849 2003, Burke NJ, Burrows AD, Donovan AS, Harrington RW, Mahon MF, Price CE

3. Disorder within dicarboxylates and supramolecular structural control in hydrogen-bonded networks.
   CrystEngComm 5: 355-357 Sep 29 2003, Burke NJ, Burrows AD, Mahon MF, Pritchard LS

4. Hydrogen-bonded linear thiourea hexads in tetra-n-butylammonium terephthalate inclusion compounds.
   CrystEngComm 5: 226-230 Jun 12 2003, Babb JEV, Burke NJ, Burrows AD, Mahon MF, Slade DMK

Other manuscripts are also anticipated.

List of abbreviations

Schematic	Chemical/full name	Abbreviation
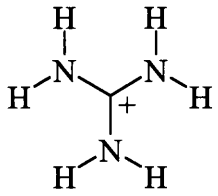	Guanidinium	$[Gu]^+$
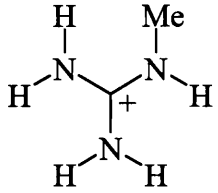	Methylguanidinium	$[MeGu]^+$
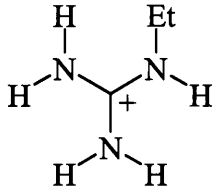	Ethylguanidinium	$[EtGu]^+$
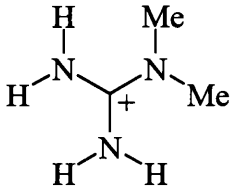	*N,N*-Dimethylguanidinium	$[DiMeGu]^+$
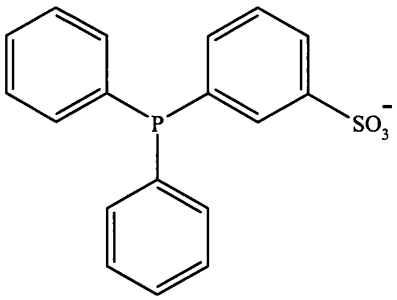	Triphenylphosphine-monosulfonate	$[mTPPMS]^-$
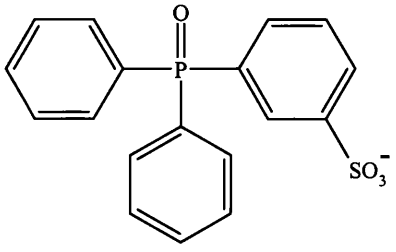	Triphenylphosphine-monosulfonate oxide	$[mTPPMSO]^-$

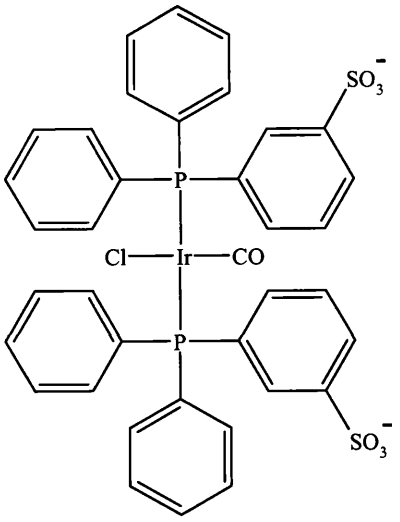	Sulfonated-Vaska's compound	$[IrCl(CO)(mTPPMS)_2]^{2-}$
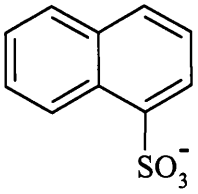	1-Naphthalenesulfonate	$[1\text{-}NapSO_3]^-$
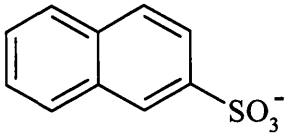	2-Naphthalenesulfonate	$[2\text{-}NapSO_3]^-$
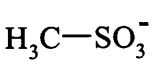	methylsulfonate	$[MeSO_3]^-$
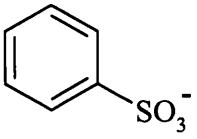	phenylsulfonate	$[PhSO_3]^-$
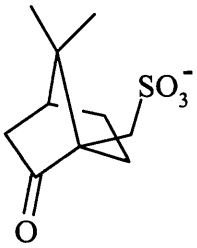	10-camphorsulfonate	$[10\text{-}CamphorSO_3]^-$

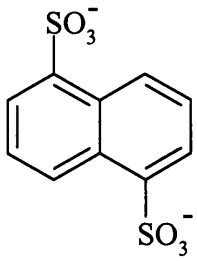	1,5-Naphthalenedisulfonate	$[1,5\text{-}Nap(SO_3)_2]^{2-}$
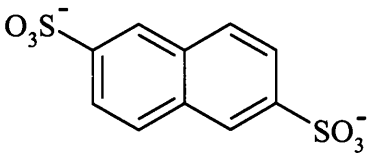	2,6-Naphthalenedisulfonate	$[2,6\text{-}Nap(SO_3)_2]^{2-}$
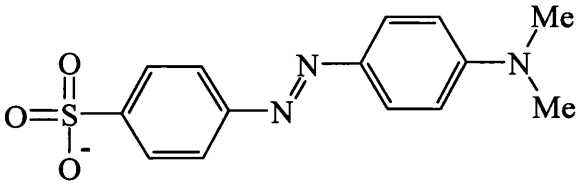	Methyl orange	$[MO]^-$
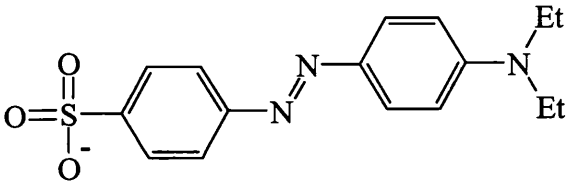	Ethyl orange	$[EO]^-$
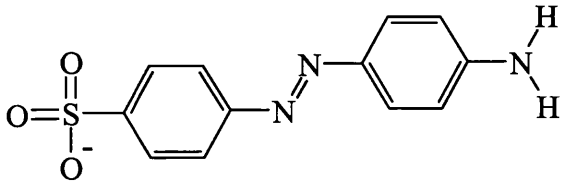	4-aminoazobenzene-4'-sulfonate	$[ABS]^-$
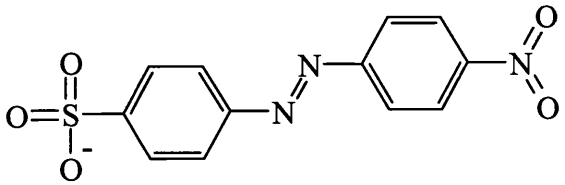	4-nitroazobenzene-4'-sulfonate	$[NBS]^-$
	θ_{IR}	Inter-ribbon angle
	GS	Guanidinium-sulfonate

Table of Contents

Accompanying cd-rom [rear cover] contains supplementary data for all new compounds, including .cif, .res and tables of data.

This thesis is dedicated to my Mum and Dad,
without whom I would not be the person I am today.

I love you both.

Thank you.

CHAPTER 1

An Introduction to Crystal Engineering and Supramolecular Chemistry

1. Introduction

1.1 Crystal Engineering and Supramolecular Chemistry

Crystal engineering can be defined as the understanding of intermolecular interactions in the context of crystal packing and in the utilisation of such understanding in the design of new solids with desired physical and chemical properties[1]. The term 'engineering' was first used by G. Schmidt and co-workers to describe the photodimerisation reaction in crystalline cinnamic acid and its derivatives[2] (Figure 1.1); *"...we shall, in the present context of synthetic and mechanistic photochemistry, be able to 'engineer' crystal structures having intermolecular contact geometries appropriate for chemical reaction..."*. Schmidt realised that the development of organic solid-state chemistry required a theory of crystal packing.

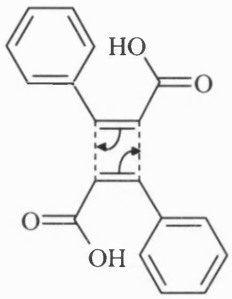

Figure 1.1; cinnamic acid undergoing photodimerisation reaction

Modern crystal engineering is a much broader subject, drawing its strengths from the design and synthesis of supramolecular crystalline materials with desired solid-state properties. The primary focus of crystal engineering is the identification or design of molecular level building blocks, whose interactions with other building blocks (including self-complementary interactions) exhibit some degree of predictability.

There are two main types of bond used in crystal engineering – coordination bonds and the intermolecular interactions, the most common of which is the hydrogen bond. The recent development of inorganic crystal engineering[3] involves metal-containing building blocks linked by non-covalent interactions. This field relies on the special role that the coordination geometry of metal ions can play in influencing the array, an example of which is given in Figure 1.2[4].

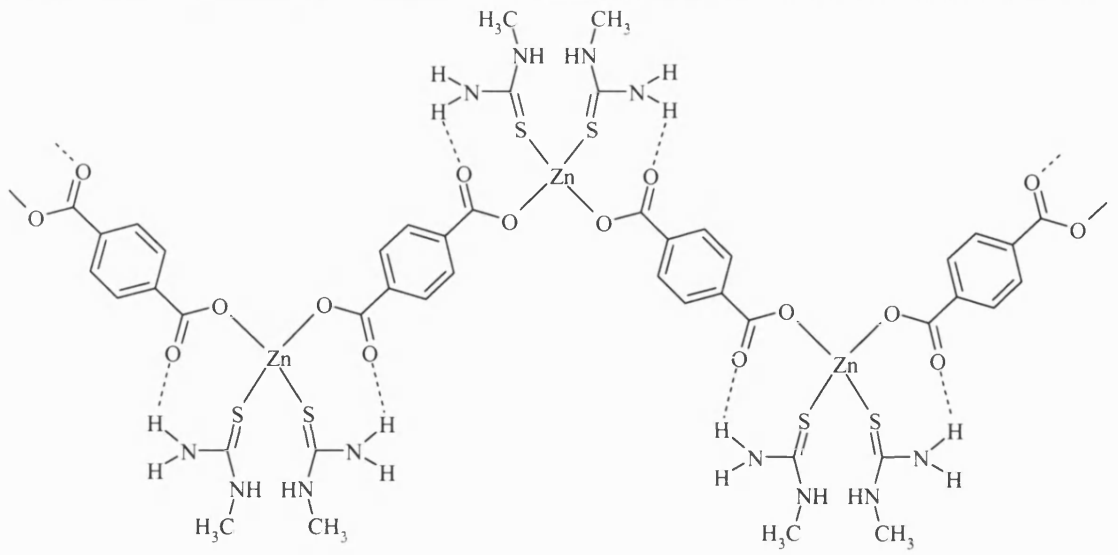

Figure 1.2; part of the coordination polymer formed in $[Zn(H_2NC(S)NHMe)_2(O_2CC_6H_4CO_2)]$ also incorporating hydrogen bonds

Coordination bonds and hydrogen bonds are valuable for the design of solid arrays since they are both directional interactions. The combination of coordination chemistry with non-covalent interactions, such as hydrogen bonding (as shown in Figure 1.3), provides a powerful method for creating predictable, metal-containing supramolecular arrays from simple building blocks[5]. Thus a wide range of inorganic-organic arrays are accessible by this coordination chemistry / hydrogen bonding approach.

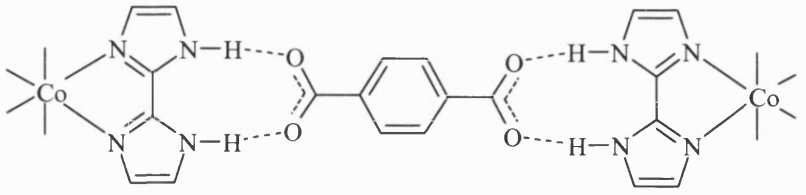

Figure 1.3; a hydrogen-bonded bridge in the structure of $[Co(Hbiim)_2(H_2biim)]_2(O_2CC_6H_4CO_2)_2{\cdot}H_2O$

Specifically chosen building blocks form hydrogen bonds with each other to produce a variety of hydrogen-bonded structural arrays. These can be one, two or three-dimensional arrays and these have been assigned specific terms. One-dimensional structures consist of chains or ribbons (the term 'tape' is sometimes used in place of 'ribbon', but both terms describe the same pattern). A chain is defined here as an infinite one-dimensional structure where components are linked by single hydrogen bonds, as shown in Figure 1.4a[6]. A ribbon

is defined as an infinite one-dimensional structure where components are linked by more than one hydrogen bond, where the hydrogen bonds are approximately co-planar (Figure 1.4b[7]). Two-dimensional arrays are formed by building blocks linked via hydrogen bonding into sheets (Figure 1.4c[8]), and three-dimensional structures are described as networks[9] which can involve a variety of hydrogen bonds.

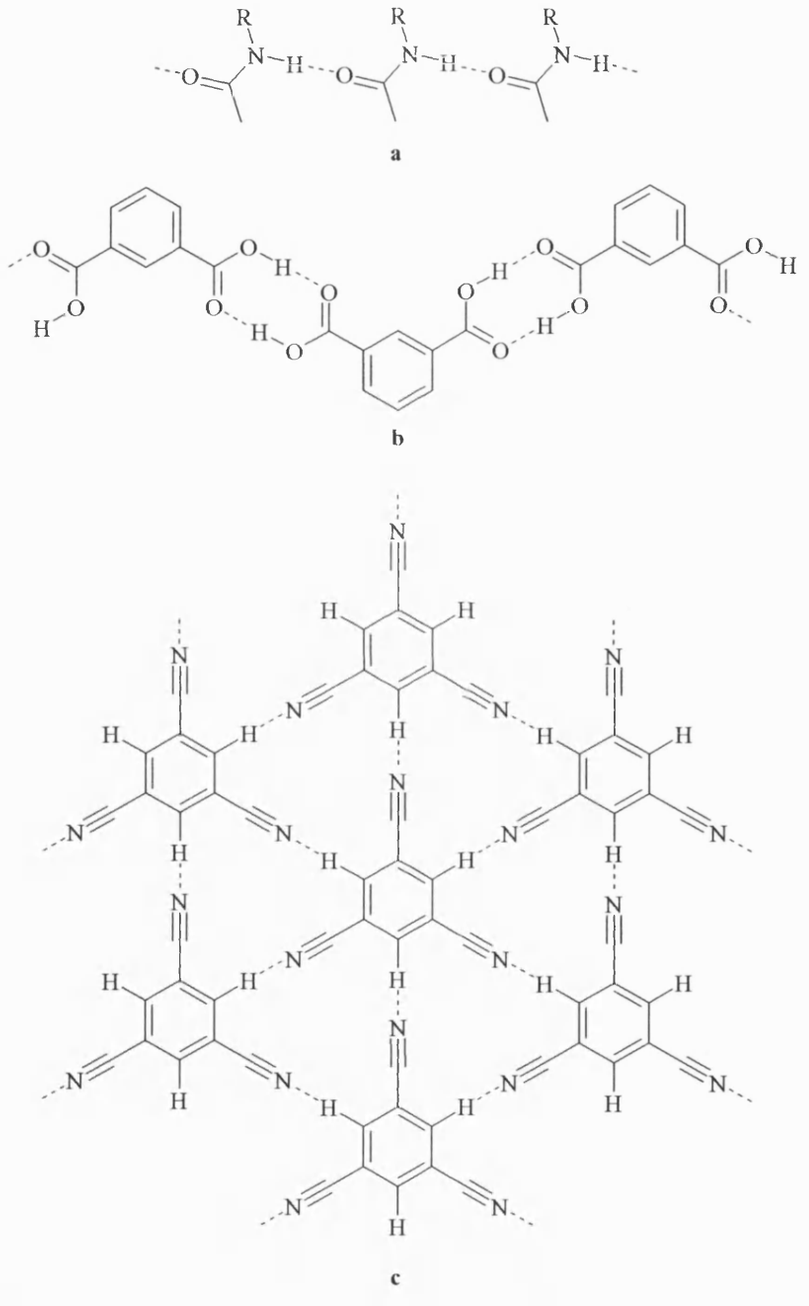

Figure 1.4; **a**) chain formation by non-cyclic secondary amides, **b**) zigzag ribbon structure of isophthalic acid, **c**) sheet formation in the structure of 1,3,5-tricyanobenzene

The use of crystal engineering approaches has led to materials with specifically tailored physical and chemical properties in a number of areas, including nanoporosity[10], magnetism[11], the formation of vapour-deposited thin films[12], non-linear optics, second harmonic generation[13] and fluorescent solid state chemosensors[14], as well as important applications in microelectronics, biomedical implants, separation technologies, catalysis, coatings[15], organic displays[16] and organic thin film transistors[17].

However, crystal engineering is hindered as the ability to genuinely predict the assembly that could arise from the innumerable possibilities available is extremely challenging, considering the number of orientations that can be formed. The presence of hydrogen bonding and other non-covalent interactions are also factors influencing crystal engineering, some of which are of a very general nature and can be difficult to control. In particular, some of these are weak interactions, the manipulation of which can fine-tune the properties of the bulk material. The formation of these interactions can be predicted, but the way in which they come together often cannot[18]. There are some predictable packing arrangements possible. For example, it is known that phenyl groups often pack with specific geometries leading to crystals that are characterised by high crystallinity and low solubility – the so called 'phenyl factor'[19].

Crystal engineering can also be hampered by the inability to maintain structural control when making even the slightest changes in the building block. Prediction of crystal structure based solely on the structure of building blocks remains a challenge[20] and examples of crystal structure prediction, i.e. crystal lattice, space group, cell dimensions and so on, based on crystal engineering strategies are rare[21].

In order to maximise the use of crystal engineering a further understanding of the subtle molecular forces responsible for linking the building blocks into the various possible arrays is needed. Competing interactions, as well as changes in experimental conditions, can also have an impact on the structural array[22]. An understanding of the steric capabilities of the constituent building blocks is also required, as well as the kinetics and thermodynamics of crystal nucleation phenomena, the requirements of crystal close packing and the relative importance of the multiplicity of interactions that go together to assemble the crystalline array[23]. This has prompted numerous investigations aimed solely at deciphering the relative importance of the specific interactions that govern solid-state structures.

Crystal structures are dominated by intermolecular interactions and the easiest way of obtaining reliable information on these interactions is through crystallography. However, in order to utilise crystallographic techniques, a single crystal must first be formed. Crystals are macroscopic objects that exhibit long-range order. The growth of a crystal is a step-wise, self-assembly process whereby molecules form small pre-nucleation aggregates, which then form nuclei that grow into macroscopic crystals[24]. Steed and Atwood have distinguished two types of self-assembly; crystal self-assembly[25] and solution self-assembly*. Crystal self-assembly is defined as '*a non-equilibrium phenomenon in which both kinetics and thermodynamic aspects contribute to the eventual structure. The final structure is a function in many cases of crystallisation conditions... [and] structures that form faster may well predominate over structures that are most stable'.* Crystals can be thought of as supermolecules as their main features are best described by using patterns of interactions, rather than by using molecular descriptors, *i.e.* functional groups. The term 'supramolecular' signifies that which is beyond the molecule. Supermolecules are not merely collections of molecules but have structural features and properties that are characteristic not of the molecules themselves but of the extended assemblies built by the linking of these molecules via non-covalent interactions[26]. A crystal structure, defined as a network of intermolecular interactions, can be seen as the supramolecular equivalent of molecular structure when defined as a networking of covalent bonds.

Supramolecular synthesis involving two or more components is hindered by the problem that a single component might crystallise individually instead of interacting with another component to form crystals of the desired product. The solubility of the individual components is a major factor influencing crystallisation reactions. Computer simulations also show that when there are competing functional groups many different structures can be predicted. These different structures are often closely related enthalpically and the global minimum structure is not always the one that is obtained experimentally, either because the computations are approximate or because the crystallisation process is subject to both kinetic and thermodynamic factors[27]. The vast majority of supramolecular structures are best considered as an interplay between the medium range, non-directional forces (e.g. van der Waals) and the long range, directional forces (e.g. hydrogen bonding). Sometimes the directional requirements of these forces act in harmony, at other times they are in conflict

* As this thesis is focused on crystal analysis, solution self-assembly is not discussed

and it is difficult in any given situation to predict whether the non-directional or directional forces will dominate[28].

The 'black magic' of the process of crystallisation remains a challenge[29]. There is no guaranteed process to follow that will form crystals from an attempted crystallisation. No method exists to predict the size or shape of the crystals that may eventually form, if the crystals will include solvent molecules upon crystallisation or if phase changes would be observed with temperature or pressure. There is also no way of predicting whether crystallisation reactions will yield single crystals, a crystalline powder or amorphous materials[30] or all these together. Many structures are disordered and their characterisation is a challenge[31].

Single crystal diffraction techniques, although rapid and accurate, provide partially *biased* information. Only those materials that produce single crystals of adequate size can be analysed by laboratory diffractometers. Microcrystalline samples require more effort and more sophisticated techniques. Since the products are solids, routine analytical and spectroscopic tools are much less useful that in the case of solution chemistry. In these cases, powder diffraction is often the only way to ascertain whether the bulk solid material has the same structure as that characterised by single crystal diffraction. However, it is also possible that grinding single crystals to a powder, a common method of sample preparation, may lead to solid state transformations[32] making it more difficult to confirm the structure of the bulk material.

1.2 Hydrogen bonding and other non-covalent interactions

The hydrogen bond can be sufficiently strong and directional to control and direct the structures of molecular assemblies, and can also be both reliable and reproducible. There are a vast number of types of hydrogen bond possible, spanning an energy range between that for van der Waals interactions and covalent bonds, allowing them to both associate and dissociate quickly at ambient temperatures in solution.

The definition of a hydrogen bond involves a hydrogen bond donor D–H and a hydrogen bond acceptor A, forming the hydrogen bond D–H···A. To interact with the donor D–H group, the acceptor A must have a lone-pair of electrons or another available filled orbital.

There are a variety of parameters used to describe a hydrogen bond; the most common are shown in Figure 1.5.

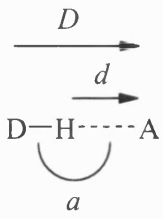

Figure 1.5; the definition of some of the common geometrical parameters used to describe a hydrogen bond, where *d* is the distance between H and A, *D* is the distance between D and A, and *a* is the angle D–H···A

One of the most important articles on hydrogen bonding was written by Pauling[33] in which the term 'hydrogen bond' was used for the first time to account for some of the properties of ice. Pauling was also responsible for bringing the subject of hydrogen bonding into the chemical mainstream. In the chapter on hydrogen bonding in *The Nature of the Chemical Bond* [34], Pauling was clear and unambiguous in the use of the word *bond* when he stated that '*under certain conditions an atom of hydrogen is attracted by rather strong forces to two atoms, instead of only one, so that it may be considered to be acting as a bond between them*'. Pauling also recognised the hydrogen bond as an electrostatic interaction. He stated that '*it is now recognised that the hydrogen atom, with only one stable orbital (the 1s orbital) can form only one covalent bond, that the hydrogen bond is largely ionic in character, and that it is formed only between the most electronegative atoms*'. The electrostatic nature of the hydrogen bond is due to the fact that the solitary electron on the H atom is delocalised between H and D (in the hydrogen bond D–H···A), and that with the increasing electronegativity of D, the H atom is increasingly forced to be more positive in nature. Pauling assumed that only if D and A are very electronegative would the positive nature of H, and in turn the electrostatic attraction between H and A, be sufficiently high to term the interaction a hydrogen bond. However, this restricts hydrogen bonding to cases where D and A can be F, O, Cl, N, Br and I.

The concept of hydrogen bonding has been developed since Pauling's work, and the definition of a hydrogen bond now most commonly used is that described by Pimentel and McClellan[35] which states that '*a hydrogen bond is said to exist when there is evidence of a*

bond, and there is evidence that this bond sterically involves a hydrogen atom already bonded to another atom'. This definition does not restrict the nature of D and A to any specific atoms and allows the existence of the potential hydrogen bond donors C–H and P–H and potential hydrogen bond acceptors such as π-orbitals.

There are many different arrangements possible for the hydrogen bond, other than the simple case of D–H···A, as shown in Figure 1.6. Hydrogen bonds are long-range interactions and a group D–H can interact with more that one acceptor at the same time. In the case where there are two hydrogen bond acceptors, A and A', a *bifurcated hydrogen bond* D–H···(A, A') is formed.

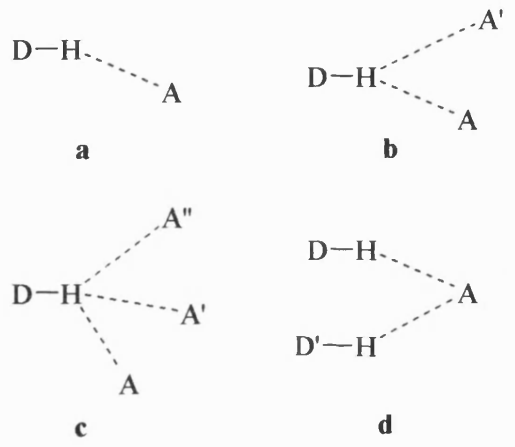

Figure 1.6; different types of hydrogen bond. **a**) the simple hydrogen bond, **b**) a bifurcated donor, **c**) a trifurcated donor, **d**) a bifurcated acceptor

The exact location of the hydrogen atom involved in a hydrogen bond is extremely difficult if not impossible to determine by X-ray diffraction[36]. In X-ray structure determinations the observed distances of the hydrogen atoms to the bonded heavier atoms are shorter than the internuclear distances. This is due to X-rays being scattered by electrons and the position derived for a hydrogen atom from X-ray analysis approximates the centre of the electron density. The latter is not centred around the nucleus of the hydrogen atom, but is displaced towards the atom D. The hydrogen atoms in crystal structures are usually fixed at specific distances from the heavy atoms they are bonded to. Hence the description of a hydrogen bond involves the two heavier atoms D and A, as well as the hydrogen atom itself.

As previously mentioned, there are a great variety of hydrogen bonds possible which cover a wide energy scale. Hydrogen bonds have therefore been classified as weak, strong or very strong and are categorised by taking into account certain properties of the hydrogen bond, for example bond energy and comparative bond lengths. Some of these properties are given in Table 1.1, along with examples of the different types of hydrogen bond formed[37]. However, others working in the field of hydrogen bonding have introduced different terminology. Jeffrey and Saenger[38] have classified hydrogen bonds as 'strong' and 'weak', and Jeffrey later elaborated this to 'strong', 'moderate' and 'weak'[39]. The terminology quoted by Desiraju and Steiner originates from supramolecular considerations. 'Strong' hydrogen bonds are able to control the crystal and supramolecular structure effectively, and include hydrogen bonds of the type O–H···O=C, N–H···O=C and O–H···O–H, whereas 'weak' hydrogen bonds have a variable influence on the packing in a crystal structure.

	Very strong	Strong	Weak
Bond energy (kJ/mol)	60-170	15-60	<15
Examples	$[F\cdots H\cdots F]^-$	O–H···O=C	C–H···O
	$[N\cdots H\cdots N]^+$	N–H···O=C	O–H···π
	P–OH···O=P	O–H···O–H	
Bond lengths	H···A ≈ D–H	H···A > D–H	H···A >> D–H
Lengthening of D–H (Å)	0.05-0.2	0.01-0.05	≤0.01
(D···A) distance range (Å)	2.2-2.5	2.5-3.2	3.0-4.0
(H···A) distance range (Å)	1.2-1.5	1.5-2.2	2.0-3.0
Bonds shorter than vdW	100%	Almost 100%	30-80%
(D–H···A) range (°)	175-180	130-180	90-180
Effect on crystal packing	Strong	Distinctive	Variable
Utility in crystal engineering	Unknown	Useful	Partly useful
Covalency	Pronounced	Weak	Vanishing

Table 1.1; some properties of very strong, strong and weak hydrogen bonds.

Hydrogen bonds are soft interactions, meaning that although energies are maximised if the D–H···A angle is 180°, significant distortion from this angle can occur with little loss of energy. Consequently, hydrogen bonds have a wide spread of lengths and angles when observed in the crystalline state, especially where there is a compromise with other packing

forces. It should also be noted that, as shown in Table 1.1, the H···A bond lengths are normally considerably longer than the D–H bond lengths, meaning that the proton is closer to the donor than the acceptor. Very strong hydrogen bonds are observed between groups where the donor is electron deficient, i.e., D^{+}–H, or the acceptor is electron rich, i.e., A^{-}. This is expected as an electron deficiency in the donor further deshields the H atom increasing its positive charge, while an excess of electrons on the acceptor increases its negative charge and hence increases the strength of the interaction with the deshielded hydrogen atom. This has the consequence of the hydrogen atom position being almost at equal distances from the donor and acceptor.

The use of multiple hydrogen bonds to link building blocks into supramolecular arrays has lead to the concept of 'supramolecular synthons'. The term supramolecular synthon is used to describe the structural units within supermolecules that can be formed by known or conceivable synthetic operations involving intermolecular interactions[40]. These synthons can involve the same component or different components. Examples of hydrogen-bonded synthons are shown in Figure 1.7.

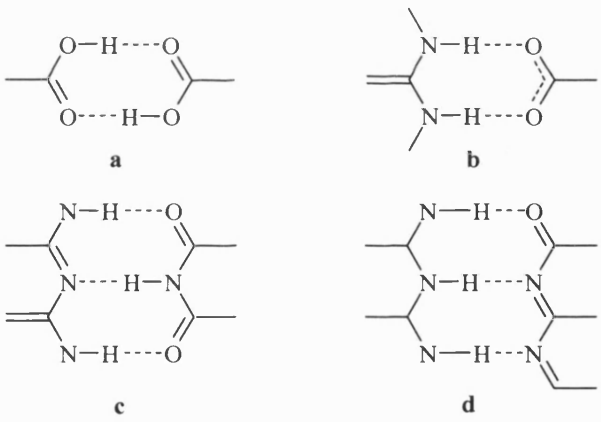

Figure 1.7; examples of supramolecular synthons;
a) DA:AD, **b**) DD:AA, **c**) DAD:ADA and **d**) DDD:AAA motifs

The formation of multiple hydrogen bonds also leads to the presence of secondary interactions, as shown in Figure 1.8. Secondary interactions can be attractive or repulsive, and can make a great difference to the observed association constants[41]. Supramolecular synthons in which the donors and acceptors form parts of different building blocks result in

stronger secondary interactions than those in which there are donors and acceptors on individual building blocks. Therefore, the DD:AA and DDD:AAA motifs are expected to be more favourable than the DA:AD and DAD:ADA motifs, respectively. Hydrogen-bonded networks that form between molecules that have all donors on one face and all acceptors on the other face of the synthon often lead to robust arrays. Robustness is defined here as an aggregate that retains the principal characteristics of its supramolecular structure regardless of ancillary functional groups or the presence of other molecular species in the lattice.

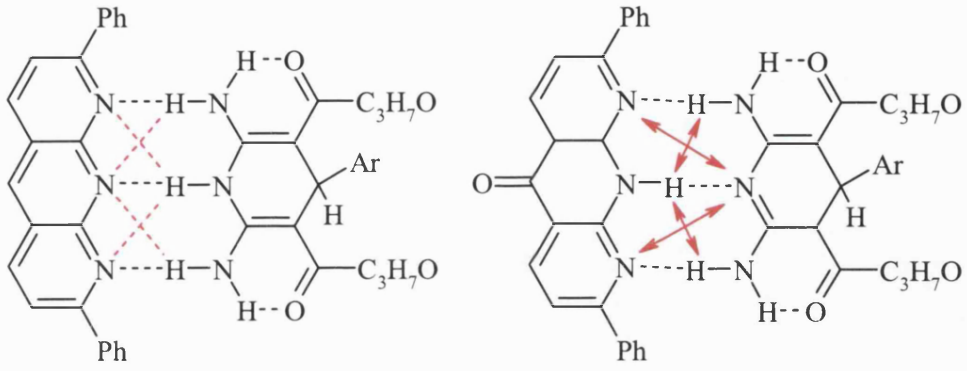

DDD:AAA
attractive secondary
interactions (in red)

DAD:ADA
repulsive secondary
interactions (in red)

Figure 1.8; attractive and repulsive hydrogen bonding interactions

In order to compare the hydrogen bonding observed in different crystal structures, Etter, using the Cambridge Structural Database (CSD), carried out a study of hydrogen bonding[42]. Etter assigned 'graph sets' to different hydrogen-bonding motifs in order to characterise them. This characterisation begins with identifying the number of different types of hydrogen bonds as defined by the nature of the donors and acceptors that form the interaction. The set of molecules that are hydrogen-bonded to another by repetition of one of these types is called a 'motif' and can be characterised in one of four ways. Intramolecular hydrogen bonds are denoted by **S**. Intermolecular hydrogen bonds can be involved in the formation of a chain (**C**), a ring (**R**) and a dimer, or other finite set, (**D**).

The number of hydrogen bond donors (**d**) is assigned as a subscript and the number of hydrogen bond acceptors (**a**) as a superscript. The number of atoms involved in the repeating unit (**n**) is then indicated in parentheses. These parameters combine to form the graph set designator $X_d^a(n)$. Examples of these graph set motifs can be seen in Figure 1.9.

From this study, Etter also devised three rules dealing with stereoelectric or structural factors, which are;

1. all good proton donors and acceptors are used in hydrogen bonding
2. six-membered-ring intramolecular hydrogen bonds form in preference to intermolecular hydrogen bonds
3. the best hydrogen bonding donors and acceptors remaining after intramolecular hydrogen bond formation form intermolecular hydrogen bonds.

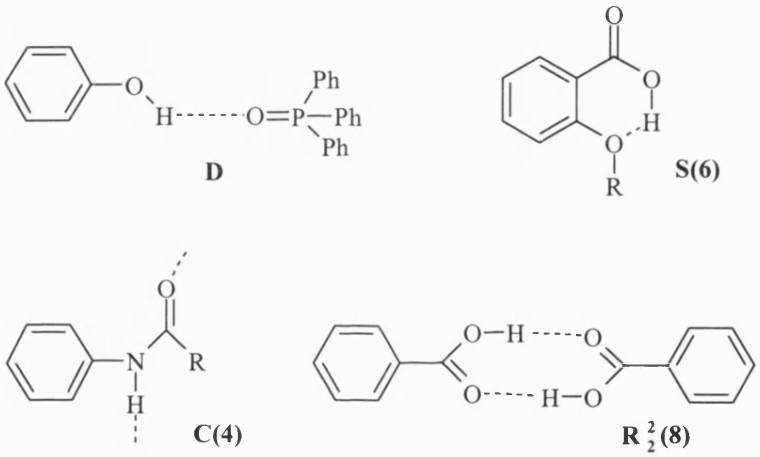

Figure 1.9; graph set notation as assigned by Etter

Raithby and co-workers have undertaken a study of the hydrogen bonding that occurs in the crystal structures in the CSD[43]. This work has identified and classified all intermolecular ring motifs comprising ≤20 atoms formed with N–H···N, N–H···O, O–H···N and O–H···O hydrogen-bonds in organic structures. Also studied was the frequency of occurrence of specific hydrogen bonding compared to the potential for that hydrogen bonding being observed. They found that the ring motif $R_2^2(8)$ that forms between an aminopyridine and an amide occurred in more than 80% of possible structures.

Duchamp and Marsh have reported the crystal structure of trimesic acid[44], as shown in Figure 1.10. The 'chicken wire' motif is observed via the DA:AD $R_2^2(8)$ hydrogen bond motif, however the apparent presence of large voids in this structure is countered by interpenetration, where the voids associated with one supramolecular array are occupied by one or more independent arrays[45].

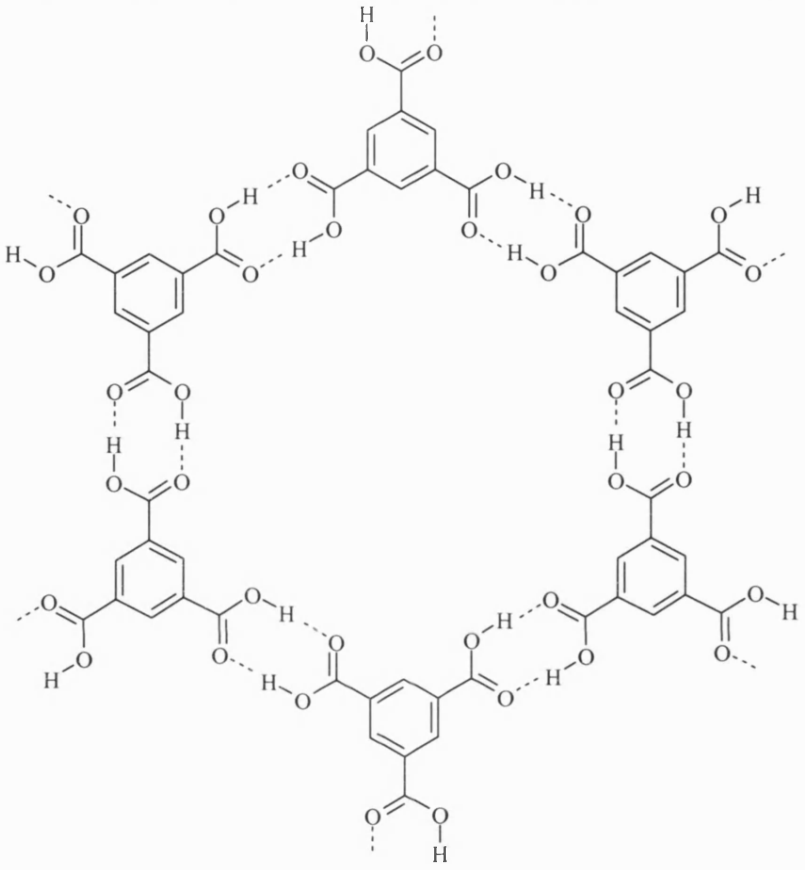

Figure 1.10; the chicken wire motif observed in the crystal structure of trimesic acid

Hamilton and co-workers developed a hydrogen-bonding motif based on carboxylic acids and 2-aminopyridine derivatives[46]. Linking two aminopyridine groups through a rigid aromatic spacer provides a receptor unit that can form hydrogen-bonded compounds with dicarboxylic acids. There are two possible arrangements of bis(aminopyridine) that can be formed. The *anti* configuration has outwardly directed hydrogen bonds and the *syn*

configuration has inwardly directed binding groups. These two arrangements are shown in Figure 1.11.

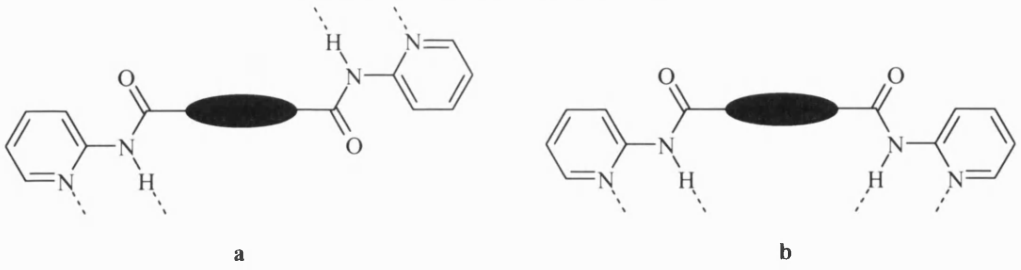

a **b**

Figure 1.11; the anti (**a**) and syn (**b**) arrangements of a bis(aminopyridine)

Four derivatives of bis(aminopyridine) were synthesised with different spacer lengths, including phenyl ***1***, and biphenyl ***2***. ***1*** forms a 1:1 compound with adipic acid [$HO_2CCH_2CH_2CH_2CH_2CO_2H$]. This is due to the distance between the aminopyridine groups in the receptor and between the carboxylate groups in the diacid being complementary, hence the syn arrangement of binding groups is formed, as shown in Figure 1.12. The hydrogen-bonding involves two sets of DA:AD $R_2^2(8)$ motifs in each dimer unit.

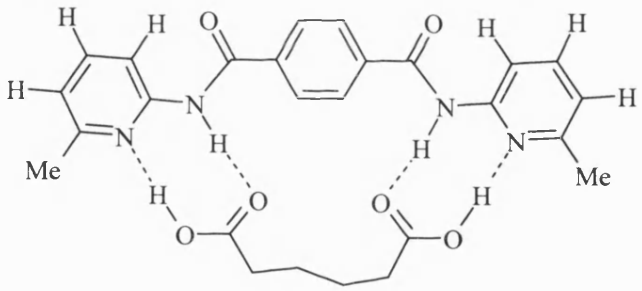

Figure 1.12; syn arrangement of binding groups observed in the 1:1 compound formed from ***1*** and adipic acid

However, in the crystal structure of ***2*** and 1,12-dodecanedicarboxylic acid, the acid is too long to form 1:1 complexes and instead ***2*** adopts the anti arrangement, with an alternating arrangement of diacid and diamide linked via hydrogen bonding leading to a ribbon structure, as shown in Figure 1.13. Even though the arrangement of the supramolecular structure is different to that mentioned above, the same DA:AD $R_2^2(8)$ motifs are observed.

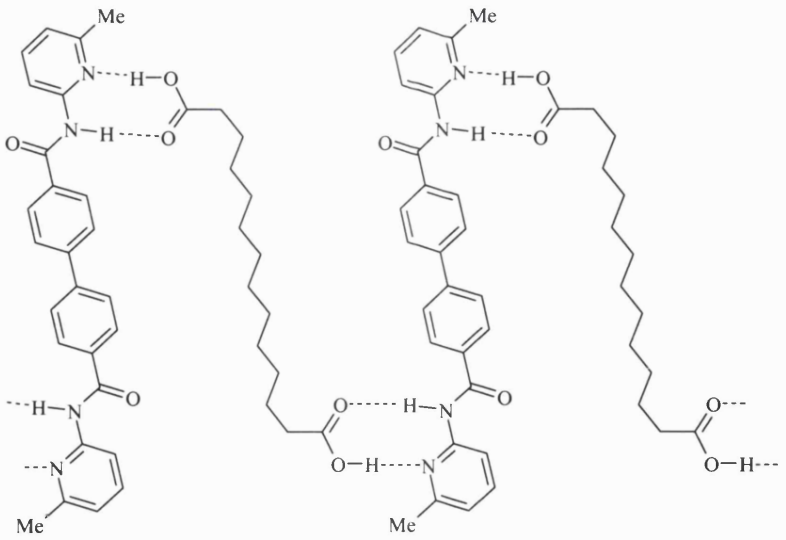

Figure 1.13; due to the length of the acid group, the anti arrangement is observed in ***2*** and 1,12-dodecanedicarboxylic acid

Whitesides and co-workers have used the hydrogen bonding between barbituric acid and melamine derivatives to force the formation of ribbons rather than sheets[47]. This work is based on the robust sheet formed between cyanuric acid and melamine, shown in Figure 1.14. These sheets are held together via multiple N–H···N and N–H···O hydrogen bonds between the three DAD:ADA faces of the two molecules.

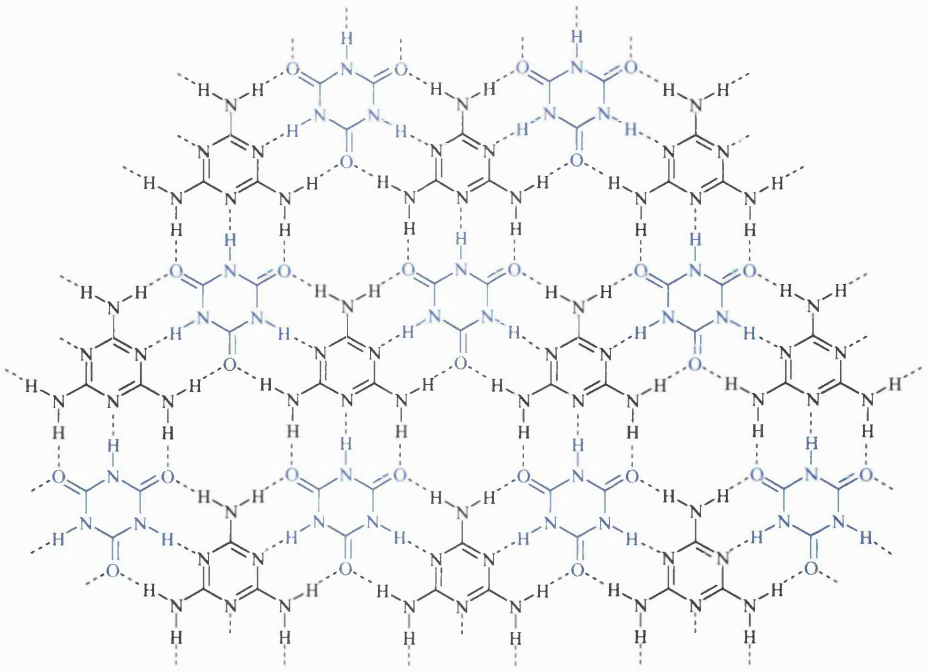

Figure 1.14; hydrogen-bonded sheet formed between cyanuric acid and melamine

When the DAD:ADA faces are disrupted by substitution of the N–H donors for alkyl groups the sheets are no longer formed and ribbons are observed, as shown in Figure 1.15.

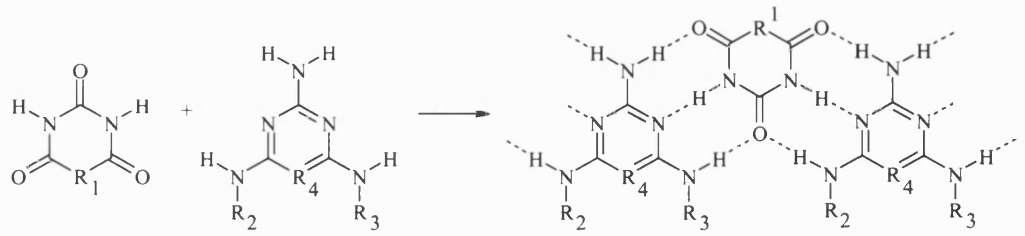

Figure 1.15; derivatives of barbituric acid and melamine and their formation into hydrogen bonded ribbons via DAD:ADA hydrogen bonding motifs

The steric interactions between substituents being varied on the melamine molecules govern the nature of the ribbons formed. Small substituents such as *p*-tolyl lead to linear tapes being observed whereas larger groups, *p*-CO_2CH_3, form crinkled ribbons while rosettes are formed as the steric bulk increases, *p*-^{t}Buphenyl, as shown in Figure 1.16.

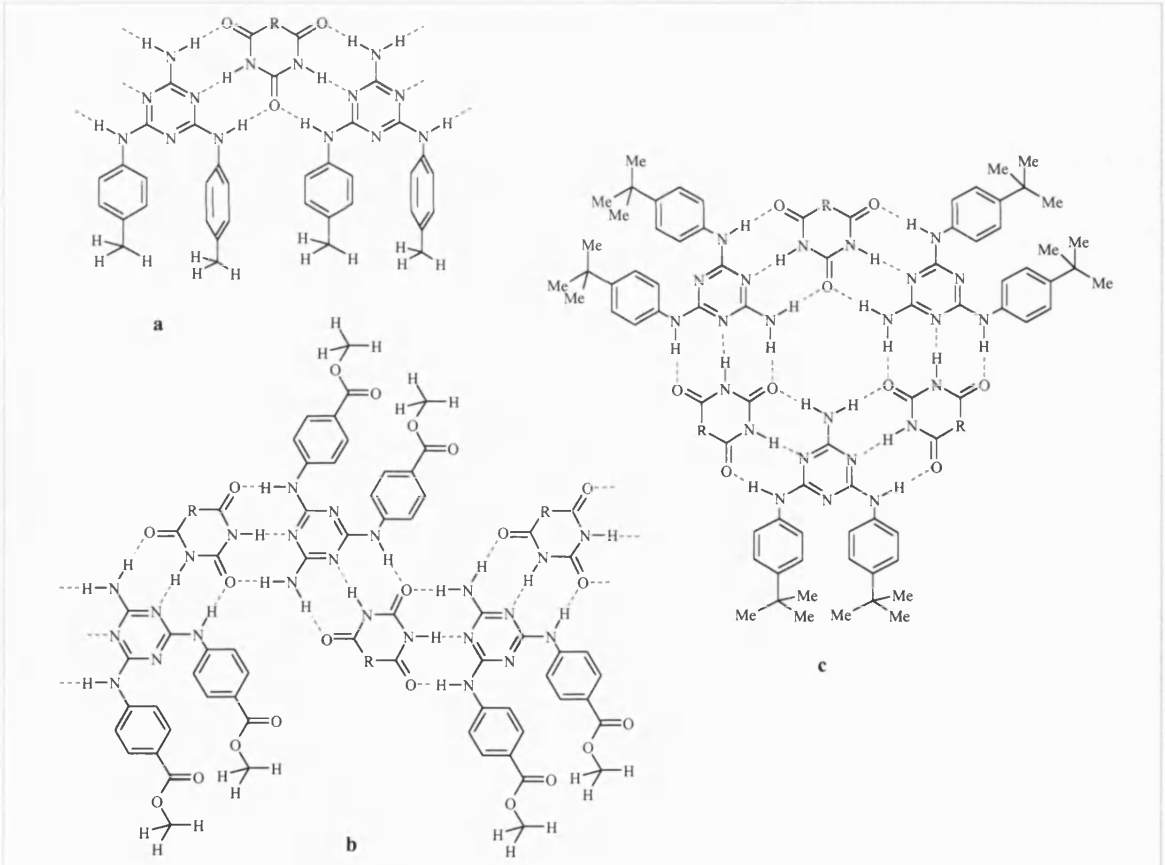

Figure 1.16; **a**) linear ribbon, **b**) crinkled ribbon and **c**) rosette motifs formed by derivatives of barbituric acid and melamine derivatives

Lehn and co-workers have used the DDA:AAD hydrogen-bonding motif in the self-assembly of pyrimidinone ***3*** and pyrimidinedione ***4*** to form molecular ribbons[48]. Compounds ***3*** and ***4***, which each have two hydrogen-bonding faces, are complementary and also self-complementary with regards to hydrogen bonding. When ***3*** and ***4*** interact with each other, a hydrogen-bonded ring comprising of six building blocks is observed. However, the self-association of either ***3*** or ***4*** leads to ribbon formation (see Figure 1.17). In both the ring and the ribbon, the $R_2^2(8)$ hydrogen-bonding motif is present.

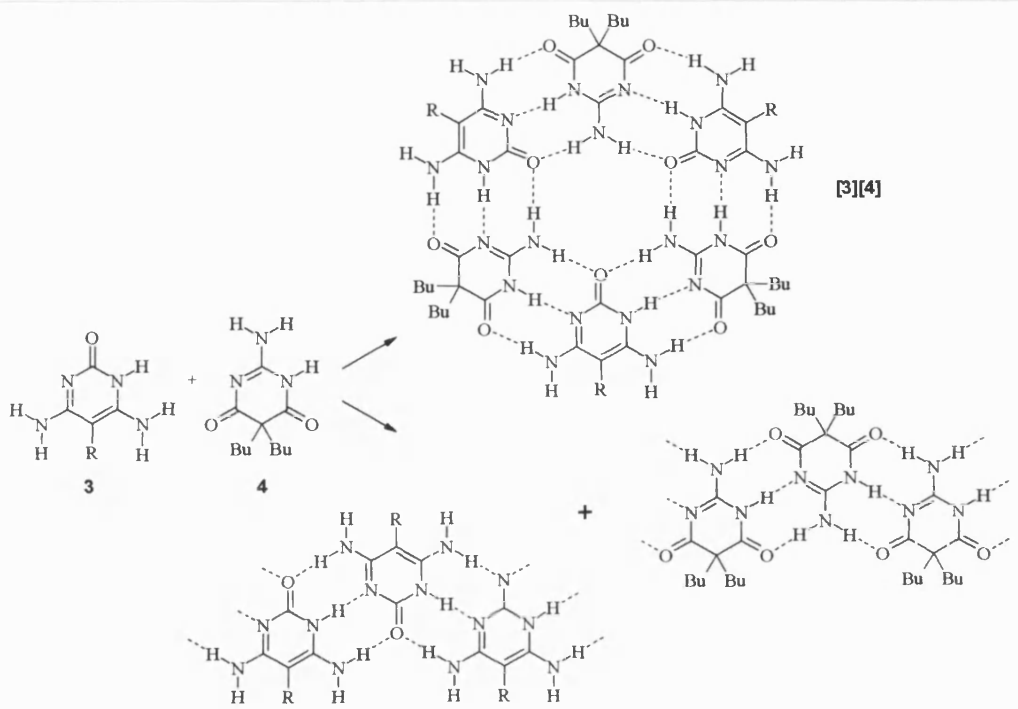

Figure 1.17; a ring is formed when ***3*** and ***4*** hydrogen bond with each other, but self association of either component leads to a hydrogen-bonded ribbon

The pyrimidinetriamine compound ***5*** also forms a ribbon polymer where there are three sites available for hydrogen-bonding forming DAD:ADA motifs, which are further strengthened by hydrogen bonds formed by DMSO molecules, as shown in Figure 1.18.

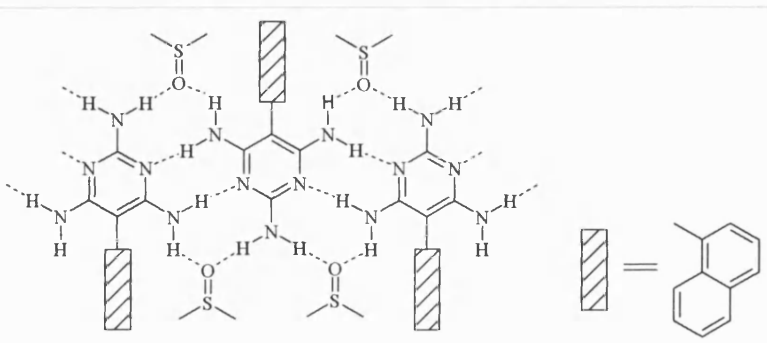

Figure 1.18; ribbon formation observed in ***5***

Ballabh and co-workers have studied a variety of crystal structures of dicarboxylic acids and amines[49]. They found that the salt ***6*** (Figure 1.19a), formed two-dimensional sheets.

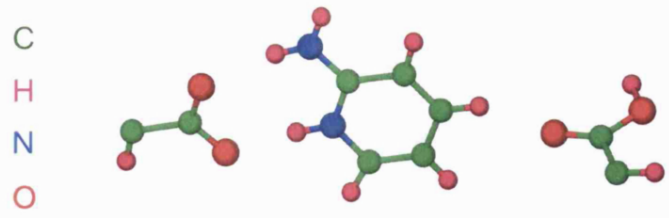

Figure 1.19a; the asymmetric unit in ***6*** (bis(2-aminopyridinium) fumarate-fumaric acid (1:1)

The sheets are formed using O–H···O and N–H···O hydrogen bonds, as shown in Figure 1.19b.

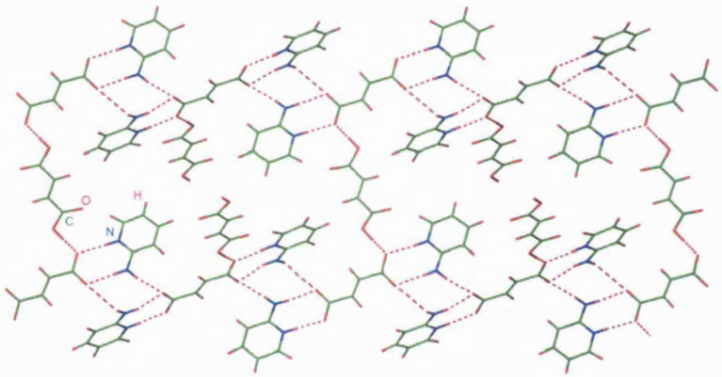

Figure 1.19b; sheet structure observed in ***6***

Hamilton and co-workers have utilised hydrogen bonding to control the aggregation of self-complementary guanidinium-carboxylate derivatives[50]. They have introduced the synthesis of two guanidinium-carboxylate zwitterionic molecules. The crystal structures of flexible *7* and rigid ***8*** guanidinium-carboxylates show DD:AA hydrogen-bonding between the guanidinium and the carboxylate groups. In *7* a non-planar structure leads to extensive interaction between adjacent layers. However, in ***8*** (see Figure 1.20) an intramolecular hydrogen bond directs planarity and minimises available hydrogen bonding groups for inter-layer interactions.

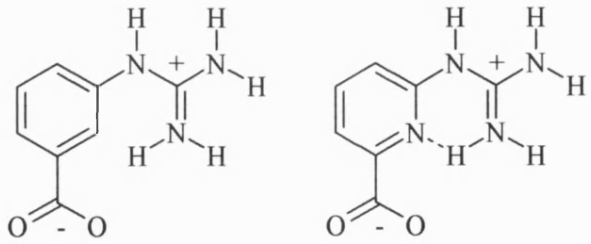

7 8

Figure 1.20; **7** forms a non-planar structure where there is extensive interaction between layers, whereas the intramolecular hydrogen bond in **8** directs planarity minimising the available hydrogen bond groups for interactions between layers.

1.2.1 O–H···O hydrogen bonds

O–H···O hydrogen bonds are employed in self-complementary carboxylic acids that hydrogen bond to form a variety of arrays, depending on the number of carboxylic acid groups in the molecule. Discrete dimers are observed between molecules containing a single carboxylic acid group. Dicarboxylic acids form ribbons, as shown in Figure 1.21, whereas tricarboxylic acids form sheets. In all these examples the $R_2^2(8)$ hydrogen-bonding motif is observed between the DA:AD faces.

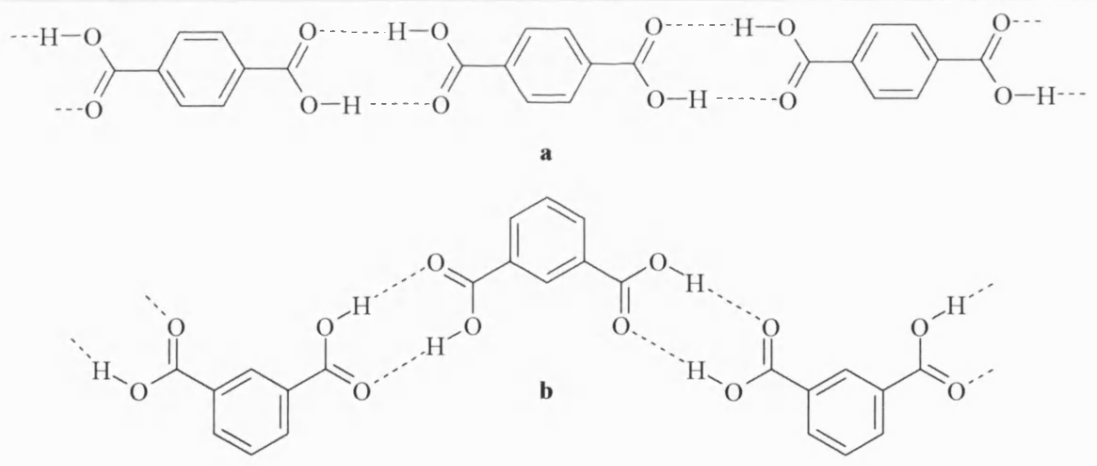

Figure 1.21; the linear ribbon and zigzag ribbon structures observed in self-complementary hydrogen bonding in terephthalic acid (**a**) and isophthalic acid (**b**) respectively

Mao *et al* have reported a metal-containing complex that forms O–H···O hydrogen-bonded ribbons[51], as shown in Figure 1.22. DA:AD faces are present with hydroxy groups forming the O–H···O hydrogen bonds.

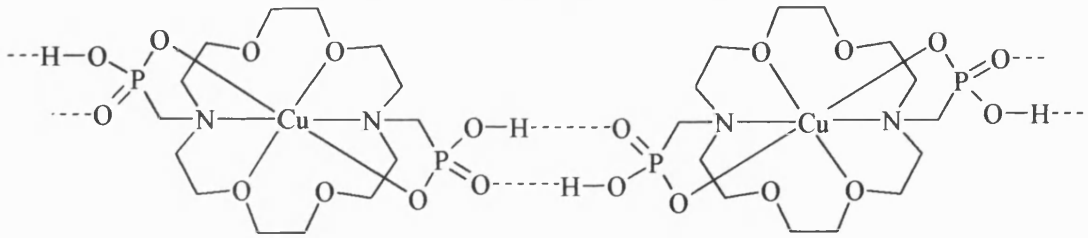

Figure 1.22; ribbon formation via $R_2^2(8)$ hydrogen bonding between DA:AD faces in a copper bis(phosphonomethyl)azacrown complex

Bishop and co-workers[52] have recently reported results of their continuing work developing the helical tubuland family of alicyclic diols. In these compounds hydroxy-group hydrogen bonding results in formation of a network of helical arrays of diol molecules that enclose channels, as shown in Figure 1.23. The formation of this hydrogen bonding results in the compounds being capable of trapping a wide range of guest species in these channels. One of the diols that Bishop *et al* have isolated that forms a helical tubuland structure is 2,6-dimethylbicyclo[3.3.2]decane-*exo*-2,*exo*-6-diol ($C_{12}H_{22}O_2$), which traps chloroform guest molecules in the channels of the lattice.

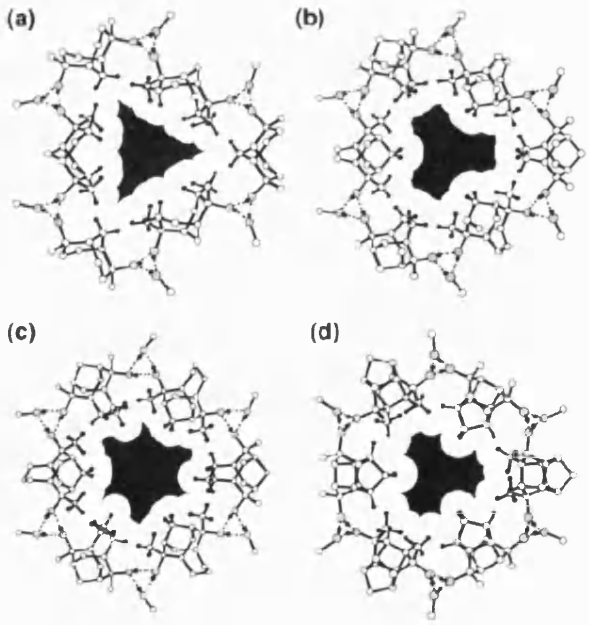

Figure 1.23; (**a-d**) represent partial lattice structures of the typical helical tubuland diols formed via hydroxy group hydrogen bonding

1.2.2 N–H···N hydrogen bonds

Harris and co-workers[53] have reported N–H···N hydrogen bonds in the crystal structure of ammonium cyanate, shown in Figure 1.24. This structure had previously been reported as the NH_4^+ cation forming hydrogen bonds to the four cyanate oxygen acceptors via N–H···O hydrogen bonds.

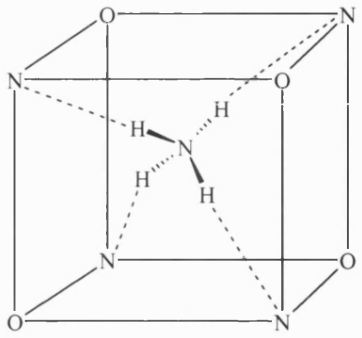

Figure 1.24; schematic illustration of the distorted cube in the crystal structure of ammonium cyanate showing the N–H···N hydrogen bonding.

This structure had been solved using Rietveld refinement of the laboratory X-ray powder diffraction data. The revised structure solution came from Rietveld refinement of improved X-ray powder diffraction data from a synchotron source.

Tadokoro and co-workers have shown that 2,2'-biimidazole (H_2bim) can form a variety of hydrogen bonding motifs[54]. When deprotonated it can be used to form many different arrays when coordinated to a metal centre. For example, the complex [Ni(Hbim)$_2$(bipy)] forms pairs of N–H···N hydrogen bonds which link the molecules into DA:AD zigzag ribbons, as shown in Figure 1.25.

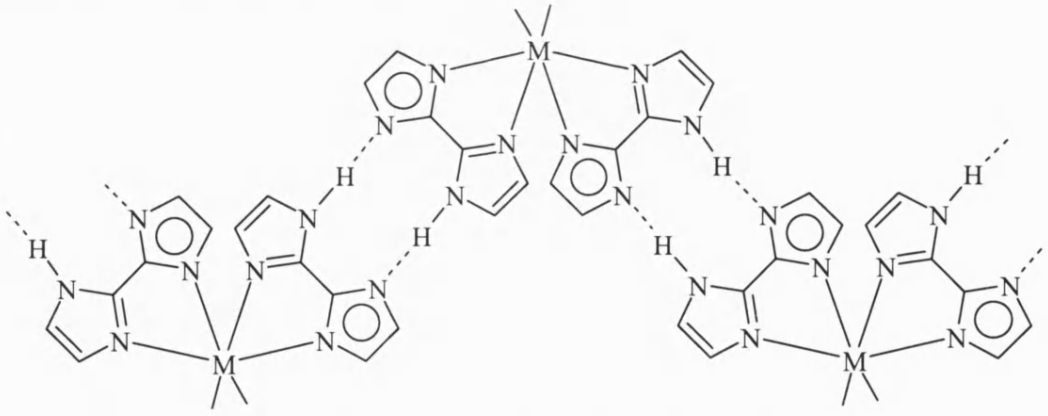

Figure 1.25; zigzag ribbons formed in [Ni(Hbim)$_2$(bipy)]

1.2.3 N–H···O hydrogen bonds

Pedireddi and Belhekar report the DA:AD hydrogen bonding formed in cyanuric acid[55]. This molecule has three ADA faces but can self-assemble in the absence of other molecules with complementary DAD faces. The hydrogen bonds form via $R_2^2(8)$ motifs linking the molecules into hydrogen-bonded ribbons using two of the three available faces of the molecules, as shown in Figure 1.26. These ribbons are further linked into sheets by single N–H···O hydrogen bonds via the third face.

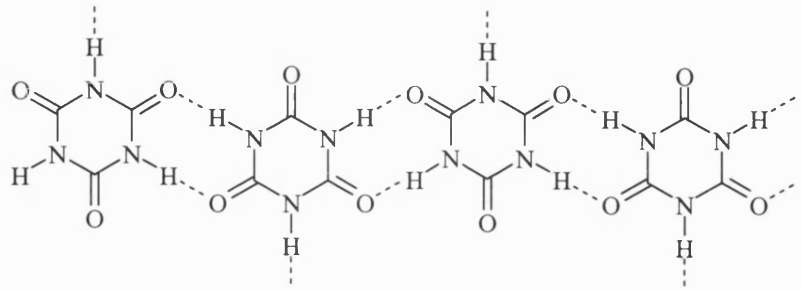

Figure 1.26; hydrogen-bonded ribbons observed in the crystal structure of self-assembled cyanuric acid

1.2.4 C–H···O and C–H···N hydrogen bonds

Sutor published a study on C–H···O hydrogen bonds in crystal structures[56]; an example of one of the structures examined is shown in Figure 1.27. Taylor and Kennard[57] also published a survey of 113 neutron diffraction crystal structures from which they concluded that C–H···O and C–H···N contacts were attractive in nature and these contacts can be described as a type of hydrogen bond.

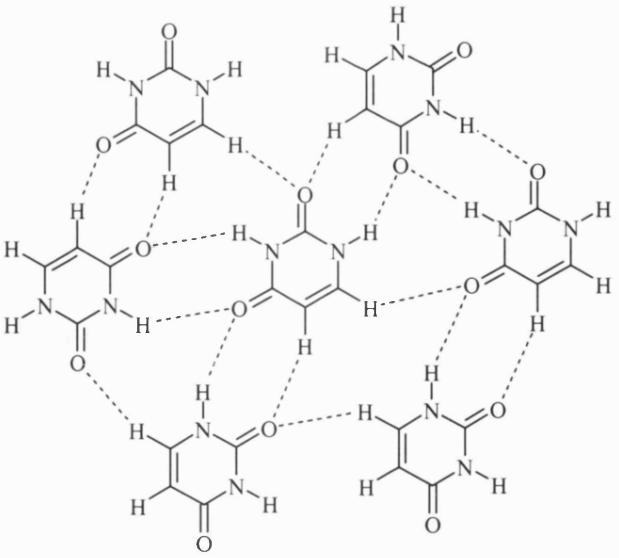

Figure 1.27; the structure of uracil, which incorporates C–H···O (and N–H···O) hydrogen bonding.

Chang and co-workers have looked in detail at the C–H···O hydrogen bond, highlighting the fact that this type of interaction may act as an additional stabilising factor in protein structures[58]. 1-acetamido-3-(2-pyrimidinyl)-imidazolium bromide exhibits a bilayer stacking structure, whereas the PF_6^- salt reveals a sheet structure, as shown in Figure 1.28. C–H···O hydrogen bonds were concluded to be important determinants for the stability of the PF_6^- salt.

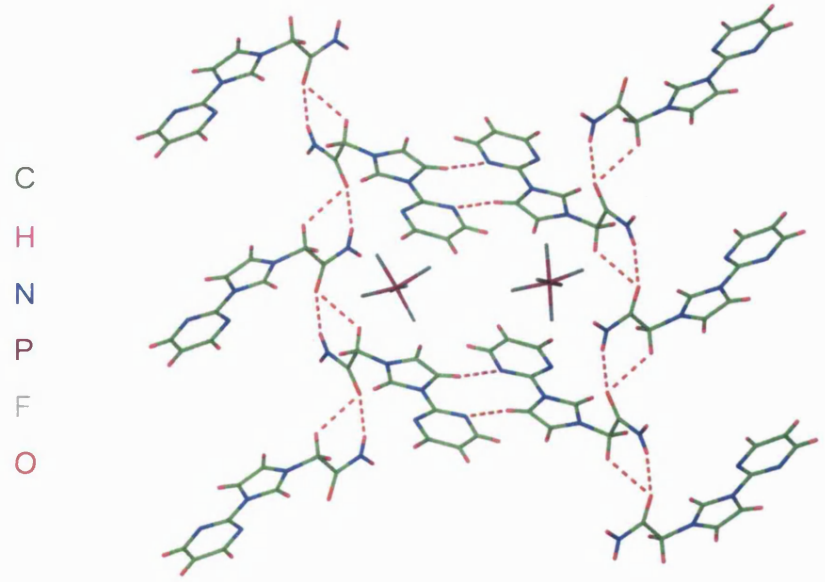

Figure 1.28; the structure of 1-acetamido-3-(2-pyrimidinyl)-imidazolium PF_6 showing the sheet structure incorporating C–H···O and C–H···N hydrogen bonds

Ohkita, Tsuji and co-workers have reported the crystallisation of 4-(4-ethynylphenyl)ethynylpyridine utilising C–H···N hydrogen bonds[59]. In the crystal the molecules are arranged in parallel through C–H···N hydrogen bonds as shown in Figure 1.29.

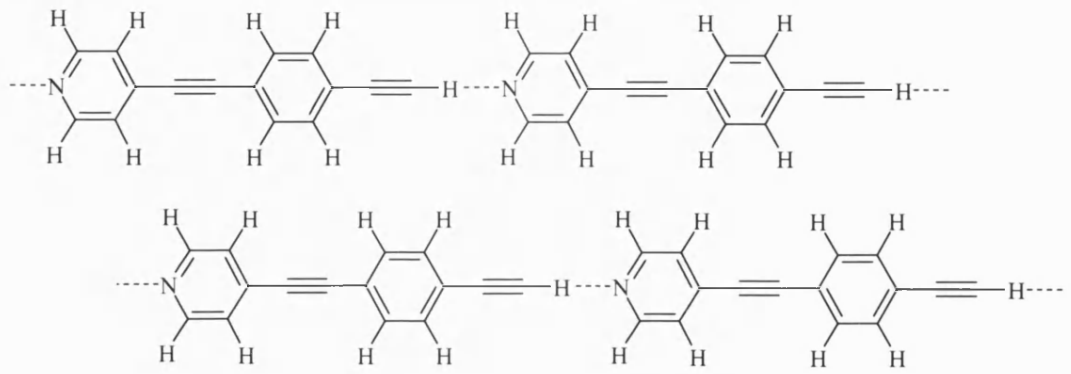

Figure 1.29; the parallel arrangement and C–H···H hydrogen bonding in 4-(4-ethynlphenyl)ethynylpyridine

1.2.5 O–H···π and N–H···π interactions

O–H···π and N–H···π interactions are rare, as carbon is not as electronegative as oxygen and also because carbon atoms are often crowded by other substituents or bulky groups. However, sufficiently electron-rich C–C bonds, for example alkynes, alkenes and aromatic carbons, have the ability to form a hydrogen bond like interaction with O–H or N–H donors. From purely electrostatic considerations, these may be regarded as the interaction of a donor with the electron density in the π orbital.

Atwood and co-workers have called this interaction a π-hydrogen bond[60] and describe an example of a calixarene host-guest complex where aromatic rings of the host molecule are splayed apart by water guest molecules forming O–H···π interactions, as shown in Figure 1.30.

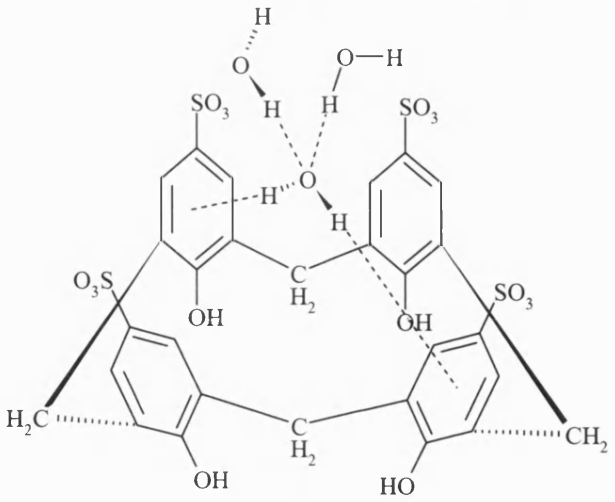

Figure 1.30; O–H···O hydrogen bonding formed between a molecule of water and calix[4]arene

An example of an intramolecular O–H···π interaction is shown in Figure 1.30, as reported by Baert *et al* [61].

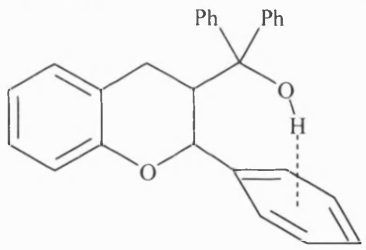

Figure 1.31; an example of intramolecular O–H···π hydrogen bonding [*cis*-diphenyl(2-phenyl-3-chromanyl)methanol]

1.2.6 C–H···π interactions

The C–H···π interaction has been recognised to play a role in a variety of chemical and biological phenomena[62]. Iitaka *et al* [63] reported crystallographic results showing that the *t*-butyl group in a pair of sulfoxide diastereoisomers (PhCHMeSO-^{t}Bu) was close to the phenyl group at the other end of the molecule, and suggested that there was an attractive force between these groups. A calix[4]arene derivative in a complex with toluene was studied by Andreetti *et al* and the guest was shown to be tightly held in the cavity of the host via C–H···π interactions[64].

Ciunik and Jarosz[65] have isolated two types of motifs formed in benzyl groups, as shown in Figure 1.32. The first kind (Figure 1.33a) has parallel benzyl groups that form columns. In the second type (Figure 1.33b) antiparallel benzyl groups form dimers. In both cases the interplanar distances are in the range 3.4 – 3.7Å.

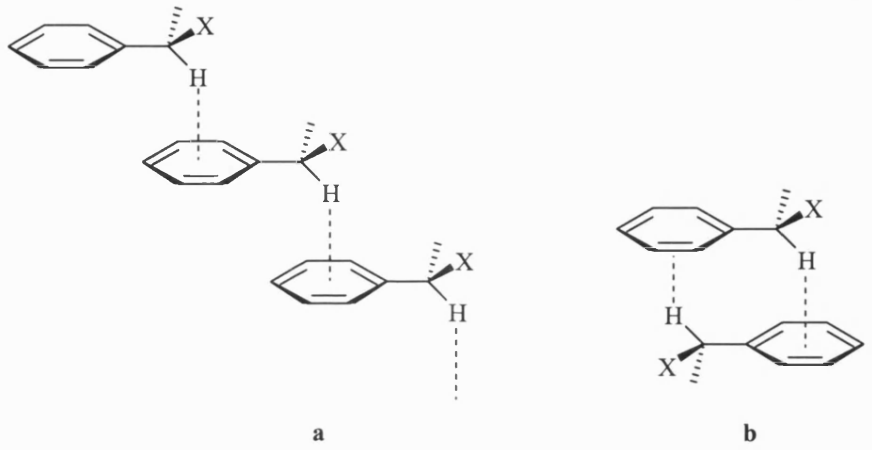

Figure 1.32; the parallel and antiparallel arrangements of benzoyl groups interacting via C–H···π interactions

Re and Nagase have also reported that the C–H···π interactions significantly contribute to host-guest complexation[66]. They used a cyclic tetramer (Figure 1.33a) as the host molecule and compared the results of complexation with 3-oxo-1-butanol (Figure 1.33b) and 1-butanol (Figure 1.33c). The adduct formed between the tetramer and 3-oxo-1-butanol has shorter contacts than those in the 1-butanol adduct as the presence of the carbonyl group in 3-oxo-1-butanol increases the acidity of the C–H groups involved in the hydrogen bonding.

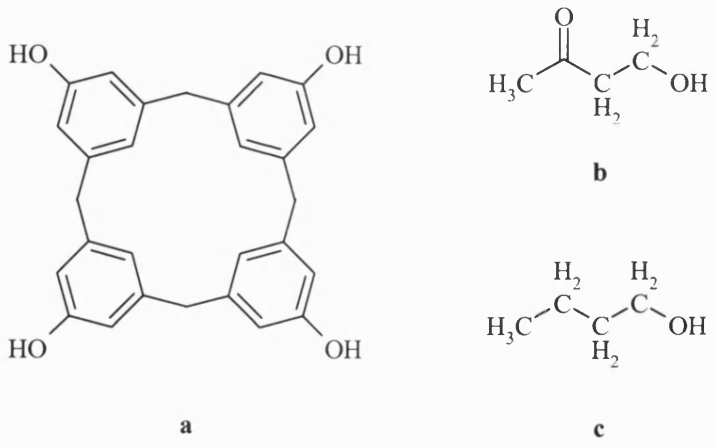

Figure 1.33; the structures of (**a**) a cyclic tetramer, (**b**) 3-oxo-1-butanol and (**c**) 1-butanol

1.2.7 π···π interactions

π···π interactions arise between aromatic rings, often in situations where one is relatively electron rich and the other is electron poor. There are two general types of π···π interactions: face-to-face and edge-to-face, though a wide variety of intermediate geometries are known[67]. Edge-to-face interactions are responsible for the herringbone packing in crystal structures of a range of small aromatic hydrocarbons, including benzene, and are regarded as C–H···π interactions.

Sanders and Hunter have devised a model based on competing electrostatic and van der Waals influences to explain the variety of geometries observed for π···π interactions[68]. The model they propose is based on overall attractive van der Waals interactions, which are proportional to the contact surface area of the two π-systems. The attractive interaction contributes highly to the overall energy of the π···π interaction. The relative orientation of the two interacting molecules is determined by the electrostatic repulsions between the two negatively charged π-systems. These interactions are shown in Figure 1.34.

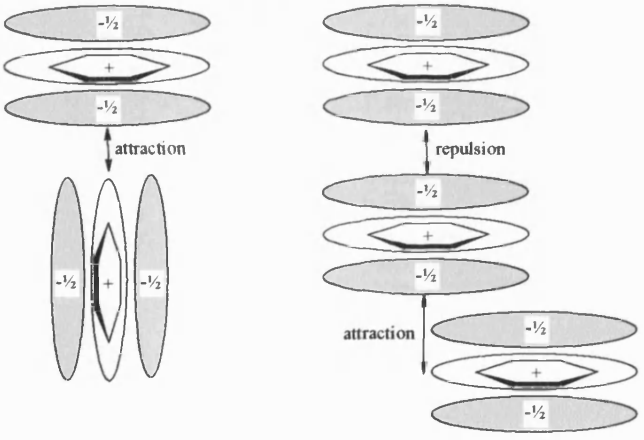

Figure 1.34; the attractive and repulsive forces in π···π interactions

Janiak has reported that π···π interactions have contributed to self-assembly and molecular recognition processes when extended structures are formed from building blocks constituting of aromatic moieties[69]. π···π interactions are stabilised by:

a) Dipole-dipole interactions: the interactions between the different permanent and static molecular charge distributions (Figure 1.35a)

b) Dipole-induced dipole interactions between the static molecular charge distribution of one molecule with a proximity-induced change in charge distribution of another molecule (Figure 1.35b)
c) Induced dipole-induced dipole (London) dispersion interactions: the instantaneous dipole moment from a fluctuating electron cloud polarises a neighbouring molecule and induces in it an instantaneous dipole (Figure 1.35c)

These van der Waals interactions (a-c) are inherently attractive and their potentials fall off rapidly with distance.

d) Pauli repulsion: at very short distances the filled electron clouds of the interacting molecules begin to overlap and the repulsion between the electron shells becomes dominating (Figure 1.35d).

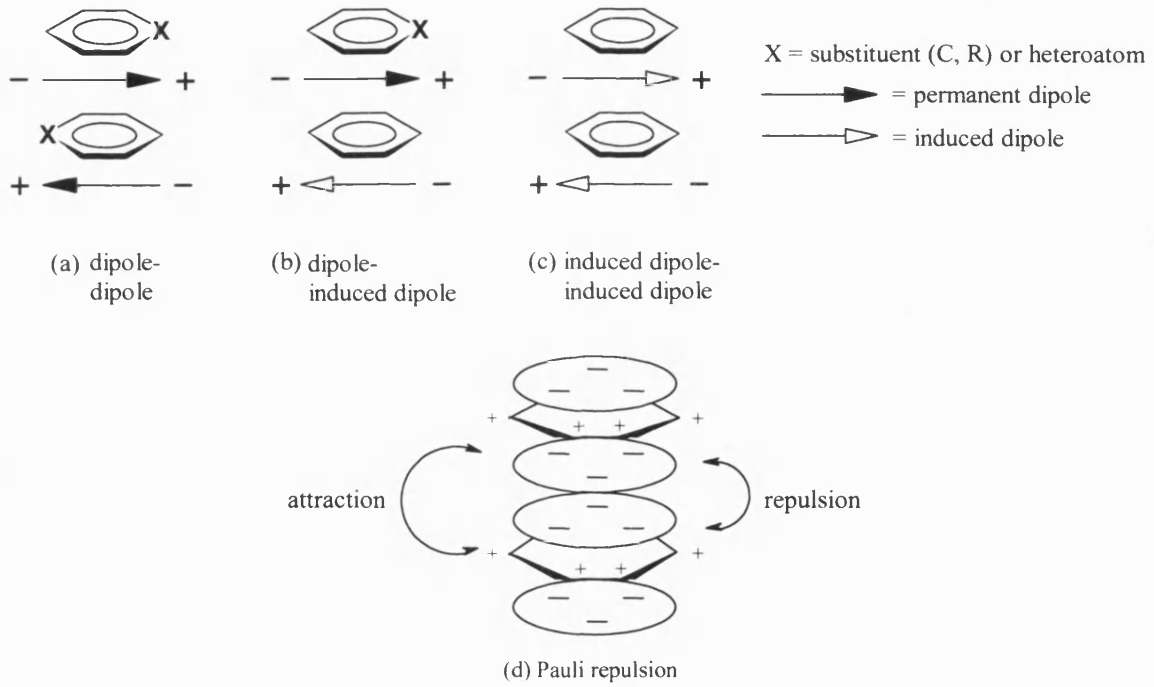

Figure 1.35; electrostatic interactions that stabilise π···π interactions
(*for simplicity, the two arene moieties are drawn in perfect face-to-face alignment*).

Nguyen and co-workers have utilised π-stacking as a route to plastic materials that could have utility in electronic applications[70]. They report that the functionalisation of disk-shaped aromatic molecules with hydrocarbon chains as a useful method to influence π-stacking and to create one-dimensional electronic materials. Two specific compounds were studied, ***9*** and ***10***, the structures of which are shown in Figure 1.36.

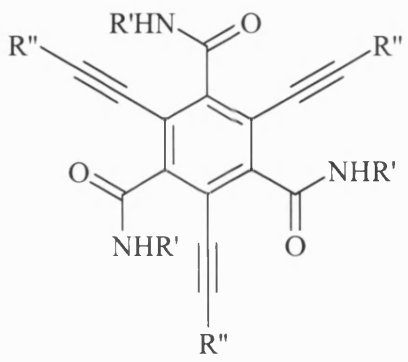

9 R' = 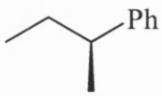 R" = $C_{10}H_{21}$

10 R' = $C_{12}H_{25}$ R" = Ph

Figure 1.36; structures of disk-shaped compounds ***11*** and ***12***

Nguyen suggests four different possibilities for the molecular arrangements of these compounds, as shown in Figure 1.37.

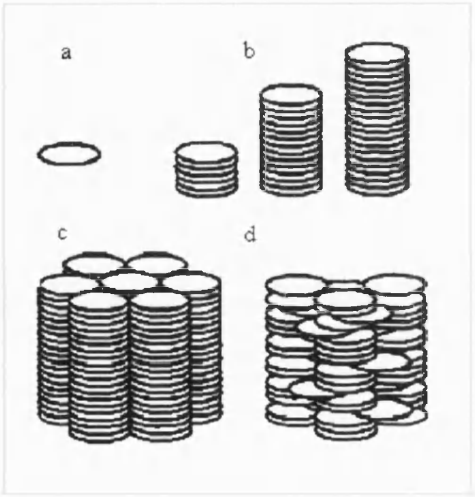

Figure 1.37; schematic representation of possible molecular arrangements: (**a**) monomer, (**b**) aggregates/fibres of different sizes, (**c**) a bundle of aggregates/fibres, (**d**) a complex ill-defined packing structure

The size of the group that flanks the amides determines the degree that the amide twists out of the ring-plane and therefore how far the π-systems are from their nearest neighbours in the stack.

Hannon and co-workers have assembled a nano-scale circular supramolecular array through π···π interactions between arc-shaped helicate units[71]. They have used metal-ligand and π···π interactions to achieve aggregation of metallo-supramolecular units into polymeric arrays. While probing the effects of modifications to the ligand backbone with a view to controlling the precise structural array formed, they chanced upon a method of controlling the way in which helicate units aggregate into discrete, rather than polymeric, arrays. The structure of

$[Cu_2(L)_2]^{2+}$ shows that each copper centre occupies a four-coordinate pseudo-tetrahedral environment bound to two pyridylimine units, one from each ligand. The arc-shaped helicates aggregate forming a cyclic array of four metallo-supramolecular units held together by π···π interactions, as shown in Figure 1.38.

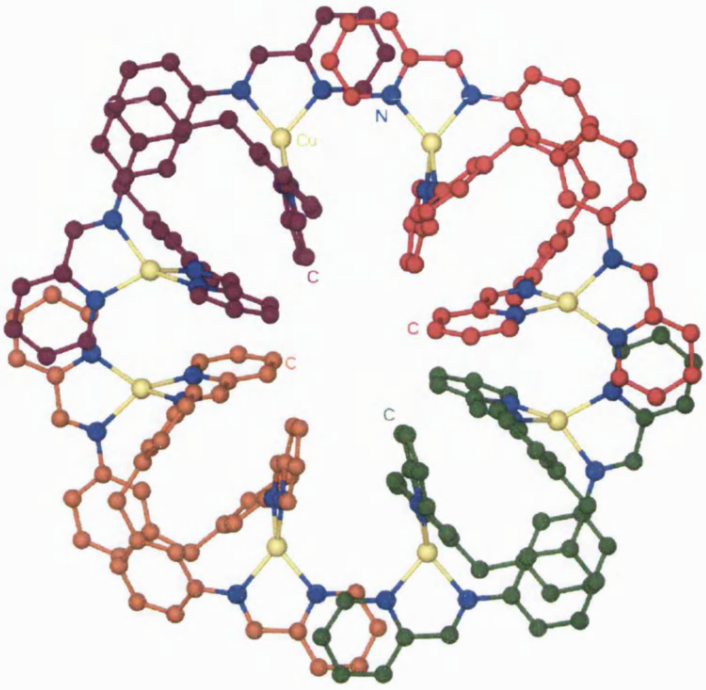

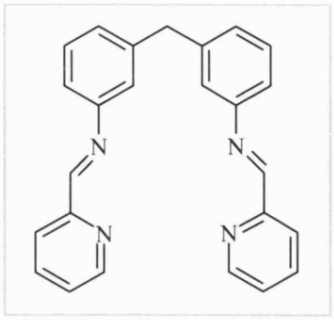

Figure 1.38; the cyclic array resulting from the aggregation of four $[Cu_2(L)_2]^{2+}$ helicates; each helicate is shown in a different colour
Inset: the structure of the ligand L

Dance and co-workers have reported the presence of π···π interactions between the phenyl rings of PPh_3 moieties[72], described as a phenyl embrace. Multiple phenyl embraces involve two or more phenyl groups of each molecule that engage in intermolecular edge-to-face and offset face-to-face interactions, often in concert, with an overall attraction. The most commonly occurring embrace is the six-fold phenyl embrace (6PE) where all six rings of two PPh_3 groups are involved in a concerted cycle of six attractive edge-to-face interactions, as shown in Figure 1.39. Where a PPh_3 group is bonded to a metal (M), the conformation of phenyl rings in M–PPh_3 influences the ability of the PPh_3 groups to engage in multiple phenyl embraces. In M–PPh_3 compounds the M–P–C angles average 115°, which is higher than the ideal tetrahedral angle of 109.5°. The three phenyl rings are therefore closed slightly, relative to $[PPh_4]^+$.

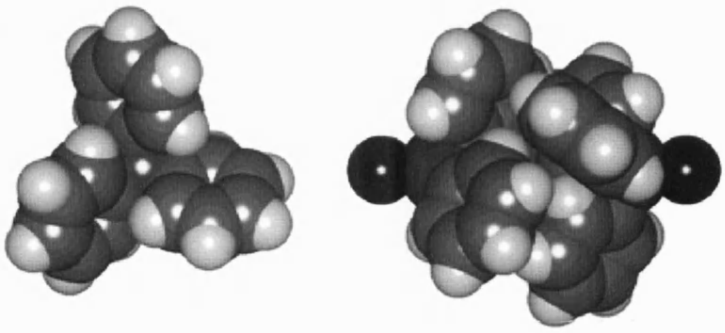

Figure 1.39; the ideal six-fold-phenyl embrace

In a four-fold phenyl embrace, there are four phenyl rings that interact via π···π interactions, the most common of which is the parallel four-fold embrace (P4FE) as shown in Figure 1.40. This embrace involves two edge-to-face interactions and can be accompanied by an offset face-to-face interaction.

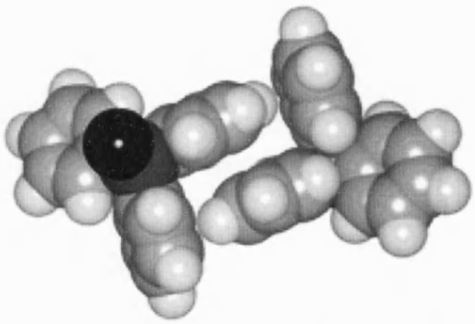

Figure 1.40; the parallel four-fold phenyl embrace

1.2.8 Polymorphism

It is possible for a compound to adopt more than one crystal structure under different conditions, for example different concentrations or temperatures of crystallisation. These structures are termed *polymorphs* and their existence is common[73]. If a crystal is seen as a giant supramolecule, polymorphs are the corresponding supramolecular isomers[74]. Polymorphs can differ in solid-state properties, such as melting point, colour, conductivity *etc.* This is particularly important for the pharmaceutical industry where two polymorphs of the same drug compound may have different physical properties, such as solubility, which can have a dramatic effect on the activity of the drug. However, McCrone's statement that

the number of polymorphs possible relates to the time spent looking for them[75] demonstrates that the task of identifying any polymorphs of a specific crystal structure can be troublesome. It is therefore of paramount importance to control crystallisation conditions to assure reproducibility.

Some researchers actively strive to identify routes to new polymorphs. Pulham *et al* have utilised high-pressure recrystallisation to form new polymorphs[76]. The basis for using high-pressure relies on the theory that the structure formed in the solid state is governed by inter-atomic and inter-molecular interactions. These interactions depend on distance and are therefore greatly affected by the application of pressure. Using this method, new polymorphs of simple compounds, such as phenanthrene (Figure 1.41), have been obtained.

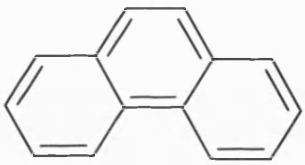

Figure 1.41; structure of phenanthrene

At ambient temperatures phenanthrene forms a regular herringbone structure. However, under high-pressure a higher density polymorph of this structure is observed, the packing in which is shown in Figure 1.42.

Figure 1.42; the structure of phenanthrene at high pressure
(*some layers have been removed for clarity*)

The crystal structure is dominated by the herringbone-type packing, which is commonly observed in planar aromatic compounds. A 12% increase in density is observed in the high-pressure polymorph indicative of more efficient packing of the molecules. The distance between the π-stacked parallel planes of molecules is substantially reduced in the high pressure polymorph, from 2.8 to 2.3Å respectively (the short distance) and from 4.4 to 3.5Å respectively (the longer distance).

1.2.9 Solvated structures

Co-crystallisation typically occurs via dissolving the chosen molecules independently in a suitable solvent, adding one to the other and waiting for crystals to form. However, these systems often crystallise with one or more solvent molecules in the asymmetric unit. Water can be trapped in the lattice from aqueous solvents or even by absorption from the atmosphere. In some cases the solvent molecules hold together an otherwise unstable crystal lattice and help remedy a donor/acceptor imbalance. In other cases, solvent molecules are incorporated to fill voids that would otherwise be present in the lattice.

Infantes *et al* have recently completed a detailed study of hydrated structures in the Cambridge Structural Database[77]. They have concluded that there is no clear answer to the question of when a hydrate may be observed, but they have found some patterns in the occurrence of hydrated structures. They find that the most frequently occurring hydrates are those compounds containing atoms or groups with ionic charge. Another major factor is the abundance of donor and acceptor groups and the balance between them. When the ratio of acceptor/donor groups is unbalanced, this ratio can be redressed by the incorporation of water molecules. It is also likely that due to the complete freedom and orientation of incorporated water molecules, a more ideal hydrogen-bonding geometry is favoured when the structure is hydrated.

Scott and co-workers have reported the structure of a cholic acid inclusion compound with acetone and water guest molecules that exhibits extensive hydrogen bonding[78] (Figure 1.43).

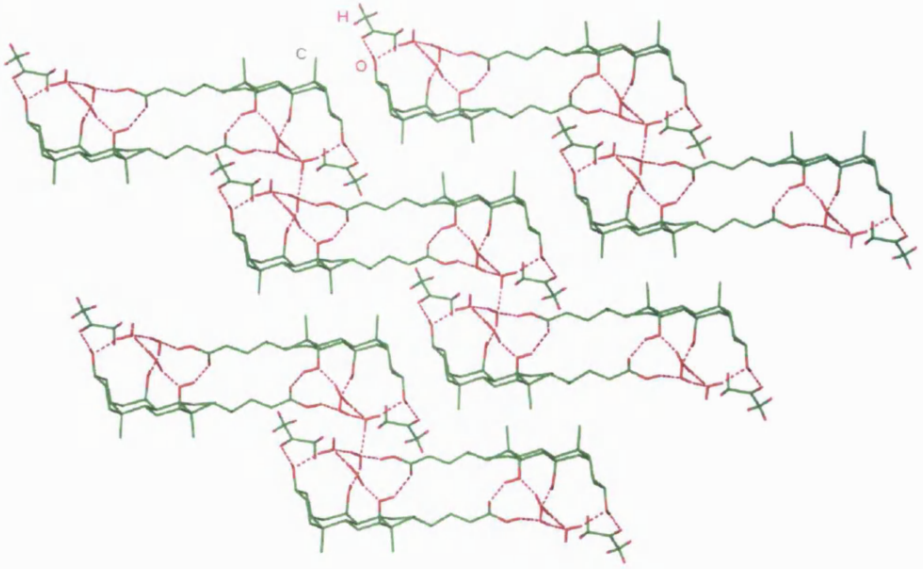

Figure 1.43; cholic acid crystallised with guest molecules of water and acetone

The hydroxy group acceptors of the host form hydrogen bonds with the acetone donor group and with molecules of water, which act as both donors and acceptors forming a bilayer structure.

1.3 Guanidinium-Sulfonate networks

Guanidinium sulfonates have attracted considerable interest as they form robust hydrogen bonded sheets, with the major contribution from Ward and co-workers[79,80,81]. The guanidinium and sulfonate ions interact with each other via pairs of DD:AA, $R_2^2(8)$ motif N–H···O hydrogen bonding forming ordered two-dimensional sheets. This is due to the equal number of hydrogen-bond donor and acceptor sites and a three-fold molecular topology common to both the cation and anion, as shown in Figure 1.44.

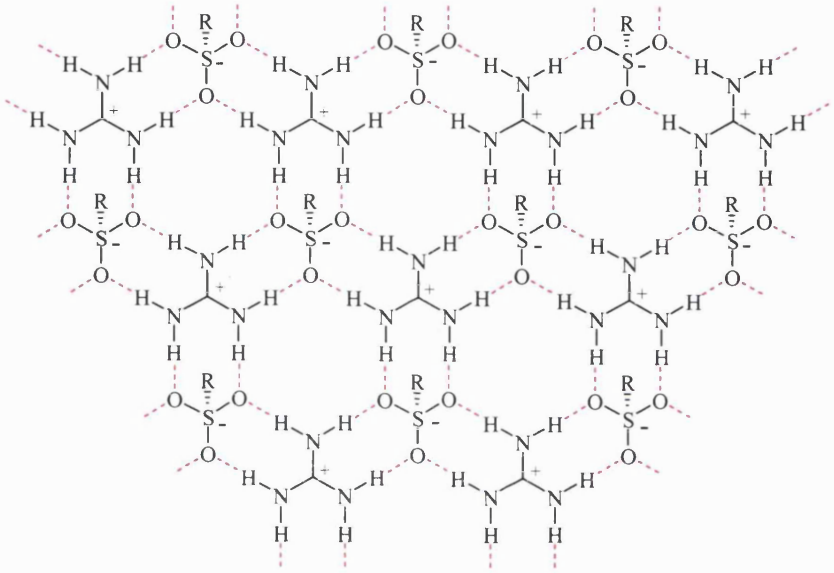

Figure 1.44; hexagonal GS sheet formed by hydrogen bonding linking guanidinium cations and sulfonate anions

Ward anticipated many applications for this type of compound as the strong intermolecular interactions in these networks favour the formation of low-density solids that would be potentially useful as host lattices. Robust supramolecular networks can reduce significantly the number of possible solid-state packing motifs, a key goal of crystal engineering[82]. Robust networks have been utilised in the design of zeolites and clays, often used to separate small molecules by size discrimination[83]. By using guanidinium sulfonate networks, all of the hydrogen bonding capacity is fulfilled which is important in forming robust networks[84]. Indeed, the guanidinium sulfonate network has been shown to be present in over 100 structures synthesised from a diverse variety of sulfonates. There is also the added benefit of the flexibility provided by the ready substitution of the sulfonate R group.

The integrity of the hydrogen-bonded network is attributed to the complementary hydrogen-bond donors and acceptors present, their similar sizes, which allows optimum hydrogen-bonding geometries, and the electrostatic interaction between the oppositely charged ions. The preservation of the hydrogen-bonded motif is also favoured by the absence of hydrogen-bonding sites on the sulfonate R groups that would otherwise compete for hydrogen-bonding sites on the guanidinium or sulfonate ions.

The guanidinium sulfonate hydrogen-bonded sheets can be thought of as assembling from one-dimensional cation-anion ribbons, in which the ribbons are connected into sheets by a hydrogen bonding 'hinge' parallel to the ribbon axes. In many guanidinium sulfonates the two-dimensional sheet is planar. In other examples the sheets are 'puckered' about the hinge resulting in corrugated sheets. The degree of corrugation can be described by the inter-ribbon angle[85] (θ_{IR}) as shown in Figure 1.45. This value describes the planarity of the hydrogen-bonded sheets, an ideally planar sheet having θ_{IR} of 180°.

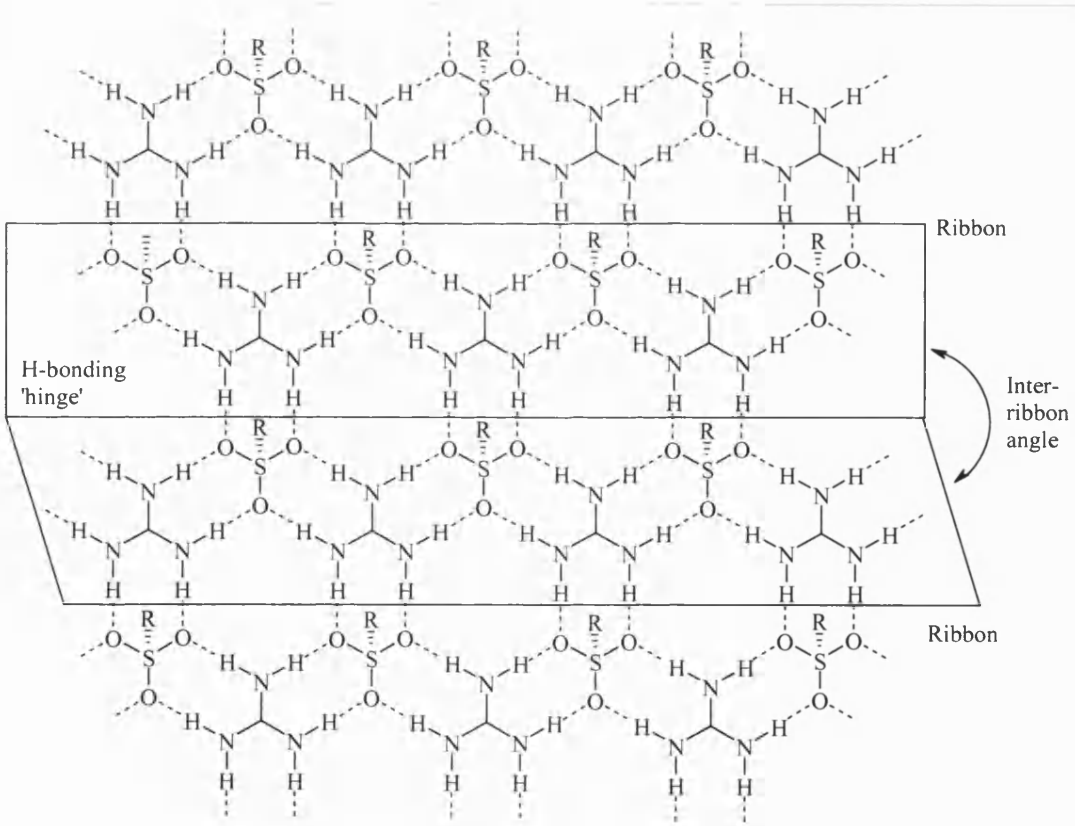

Figure 1.45; the inter-ribbon angle θ_{IR} in guanidinium sulfonate sheets

The two-dimensional sheet is controlled by the hydrogen-bonding interactions between the cations and anions. The hydrogen-bonded networks are able to incorporate a number of different sulfonate substituents while retaining the guanidinium sulfonate sheets. This is due to the different stacking motifs that can be formed and the softness of the sheets, which are able to corrugate, decreasing θ_{IR}, to minimise void space in the structure. However, assembly into the third dimension is influenced by the sulfonate group R. The factors that determine this third-dimensional assembly include steric constraints for the bulky R groups as well as favourable inter-layer interactions, such as van der Waals and $\pi\cdots\pi$ interactions[80].

Open molecular frameworks are often not stable by themselves, as the non-covalent forces holding them together are relatively weak when compared to covalent bonding, therefore favouring conversion to more dense phases[86]. The molecules in a network assemble in a way that minimises void space as dense packing balances the attractive and repulsive forces. Therefore, the arrangement that requires the least space is likely to be the one that minimises the total energy of all the forces among the molecules[87]. Inclusion of 'guest' molecules in the voids of an array can stabilise open frameworks, where the molecular framework can be described as a 'host'. Low-density networks can also be stabilised by interpenetration of one or more crystallographically identical networks.

The guanidinium-sulfonate structures reported by Ward *et al* that are relevant to the continued work included in this thesis are shown in Table 1.2.

Guanidinium sulfonate	**Abbreviation**
Guanidinium 1-naphthalenesulfonate	[Gu][1-NapSO_3]
Guanidinium 2-naphthalenesulfonate	[Gu][2-NapSO_3]
Guanidinium 10-camphorsulfonate	[Gu][10-CamphorSO_3]
Guanidinium methanesulfonate	[Gu][MeSO_3]
Guanidinium benzenesulfonate	[Gu][PhSO_3]
Guanidinium 1,5-naphthalenedisulfonate	$[Gu]_2$[1,5-Nap$(SO_3)_2$]
Guanidinium 2,6-naphthalenedisulfonate	$[Gu]_2$[2,6-Nap$(SO_3)_2$]

Table 1.2; guanidinium sulfonates reported by Ward *et al* that are specifically relevant to the work completed in this thesis

1.3.1 Guanidinium Monosulfonates

There are two main structural types observed - bilayers and single layers - and the one that is formed is dictated by the steric requirements of the R groups[84]. In the bilayer structure the sulfonate R groups of each sheet are directed to the same side, with interpenetrating R groups within the bilayer directed towards each other (shown in Figure 1.46a). In the single layer structure the sulfonate R groups within a ribbon are located on one side of each ribbon but alternate sides on neighbouring ribbons and are hence directed to both sides of the sheet (shown in Figure 1.46b). Both these structures result in partitioning of the gross structure into hydrophobic regions containing the R groups and polar regions containing the guanidinium sulfonate hydrogen-bonded sheet. In all cases the R groups inter-digitate to maximise the favourable van der Waals contacts and to minimise void space in the lattice[80].

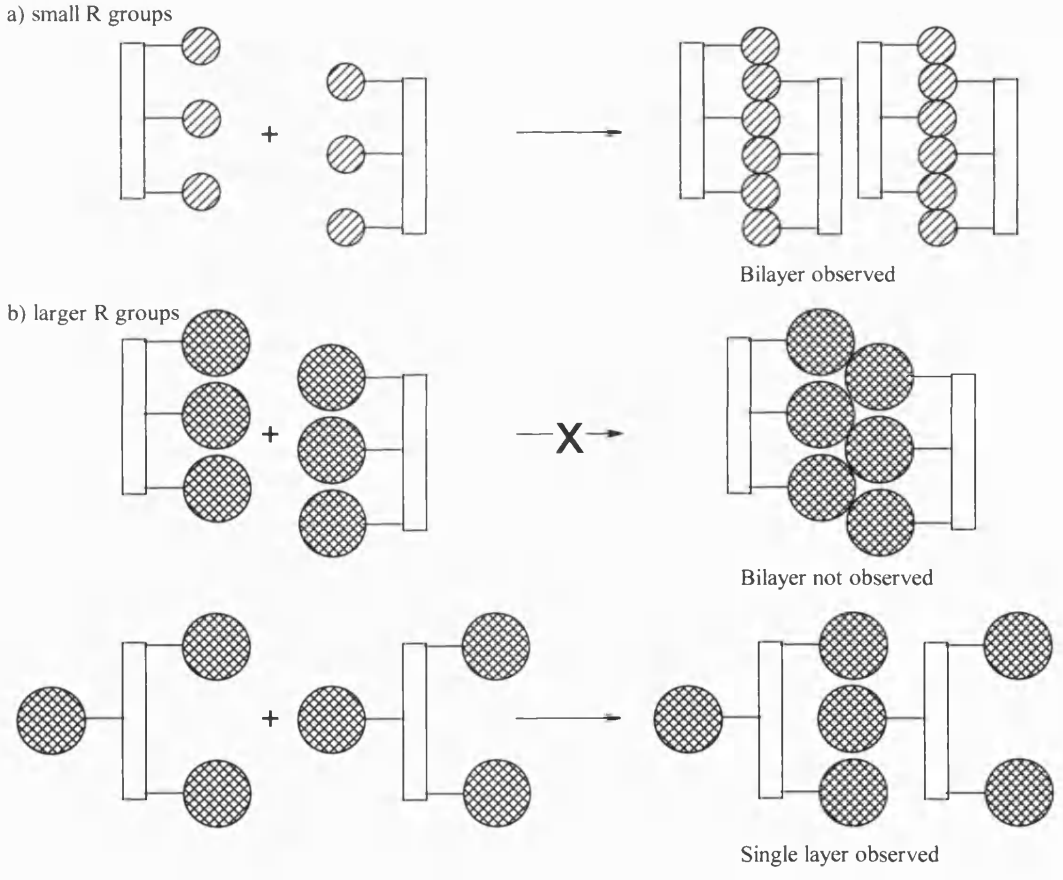

Figure 1.46; the different types of layer structure observed in guanidinium monosulfonate structures

Bilayer structures are favoured for small R groups such as methyl or phenyl, as shown in Figure 1.47, as the low density of hydrocarbon content allows for inter-digitation of the layers. The hydrogen-bonded sheets can distort from planarity to relieve steric crowding or to accommodate closer packing of the R groups.

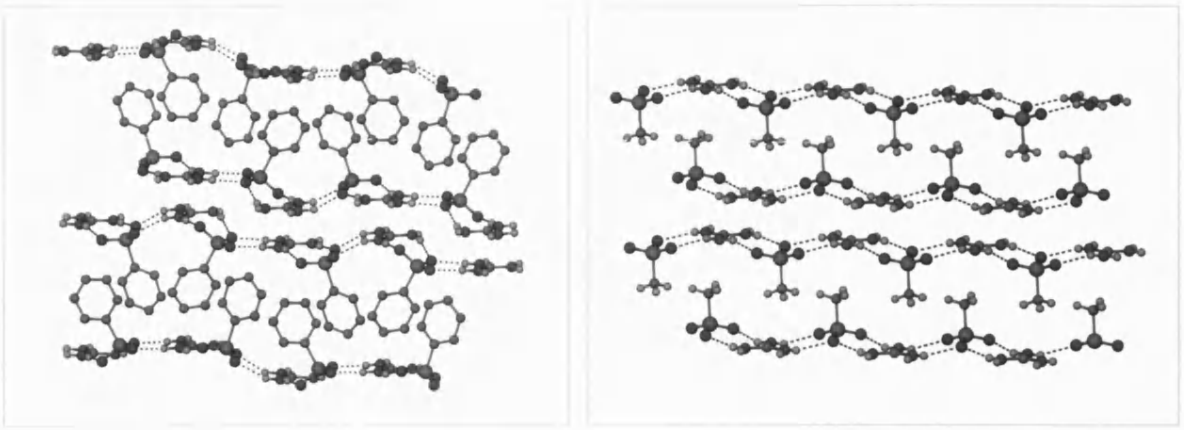

Figure 1.47; the bilayer formation observed in [Gu][$PhSO_3$] (left) and [Gu][$MeSO_3$] (right)

As the R groups become larger, there can be a difficulty in predicting which type of structure will be observed. The crystal structure of [Gu][2-$NapSO_3$] reveals bilayer formation with inter-digitating naphthalene groups, as shown in Figure 1.48a. However, the crystal structure of [Gu][1-$NapSO_3$] does not form bilayers, even though only a small modification has been made to the sulfonate. Instead, single layers are observed, as shown in Figure 1.48b.

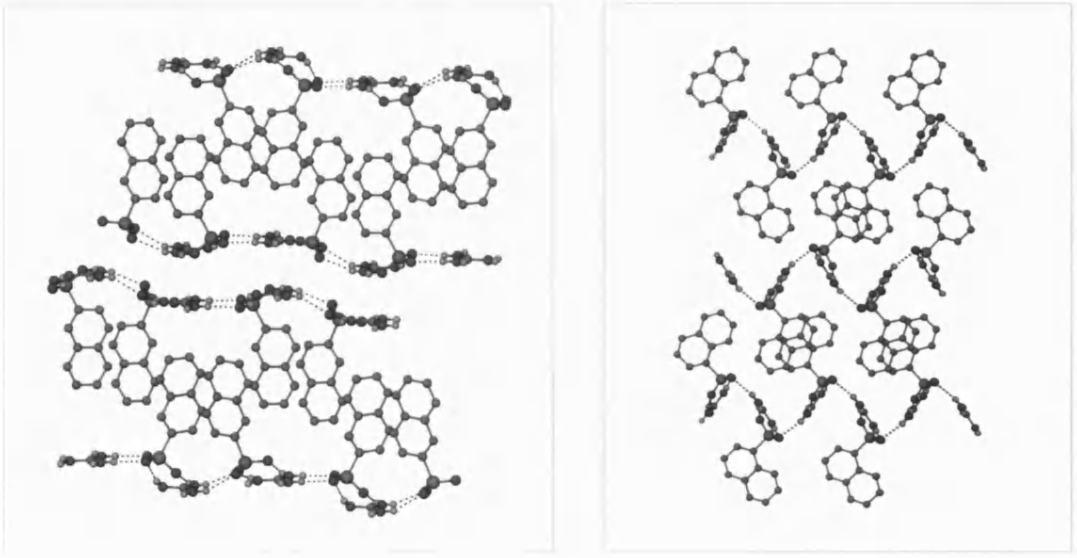

Figure 1.48; **a**) bilayer formation observed in [Gu][2-NapSO3] (left) and **b**) single later structure observed in [Gu][1-NapSO3] (right)

In compounds with larger R groups (groups wider than the ion centre-to-centre distance of 4.75Å) orientation of these R groups to the same side of each hydrogen-bonded sheet is still permitted on the basis of steric considerations. However, the R groups residing on the hydrogen-bonded sheet would be very close packed thus reducing the van der Waals contacts between the R groups of two approaching sheets. This means that interpenetration of R groups from different sheets would not be possible without severe disruption of the hydrogen-bonded motif. Therefore in these cases, hydrogen-bonded sheets where the R groups are directed to both sides of the sheet lead to single layer formation. This arrangement permits inter-digitation of R groups, which maximises van der Waals forces between sulfonate R groups[80].

Sheet formation in bilayer and in single layer structures is different. In bilayer structures the sheets are approximately coplanar (θ_{IR} approaching 180°), whereas in the single layer structures there can be distortion of the hydrogen-bonded sheets from planarity. Therefore the structures observed reflect a balance between hydrogen-bonding forces associated with the guanidinium-sulfonate sheet and the van der Waals forces between sulfonate R groups.

1.3.2 Guanidinium Disulfonates

When guanidinium cations are crystallised with disulfonate anions, pillared structures with parallel two-dimensional hydrogen-bonding sheets are formed when the sulfonate groups are located at opposite ends of the anion. Here the sulfonate acts as a pillar linking two hydrogen-bonded sheets. The formation of voids in the structure is observed with sizes, heights, shapes and chemical environments that can be manipulated by the choice of molecular pillar. The same two main structures observed with monosulfonates are also observed when employing disulfonates: the pillared bilayer and the pillared brick continuous single layer. Representations of both these structures are shown in Figure 1.49 and each one has one-dimensional channels between the linked hydrogen-bonded sheets, which can be occupied with guest molecules[83]. The size and shape of these channels can also be tailored by the choice of molecular pillar[88].

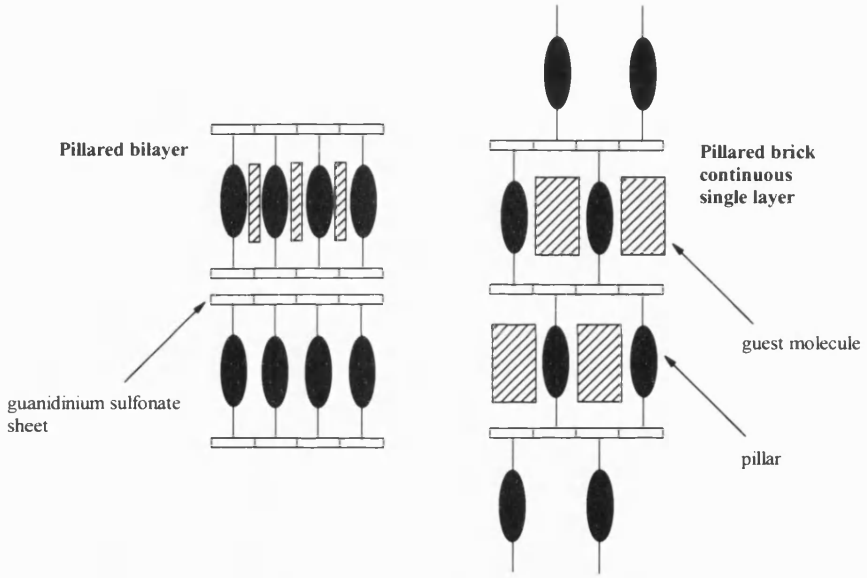

Figure 1.49; the stacking motifs observed in guanidinium disulfonate structures

Small guests favour a bilayer motif whereas large guests favour a continuous single-layer 'pillared brick' stacking motif. Large pillars favour single layer pillared brick motifs with small guests or can even exclude guest molecules[87]. The single layer pillared brick motif can also be induced by the incorporation of guest molecules that are identical to the sulfonate substituent, as shown in Figure 1.50a. Many guanidinium-disulfonate assemblies have been studied and the results show that it is the combined steric requirements of the pillars and guests that govern which framework is adopted. Therefore, the host architecture of these materials can be rationally manipulated by systematic, stepwise changes in the size of the host and guest components[85].

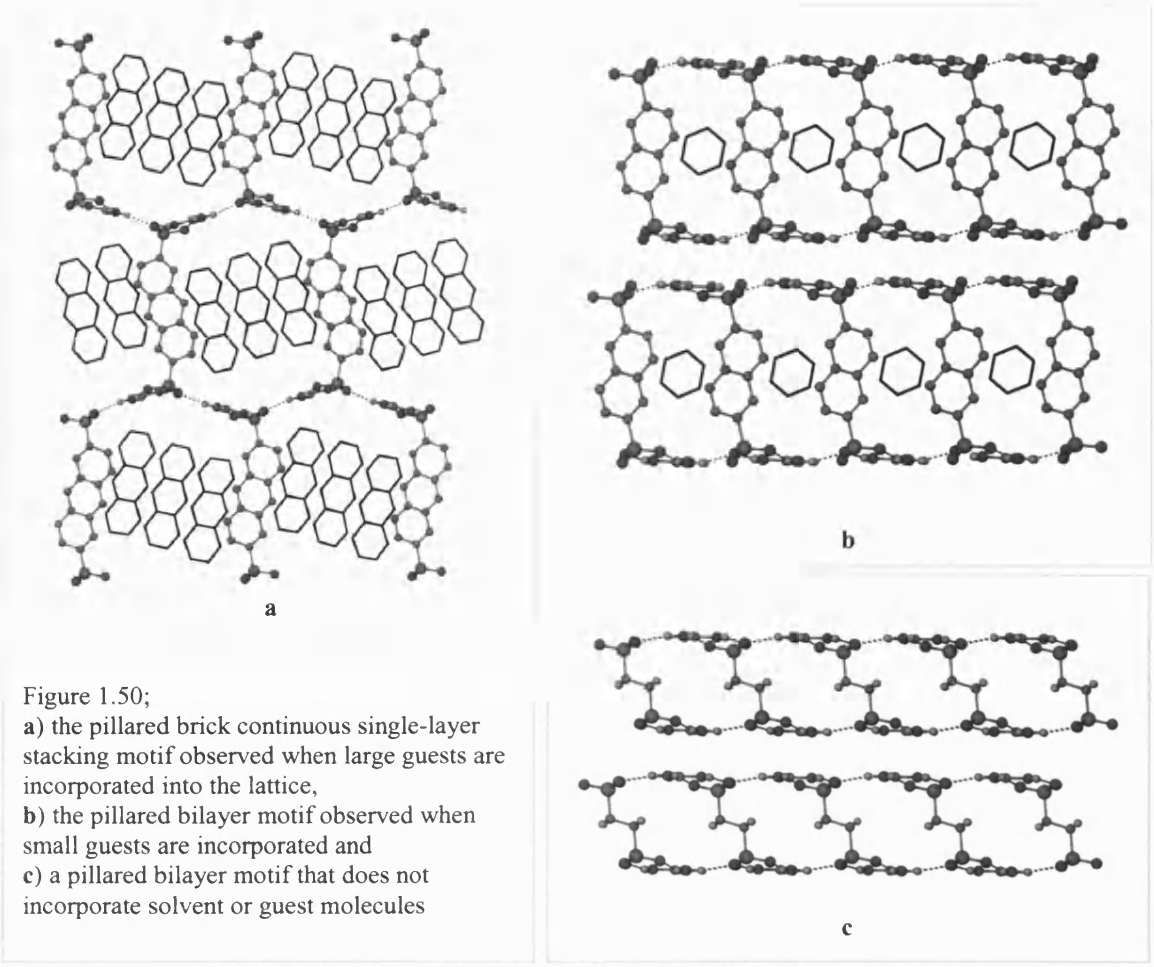

Figure 1.50;
a) the pillared brick continuous single-layer stacking motif observed when large guests are incorporated into the lattice,
b) the pillared bilayer motif observed when small guests are incorporated and
c) a pillared bilayer motif that does not incorporate solvent or guest molecules

However, as seen in the guanidinium monosulfonate examples, it can be difficult to predict which packing motif will be formed. The structures of 2,6-naphthalenedisulfonate and 4,4-biphenyldisulfonate are similar, as shown in Figure 1.51.

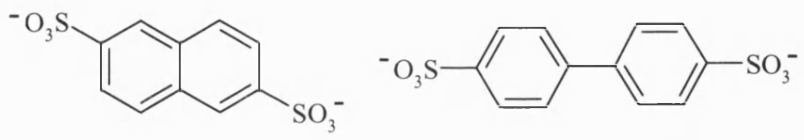

Figure 1.51; structures of 2,6-naphthalenedisulfonate (left) and 4,4-biphenyldisulfonate (right)

When the sodium salt of 2,6-naphthalenedisulfonate is crystallised with guanidinium cations in the presence of naphthalene, the pillared continuous single-layer structure is observed, as shown in Figure 1.52a. However, when the same crystallisation is carried out using 4,4-biphenyldisulfonate in place of 2,6-naphthalenedisulfonate the stacking pillared bilayer structure is observed, as shown in Figure 1.52b.

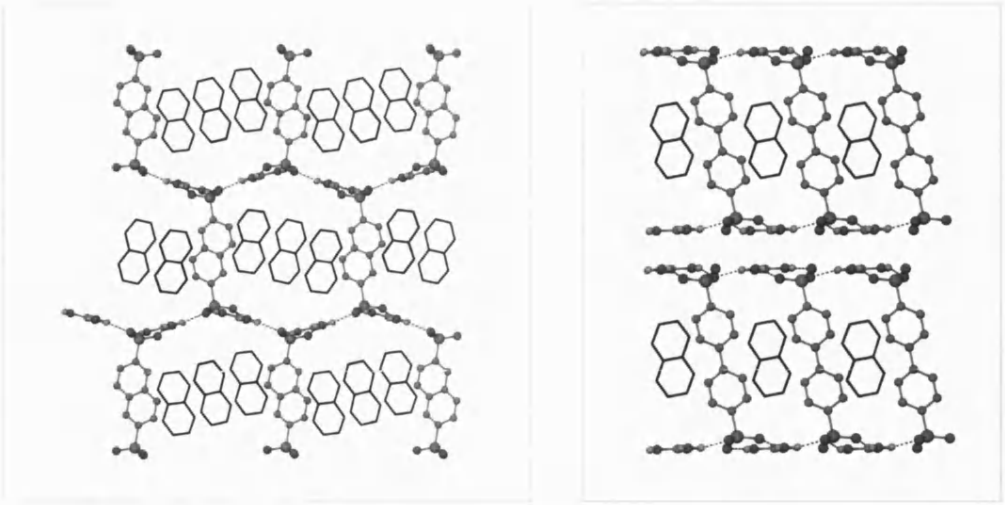

Figure 1.52; a) the pillared continuous single-layer structure of [Gu][2,6-naphthalenedisulfonate] (left) and b) the continuous single-layer structure of [Gu][4,4-biphenyldisulfonate] (right) both incorporating naphthalene guest molecules

In some cases when guanidinium disulfonates are crystallised with guests incorporated into the lattice, a 'shifted' guanidinium sulfonate sheet is observed, as shown in Figure 1.53 [89].

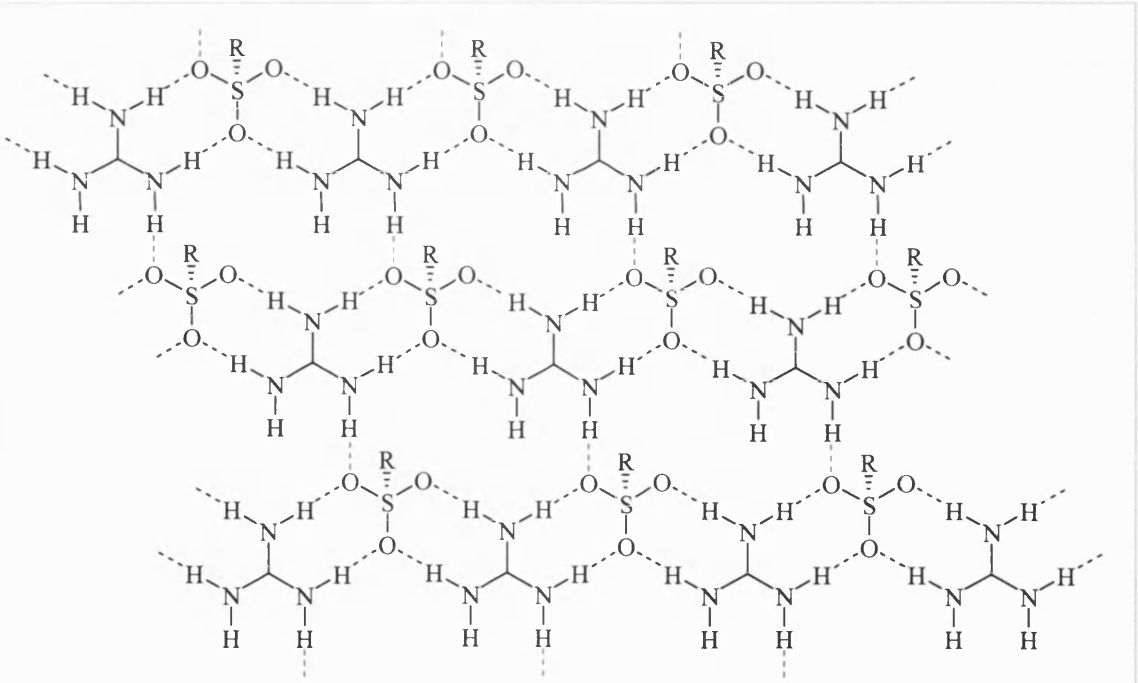

Figure 1.53; shifted guanidinium sulfonate sheet observed in some guanidinium disulfonates.

The DD:AA ribbons are linked into sheets by a single N–H···O hydrogen bond, in place of the DD:AA $R_2^2(8)$ motif observed between ribbons to form the hexagonal guanidinium sulfonate sheet.

The two crystal structures of $[Gu]_2[2,6\text{-}Nap(SO_3)_2]$ with naphthalene ***11*** and benzene ***12*** incorporated as guests reveal these two different sheet structures as well as different three-dimensional arrays. ***11*** forms the pillared brick continuous single-layer structure, where hexagonal hydrogen-bonded guanidinium sheets are observed. The pillars in ***11*** are rotated so that the arene planes (of the $2,6\text{-}Nap(SO_3)_2$) lie parallel to the DD:AA ribbons, as shown in Figure 1.54. However, ***12*** forms the pillared bilayer structure and the shifted guanidinium sulfonate sheets are observed. The pillars in ***12*** are rotated with the arene planes (of the $2,6\text{-}Nap(SO_3)_2$) nearly orthogonal to the DD:AA ribbons, as shown in Figure 1.55. In both hexagonal and shifted guanidinium sheet structures the pillars can rotate about the C-S bond allowing the different conformations of the pillar with respect to the DD:AA ribbons of the different sheets.

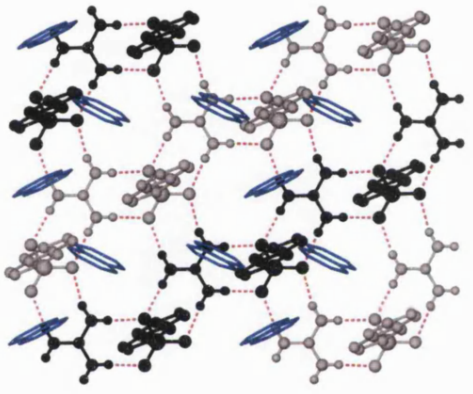

Figure 1.54; hexagonal sheet in ***11*** showing the arene groups of the sulfonate rotated parallel to the ribbons. Guest molecules are shown in blue.

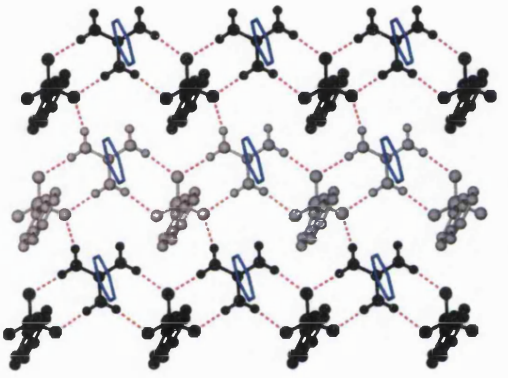

Figure 1.55; shifted sheet in ***12*** showing arene groups of the sulfonate rotated orthogonal to the ribbons. Guest molecules are shown in blue.

1.4 Incorporation of metals into guanidinium sulfonate networks

In order to incorporate metal centres into the guanidinium sulfonate arrays, Harrington[90] utilised the triphenylphosphine monosulfonate [mTPPMS]$^-$, [$PPh_2C_6H_4$-3-SO_3]$^-$, along with its derivatives; [AuCl(mTPPMS)]$^-$, [S(mTPPMS)]$^-$ and [Se(mTPPMS)]$^-$. These sulfonates were crystallised with guanidinium [Gu] and the crystal structures determined. In [Gu][mTPPMS] (***13***) the hexagonal hydrogen bonded two-dimensional array is formed despite the bulky group being incorporated into the sulfonate (Figure 1.56a). The sheet is corrugated, as shown in Figure 1.56b, with θ_{IR} of 103°, which minimises void space in the array. The mTPPMS groups are directed to both sides of this sheet forming a continuous inter-digitated single layer structure, with neighbouring mTPPMS groups interacting via a six-fold phenyl embrace. There are also C–H···O hydrogen bonds present between the phenyl rings (directed towards the anion) and the sulfonate oxygen acceptors.

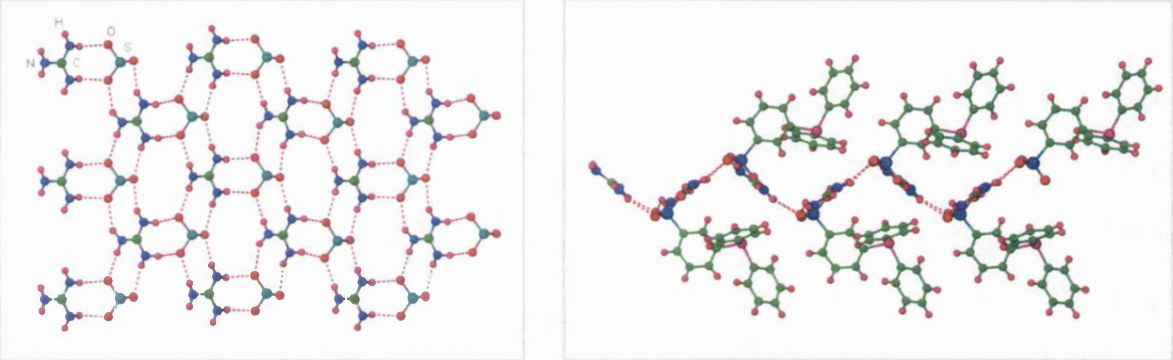

Figure 1.56 a) the hexagonal hydrogen bonded sheet observed in [Gu][mTPPMS] (left) and b) the side view showing the corrugation present (right)

The gold complex [Gu][AuCl(mTPPMS)] (***14***) also forms hexagonal sheets, as shown in Figure 1.57a. However, in contrast to ***13*** these are relatively flat, with θ_{IR} of 161°, as shown in Figure 1.57b. The sheet has been flattened due to the presence of AuCl bonded to the phosphine. As seen in ***13*** the (AuCl(mTPPMS)) groups are directed to both sides of this sheet forming a continuous inter-digitated single layer structure. The incorporation of AuCl into the sulfonate leads to a pseudo-six-fold phenyl embrace linking AuCl(PPh_3) units into chains that run perpendicular to the hydrogen bonded ribbons. These pseudo-phenyl embraces form between three phenyl rings of one anion and two phenyl rings and the AuCl group on the other, with the AuCl group acting in a similar manner to a phenyl ring. It should also be noted that although Au···Au interactions have been employed in hydrogen-bonded networks, these interactions are not observed in this structure.

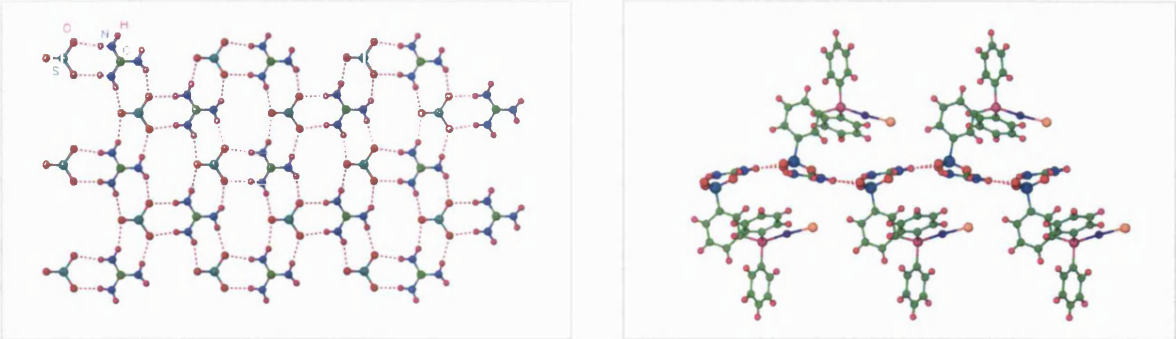

Figure 1.57 a) the hexagonal hydrogen bonded sheet observed in [Gu][AuCl(mTPPMS)] (left) and b) the side view showing the corrugation observed (right)

The compounds [Gu][S(mTPPMS)] (***15***) and [Gu][Se(mTPPMS)] (***16***) are essentially isostructural. Guanidinium sulfonate sheets are observed in ***15*** and ***16*** with the bulky groups of the sulfonate directed to both sides of the sheets, forming a continuous single-layer structure with inter-digitating sulfonate groups. Both ***15*** and ***16*** are disordered with respect to the sulfonate oxygen and the guanidinium cation positions. Guanidinium sulfonate sheets are observed in both structures, however these are not the regular hexagonal structure but are disordered, as shown in Figure 1.58a. It is not possible to accurately determine the inter-ribbon angle in ***15*** and ***16*** due to the disorder, however estimated values are 150° and 153° respectively. As seen in ***14***, there are pseudo-six-fold phenyl embrace interactions observed in ***15*** and ***16*** involving three phenyl rings of one anion and two phenyl rings of the S or Se group respectively. In addition to these interactions, each $S(PPh_3)$ or $Se(PPh_3)$ unit forms a second pseudo-six-fold phenyl embrace, approximately perpendicular to the first. These interactions between anions dictate the positions of the sulfonate groups in ***15*** and ***16***. The sulfonates are forced too close together to form regular hexagonal hydrogen bonded sheets, hence the disordered sheets are observed.

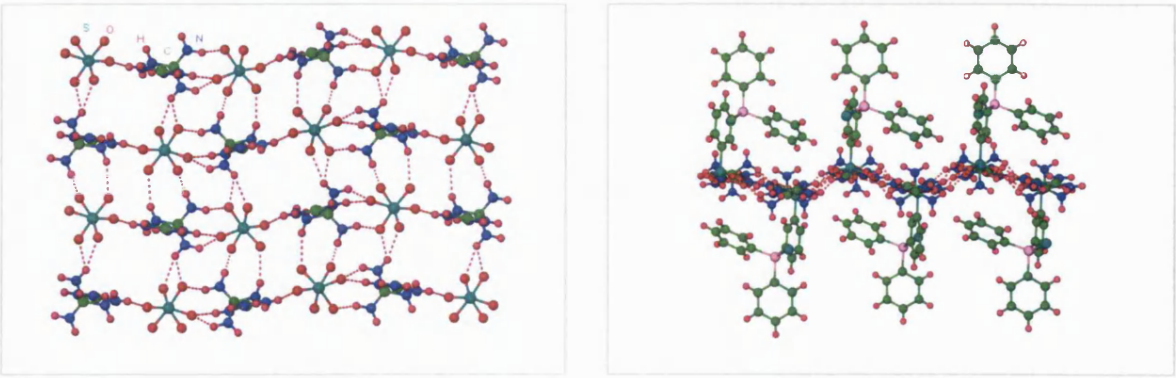

Figure 1.58 a) the disordered hydrogen bonded sheet observed in [Gu][S(mTPPMS)] (left) and b) the side view (right)

1.5 Aims and objectives of this thesis

It has been demonstrated that guanidinium sulfonate compounds form solid state structures based on hydrogen bonded layers. Each cation is linked to three anions (and *vice versa*) by two hydrogen bonds via the $R_2^2(8)$ hydrogen bonded motif that generally leads to hexagonal arrays.

All structures incorporating GS arrays reported to date have utilised the guanidinium cation $[C(NH_2)_3]^+$. Thus, to examine the robustness of the GS arrays, methylguanidinium $[C(NH_2)_2(NHMe)]^+$, ethylguanidinium $[C(NH_2)_2(NHEt)]^+$ and dimethylguanidinium $[C(NH_2)_2(NMe_2)]^+$ cations were crystallised with a variety of mono- and disulfonates. The substituted cations vary in the number and location of hydrogen bond donors, perhaps reducing the possibility of forming the GS sheet. Steric effects of the sulfonate alkyl groups on the hydrogen-bonded array formed were also investigated. The use of sulfonates with competing hydrogen bond donors was also examined, for example Na[mTPPMSO] $Na[OPPh_2(C_6H_4\text{-}3\text{-}SO_3)]$ to see how the presence of a competing hydrogen-bonding site affects the formation of GS arrays. The results are reported herein, along with comparisons to analogous structures based on the unsubstituted guanidinium cation.

Moreover, most of the GS structures reported to date have been completely organic, however the use of sulfonates incorporating inorganic moieties provides a simple method of introducing metal atoms into these arrays. Such an ideal ligand is a sulfonated phosphine, as co-ordinatively unsaturated metal centres are stabilised by π-acceptor ligands. These compounds have received a great deal of attention due to their ability to solubilise organometallic compounds in water. A obvious example is that of Na[mTPPMS], $Na[PPh_2(C_6H_4\text{-}3\text{-}SO_3)]$ as the chemistry of this compound is well known. The incorporation of metallated-mTPPMS into GS arrays has already been probed by Burrows *et al* and results show that hydrogen bonded arrays are observed. The successful incorporation of unsaturated metal centres into guanidinium sulfonate arrays would lead to the potential for reversible co-ordination of small molecules, either by coordinative or oxidative addition. Therefore the compound $Na_2[IrCl(CO)(mTPPMS)_2]$ was prepared and crystallised with the substituted and unsubstituted guanidinium cations. The resulting compounds were then be exposed to reagents such as SO_2 and CO to ascertain if these molecules can be reversible coordinated to the metal.

The incorporation of dye sulfonates into GS networks has been investigated. These dyes in the solid state are sensitive to pH conditions. Therefore the aim was to form hydrogen-bonded crystalline solids with the guanidinium and substituted guanidinium cations and then to ascertain whether the same solid state transitions could take place when the pH environment is altered, while retaining the crystalline state. To this end, the guanidinium and substituted guanidinium cations were crystallised with the sodium salts of methyl orange $Na[O_3SC_6H_4N{=}NC_6H_4NMe_2]$, ethyl orange $Na[O_3SC_6H_4N{=}NC_6H_4NEt_2]$ and 4-aminoazobenzene-4'-sulfonate $Na[O_3SC_6H_4N{=}NC_6H_4NH_2]$ (which also contains a competing hydrogen bonding site via the amine group). The resulting crystalline solids were exposed to cycles of acidic and basic conditions, and the results studied using single crystal X-ray crystallography and X-ray powder diffraction are reported herein.

1.6 References

[1] G. R. Desiraju, *Crystal Engineering. The design of Organic Solids,* Materials Science Monographs 54, Elsevier, Amsterdam, 1989.

[2] G. M. Schmidt, *J. Pure Appl. Chem.,* 1971, 27, 647

[3] *J. Chem. Soc., Dalton Trans.,* 2000, 3705. Entire issue devoted to Dalton Discussions 3: Inorganic Crystal Engineering; D. Braga, F. Grepioni, *Acc. Chem. Res.,* 2000, 33, 601; D. Braga, *Chem. Commun.,* 2003, 2751; L. Brammer, J. C. M. Rivas, R. Atencio, S. Fang, F. C. Pigge, *J. Chem. Soc., Dalton Trans.,* 2000, 3855; C. B. Aakeröy, A. M. Beatty, in *Comprehensive Coordination Chemistry-II: From Biology to Nanotechnology,* Vol. 1, ed. J. A. McCleverty and T. J. Meyer, vol. Ed. A. B. P. Lever, Elsevier, Amsterdam, 2003, 679; T. J. Burchell, D. J. Eisler, R. J. Pudephett, *Chem. Commun.,* 2004, 944 and references therein.

[4] N. J. Burke, A. D. Burrows, A. S. Donovan, R. W. Harrington, M. F. Mahon, C. E. Price, *Dalton Trans.,* 2003, 3840

[5] G. R. Desiraju, *Acc. Chem. Res.,* 2002, 35, 565

[6] T.-J. M. Luo, G. T. R. Palmore, *J. Phys. Org. Chem.,* 2000, 13, 870

[7] D. J. Duchamp, R. E. Marsh, *Acta. Cryst. B.,* 1969, 25, 5

[8] D. S. Reddy, B. S. Goud, K. Panneerselvam, G. R. Desiraju, *J. Chem. Soc., Chem. Commun.,* 1993, 663

[9] A. D. Burrows, *Structure and Bonding,*2004, 108, 55

[10] S. Bordiga, I. Roggiero, P. Ugliengo, *J. Chem. Soc., Dalton Trans.,* 2000, 3921

[11] A. Caneshi, D. Gatteschi, *J. Chem. Soc., Dalton Trans.,* 2000, 3907

[12] P. Zhu, H. Kang, A. Facchetti, G. Evmenenko, P. Dutta, T. J. Marks, *J. Am. Chem. Soc.,* 2003, 125, 11496

[13] W. B. Lin, L. Ma, O. R. Evans, *Chem. Comm.,* 2000, 22, 2263; O. R. Evans, R. G. Xiong, Z. Wang, G. K. Wong, W. Lin, *Angew. Chem. Int.,* 1999, 38, 536

[14] J. Tao, M. L. Tong, J. X. Shi, X. M. Chen, S. W. Ng, *Chem. Comm.,* 2000, 2043

[15] H. Li, M. Eddaoudi, T. L. Groy, O. Yaghi, *J. Am. Chem. Soc.,* 1998, 120, 8571

[16] S. R. Forest, *Chem. Rev.,* 1997, 97, 1793

[17] *Thin-Film Transistors,* ed. C. R. Kagan and A. Paul, Marcel Dekker, Inc., New York, 2003

[18] A. J. Blake, N. R. Champness, P. Hubberstey, W. S. Li, M. Withersby, M. Schroder, *Coord. Chem. Rev.,* 1999, 117

[19] I.G Dance, *Perspectives in Supramolecular Chemistry: The Crystal as a Supramolecular Entity,* ed G. R. Desiraju, Wiely, Chichester, 1996, vol. 2

[20] A. Gavezzotti, *Acc. Chem. Res.,* 1994, 27, 309

[21] K. T. Holman, A. M. Pivovar, M. D. Ward, *Science,* 2001, 294, 1907

[22] S. Bourne, Z. Mangombo, *CrystEngComm,* 2004, 6, 437

[23] J. Steed, J. Atwood, *Supramolecular Chemistry,* Wiley, 2000

[24] P. Carter, M. Ward, *J. Am. Chem. Soc.,* 1993, 115, 11521

[25] J. Steed, J. Atwood, *Supramolecular Chemistry,* Wiley, 2000

[26] J.–M. Lehn, *Supramolecular Chemistry: Concepts and perspectives*, VCH, Weinheim, 1995

[27] M. T. Kirchner, R. Boese, A. Gehrke, D. Bläser, *CrystEngComm,* 2004, 6, 1

[28] G. R. Desiraju, *Chem. Commun.,* 1997, 1475

[29] P. Ball, *Nature*, 1996, 381, 648

[30] J. Aizenberg, G. Lambert, S. Weiner, L. Addadi, *J. Am. Chem. Soc.,* 2002, 124, 32

[31] D. Braga, *Chem. Commun.,* 2003, 2751, focus article

[32] R. Kuroda, K. Higashiguchi, S. Hasebe, Y. Imai, *CrystEngComm,* 2004, 6, 463

[33] L. Pauling, *J. Am. Chem. Soc.,* 1935, 57, 2680

[34] L. Pauling, *The nature of the chemical bond,* Cornell University Press, Ithaca, New York, 1939

[35] G. C. Pimentel, A. L. McClellan, *The hydrogen bond.* W. H. Freeman, San Francisco, 1960

[36] J. P. Glusker, M. Lewis, M. Rossi, *Crystal structure analysis for chemists and biologists.* VCH, New York, 1994

[37] G. R. Desiraju, T. Steiner, *The Weak Hydrogen Bond,* Oxford University Press, 1999

[38] G. A. Jeffrey, W. Saenger, *Hydrogen bonding in biological structures.* Springer-Verlag, Berlin, 1991

[39] G. A. Jeffrey, *An introduction to hydrogen bonding,* Oxford University Press, New York, 1997

[40] G. R. Desiraju, *Chem. Commun.,* 1997, 1475

[41] P. D. Beer, P. A. Gale, D. K. Smith, *Supramolecular Chemistry,* Oxford University Press, 1999

[42] M. Etter, *J. Physical. Chem.* 1991, 95, 4601

[43] P. Raithby, F. Allen, W. Motherwell, G. Shields, R. Taylor, *New J. Chem.,* 1999, 25

[44] D. J. Duchamp, R. E. Marsh, *Acta. Cryst. B,* 1969, 25, 5

[45] S. R. Batten, R. Robson, *Angew, Chem, Int, Ed.,* 1998, 37, 1460

[46] F. G.-Tellado, S. Geib, S. Goswami, A. Hamilton, *J. Am. Chem. Soc.,*1991, 113, 9265

[47] J. A. Zerkowski, C. T. Seto, D. A. Wierda, G. M. Whitesides, *J. Am. Chem. Soc.,* 1990, 112, 9025; J. A. Zerkowski, C. T. Seto, G. M. Whitesides, *J. Am. Chem. Soc.,* 1992, 114, 5473; J. A. Zerkowski, C. T. Seto, D. A. Wierda, G. M. Whitesides, *J. Am. Chem. Soc.,* 1994, 116, 2382; J. A. Zerkowski, G. M. Whitesides, *J. Am. Chem. Soc.,* 1994, 116, 4298; J. A. Zerkowski, J. P. Mathias G. M. Whitesides, *J. Am. Chem. Soc.,* 1994, 116, 4305

[48] J.-M. Lehn, M. Mascal, A. DeCian, J. Fischer, *Chem. Soc. Perkin Trans.2,* 1992, 461

[49] A. Ballabh, D. Trivedi, P. Dastidar, E. Suresh, *CrystEngComm,* 2002, 4(24), 135

[50] A. Zafar, R. Melendez, S. Geib, A. Hamilton, *Tetrahedron,* 2002, 58, 683

[51] J.-G. Mao, Z. Wang, A. Clearfield, *Inorg. Chem.,* 2002, 41, 3713

[52] S. Kim, R. Bishop, D. C. Craig, I. G. Dance, M. L. Scudder, *J. Org. Chem.* 2002, *67*, 3221

[53] E. J. Maclean, K. D. M. Harris, B. M. Kariuki, S. J. Kitchin, R. R. Tykwinski, I. P. Swainson, J. D. Dunitz, *J. Am. Chem. Soc.*, 2003, 125, 14449

[54] M. Tadokoro, H. Kanno, T. Kitajima, H. S.-Umemoto, N. Nakanishi, K. Isobe, K. Nakasuji, *Proc. Natl. Acad. Sci. USA.*, 2002, 99, 4950

[55] V. R. Pedireddi, D. Belhekar, *Tetrahedron*, 2002, 58, 2937

[56] D. J. Sutor, *J. Chem. Soc.*, 1963, 1105

[57] R. Taylor, O. Kennard, *J. Am. Chem. Soc.*, 1982, 104, 5063

[58] K. M. Lee, H.-C. Chang, J.-C. Jiang, J. C. C. Chen, H.-E. Kao, S. H. Lin, I. J. B. Lin, *J. Am. Chem. Soc.*, 2003, 125, 12358

[59] M. Ohkita, T. Suzuki, K. Nakatani, T. Tsuji, *Chem. Commun.*, 2001, 1454

[60] J. L. Atwood, F. Hamada, K. D. Robinson, G. W. Orr, L. R. Vincent, *Nature (London)*, 1991, 349, 683

[61] F. Baert, R. Fouret, H. Sliwa, H. Sliwa, *Acta. Cryst. B*, 1983, 39, 444

[62] M. Nishio, *CrystEngComm,* 2004, 6(27), 130

[63] Y. Iitaka, Y. Kodama, K. Nishihata, M. Nishio, *Chem. Commun.*, 1974, 389; Y. Kodama, K. Nishihata, M. Nishio, Y. Iitaka, *J. Chem. Soc. Perkin. Trans. 2.*, 1976, 1490

[64] G. D. Andreetti, R. Ungaro, A. Pochini. *J. Chem. Soc., Chem. Commun.*, 1979, 1005

[65] Z. Ciunik, S. Jarosz, *J. Mol. Structure*, 1998, 442, 115

[66] S. Re, S. Nagase, *Chem. Commun.*, 2004, 658

[67] P. D. Beer, P. A. Gale, D. K. Smith, *Supramolecular Chemistry,* Oxford University Press, 1999

[68] C. A. Hunter, J. K. M. Sanders, *J. Am. Chem. Soc.*, 1990, 112, 5525

[69] C. Janiak, *J. Chem. Soc., Dalton Trans.*, 2000, 3885

[70] T.-Q. Nguyen, R. Martel, P. Avouris, M. L. Bushey, L. Brus, C. Nuckolls, *J. Am. Chem. Soc.*, 2004, 126, 5234

[71] L. J. Childs, N. W. Alcock, M. J. Hannon, *Angew. Chem. Int. Ed.*, 2001, 40, Number 6, 1079

[72] I. Dance, M. Scudder, *J. Chem. Soc., Dalton Trans.*, 2000, 1579

[73] W. Clegg, *Crystal Structure Determination,* Oxford Primer, 1998

[74] P. Erk, R. van Gelder, M. F. Haddow, H. Hengelsberg, *CrystEngComm,* 2004, 6, 474

[75] W. C. McCrone, *Physics and chemistry of the organic solid state,* ed. D. Fox, M. M. Labes, A. Weissberger, Wiley Interscience, New York, 1965, vol.2

[76] F. P. A. Fabbiani, D. R. Allan, W. I. F. David, S. A. Moggach, S. Parsons, C. R. Pulham, *CrystEngComm,* 6, 504

[77] L. Infantes, J. Chisholm, S. Motherwell, *CrystEngComm,* 2003, 5(85), 480

[78] M. R. Caira, L. R. Nassimbeni, J. L. Scott, *J. Chem. Soc., Perkin Trans.*, 1994, 1403

[79] V. A. Russell, M. C. Etter, M. D. Ward, *J. Am. Chem. Soc.*, 1994, 116, 1941

[80] V. A. Russell, C. C. Evans, W. Li, M. D. Ward, *Science*, 1997, 276, 575

[81] K. T. Holman, M. D. Ward, *Angew. Chem., Int. Ed.*, 2000, 39, 1653

[82] V. Russell, M. Ward, *Chem. Mater.* 1996, 8, 1654

[83] G. Wu, T. Bein, *Chem. Mater.* 1994, 6, 1109

[84] V. Russell, M. Ward, *J. Mater. Chem.*, 1997, 7, 1123

[85] V. Russell, M. Etter, M. Ward, *Chem. Mater.*, 1994, 6, 1206

[86] M. D. Ward, *Chemistry in Britain*, 1998, 52

[87] P. Fagan, M. Ward, *Sci. Am.*, 1992, 28

[88] C. Evans, L. Sukarto, M. Ward, *J. Am. Chem. Soc.*, 1999, 121, 320

[89] D. J. Plaut, K. T. Holman, A. M. Pivovar, M. D. Ward, *J. Phys. Org. Chem.*, 2000, 13, 858

[90] A. D. Burrows, M. F. Mahon, R. W. Harrington, S. J. Teat, *Eur. J. Inorg. Chem.*, 2003, 1433; R. W. Harrington, PhD Thesis, University of Bath, 2002

CHAPTER 2

The reactions of sulfonated phosphines with guanidinium and substituted guanidinium derivatives

2.0 Introduction

The guanidinium sulfonate hydrogen-bonded sheet is flexible towards steric changes in the sulfonate substituent. The synthesis and crystal structure of [Gu][mTPPMS] has been previously investigated (Chapter 1, section 1.4) and results show that the hexagonal guanidinium sulfonate (GS) array remains intact[1]. Therefore the incorporation of the substituted cations methylguanidinium, ethylguanidinium and *N*,*N*-dimethylguanidinium into GS arrays is investigated here to see what effect reducing the number of hydrogen bond donors has on the formation of the hexagonal sheet. To this end, the compounds guanidinium chloride; GuCl, $[C(NH_2)_3]Cl$, methylguanidinium chloride; MeGuCl, $[C(NH_2)_2(NHMe)]Cl$, ethylguanidinium sulfate; $(EtGu)_2SO_4$, $[C(NH_2)_2(NHEt)]_2SO_4$ and *N*,*N*-dimethylguanidinium sulfate $(DiMeGu)_2SO_4$, $[C(NH_2)_2(NMe_2)]_2SO_4$, were crystallised with the sulfonated phosphines Na[mTPPMS], $Na[PPh_2C_6H_4SO_3\text{-}3]$, Na[mTPPMSO], $Na[O{=}PPh_2C_6H_4SO_3\text{-}3]$ and the sulfonated phosphine complex $Na_2[IrCl(CO)(PPh_2C_6H_4SO_3\text{-}3)_2]$. The structures of these sulfonates are shown in Figure 2.1.

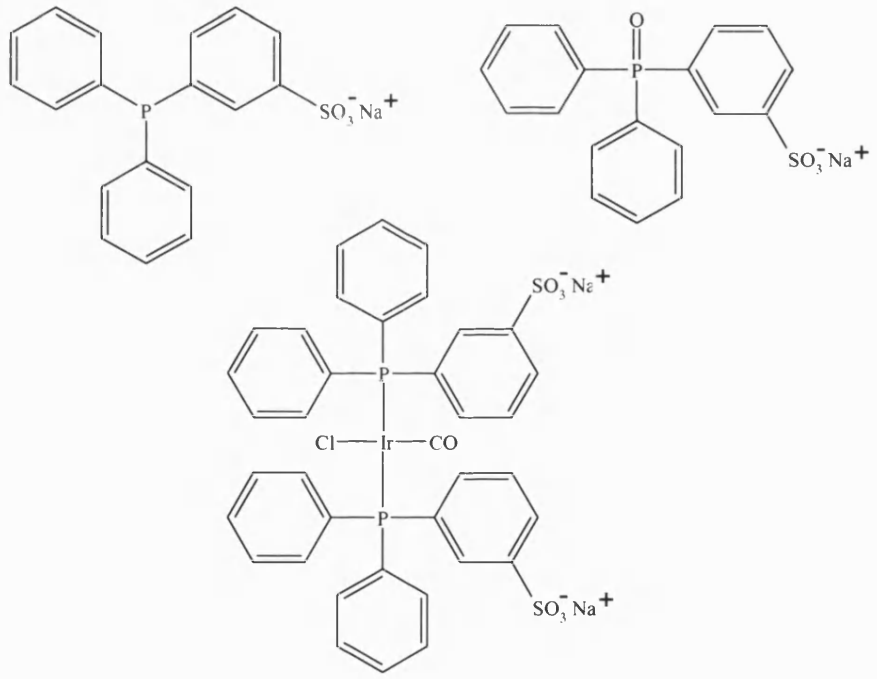

Figure 2.1; structures of sulfonated phosphines Na[mTPPMS], $Na[PPh_2C_6H_4SO_3\text{-}3]$ (top left), Na[mTPPMSO], $Na[O{=}PPh_2C_6H_4SO_3\text{-}3]$ (top right) and $Na_2[IrCl(CO)(PPh_2C_6H_4SO_3\text{-}3)_2]$ (bottom)

These sulfonates were chosen to investigate how flexible the regular hexagonal GS sheet is to the increasing bulk of the sulfonate substituents, as well as the other potential non-covalent interactions, such as phenyl embraces. The crystal structures of [MeGu][mTPPMS] **1**, [EtGu][mTPPMS] **2** and [DiMeGu][mTPPMS] **3** are described herein, and compared with that for [Gu][mTPPMS] **I**.

The inclusion of functional groups that could compete in the formation of hydrogen bonds is also examined, to ascertain if the regular hexagonal sheet persists in the presence of these groups. The incorporation of $[mTPPMSO]^-$ into GS arrays has not been reported to date. $[mTPPMSO]^-$ is very similar to $[mTPPMS]^-$ in shape and size, therefore might be expected to form related arrays when crystallised with the substituted and unsubstituted guanidinium salts. However, $[mTPPMSO]^-$ is a phosphine oxide, and incorporates an additional hydrogen bond acceptor which could act as a competing site with the sulfonate group in hydrogen bond formation. The crystallisations of Na[mTPPMSO] with the four guanidinium salts were investigated and the structures of [EtGu][mTPPMSO] **6** and [DiMeGu][mTPPMSO]·H_2O **7** are described. The crystal structure of [Gu][oTPPMSO] has been reported by Katho *et al*[2] and is discussed and compared to the structures observed in the $[mTPPMS]^-$ and $[mTPPMSO]^-$ series.

The use of sulfonated phosphines introduces a straightforward route to the incorporation of metal-containing ligands into guanidinium sulfonate arrays. The successful incorporation of unsaturated metal centres into these arrays affords the potential for reversible coordination of small molecules, such as SO_2 and CO. Previous results reported by the Burrows group[1] (Chapter 1, section 1.4) have shown that metal centres can be incorporated into GS arrays with little or no disruption to the formation of the GS sheet, as in most cases a monosulfonated metal-containing phosphine was explored and single GS layers were formed. One structure of a disulfonated metal-containing phosphine $[Gu]_2\{cis\text{-}[PdCl_2(mTPPMS)_2]\}$ has also been reported, where it was observed that both sulfonate groups are directed into the same GS layer (Figure 2.2). Consequently, major disruption to the GS array ensued, to the extent that the regular hexagonal sheet is no longer observed, as shown in Figure 2.3.

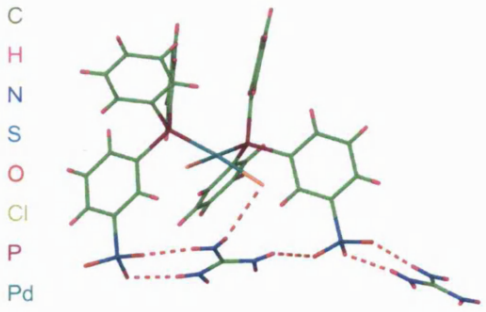

Figure 2.2; both sulfonates directed into the same plane in $[Gu]_2\{cis\text{-}[PdCl_2(mTPPMS)_2]\}$

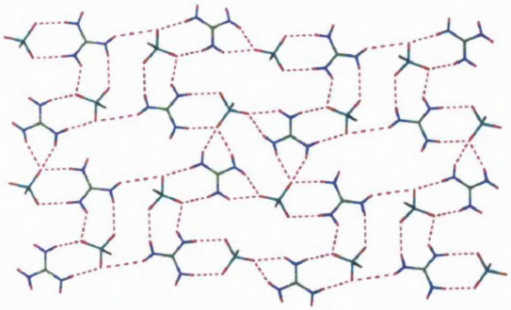

Figure 2.3; hydrogen bonded sheet formed in $[Gu]_2\{cis\text{-}[PdCl_2(mTPPMS)_2]\}$

Complexes containing mutually *trans* $[mTPPMS]^-$ ligands are more likely to be the most effective with respect to forming a pillared brick array where the GS sheets are bridged by the disulfonate anion, as the hydrogen-bonding of the two *trans* sulfonates within the same GS layer would be expected to be less sterically favourable. Hence, the complex $Na_2\{trans\text{-}[IrCl(CO)(mTPPMS)_2]\}$ was prepared and crystallised with GuCl, MeGuCl, $(EtGu)_2SO_4$ and $(DiMeGu)_2SO_4$. The chemistry of $[IrCl(CO)(PPh_3)_2]$, Vaska's compound, is well developed and the complex reversibly adds a number of small molecules such as SO_2, CO and O_2 into one of the axial positions on the metal. It can also interact with other small molecules such as HCl and H_2 by oxidative addition. Coordinative addition can lead to either square pyramidal or trigonal bipyramidal metal geometries, though in both cases the *trans* orientation of the phosphines is maintained in the product[3]. Oxidative addition, when concerted, normally occurs across the Cl–Ir–CO vector, again forming a product with mutually *trans* phosphines[4]. Therefore both types of reaction are unlikely to disrupt the crystalline structure of the GS array.

There is precedence for coordination compounds in the solid state reacting with gases such as SO_2. McAuliffe and co-workers[5] have reported the reaction of $[MnI_2(PPh_3)_2]$ with SO_2 to give $[MnI_2(PPh_3)_2]\cdot{}^2/_3SO_2$ and Burrows *et al* have reported that the palladium cluster compound $NEt_3Bz[Pd_3(\mu\text{-}SO_2)_2(\mu\text{-}Cl)(PPh_3)_3]$ reacts reversibly with SO_2 to give a compound where the SO_2 is bound to the chloride[6]. Compounds containing pincer ligands such as $[\{C_6H_3(CH_2NMe_2)_2\text{-}2,6\text{-}C,N,N\}PtCl]$ (see Figure 2.4) have been shown by van Koten and co-workers to

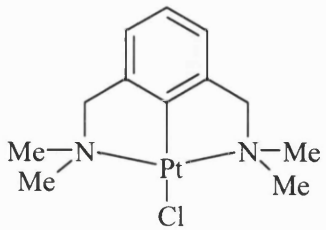

Figure 2.4; structure of $[\{C_6H_3(CH_2NMe_2)_2\text{-}2,6\text{-}C,N,N\}PtCl]$

reversibly coordinate SO_2 with a colour change from colourless to orange. This absorption occurs with no loss of crystallinity therefore allowing the reaction to be followed by X-ray diffraction[7].

2.1 Reactions of sulfonated phosphines with guanidinium and substituted guanidinium cations

The guanidinium and substituted guanidinium salts GuCl, MeGuCl, $(EtGu)_2SO_4$ and $(DiMeGu)_2SO_4$ were crystallised in a 1:1 molar ratio with the sulfonated phosphines. The compounds Na[mTPPMS], Na[mTPPMSO] and $Na_2[IrCl(CO)(mTPPMS)_2]$ and the guanidinium salts were each dissolved in methanol, mixed together, and the solvent allowed to slowly evaporate. This procedure was also repeated in water.

Using this method, crystals of [MeGu][mTPPMS] **1**, [EtGu][mTPPMS] **2** and [DiMeGu][mTPPMS] **3** as well as $[Gu]_2[IrCl(CO)(mTPPMS)_2]$ **8** were isolated from methanol, whereas crystals of [EtGu][mTPPMSO] **6** and [DiMeGu][mTPPMSO]·H_2O **7** were isolated from water.

Unfortunately, the reactions of Na[mTPPMSO] with GuCl and MeGuCl did not yield single crystals or powders of the desired products, despite attempts involving many different conditions.

This synthetic method did not afford crystals or powder from the reactions of $Na_2[IrCl(CO)(mTPPMS)_2]$ with the substituted guanidinium salts. The compounds $Na_2[IrCl(CO)(mTPPMS)_2]$ and MeGuCl, $(EtGu)_2SO_4$ and $(DiMeGu)_2SO_4$ were dissolved in methanol and mixed together under an atmosphere of nitrogen. Hexane was then gently layered onto the reaction mixture. Crystals of $[MeGu]_2[IrCl(CO)(mTPPMS)_2]\cdot{}^3/_8H_2O$ **9** formed at the interface between the two solvents. Analogous compounds incorporating the ethylguanidinium or dimethylguanidinium cations could not be obtained however, despite numerous attempts. Indeed, no solid precipitate was observed from these reactions.

The crystal structures of **1**, **2**, **3**, **6**, **7**, **8** and **9** are described in this chapter (crystallographic data are given in Table 2.1).

1: [MeGu][mTPPMS] : $[C(NH_2)_2(NHMe)][PPh_2C_6H_4SO_3\text{-}3]$

2: [EtGu][mTPPMS] : $[C(NH_2)_2(NHEt)][PPh_2C_6H_4SO_3\text{-}3]$

3: [DiMeGu][mTPPMS] : $[C(NH_2)_2(NMe_2)][PPh_2C_6H_4SO_3\text{-}3]$

6: [EtGu][mTPPMSO] : $[C(NH_2)_2(NHEt)][OPPh_2C_6H_4SO_3\text{-}3]$

7: [DiMeGu][mTPPMSO]·H_2O : $[C(NH_2)_2(NMe_2)][OPPh_2C_6H_4SO_3\text{-}3]\cdot H_2O$

8: $[Gu]_2[IrCl(CO)(mTPPMS)_2]$: $[C(NH_2)_3]_2\{trans\text{-}[IrCl(CO)(PPh_2C_6H_4SO_3\text{-}3)_2]\}$

9: $[MeGu]_2[IrCl(CO)(mTPPMS)_2]\cdot{}^3/_8H_2O$:

$[C(NH_2)_2(NHMe)]_2\{trans\text{-}[IrCl(CO)(PPh_2C_6H_4SO_3\text{-}3)_2]\}\cdot{}^3/_8H_2O$

Crystallographic measurements for compounds **1**, **6**, and **7** were made at 150 K, compound **2** at 293 K and compound **8** at 240 K on a Nonius Kappa CCD diffractometer. Crystallographic measurements for compounds **3** and **9** were made at 150 K on the Bruker SMART CCD diffractometer at Daresbury SRS Station 9·8.

All of the structure determinations have been carried out using X-ray crystallography. In compound $[MeGu]_2[IrCl(CO)(mTPPMS)_2]\cdot{}^3/_8H_2O$ **9** there is disorder in the carbonyl and chloride ligands, where the atoms of the minor part were refined isotropically. In the remaining structures, all non-hydrogen atoms were allowed to vibrate anisotropically in the least squares cycles. In compounds **7** and **9** molecules of water are included in the lattice. The positions of the water hydrogen atoms in **7** were determined from the electron density map, and subsequently refined subject to having O–H bond lengths fixed at 0.89(3)Å. The positions of the water hydrogen atoms in **9** could not be determined. All other hydrogen atoms were included at calculated positions.

Compound	**1**	**2**	**3**	**6**	**7**	**8**	**9**
Empirical formula	$C_{20}H_{22}N_3O_3PS$	$C_{21}H_{24}N_3O_3PS$	$C_{21}H_{24}N_3O_3PS$	$C_{21}H_{24}N_3O_4PS$	$C_{21}H_{26}N_3O_5PS$	$C_{39}H_{40}Cl_1Ir_1N_6O_7P_2S_2$	$C_{41}H_{44}Cl_1Ir_1N_6O_{7.375}P_2S_2$
M	415.44	429.46	429.46	445.46	463.48	1058.48	1092.53
Crystal system	Monoclinic	Monoclinic	Triclinic	Monoclinic	Monoclinic	Monoclinic	Orthorhombic
Space group	$P2_1/n$	$P2_1/n$	P-1	$P2_1/c$	Cc	$P2_1/a$	$P2_1ca$
Wavelength / Å	0.71073	0.71073	0.68670	0.71073	0.71073	0.71073	0.67780
a / Å	6.3010(1)	6.7430(1)	8.2503(4)	11.8720(2)	10.1640(2)	12.7340(1)	48.848(2)
b / Å	29.1970(6)	29.9410(4)	9.4097(5)	12.6140(2)	15.4510(2)	14.2640(2)	14.0177(6)
c / Å	11.8190(3)	11.6940(2)	13.9516(7)	14.7520(2)	15.3750(3)	24.3880(3)	12.7941(6)
α / °	90	90	92.899(2)	90	90	90	90
β / °	104.742(1)	104.331(1)	98.098(2)	99.315(1)	107.981(1)	100.1938(4)	90
γ / °	90	90	96.580(2)	90	90	90	90
U / Å^3	2102.77(8)	2287.46(6)	1062.14(9)	2180.03(6)	2296.62(7)	4359.85(9)	8760.7(7)
Z	4	4	2	4	4	4	8
μ(Mo-Kα) / mm^{-1}	0.255	0.237	0.255	0.255	0.247	3.347	3.335
Reflections collected	30503	21765	10110	26029	17420	60347	69787
Independent reflections	4828	5191	5645	4981	5098	9980	17597
R(int)	0.1404	0.0512	0.0272	0.0923	0.0683	0.0933	0.0542
*R*1, w*R*2	0.0507, 0.0958	0.0522, 0.1051	0.0456, 0.1242	0.0489, 0.1214	0.0361, 0.0774	0.0464, 0.0925	0.0355, 0.0804
R indices (all data)	0.1496, 0.1203	0.1180, 0.1318	0.0610, 0.1306	0.0620, 0.1306	0.0519, 0.0828	0.0792, 0.1035	0.0402, 0.0827

Table 2.1; X-ray crystallographic parameters for compounds **1, 2, 3, 6, 7, 8, 9**

2.2 Triphenylphosphine-monosulfonates

In this section the structures of [MeGu][mTPPMS] **1**, [EtGu][mTPPMS] **2** and [DiMeGu][mTPPMS] **3** are described. The structural effects of substitution on the guanidinium cation are also compared with the previously reported structure of [Gu][mTPPMS] **I** which contains the unsubstituted guanidinium cation.

[MeGu][mTPPMS] : $[C(NH_2)_2(NHMe)][PPh_2C_6H_4SO_3\text{-}3]$ 1

Asymmetric Unit

The asymmetric unit of **1** is shown in Figure 2.5 and consists of one $[MeGu]^+$ cation and one $[mTPPMS]^-$ anion.

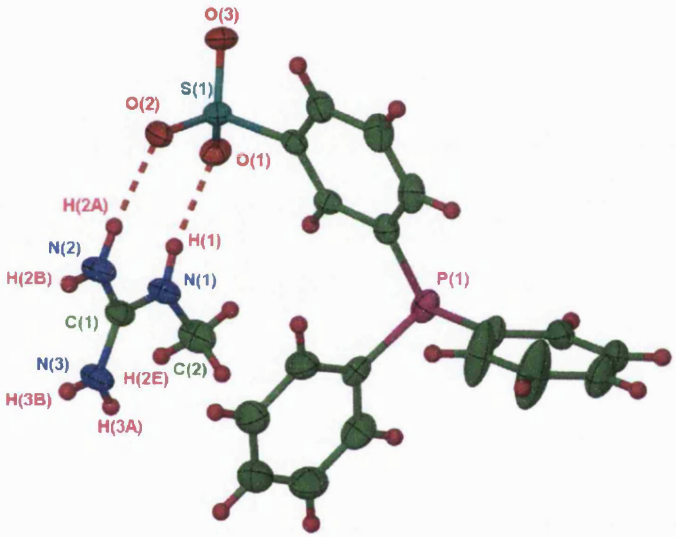

Figure 2.5; asymmetric unit of **1**. Ellipsoids are depicted at 50% probability level.

Extended Structure

The cation has two unsubstituted faces available to form hydrogen bonds via the DD:AA motif, giving two $R_2^2(8)$ rings with the sulfonates and leading to the formation of ribbons. The third face of the cation has only one N–H donor, due to the substitution of a hydrogen atom by a methyl group. This donor forms a single hydrogen bond with a sulfonate oxygen atom of a neighbouring anion. These hydrogen-bonded motifs repeat to form a sheet, as shown in Figure 2.6, which has a similar structure to the hexagonal array observed in the analogous structures containing unsubstituted guanidinium cations (as described in section 1.3). However, in **1** one N–H···O hydrogen bond has been replaced with a weaker C–H···O

hydrogen bond. Although the hydrogen atoms are included at calculated positions, their locations are very close to those determined from the electron density map. See Table 2.2 for hydrogen bond details. The triphenylphosphine groups of the sulfonates are directed to both sides of the sheets, which are corrugated with an inter-ribbon angle of 121°, and these interdigitate to produce single layers in the gross structure. There are also interactions between phenyl rings in the $[mTPPMS]^-$ units of different sheets. Each $[mTPPMS]^-$ forms a 4-fold-phenyl-embrace (4PE) with a P···P distance within the embrace of 8.4Å.

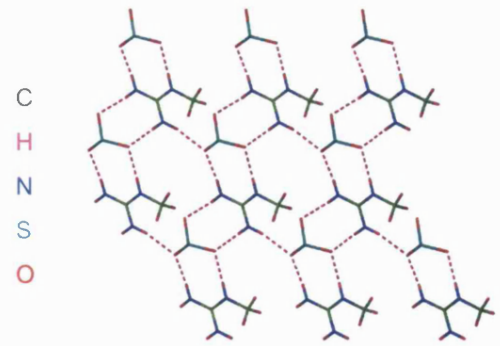

Figure 2.6; hexagonal hydrogen-bonded sheet formed in **1**.

D–H···A	D···A /Å	H···A /Å	D–H···A /°	Symmetry operation generating D···A
N(1)–H(1)···O(1)	2.857(3)	1.99	169	*x*, *y*, *z*
N(2)–H(2A)···O(2)	2.847(3)	1.97	172	*x*, *y*, *x*
N(2)–H(2B)···O(3)	3.054(3)	2.18	174	*x*-½, ½-*y*, *z*-½
N(3)–H(3A)···O(2)	2.839(2)	2.10	142	½+*x*, ½-*y*, *z*-½
N(3)–H(3B)···O(1)	2.792(3)	1.92	171	*x*-½, ½-*y*, *z*-½
C(2)–H(2E)···O(1)	4.009(3)	3.15	147	½+*x*, ½-*y*, *z*-½

Table 2.2; details of the hydrogen bonding in **1**

[EtGu][mTPPMS] : $[C(NH_2)_2(NHEt)][PPh_2C_6H_4SO_3\text{-}3]$ 2

Asymmetric Unit

The asymmetric unit of **2** consists of one $[EtGu]^+$ cation and one $[mTPPMS]^-$ anion and is shown in Figure 2.7. There is disorder in the ratio 50:50 between the atoms C(2), H(2C), H(2D), C(3), H(3C), H(3D), H(3E) and their counterparts C(2A), H(2A1), H(2A2), C(3A), H(3A1), H(3A2), H(3A3) respectively, in the ethyl group of the cation.

The single crystal data for **2** were collected at 293 K. Data were originally collected at 150 K where a different unit cell was determined, with the space group $P\bar{1}$ with four cations and four anions in the asymmetric unit and twice the volume of that presented here due to the doubling of one cell axis. These two structures are different phases. The data collected for

the high temperature phase resulted in optimum convergence, whereas convergence is not satisfactory in the low temperature phase possibly due to the phase change being incomplete.

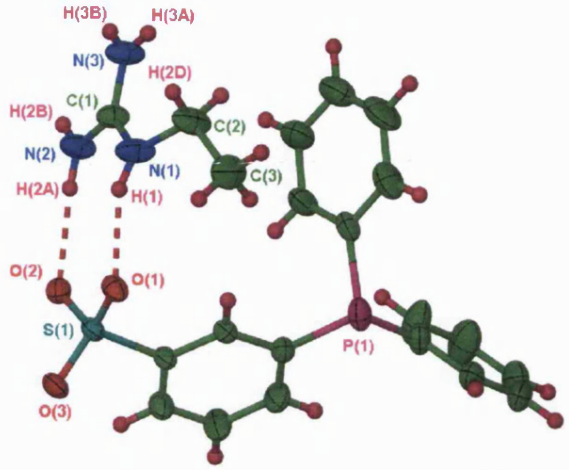

Figure 2.7; asymmetric unit of **2**. Ellipsoids are depicted at 30% probability level.
(*only one of the disordered parts is shown for clarity*)

Extended Structure

The cation has two unsubstituted faces with which to form two $R_2^2(8)$ motifs via DD:AA hydrogen bonds with the sulfonate, forming ribbons. The third face of the cation has only one N–H donor due to substitution by an N–Et group. The single N–H donor of this substituted cation face forms a hydrogen bond with an oxygen atom of a sulfonate in a neighbouring ribbon, linking them into sheets (Figure 2.8). The details of the hydrogen bonds are given in Table 2.3.

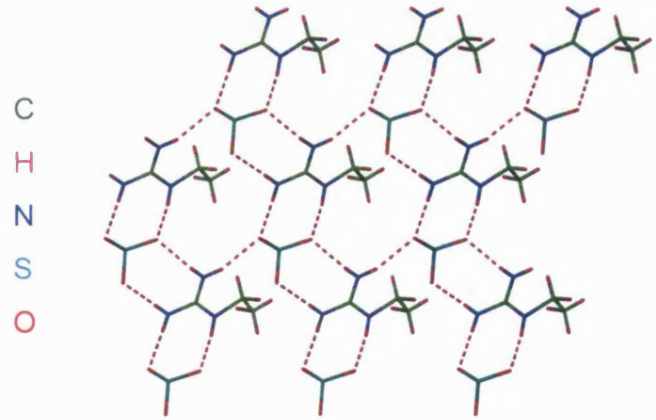

Figure 2.8; hexagonal sheet formed in **2**

As seen in [MeGu][mTPPMS] **1**, the sheet formed is similar to the hexagonal array, with a C–H···O interaction forming in place of the missing N–H···O hydrogen bond. The sheets are corrugated (θ_{IR} of 120°) with the triphenylphosphine groups directed to either side, forming

continuous single layers in the gross structure. Similar to **1**, each $[mTPPMS]^-$ forms a 4PE with a P···P distance of 8.2Å.

D–H···A	D···A /Å	H···A /Å	D–H···A /°	Symmetry operation generating D···A
N(1)–H(1)···O(1)	2.838(3)	2.02	158	*x*, *y*, *z*
N(2)–H(2A)···O(2)	2.957(3)	2.10	175	*x*, *y*, *z*
N(2)–H(2B)···O(3)	3.030(3)	2.17	178	½+*x*, ½-*y*, ½+*z*
N(3)–H(3A)···O(2)	2.980(3)	2.16	158	*x*-½, ½-*y*, ½+*z*
N(3)–H(3B)···O(1)	2.828(3)	2.02	157	½+*x*, ½-*y*, ½+*z*
C(2)–H(2D)···O(3)	3.717(2)	2.89	144	*x*-½, ½-*y*, ½+*z*

Table 2.3; details of the hydrogen bonding in **2**

[DiMeGu][mTPPMS] : $[C(NH_2)_2(NMe_2)][PPh_2C_6H_4SO_3\text{-}3]$ 3

Asymmetric Unit

The asymmetric unit of **3** is shown in Figure 2.9 and consists of one $[DiMeGu]^+$ cation and one $[mTPPMS]^-$ anion.

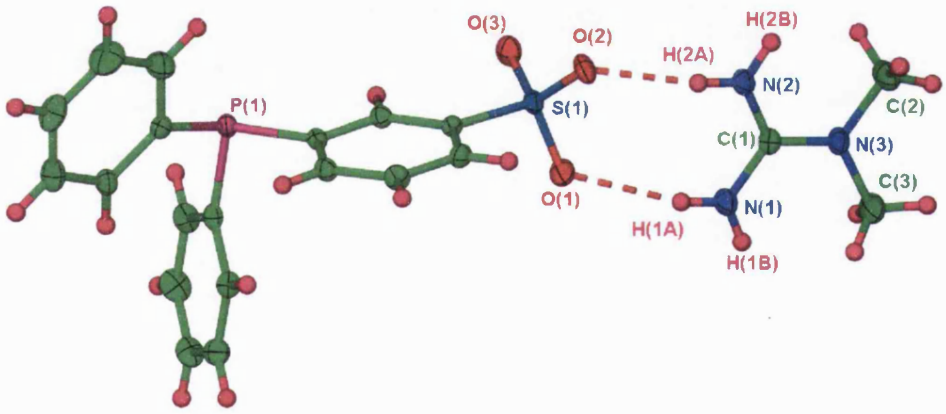

Figure 2.9; asymmetric unit in **3**. Ellipsoids are depicted at 50% probability level.

Extended Structure

The unsubstituted face of the cation forms the DD:AA hydrogen-bonded motif with the sulfonate. Two faces of the cation are disrupted by replacing NH_2 with NMe_2, and can no longer form DD:AA hydrogen bonds. Both N–H donors in the substituted cation faces form hydrogen bonds with an oxygen atom in a neighbouring sulfonate to generate motifs with the hydrogen-bonded graph sets $R_4^2(8)$ and $R_4^4(12)$, which propagate to afford ribbons as shown

in Figure 2.10. All of the N–H donors and sulfonate oxygen atoms are used in the formation of these ribbons, which stack in flat planes separated by regions containing the sulfonate triphenylphosphine groups. Details of the hydrogen bonds are given in Table 2.4.

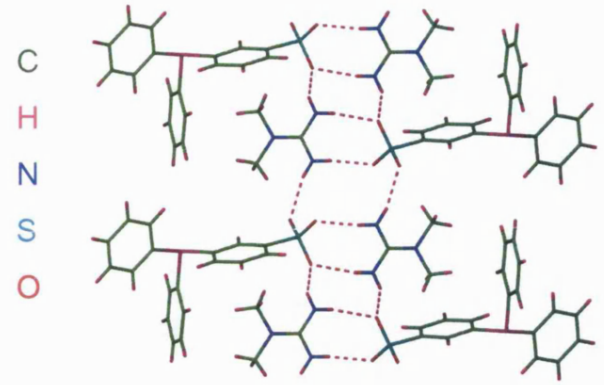

Figure 2.10; ribbon formation in **3**

There are also interactions between the phenyl groups of ribbons that lie in the same plane. The $[mTPPMS]^-$ units form a 6PE, in contrast to the 4PE observed in **1** and **2**, with a shorter P···P distance of 7.1Å.

D–H···A	D···A /Å	H···A /Å	D–H···A /°	Symmetry operation generating D···A
N(1)–H(1A)···O(1)	2.963(2)	2.24	139	*x*, *y*, *z*
N(1)–H(1B)···O(1)	2.869(2)	2.12	142	-*x*+1, -*y*, -*z*
N(2)–H(2B)···O(3)	2.985(2)	2.13	163	-*x*+1, -*y*+1, -*z*
N(2)–H(2A)···O(2)	2.885(2)	2.04	161	*x*, *y*, *z*

Table 2.4; details of the hydrogen bonding in **3**

2.2.1 The structural effects of alkyl substitution in guanidinium ions when crystallised with triphenylphosphine-monosulfonate

The hydrogen-bonding patterns observed in most of the structures in the $[mTPPMS]^-$ series have hardly been affected by the substitution of the N–H groups in the cation. In [Gu][mTPPMS][1] **I** the regular hexagonal sheet is observed, and in [MeGu][mTPPMS] **1** and [EtGu][mTPPMS] **2** adapted hexagonal sheets are formed. These compounds exhibit repeating single layers in the gross structure. In contrast, independent ribbons are formed in [DiMeGu][mTPPMS] **3**. These results show that the hexagonal sheet can be retained when one NH group in the cation is lost, as seen in **1** and **2**, but when two NH groups are lost this array is no longer observed. Even though **3** forms different packing arrangements to **I**, **1** and **2**, all four structures have regions of hydrogen-bonded cations and anions, separated by regions of the sulfonate triphenylphosphine groups.

Compound [Gu][mTPPMS] **I** is the only example in this system to have two cations and two anions in the asymmetric unit. The regular hexagonal hydrogen-bonded GS sheet is formed using the three unsubstituted faces of each cation, forming DD:AA hydrogen bonds with the sulfonates. The sheets are highly corrugated with an inter-ribbon angle of 107°. The sulfonate triphenylphosphine groups are directed to both sides, which interdigitate forming repeating single layers. The $[mTPPMS]^-$ groups interact via a 6PE, with a P···P distance of 7.1Å.

In compounds [MeGu][mTPPMS] **1** and [EtGu][mTPPMS] **2**, hydrogen bonds between the cations and anions afford corrugated hexagonal sheets, with the triphenylphosphine groups directed to either side leading to interdigitating single layers. The extended structures in **1** and **2** are remarkably similar, forming the same hydrogen-bonded motifs with similar inter-ribbon angles and phenyl-embrace interactions between the triphenylphosphine groups.

Compound [DiMeGu][mTPPMS] **3** is the only structure in this series where the planes of the nitrogen atoms in the cations are not coplanar with the sulfonate oxygens, but instead are almost perpendicular to them. The cation has lost two N–H donors due to substitution by methyl groups, leading to the formation of ribbons. The triphenylphosphine groups of the sulfonates are directed to either side of the ribbons, which pack in layers in the gross structure.

All four structures exhibit a phenyl embrace between proximate $[mTPPMS]^-$ groups. Compounds **1** and **2** exhibit a 4PE whereas there is a 6PE in **I**, even though similar arrays are formed in these structures. This is due to the arrangement of the triphenylphosphine groups in these compounds. In **I** the $[mTPPMS]^-$ groups of one ribbon face the opposite direction to those of the neighbouring ribbons, and alternate along the sheet (see Figure 2.11). These alternating $[mTPPMS]^-$ groups interdigitate with those of a neighbouring sheet leading to a 6PE. However, in **1** and **2** all of the $[mTPPMS]^-$ groups are facing the same direction, and the interdigitating $[mTPPMS]^-$ groups of the neighbouring sheet are facing the opposite direction leading to a 4PE (see Figure 2.11).

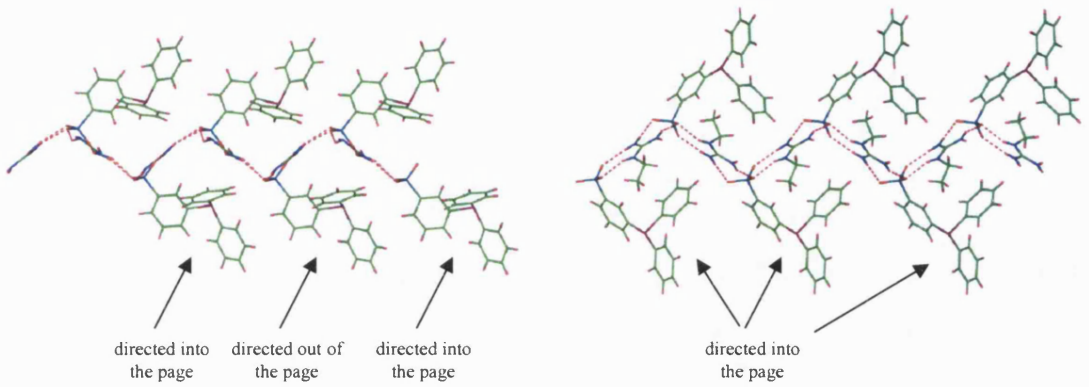

Figure 2.11; (*left*) the triphenylphosphine groups of one ribbon in **I** are directed into the page, whereas those of the neighbouring ribbon are directed out of the page, and (*right*) the triphenylphosphine groups in **2** are all directed into the page.

This difference in conformation of the triphenylphosphine groups in **1** and **2** results from the presence of the alkyl groups in the cation in these compounds. In **I** there is very little void space between the triphenylphosphine groups and the sheet, whereas in **1** and **2** the orientation of the triphenylphosphine group is different such that a space is made available for the bulk of the Me or Et groups in the substituted cations. This difference in orientation of the $[mTPPMS]^-$ groups also has a direct effect on the corrugation of the sheets, increasing the θ_{IR} in **1** and **2** from that in **I**. This suggests that in the $[mTPPMS]^-$ series the formation of the regular hexagonal hydrogen-bonded array in **I**, **1** and **2** has a higher priority than the corrugation or phenyl embrace observed.

2.3 Triphenylphosphine-monosulfonate oxides

The structures of [EtGu][mTPPMSO] **6** and [DiMeGu][mTPPMSO]·H_2O **7** are described, and the structural affects of substitution on the guanidinium cation are also discussed.

[EtGu][mTPPMSO] : $[C(NH_2)_2(NHEt)][PPh_2C_6H_4SO_3\text{-}3]$ 6

Asymmetric Unit

The asymmetric unit of **6** is shown in Figure 2.12 and consists of one $[EtGu]^+$ cation and one $[mTPPMSO]^-$ anion. There is disorder in the ratio 60:40 between the atoms C(3), H(3B), H(3C), H(3D) and their counterparts C(3A), H(3A1), H(3A2), H(3A3) respectively, in the methyl group in the cation.

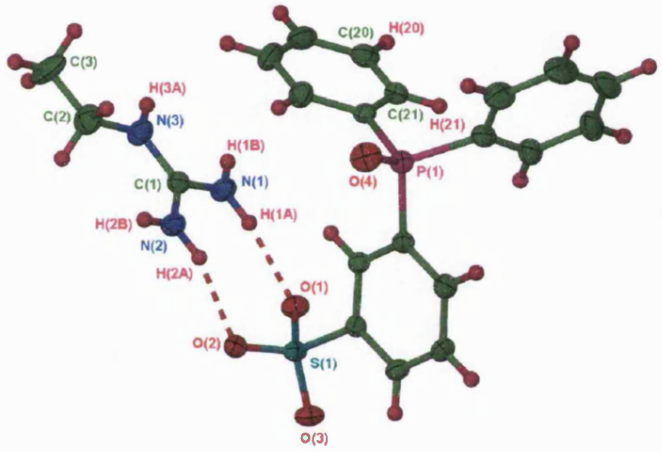

Figure 2.12; asymmetric unit of **6**. Ellipsoids are depicted at 50% probability level. (*disordered part of 40% occupancy is not shown for clarity*)

Extended Structure

The two unsubstituted faces of the cation form DD:AA hydrogen-bonded motifs with the sulfonate, forming ribbons, as shown in Figure 2.13. The third face of the cation has only one N–H donor due to substitution by an ethyl group. The $[mTPPMSO]^-$ groups are directed to either side of the ribbons.

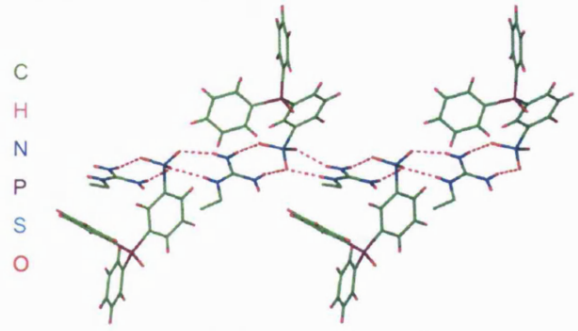

Figure 2.13; ribbon formed in **6**

Neighbouring ribbons are linked by the N–H donor of the substituted cation face forming a hydrogen bond to the P=O acceptor of a neighbouring ribbon, as shown in red in Figure 2.14. This repeating motif leads to two-dimensional hydrogen-bonded arrays which are linked through hydrogen bonds from two C–H donors of a phenyl ring in the triphenylphosphine group, and two oxygen acceptor atoms of a sulfonate generating a $R_2^2(7)$ motif. This generates a three-dimensional hydrogen-bonded array in the gross structure (Figure 2.15). Details of the hydrogen bonds are given in Table 2.6. There is also a 4PE between the $[mTPPMSO]^-$ groups of interdigitating anions, with a P···P distance of 7.6Å.

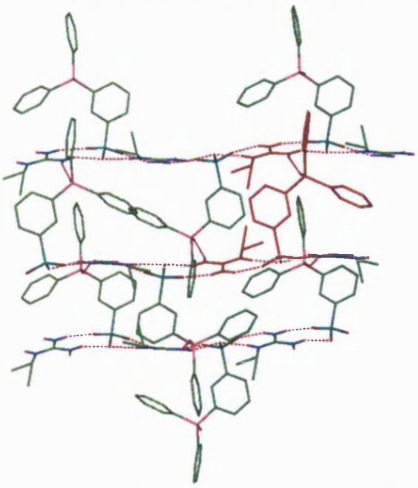

Figure 2.14; ribbons linked via P=O hydrogen bonding

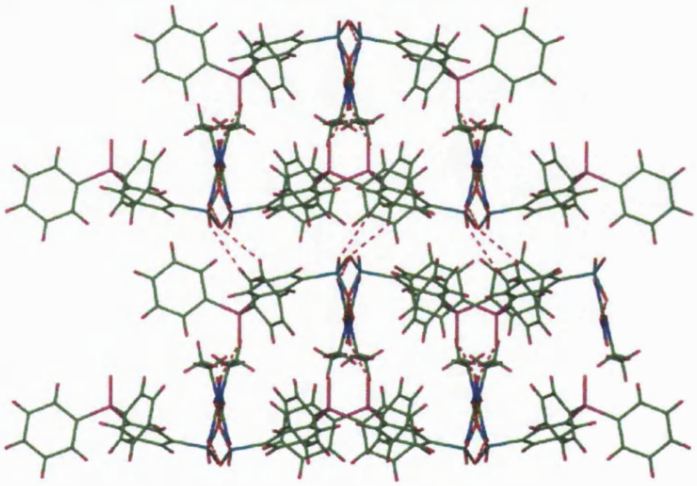

Figure 2.15; two-dimensional layers hydrogen-bonded into a three-dimensional network in **6**

D–H···A	D···A /Å	H···A /Å	D–H···A /°	Symmetry operation generating D···A
N(1)–H(1A)···O(1)	2.901(2)	2.03	169	*x*, *y*, *z*
N(1)–H(1B)···O(3)	2.922(2)	2.07	163	*x*, -*y*-½, ½+*z*
N(2)–H(2A)···O(2)	2.884(2)	2.03	163	*x*, *y*, *z*
N(2)–H(2B)···O(4)	2.762(2)	1.94	155	2-*x*, *y*-½, ½-*z*
N(3)–H(3A)···O(2)	2.879(2)	2.00	172	*x*, -*y*-½, ½+*z*
C(20)–H(20)···O(3)	3.542(3)	2.75	142	1-*x*, *y*+½, ½-*z*
C(21)–H(21)···O(1)	3.401(3)	2.59	144	1-*x*, *y*+½, ½-*z*

Table 2.6; details of the hydrogen bonding in **6**

[DiMeGu][mTPPMSO]·H_2O : $[C(NH_2)_2(NMe_2)][OPPh_2C_6H_4SO_3\text{-}3]\cdot H_2O$ 7

Asymmetric Unit

The asymmetric unit of **7** consists of one $[EtGu]^+$ cation, one $[mTPPMSO]^-$ anion and a molecule of water, as shown in Figure 2.16.

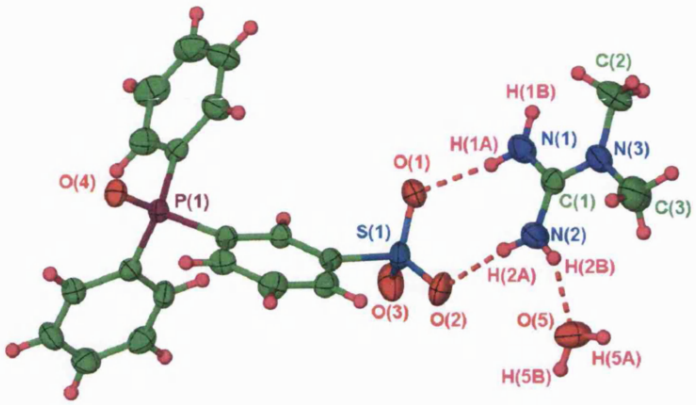

Figure 2.16; asymmetric unit of **7**. Ellipsoids are depicted at 50% probability level.

Extended Structure

The unsubstituted face of the cation forms DD:AA hydrogen bonds with the sulfonate. The water molecules act as hydrogen-bond donors and acceptors, linking the cation-anion pairs into chains. These chains are linked by hydrogen-bonding involving the P=O functionality of the $[mTPPMSO]^-$ group to form a virtually flat sheet (θ_{IR} of 174°) with graph set $R_{10}^{8}(26)$, as shown in Figure 2.17. There are no significant C–H···O hydrogen bonds between the cations and anions. Details of the hydrogen bonds are given in Table 2.7. This is the only compound in this thesis in which there are no N–H···O hydrogen bonds between the DD:AA hydrogen-bonded cation-anion pairs (as seen in Figure 2.16). This is due to the inclusion of water molecules into the lattice and the presence of the P=O group in the anion, and their subsequent involvement in the formation of the hydrogen-bonded array.

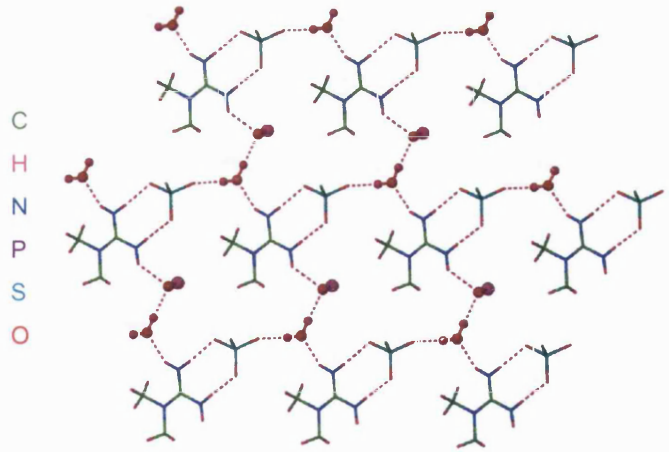

Figure 2.17; sheet formed in **7**
(*most of the anion has been removed for clarity*)

The $[mTPPMSO]^-$ groups of the anion are directed to one side of each sheet. However, bilayers are not observed in the gross structure. Instead, due to P=O involvement in the hydrogen-bonded network, the anion acts as a bridge between parallel sheets forming a three-dimensional array, as shown in Figure 2.18. This array is similar to a pillared brick architecture, normally observed when disulfonates are incorporated into GS arrays (Chapter 1, section 1.3). There are also edge-to-face C–H···π interactions between $[mTPPMSO]^-$ groups of neighbouring anions.

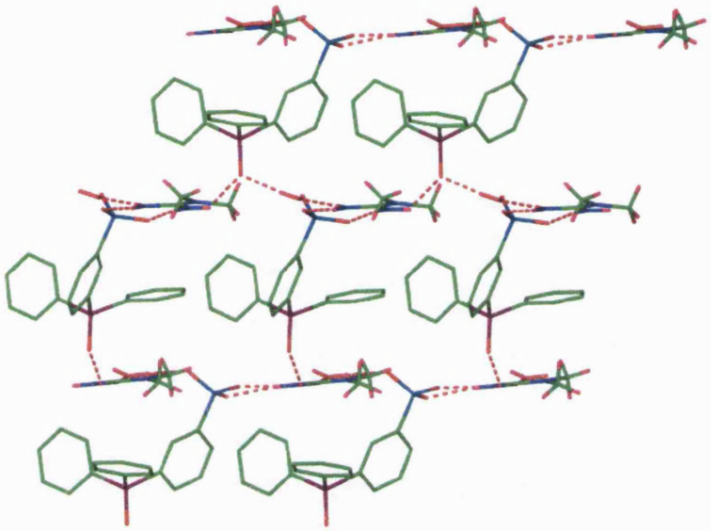

Figure 2.18; pillared brick architecture formed in **7**
(*the hydrogen atoms of the anion have been removed for clarity)*

D–H···A	D···A /Å	H···A /Å	D–H···A /°	Symmetry operation generating D···A
N(1)–H(1A)···O(1)	2.928(3)	2.05	172	*x*, *y*, *z*
N(1)–H(1B)···O(4) $_{(P=O)}$	2.923(2)	2.27	131	*x*-1, 2-*y*, *z*-½
N(2)–H(2A)···O(2)	2.850(3)	1.97	174	*x*, *y*, *z*
N(2)–H(2B)···O(5) $_w$	2.786(3)	1.98	152	*x*, *y*, *z*
O(5)$_w$–H(5A)···O(3)	2.703(3)	1.81	175	*x*-½, ½+*y*, *z*
O(5)$_w$–H(5B)···O(4)$_{(P=O)}$	2.808(2)	1.92	174	*x*-½, $^5/_2$-*y*, *z*-½

Table 2.7; details of the hydrogen bonding in **7**

2.3.1 The structural effects of alkyl substitution in guanidinium ions when crystallised with triphenylphosphine-monosulfonate oxide

The compounds [EtGu][mTPPMSO] **6** and [DiMeGu][mTPPMSO]·H_2O **7** have very different hydrogen-bonded architectures. This reflects the loss of only one N–H group in **6** but the loss of two N–H groups and the incorporation of water into the lattice in **7**, changing the number of hydrogen bond donors and acceptors available in this compound. The presence of the P=O hydrogen-bond competing group in the anion has also affected the hydrogen bonded network.

In the supramolecular structure of compound **6** ribbons are observed, while in **7** sheets disrupted by the inclusion of water are linked into a pillared brick array. There are also distinct regions of hydrogen bonding separated by regions of the sulfonate substituent in the latter. However, in compound **6** similar distinct regions are not observed as the ribbons are staggered in relation to each other.

Compounds **6** and **7** form very different structures to their $[mTPPMS]^-$ analogues [EtGu][mTPPMS] **2** and [DiMeGu][mTPPMS] **3**, respectively. In particular, adapted hexagonal sheets are stacked in repeating single layers in **2** and independent ribbons are formed in **3**. It is surprising that in [EtGu][mTPPMSO] **6** the loss of one NH group leads to independent ribbons, whereas in [DiMeGu][mTPPMSO]·H_2O **7** a sheet is observed even though there is a loss of two NH groups. This behaviour can be accounted for by the inclusion of water in **7**, increasing the number of donors and acceptors available. Compound **6** is the only example reported in this thesis where the inclusion of $[EtGu]^+$ into a GS array does not lead to sheets being observed.

The structure of [Gu][oTPPMSO] has been previously reported by Katho *et al*[2], where the sulfonate functionality occupies the *ortho* position. In contrast to the $[mTPPMSO]^-$ series, in [Gu][oTPPMSO] an NH donor involved in forming DD:AA hydrogen bonds with the sulfonate also forms a hydrogen bond with the oxygen atom of the P=O group in the anion. The P=O group is not involved in the sheet formation, however the regular hexagonal hydrogen-bonded array is not observed. Instead, there is hydrogen bonding between the cations and anions where two of the cation faces form $R_2^2(8)$ motifs, and the third cation face forms a $R_2^1(6)$ motif. The $[mTPPMSO]^-$ groups are directed to both sides of the sheets, and

interact via a 4PE (P···P distance of 6.9Å), leading to single layers. This structure is similar to those observed in [MeGu][mTPPMS] **1** and [EtGu][mTPPMS] **2**, where repeating single layers are formed with a 4PE between triphenylphosphine groups. It is noteworthy that corrugated hexagonal sheets are seen in **1** and **2** whereas virtually flat sheets are formed in [Gu][oTPPMS], due to the orientation of the $[mTPPMSO]^-$ groups (see Figure 2.19).

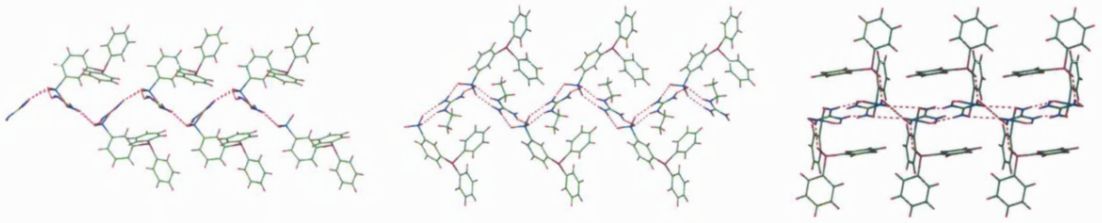

Figure 2.19; corrugated repeating single layers formed in [MeGu][mTPPMS] **1** and [EtGu][mTPPMS] **2** (*left and middle respectively*) and virtually flat repeating single layers formed in [Gu][oTPPMSO] (*right*)

2.4 Sulfonated derivative of Vaska's compound

The structures of $[Gu]_2[IrCl(CO)(mTPPMS)_2]$ **8** and $[MeGu]_2[IrCl(CO)(mTPPMSO)_2]\cdot{}^3/_8 H_2O$ **9** are described in this section, and the structural affects of substitution on the guanidinium cation are discussed and compared with $[Gu]_2\{cis\text{-}[PdCl_2(mTPPMS)_2]\}$ **A**.

$[Gu]_2[IrCl(CO)(mTPPMS)_2]$: $[C(NH_2)_3]_2$ {*trans*-$[IrCl(CO)(PPh_2C_6H_4SO_3\text{-}3)_2]$} 8

Asymmetric Unit

The asymmetric unit of **8** consists of two $[Gu]^+$ cations and one $[IrCl(CO)(TPPMS)_2]^{2-}$ anion as shown in Figure 2.20. The carbonyl group and chloride are disordered in a 55:45 ratio between positions C(37), O(7) and Cl(1) and C(37A), O(7A) and Cl(1A), respectively.

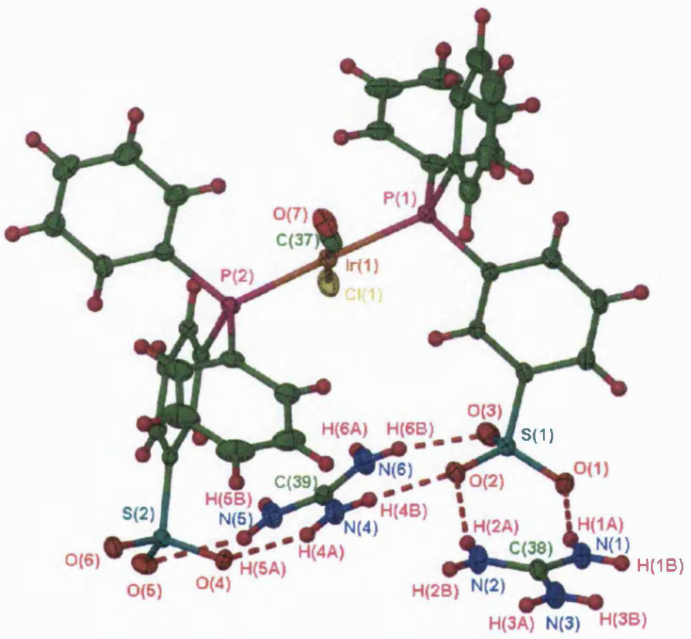

Figure 2.20; asymmetric unit of **8**. Ellipsoids are depicted at 30% probability level.
(*only one disordered part is shown for clarity*)

The single crystal data for **8** were collected at 240 K. Data were originally collected at 150 K however the single crystals undergo a phase change on cooling. The data collected at 240 K leads to optimal convergence.

Extended Structure

The guanidinium cation has three faces available to form DD:AA hydrogen-bonded motifs with the sulfonate, and forms the regular hexagonal guanidinium sulfonate array as shown in Figure 2.21. The hydrogen bond details are given in Table 2.9. The sheets are almost flat with an inter-ribbon angle of 168°, and both sulfonate groups of the anion are directed into the same GS layer. The sulfonate substituents are directed to the same side of each sheet, which stack to form bilayers, as shown in Figure 2.22. There is not a large degree of interdigitation as the anions are extremely bulky. Edge-to-face C–H···π interactions are evident between the phenyl rings of neighbouring anions within and between the sheets.

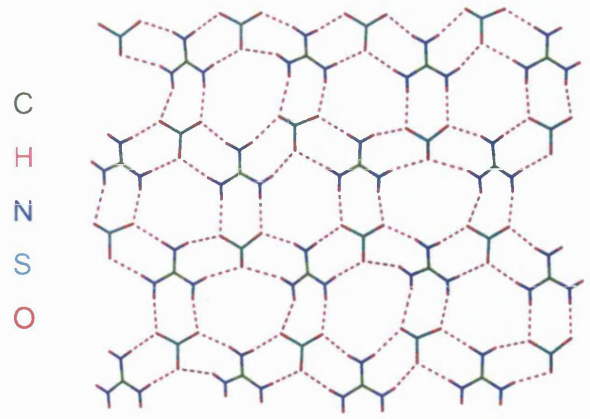

Figure 2.21; hexagonal GS sheet formation in **8**
(*most of the anion is removed for clarity*)

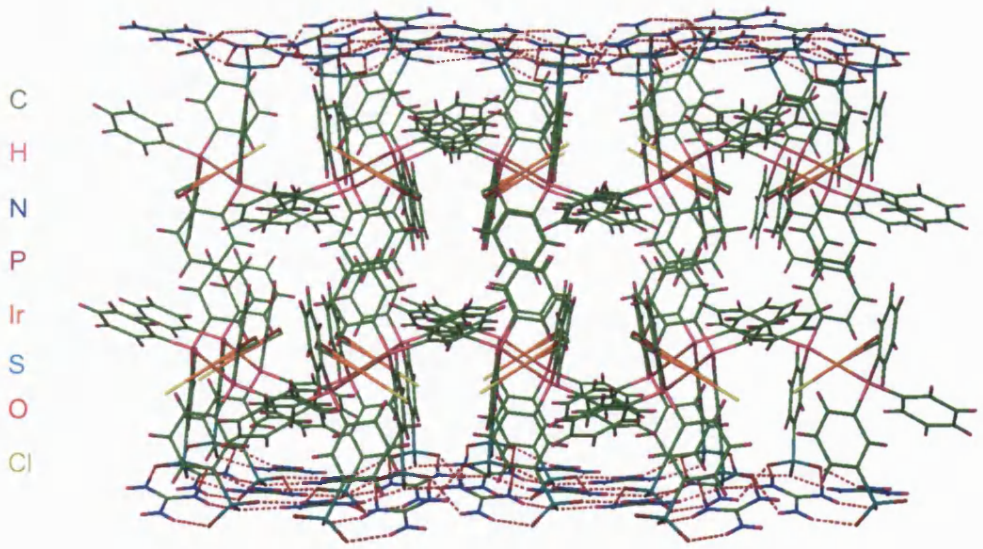

Figure 2.22; bilayer formation in **8**

D–H···A	D···A /Å	H···A /Å	D–H···A /°	Symmetry operation generating D···A
N(1)–H(1A)···O(1)	2.873(6)	2.03	164	*x*, *y*, *z*
N(1)–H(1B)···O(5)	3.052(6)	2.20	167	*x*-1, *y*, *z*
N(2)–H(2A)···O(2)	3.029(6)	2.20	160	*x*, *y*, *z*
N(2)–H(2B)···O(6)	2.986(5)	2.12	176	*x*-½, -*y*+½, *z*
N(3)–H(3A)···O(4)	2.892(6)	2.02	179	*x*-½, -*y*+½, *z*
N(3)–H(3B)···O(6)	2.998(6)	2.22	149	x-*1*, *y*, *z*
N(4)–H(4A)···O(4)	2.902(6)	2.07	160	*x*, *y*, *z*
N(4)–H(4B)···O(2)	2.988(6)	2.12	177	*x*, *y*, *z*
N(5)–H(5A)···O(5)	3.258(6)	2.44	158	*x*, *y*, *z*
N(5)–H(5B)···O(3)	3.192(6)	2.55	131	*x*+½, -*y*-½, *z*
N(6)–H(6A)···O(1)	2.906(6)	2.05	170	*x*+½, -*y*-½, *z*
N(6)–H(6B)···O(3)	2.886(6)	2.03	167	*x*, *y*, *z*

Table 2.9; details of the hydrogen bonding in **8**

$[MeGu]_2[IrCl(CO)(mTPPMS)_2]\cdot{}^3/_8H_2O$: $[C(NH_2)_2(NHMe)]_2\{$*trans*-$[IrCl(CO)(PPh_2C_6H_4SO_3\text{-}3)_2]\}\cdot{}^3/_8H_2O$ **9**

Asymmetric Unit

The asymmetric unit of **9** consists of four $[MeGu]^+$ cations, two $[IrCl(CO)(mTPPMS)_2]^{2-}$ anions and a 0.75 molecule of water as shown in Figure 2.23. There is disorder in the carbonyl groups and chlorides in the ratio 80:20 between sites C(1), O(1) and Cl(1) and C(1A), O(1A) and Cl(1A) respectively, and in the ratio 75:25 between C(38), O(2), Cl(2), and C(38A), O(2A) and Cl(2A). The water molecule is also disordered in a 50:25 ratio between positions O(15A) and O(15B). The atoms of the minor portions of the disordered water, carbonyl and chloride ligands were refined isotropically in the least squares cycles. The positions of the hydrogen atoms in the water molecule could not be determined.

Initially, it seemed that there were two space group possibilities for this compound, *Pcca* and $P2_1ca$. However, close scrutiny revealed that the absence pertaining to a possible *c* glide perpendicular to *a* is not upheld, although the intensities of the *0kl*, $l=2n+1$ reflections are systematically weak.

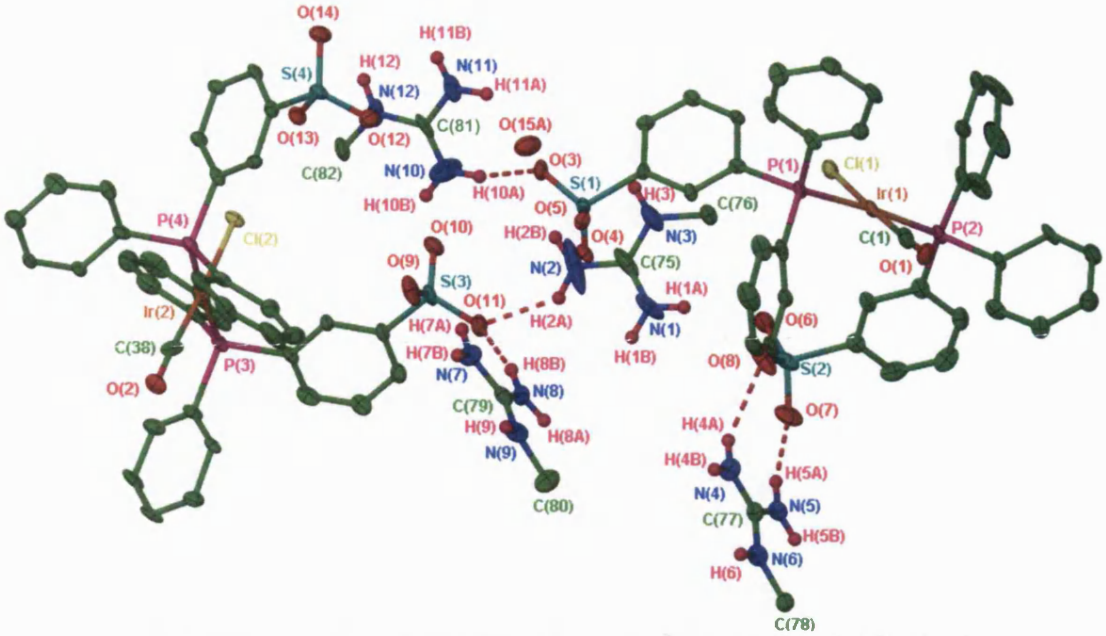

Figure 2.23; asymmetric unit in **9**. Ellipsoids are depicted at 30% probability level.
(*minor disordered fractions and some hydrogen atoms omitted for clarity*)

Extended Structure

The four cations have each lost an N–H donor due to methyl substitution. The formation of a hexagonal sheet is not observed, however a sheet is formed through hydrogen bonds incorporating the cations, anions and water molecules. The cations based on C(77) and C(79) are approximately coplanar with the oxygen atoms based on the sulfonates containing S(1) and S(2) and those containing S(3) and S(4), respectively. The unsubstituted faces of the cations based on C(77) form DD:AA hydrogen bonds with the sulfonates based on S(1) and S(2), and those on the cation based on (C79) form similar interactions with the sulfonates based on S(3) and S(4). The remaining N–H donors [N(5)–H(5A) and N(8)–H(8A)] of the substituted faces of each cation form a single hydrogen bond to a neighbouring sulfonate oxygen atom (see Figure 2.24).

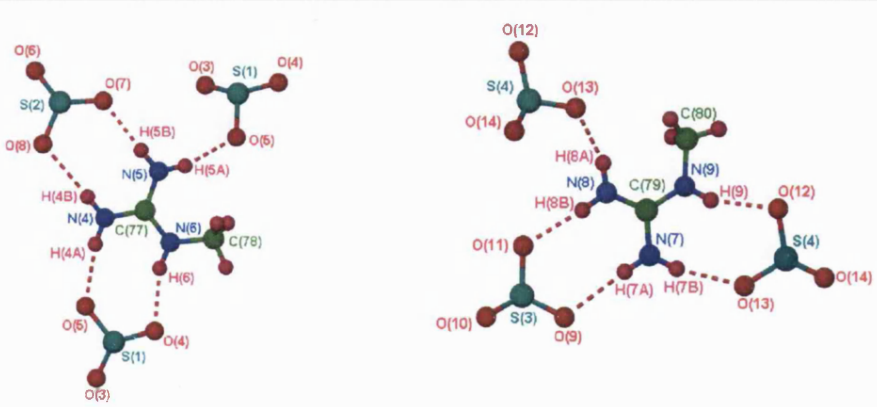

Figure 2.24; the hydrogen bonds formed by the cations based on C(77) and C(79)

However, the remaining cations based on C(75) and C(81) are almost perpendicular to the planes of the sulfonate oxygen atoms, and are not involved in any DD:AA hydrogen bonds. One of the unsubstituted faces of each cation forms a $R_2^1(6)$ motif with a neighbouring sulfonate oxygen atom, whereas the donors of the remaining unsubstituted and substituted cation faces each form single hydrogen bonds, either with neighbouring sulfonate oxygen atoms or lattice waters (see Figure 2.25).

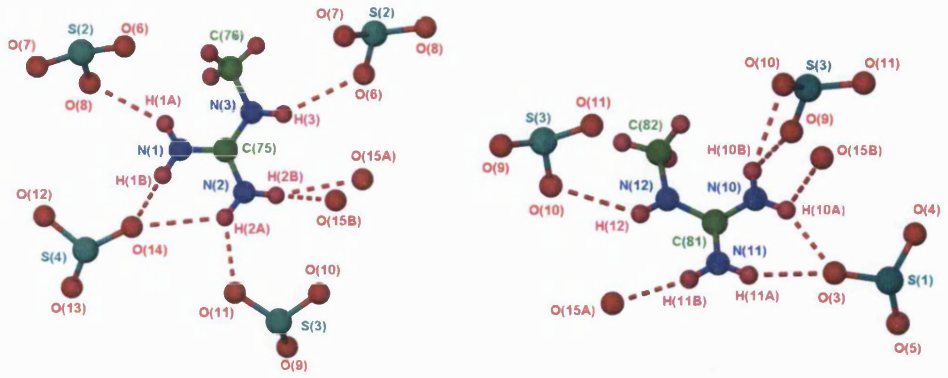

Figure 2.25; hydrogen bonds formed by the cations based on C(75) and C(81)

Two cations, related approximately parallel and perpendicular respectively to the sulfonate oxygen atoms, form hydrogen bonds with the sulfonates forming a two-dimensional array. The cations containing C(75) and C(77) form hydrogen bonds with the sulfonates based on S(1) and S(2) linking them into sheets (Figure 2.23) where all of the anions are directed to the same side. The cations containing C(79) and C(81) form hydrogen bonds with the sulfonates containing S(3) and S(4) to form a similar sheet (see Figure 2.26) and the anions are also directed to one side.

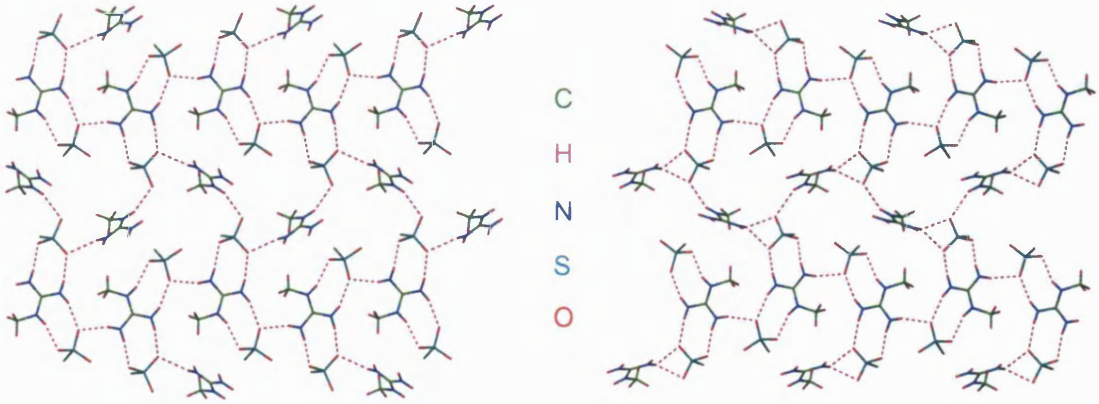

Figure 2.26; sheet formed by cations containing C(75) and C(77) and anion based on S(1) and S(2) (*left*) and sheet formed by cations containing C(79) and C(81) and anion based on S(3) and S(4) (*right*)

These two sheets are almost parallel to each other. The cations based on C(75) and C(81) form hydrogen bonds with the sulfonate oxygen atoms, linking the two sheets into a single and complex two-dimensional array (Figure 2.27).

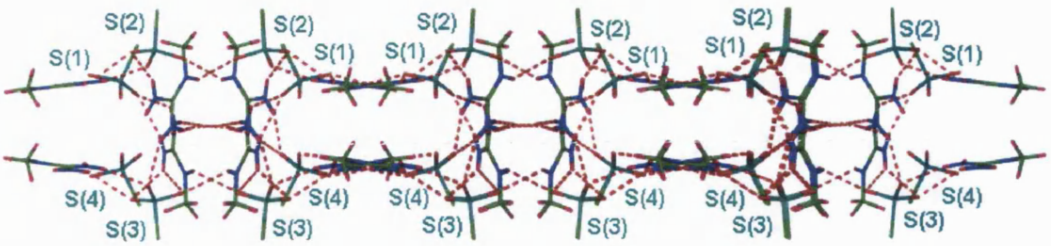

Figure 2.27; side view of the complex sheet formed in **9**
(*most of the anions are removed for clarity*)

The lattice water acts as a hydrogen bond acceptor forming hydrogen bonds with the cations reinforcing the complex array observed. There may be hydrogen bonds from the lattice water to the sulfonate oxygen atoms, however this cannot be determined as the water hydrogen atoms could not be located. However, the the D···A distances between the water oxygen atoms and proximate acceptor groups indicate the presence of possible interactions [O(15B)···O(3) 3.18(2)Å, O(15A)···O(10) 3.42(2)Å, O(15A)···O(14) 3.25(2)Å, O(15A)···O(6) 3.04(2)Å, O(15B)···O(10) 2.95(2)Å]. Details of the hydrogen bonds are given in Table 2.10.

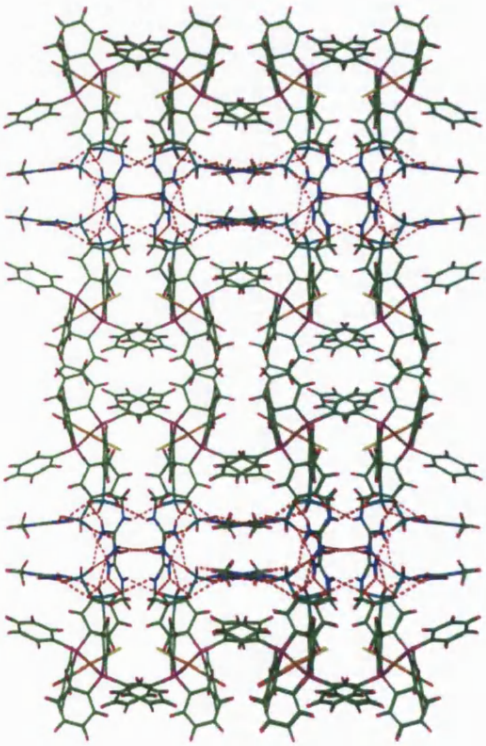

Figure 2.28; *pseudo*-bilayers formed in **9**

The anions are directed to both sides of this complex sheet, forming a *pseudo*-bilayer in the extended structure (Figure 2.28). There is a small degree of interdigitation between neighbouring anions, however this is minimal due to the large bulk of the sulfonate substituents. There are weak face-to-face and edge-to-face interactions between neighbouring phenyl rings.

D–H···A	D···A /Å	H···A /Å	D–H···A /°	Symmetry operation generating D···A
N(1)–H(1A)···O(8)	3.17(2)	2.39	148	*x*, *y*, *z*
N(1)–H(1B)···O(14)	2.88(1)	2.03	161	*x*, *y*, *z*+1
N(2)–H(2A)···O(11)	2.81(1)	2.11	136	*x*, *y*, *z*
N(2)–H(2A)···O(14)	3.23(2)	2.53	138	*x*, *y*, *z*+1
N(2)–H(2B)···O(15A)	3.26(3)	2.41	164	*x*, *y*, *z*
N(2)–H(2B)···O(15B)	2.55(3)	1.72	156	*x*, *y*, *z*
N(3)–H(3)···O(6)	3.25(1)	2.46	150	*x*, -*y*, *z*-½
N(4)–H(4A)···O(8)	3.14(1)	2.34	152	*x*, *y*, *z*
N(4)–H(4B)···O(5)	2.94(1)	2.12	156	*x*, -*y*+1, *z*+½
N(5)–H(5A)···O(7)	2.83(1)	1.97	167	*x*, *y*, *z*+1
N(5)–H(5B)···O(5)	2.85(1)	2.00	161	*x*, *y*, *z*
N(6)–H(6)···O(4)	2.86(1)	2.01	162	*x*, -*y*+1, *z*+½
N(7)–H(7A)···O(9)	3.13(1)	2.32	154	*x*, *y*, *z*
N(7)–H(7B)···O(13)	2.88(1)	2.03	164	*x*, -*y*+1, *z*+½
N(8)–H(8A)···O(13)	2.89(1)	2.09	151	*x*, *y*, *z*+1
N(8)–H(8B)···O(11)	2.92(1)	2.06	166	*x*, *y*, *z*
N(9)–H(9)···O(12)	2.80(1)	1.97	158	*x*, -*y*+1, *z*+½
N(10)–H(10A)···O(3)	2.82(1)	2.04	147	*x*, *y*, *z*
N(10)–H(10A)···O(15B)	2.60(1)	2.15	110	*x*, *y*, *z*
N(10)–H(10B)···O(10)	3.03(1)	2.35	135	*x*, *y*, *z*
N(10)–H(10B)···O(9)	3.13(1)	2.39	141	*x*, *y*, *z*
N(11)–H(11A)···O(3)	3.06(1)	2.37	135	*x*, *y*, *z*
N(11)–H(11B)···O(15A)	3.05(2)	2.19	168	*x*, -*y*, *z*-½
N(12)–H(12)···O(10)	3.36(1)	2.64	139	*x*, -*y*, *z*-½

Table 2.10; details of the hydrogen bonding in **9**

2.4.1 The structural effects of alkyl substitution in guanidinium ions when crystallised with the sulfonated phosphine complexes

The extended structures in both compounds $[Gu]_2[IrCl(CO)(mTPPMS)_2]$ **8** and $[MeGu]_2[IrCl(CO)(mTPPMS)_2]\cdot{}^3/_8H_2O$ **9** show similarities, with bilayers and *pseudo*-bilayers observed respectively in the gross structures. The structure of $[Gu]_2\{cis\text{-}[PdCl_2(mTPPMS)_2]\}$ **A** has been reported by Burrows *et al*[1]. In all three compounds, the sulfonate groups of each complex anion are directed into the same GS sheet. However, the gross structures exhibited by **8** and **9** are different to that seen in **A**.

The compound $[Gu]_2\{cis\text{-}[PdCl_2(mTPPMS)_2]\}$ **A** contains two cations and one anion in the asymmetric unit. Both of the sulfonates from each complex anion are directed into the same plane, where they form hydrogen bonds with the cations linking them into sheets. There is also hydrogen bond formation between one of the N–H donors of the cation and one of the chlorides. The sulfonate substituents are directed to both sides, to yield interdigitating single layers in the extended array (Figure 2.29).

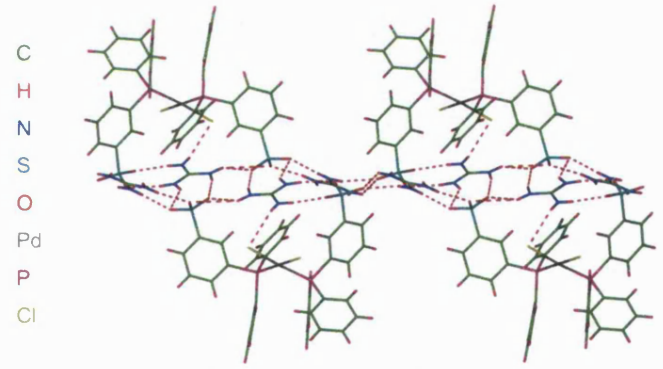

Figure 2.29; single layer formed in $[Gu]_2\{cis\text{-}[PdCl_2(mTPPMS)_2]\}$

The gross structures observed in the compounds $[Gu]_2[IrCl(CO)(mTPPMS)_2]$ **8** and $[MeGu]_2[IrCl(CO)(mTPPMS)_2]\cdot{}^3/_8H_2O$ **9** are very different to that seen in $[Gu]_2\{cis\text{-}[PdCl_2(mTPPMS)_2]\}$ **A**. The most obvious difference is that the regular hexagonal hydrogen bonded sheet is observed in **8**, whereas this is not the case in **9** or **A**.

Compounds **8** and **9** form repeating bilayers (or *pseudo*-bilayers), whereas **A** forms repeating single layers. The single layer arrangement seen in **A** is to be expected as the width of the sulfonate substituent is much larger than 4.75Å, the value derived by Ward to predict the formation of single layers in preference to bilayers[8]. It is possible that compounds **8** and **9** form bilayers due to the *trans* arrangement of the phosphines, whereas in **A** the phosphines are *cis* to each other, as this is the only major structural difference between the anions. There are also hydrogen bonds between an N–H donor of a cation and one of the chlorides in **A**, whereas this is not the case in compounds **8** or **9** as the *trans* arrangement of the $[mTPPMS]^-$ groups leads to the chlorides being remote from the cation N–H donors.

In compound **8** there is a S···S distance of 7.6Å within the same complex anion. This creates an ideal space for a guanidinium cation to occupy, where it can form DD:AA hydrogen bonds with both sulfonate groups leading to hexagonal sheets. It is notable that both sulfonate groups of the complex anion form hydrogen bonds to the same cation, leading to a chelating effect between the anion and cation. However, this chelation is not observed in compounds **9** or **A**. This results from the fact that the plane of the cation is almost perpendicular to that of the sulfonate oxygen atoms in **9**, while the *cis* orientation of the sulfonates in **A** increases the distance between the sulfonate oxygen atoms and the cation donors.

2.5 The overall effects of alkyl substitution in guanidinium ions when crystallised with triphenylphosphine-monosulfonate, triphenylphosphine-monosulfonate oxide and a sulfonated derivative of Vaska's compound

The extended structures observed in [Gu][mTPPMS] **I**, [MeGu][mTPPMS] **1**, and [EtGu][mTPPMS] **2** are remarkably similar, revealing that the substitution of the cation in compounds **1** and **2** does not significantly affect the overall array. All three compounds form a regular or adapted hexagonal sheet, though using different graph sets. However, sheets are not observed in **3**, where independent ribbons are formed instead. There are also different phenyl embrace interactions between the $[mTPPMS]^-$ units in the structures; in **I** and **3** there is a 6PE, whereas **1** and **2** (which are isostructural) exhibit a 4PE. This suggests that the formation of the hexagonal sheets in **1** and **2** takes precedence over the type of phenyl embrace formed in the $[mTPPMS]^-$ series.

The two $[mTPPMSO]^-$ structures, [EtGu][mTPPMSO] **6** and [DiMeGu][mTPPMSO]·H_2O **7**, are very different. In compound **6** ribbons are formed by DD:AA hydrogen bonds and are linked into a two dimensional array through hydrogen bonding incorporating the P=O group. However, in **7** a type of pillared brick array is formed where the P=O group and water molecules are involved in the formation of sheets. The presence of the P=O group has had a major effect on the structures formed. The unsubstituted cation faces in both compounds **6** and **7** form DD:AA hydrogen bonds with the sulfonates. However, the substituted cation face in **6** forms hydrogen bonds with the P=O group, whereas in **7** the substituted cation face forms interactions with the P=O group and molecules of water.

All of the unsubstituted faces of the cations in the $[mTPPMS]^-$ and $[mTPPMSO]^-$ compounds form the DD:AA hydrogen-bonded motif with the sulfonates generating the graph set $R_2^2(8)$. This finding may be used as a predicting tool for synthesis of further substituted guanidinium sulfonate materials. However, it is not infallible and more results are required to investigate this further.

The inclusion of a hydrogen bond acceptor or donor competing functionality has previously been seen to disrupt the hexagonal hydrogen-bonded array. The compounds [Gu][1-$HO_2CC_6H_4SO_3$-4][9] and [Gu][1-$HO_2CC_6C_4SO_3$-3][10] have been reported and both have additional hydrogen bond donors and acceptors in the $-CO_2H$ functionality. These

compounds do not exhibit regular hexagonal sheets, but ribbons are formed via DD:AA hydrogen bonds between two of the cation faces and the sulfonates. The third cation face in each compound forms DD:A hydrogen bonds with an acceptor atom of the carboxylic acid, linking the ribbons into two-dimensional arrays. These hydrogen bonding motifs are also observed in the compound [Gu][1,2-(OH)(CO_2H)$C_6H_3SO_3$-4][11].

However, the inclusion of competing moieties does not inevitably lead to disruption of the hexagonal sheet. The compounds [Gu][1-$NO_2C_6H_4SO_3$-4][9], [Gu][1-$NO_2C_6H_4SO_3$-3][12] and [Gu][1-$NO_2C_6H_4SO_3$-2][12] have been reported by Ward *et al* and each have two additional acceptor atoms in the NO_2 group that could compete for hydrogen bond formation with the sulfonate groups. However, all of these compounds exhibit the formation of regular hexagonal hydrogen-bonded sheets and no N–H···O hydrogen bonds are observed between the cations and the NO_2 groups. There are weak C–H···O hydrogen bonds formed to these functional groups from the C–H donors of the phenyl ring in the anion.

The two metal-containing compounds [Gu]$_2$[IrCl(CO)(mTPPMS)$_2$] **8** and [MeGu]$_2$[IrCl(CO)(mTPPMS)$_2$]·$^3/_8H_2O$ **9** form bilayers in the extended structure with both of the sulfonate groups directed into the same layer. However, in **8** the hexagonal GS array is observed, whereas this is not the case in **9** and water molecules are incorporated into the sheet. As seen in the [mTPPMS]$^-$ and [mTPPMSO]$^-$ structures, all of the DD faces of each cation in **8** form DD:AA hydrogen bonds with the sulfonates. However, in **9** DD:AA hydrogen bonds are observed in only two of the four cations via the unsubstituted faces, whereas the unsubstituted faces of the remaining cations form single hydrogen bonds.

2.5.1 The effects of alkyl substitution in guanidinium cations on bond and hydrogen bond parameters in triphenylphosphine-sulfonate compounds

In the $[mTPPMS]^-$ series, the DD:AA hydrogen bond distances (N···O) vary between 2.972(10)Å – 3.061(12)Å in [Gu][mTPPMS] **I**, 2.847(3)Å – 3.054(3)Å in [MeGu][mTPPMS] **1**, 2.828(3)Å – 3.030(3)Å in [EtGu][mTPPMS] **2** and 2.885(2)Å – 2.963(2)Å in [DiMeGu][mTPPMS] **3**. The mean hydrogen bond distances are 3.022(12)Å in **I**, 2.888(3)Å in **1**, 2.951(3)Å in **2** and 2.877(2)Å in **3**. The mean distance in **I** is longer than those observed in **1**, **2** and **3**, suggesting that hydrogen bond strength has increased on cation substitution. However, it should be noted that data were collected at 296 K for **I**, 293 K for **2** and 150 K for **1** and **3**.

In the $[mTPPMSO]^-$ and $[IrCl(CO)(mTPPMS)_2]^{2-}$ series the DD:AA hydrogen bond distances vary between 2.879(2)Å – 2.992(2)Å in [EtGu][mTPPMSO] **6**, 2.850(3)Å – 2.928(3)Å in $[DiMeGu][mTPPMS]\cdot H_2O$ **7**, 2.872(6)Å – 3.256(6)Å in $[Gu]_2[IrCl(CO)(mTPPMS)_2]$ **8** and between 2.81(1)Å – 3.15(1)Å in $[MeGu]_2[IrCl(CO)(mTPPMS)_2]\cdot{}^3/_8H_2O$ **9**. The mean hydrogen bond distances are 2.897(2)Å, 2.889(3)Å, 2.997(6)Å and 2.94(1)Å for **6**, **7**, **8**, and **9** respectively. The mean distances in the $[mTPPMSO]^-$ compounds are similar, as are those in the $[IrCl(CO)(mTPPMS)_2]^{2-}$ compounds, suggesting that the hydrogen bond strength is not affected by substitution of the cation.

The C–N bond lengths in the cation and the S–O bond lengths of the anion are similar in structures **1**, **2**, **3**, **6**, **7**, **8** and **9** revealing that variation in the cation and anion does not affect these parameters. The N–C–N and O–S–O bond angles are also unaffected.

2.5.2 Future Work

Despite several attempts, the reactions of GuCl and MeGuCl with Na[mTPPMSO] did not yield single crystals or powder of the desired products, and neither did the reactions of $[EtGu]_2SO_4$ and $[DiMeGu]_2SO_4$ with $Na_2[IrCl(CO)(mTPPMS)_2]$. The first goal would be to find other crystallisation techniques to try and isolate these compounds, on the basis of the number of structures reported in this chapter and their associated differences it is difficult to extract any specific structure predicting tools. Therefore, the additional GS structures must be determined so that they can be compared to those reported here and overall conclusions made about the hydrogen-bonding arrays.

One of the original goals of this thesis was to use a metal containing disulfonate to bridge between two GS sheets, so that solid state chemistry could be undertaken at the metal centre. However, the metal-containing compounds $[Gu]_2[IrCl(CO)(mTPPMS)_2]$ **8** and $[MeGu]_2[IrCl(CO)(mTPPMS)_2]\cdot{}^3/_8H_2O$ **9** crystallised with both of the sulfonate groups of each anion directed into a single sheet, and bilayers were observed. Therefore the use of alternative phosphine ligands must be investigated to ascertain if the sulfonate orientation in the ligand directs the single layer or bilayer arrangement of *trans*-directed phosphines in the solid state. To this end, $Na_2\{$*trans*-$[IrCl(CO)($*ortho*-$TPPMS)_2]\}$ and $Na_2\{$*trans*-$[IrCl(CO)($*para*-$TPPMS)_2]\}$ will be prepared and crystallised with the guanidinium salts to ascertain if metal bridged GS arrays can be isolated. The synthesis of Na[pTPPMS] was attempted in the course of this work and crystallisation reactions carried out with the guanidinium salts. The desired products were not obtained in the initial experiments, though time constraints made it impossible to fully explore these reactions.

The incorporation of the disulfonated ligand $[mTPPDS]^{2-}$, $[PPh(C_6H_4SO_3\text{-}3)_2]^{2-}$, into GS arrays was also investigated briefly, however the desired products could not be obtained. The compound $Na_4\{$*trans*-$[IrCl(CO)($*meta*-$TPPDS)_2]\}$ is less likely to form GS compounds with all four sulfonates directed into the same sheet when crystallised with the guanidinium salts, due to the orientation and steric bulk of the sulfonate groups. Therefore this avenue of investigation merits further attention in the quest to synthesise materials with metal-bridged GS sheets.

It is also possible that the inclusion of guest solvent molecules might force the formation of a pillared brick array where the sulfonate groups are each directed into different sheets, with pores present in the structure occupied by these guests. Removal of such solvent from the single crystals while maintaining the GS array might facilitate the inclusion of small gas molecules, for example SO_2 and CO, such that solid-state chemistry could occur at the metal centre.

2.6 Experimental

Guanidinium chloride, $[C(NH_2)_3]Cl$, methylguanidinium chloride, $[C(NH_2)_2(NHMe)]Cl$, ethylguanidinium sulfate, $[C(NH_2)_2(NHEt)]_2SO_4$ and *N,N*-dimethylguanidinium sulfate, $[C(NH_2)_2(NMe_2)]_2SO_4$ were purchased from Aldrich Chemical Co. The sulfonated phosphines Na[mTPPMS], $Na[PPh_2C_6H_4\text{-}3\text{-}SO_3]$ and $Na_2[IrClCO(mTPPMS)_2]$, $Na_2[IrClCO(PPh_2C_6H_4\text{-}3\text{-}SO_3)_2]$ were prepared following the literature methods[13, 14]. The oxidised ligand Na[mTPPMSO], $Na[OPPh_2C_6H_4\text{-}3\text{-}SO_3]$, was prepared via the oxidation of Na[mTPPMS][15] with hydrogen peroxide. Microanalysis (C, H and N) were carried out by Mr. Alan Carver (University of Bath Microanalytical Service). It is notable that the microanalysis results repeatedly showed lower than anticipated percentages of carbon, hydrogen and nitrogen. This may be the result of the presence of impurities, or be a consequence of incomplete combustion.

Synthesis of [MeGu][mTPPMS] 1

A solution of $[C(NH_2)_2(NHMe)]Cl$ (0.027g, 0.25mmol) in methanol ($2cm^3$) was added to a solution of $Na[PPh_2C_6H_4\text{-}3\text{-}SO_3]$ (0.100g, 0.25mmol) in methanol ($5cm^3$) and allowed to slowly evaporate. Small colourless crystals of $[C(NH_2)_2(NHMe)][PPh_2C_6H_4\text{-}3\text{-}SO_3]$ **1** were collected. Calc for $C_{20}H_{22}N_3PO_3S$: C, 57.8; H, 5.34; N, 10.11. Found: C, 56.4; H, 5.16; N, 9.90%. There are peaks present in the powder diffraction pattern that are not present in the powder pattern simulated from single crystal data, which confirm the presence of a small amount of MeGuCl in the bulk material.

Synthesis of [EtGu][mTPPMS] 2

A solution of $[C(NH_2)_2(NHEt)]_2SO_4$ (0.034g, 0.12mmol) in methanol ($5cm^3$) was added to a solution of $Na[PPh_2C_6H_4\text{-}3\text{-}SO_3]$ (0.100g, 0.25mmol) in methanol ($5cm^3$) and allowed to slowly evaporate. Small colourless crystals of $[C(NH_2)_2(NHEt)][PPh_2C_6H_4\text{-}3\text{-}SO_3]$ **2** were collected. Calc for $C_{21}H_{24}N_3PO_3S$: C, 58.7; H, 5.63; N, 9.78. Found: C, 57.5; H, 5.61; N, 9.74%. The powder diffraction pattern is consistent with the simulated powder pattern confirming that the single crystal is representative of the bulk material.

Synthesis of [DiMeGu][mTPPMS] 3

A solution of $[C(NH_2)_2(NMe_2)]_2SO_4$ (0.034g, 0.12mmol) in methanol ($5cm^3$) was added to a solution of $Na[PPh_2C_6H_4\text{-}3\text{-}SO_3]$ (0.100g, 0.25mmol) in methanol ($5cm^3$) and allowed to slowly evaporate. Small colourless crystals of $[C(NH_2)_2(NMe_2)][PPh_2C_6H_4\text{-}3\text{-}SO_3]$ **3** were collected. Calc for $C_{21}H_{24}N_3PO_3S$: C, 58.7; H, 5.63; N, 9.8. Found: C, 52.6; H, 6.01; N, 8.41%. The powder diffraction pattern is consistent with the simulated powder pattern confirming that the crystalline bulk material is the same compound as that observed from the crystal structure. It is possible that an amorphous impurity is present in the bulk material.

Synthesis of [EtGu][mTPPMSO] 6

A solution of $[C(NH_2)_2(NHEt)]_2SO_4$ (0.033g, 0.12mmol) in water ($2cm^3$) was added to a solution of $Na[OPPh_2C_6H_4\text{-}3\text{-}SO_3]$ (0.100g, 0.24mmol) in water ($4cm^3$) and allowed to slowly evaporate. Small colourless crystals of $[C(NH_2)_2(NHEt)][OPPh_2C_6H_4\text{-}3\text{-}SO_3]$ **6** were collected. Calc for $C_{21}H_{24}N_3PO_4S$: C, 56.6; H, 5.43; N, 9.4. Found: C, 49.6; H, 5.27; N, 10.9%. The microanalysis results are reproducibly poor. However, the powder diffraction pattern and simulated pattern show good agreement. An amorphous impurity may be present in the bulk material.

Synthesis of [DiMeGu][mTPPMSO]·H_2O 7

A solution of $[C(NH_2)_2(NMe_2)]_2SO_4$ (0.033g, 0.12mmol) in water ($2cm^3$) was added to a solution of $Na[OPPh_2C_6H_4\text{-}3\text{-}SO_3]$ (0.100g, 0.24mmol) in water ($4cm^3$) and allowed to slowly evaporate. Small colourless crystals of $[C(NH_2)_2(NMe_2)][OPPh_2C_6H_4\text{-}3\text{-}SO_3]$ **7** were collected. Calc for $C_{21}H_{26}N_3PO_5S$: C, 54.4; H, 5.65; N, 9.07. Found: C, 53.4; H, 5.47; N, 9.03%. The powder diffraction pattern reveals the presence of a small amount $(DiMeGu)SO_4\cdot H_2O$ in the bulk material.

Synthesis of $[Gu]_2[IrClCO(mTPPMS)_2]$ 8

A solution of $C(NH_2)_3Cl$ (0.043g, 0.45mmol) in degassed methanol (3 cm^3) was added to a solution of $Na_2[IrClCO(PPh_2C_6H_4SO_3\text{-}3)_2]$ (0.100g, 1.00mmol) in degassed methanol (1 cm^3) under an inert atmosphere. The sealed vessel containing the reaction mixture, under nitrogen, was then left in the fridge to crystallise. After approximately one month small yellow crystals of $[C(NH_2)_3][IrClCO(PPh_2C_6H_4SO_3\text{-}3)_2]$ **8** were collected. Calc for $C_{39}H_{40}N_6P_2O_7S_2IrCl$: C, 44.3; H, 3.81; N, 7.9. Found: C, 43.2; H, 3.78; N, 7.6%. The powder pattern and powder diffraction patterns show good agreement confirming the single crystal is representative of the bulk material.

Synthesis of $[MeGu]_2[IrClCO(mTPPMS)_2]\cdot{}^3/_8H_2O$ 9

A solution of $[C(NH_2)_2(NHMe)]Cl$ (0.049g, 0.48mmol) in degassed methanol (3 cm^3) was added to a solution of $Na_2[IrClCO(PPh_2C_6H_4SO_3\text{-}3)_2]$ (0.100g, 1.00mmol) in degassed methanol (1 cm^3) under an inert atmosphere. Hexane was then gently layered onto the reaction mixture. The sealed vessel containing the reaction mixture, under nitrogen, was then left to crystallise. After approximately one month small yellow crystals of $[C(NH_2)_2(NHMe)]_2[IrClCO(PPh_2C_6H_4SO_3\text{-}3)_2]\cdot{}^3/_8H_2O$ **9** were collected. Calc for $C_{41}H_{45}N_6P_2O_{7.375}S_2IrCl$: C, 45.1; H, 4.06; N, 7.69. Found: C, 42.2; H, 4.12; N, 7.76%. The powder diffraction pattern and simulated pattern show good agreement.

2.7 References

[1] A. D. Burrows, M. F. Mahon, R. W. Harrington, S. J. Teat, *Eur. J. Inorg. Chem.*, 2003, 1433; R. W. Harrington, PhD Thesis, University of Bath, 2002

[2] A. Katho, A. C. Benyei, F. Joo, M. Sagi, *Adv. Synth. Catal.*, 2002, 278

[3] L. Vaska, *Science*, 1966, 152, 769, S. J. Placa, J. A. Ibers, *Inorg. Chem.*, 1966, 5, 405

[4] S. K. Hasnip, S. B. Duckett, C. J. Sleigh, D. R. Taylor, G. K. Barlow, M. J. Taylor, *Chem. Commun.*, 1999, 1717

[5] B. L. Booth, K.-S. Li, C. A. McAuliffe, *J. Chem. Soc., Dalton Trans.*, 1987, 2959; O. El-Sayrafi, G. A. Gott, D. G. Kelly, C. A. McAuliffe, P. P. MacRory, *Inorg. Chim. Acta.*, 1990, 174, 165

[6] A. D. Burrows, J. C. Machell, D. M. P. Mingos, *J. Chem. Soc., Dalton Trans.*, 1992, 1939

[7] M. Albrecht, R. A. Gossage, A. L. Spek, G. van Koten, *Chem. Commun.*, 1998, 1003; M. Albrecht, R. A. Gossage, M. Lutz, A. L. Spek, G. van Koten, *Chem. Eur. J.*, 2000, 6, 1431; M. Albrecht, M. Lutz, A. M. M. Schreurs, E. T. H. Lutz, A. L. Spek, G. van Koten, *J. Chem. Soc., Dalton Trans.*, 2000, 3797

[8] V. A. Russell, C. C. Evans, W. Li, M. D. Ward, *Science*, 1997, 276, 575

[9] V. A. Russell, M. C. Etter, M. D. Ward, *Chem. Mater.*, 1994, 1206

[10] V. V. Adrabinska, I. T. Tyrk, T. Borowiak, G. Dutkiewicz, *New. J. Chem.*, 2001, 1403

[11] X.-L. Zhang, X.-M. Chen, S. W. Ng, *Acta. Cryst. E.*, 2004, 453

[12] V. A. Russell, M. D. Ward, *J. Mater. Chem.*, 1997, 1123

[12] F. Joo, J. Kovacs, A. Katho, A. C. Benyei, T. Decuir, D. J. Darensbourg, *Inorganic Synthesis* 32

[14] H. Sertchook, *J. Mol. Cat. A: Chemical*, 1996, 108, 153

[15] D. Sinou, D. Maillard, G. Pozzi, *Eur. J. Chem.* 2002, 269

CHAPTER 3

The reactions of organic sulfonates and guanidinium and substituted guanidinium derivatives

3.0 Introduction

A series of guanidinium sulfonate compounds containing mono- and disulfonates and the unsubstituted guanidinium cation have been reported by Ward *et al*, and the regular hexagonal or shifted GS sheet is observed in all of these compounds (see Chapter 1, section 1.3).

In this chapter, the inclusion of substituted guanidinium cations into the GS array is investigated to ascertain if the hexagonal (or shifted) GS sheet structure can be maintained when the number of N–H donors on the cation is reduced. Thus, the sulfonates shown in Figure 3.1 have been crystallised with the substituted guanidinium salts MeGuCl, $(EtGu)_2SO_4$ and $(DiMeGu)_2SO_4$ and the results are discussed and compared with the analogous unsubstituted guanidinium-sulfonate compounds.

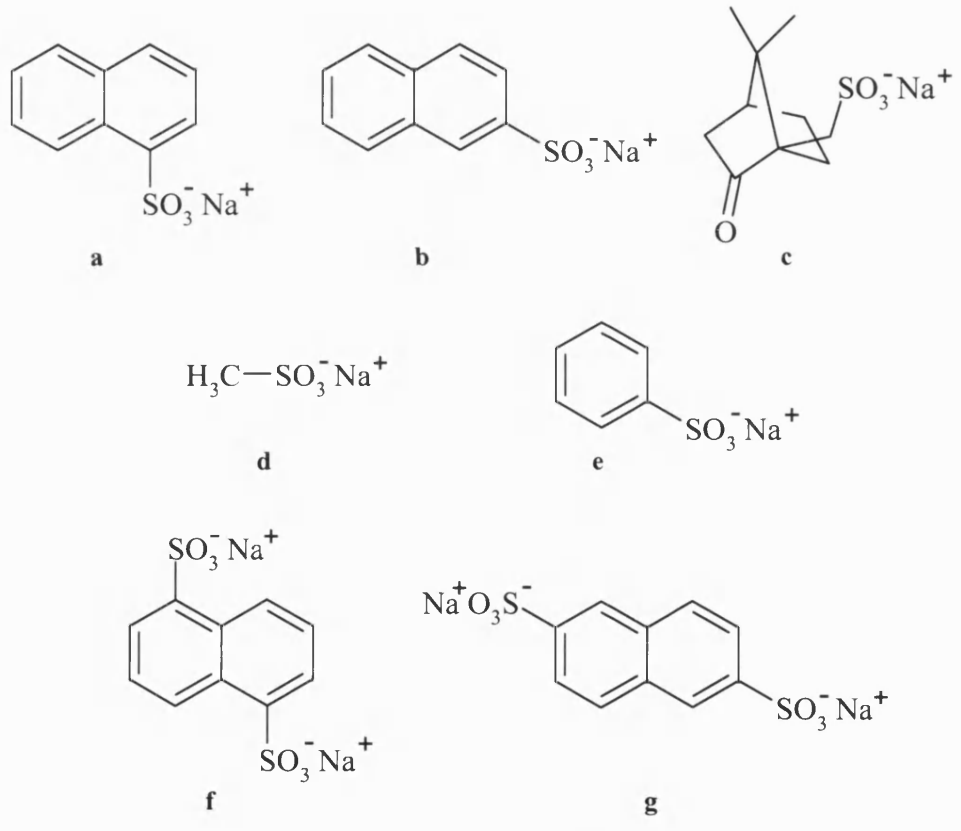

Figure 3.1, structures of the sodium salts of;
a) 1-naphthalenesulfonate (1-NapSO_3), b) 2-naphthalenesulfonate (2-NapSO_3), **c**)10-camphorsulfonate (10-CamphorSO_3), **d**) methylsulfonate (MeSO_3), **e**) phenylsulfonate (PhSO_3), **f**) 1,4-naphthalenedisulfonate (1,4-Nap$(SO_3)_2$), **g**) 2,6-naphthalenedisulfonate (2,6-Nap$(SO_3)_2$)

3.1 Reactions of mono- and disulfonates with substituted guanidinium cations

The substituted guanidinium cations were reacted in a 1:1 molar ratio with the sulfonate anions. The guanidinium chloride or sulfate and sodium sulfonate were each dissolved in methanol, mixed together and the solvent allowed to slowly evaporate. The same reactions were also carried out in water.

All of the structure determinations have been carried out using single crystal X-ray crystallography. Where crystals were not produced, either no solid precipitate was observed or the starting materials were isolated as powder or single crystals. In some cases, single crystals were formed from both methanol and water. In these instances, X-ray data were collected from both sets of crystals to verify that the same product was observed. In reactions where powder precipitates were formed as opposed to single crystals, these powders were subjected to microanalysis and X-ray powder diffraction. The results of the latter were compared with the analogous powder pattern as simulated from the single crystal X-ray data.

Crystals of the following compounds were formed and their structures are described (crystallographic data are given in Tables 3.1, 3.2 and 3.3);

12: [MeGu][1-NapSO$_3$] : [C(NH$_2$)$_2$(NHMe)][C$_{10}$H$_7$SO$_3$-1]
13: [EtGu][1-NapSO$_3$]·H$_2$O : [C(NH$_2$)$_2$(NHEt)][C$_{10}$H$_7$SO$_3$-1]·H$_2$O
14: [DiMeGu][1-NapSO$_3$]·H$_2$O : [C(NH$_2$)$_2$(NMe$_2$)][C$_{10}$H$_7$SO$_3$-1]·H$_2$O
15: [MeGu][2-NapSO$_3$] : [C(NH$_2$)$_2$(NHMe)] [C$_{10}$H$_7$SO$_3$-2]
16: [EtGu][2-NapSO$_3$] : [C(NH$_2$)$_2$(NHEt)][C$_{10}$H$_7$SO$_3$-2]
17: [DiMeGu][2-NapSO$_3$] : [C(NH$_2$)$_2$(NMe$_2$)][C$_{10}$H$_7$SO$_3$-2]
18: [MeGu][10-CamphorSO$_3$] : [C(NH$_2$)$_2$(NHMe)][C$_{10}$H$_{17}$OSO$_3$]
19: [EtGu][10-CamphorSO$_3$] : [C(NH$_2$)$_2$(NHEt)][C$_{10}$H$_{17}$OSO$_3$]
20: [DiMeGu][10-CamphorSO$_3$] : [C(NH$_2$)$_2$(NMe$_2$)][C$_{10}$H$_{17}$OSO$_3$]
21: [DiMeGu][MeSO$_3$] : [C(NH$_2$)$_2$(NMe$_2$)][CH$_3$SO$_3$]
22: [DiMeGu][PhSO$_3$] : [C(NH$_2$)$_2$(NMe$_2$)][C$_6$H$_5$SO$_3$]
23: [DiMeGu]$_2$[1,5-Nap(SO$_3$)$_2$] : [C(NH$_2$)$_2$(NMe$_2$)]$_2$[C$_{10}$H$_6$(1,5-SO$_3$)$_2$]
24: [DiMeGu]$_2$[2,6-Nap(SO$_3$)$_2$] : [C(NH$_2$)$_2$(NMe$_2$)]$_2$[C$_{10}$H$_6$(2,6-SO$_3$)$_2$]

Crystallographic measurements for compounds **13**, **14**, **15** and **24** were made at 150 K, **18** at 293 K and **19** at 240 K on a Nonius Kappa CCD diffractometer. Crystallographic measurements for compounds **12**, **16**, **17**, **21**, **22** and **23** were made at 150K, while those for **20** were obtained at 240 K on the Bruker SMART CCD diffractometer at Daresbury SRS Station 9·8. In all of the structures, the non-hydrogen atoms were allowed to vibrate anisotropically in the least squares cycles. In some compounds, molecules of water are included in the lattice. The position of the water hydrogen atoms were determined from the electron density map, and have been refined subject to having O–H bond lengths fixed at 0.89(3)Å. All other hydrogen atoms were included at calculated positions.

Compound	**12**	**13**	**14**	**15**
Empirical formula	$C_{12}H_{15}N_3O_3S$	$C_{13}H_{19}N_3O_4S$	$C_{13}H_{19}N_3O_4S$	$C_{12}H_{15}N_3O_3S$
M	281.33	313.37	313.37	281.33
Crystal system	Monoclinic	Orthorhombic	Monoclinic	Monoclinic
Space group	$P2_1/n$	$Pbca$	$P2_1/a$	$P2_1/c$
Wavelength / Å	0.67780	0.71073	0.71073	0.71073
a / Å	8.884(3)	7.3850(2)	11.0940(2)	8.7420(2)
b / Å	40.601(11)	15.9310(5)	10.6850(2)	28.3960(5)
c / Å	10.980(3)	25.394(1)	12.7100(3)	10.8770(2)
α / °	90	90	90	90
β / °	96.180(4)	90	102.9540(10)	92.953(1)
γ / °	90	90	90	90
U / Å^3	3937.7(19)	2987.61(18)	1468.29(5)	2696.50(9)
Z	12	8	4	8
μ(Mo-Kα) / mm^{-1}	0.255	0.236	0.240	0.248
Reflections collected	23498	13638	29129	31192
Independent reflections	5579	3358	3358	6046
R(int)	0.1434	0.0937	0.0529	0.0831
$R1$, w$R2$	0.0903, 0.2096	0.0559, 0.1062	0.0382, 0.0885	0.0529, 0.1098
R indices (all data)	0.1088, 0.2245	0.1248, 0.1283	0.0573, 0.0973	0.0925, 0.1255

Table 3.1; X-ray crystallographic parameters for compounds **12-15**

Compound	**16**	**17**	**18**	**19**
Empirical formula	$C_{13}H_{17}N_3O_3S$	$C_{26}H_{34}N_6O_6S_2$	$C_{12}H_{23}N_3O_4S$	$C_{13}H_{25}N_3O_4S$
M	295.36	590.71	305.39	319.42
Crystal system	Monoclinic	Orthorhombic	Orthorhombic	Monoclinic
Space group	*Cc*	*Pbca*	$P2_12_12_1$	$P2_1$
Wavelength / Å	0.68940	0.68940	0.71073	0.71073
a / Å	13.581(4)	54.44(3)	13.0450(2)	6.8940(1)
b / Å	30.358(11)	10.652(4)	13.7180(2)	17.4760(4)
c / Å	8.693(3)	10.105(3)	17.8470(3)	14.2100(3)
α / °	90	90	90	90
β / °	125.803(19)	90.17(3)	90	103.180(1)
γ / °	90	90	90	90
U / Å^3	2906.8(16)	5860(4)	3193.74(9)	1666.92(6)
Z	8	8	8	4
μ(Mo-Kα) / mm^{-1}	0.233	0.232	0.219	0.213
Reflections collected	4970	18809	34543	16900
Independent reflections	4655	8026	5567	5835
R(int)	0.0428	0.0998	0.0505	0.0450
$R1$, w$R2$	0.0447, 0.1126	0.0628, 0.1532	0.0785, 0.2162	0.0466, 0.1206
R indices (all data)	0.0547, 0.1178	0.0991, 0.1691	0.0963, 0.2357	0.0705, 0.1313

Table 3.2; X-ray crystallographic parameters for compounds **16-19**

Compound	**20**	**21**	**22**	**23**	**24**
Empirical formula	$C_{13}H_{25}N_3O_4S$	$C_4H_{13}N_3O_3S$	$C_9H_{15}N_3O_3S$	$C_8H_{13}N_3O_3S$	$C_8H_{13}N_3O_3S$
M	319.42	183.23	245.30	231.27	231.27
Crystal system	Monoclinic	Monoclinic	Orthorhombic	Monoclinic	Monoclinic
Space group	$P2_1$	$P2_1/c$	$Pca2_1$	$P2_1/c$	$P2_1/c$
Wavelength / Å	0.67780	0.68670	0.71073	0.68670	0.71073
a / Å	10.8207(16)	6.4309(5)	10.6084(4)	11.8517(7)	7.2870(6)
b / Å	13.254(2)	7.9829(6)	11.3449(5)	10.8528(7)	19.4830(12)
c / Å	11.8837(18)	16.2140(12)	10.0582(4)	9.1258(11)	14.679(2)
α / °	90	90	90	90	90
β / °	103.423(2)	92.057(2)	90	111.267(2)	94.837(5)
γ / °	90	90	90	90	90
U / Å^3	1657.8(4)	831.85(11)	1210.52(9)	1093.86(11)	2076.6(4)
Z	4	4	4	4	8
μ(Mo-Kα) / mm^{-1}	0.214	0.357	0.265	0.288	0.304
Reflections collected	14198	7977	8198	7222	4331
Independent reflections	6590	2335	3345	3028	2962
R(int)	0.0699	0.0329	0.0325	0.0399	0.0628
$R1$, w$R2$	0.0888, 0.2392	0.0440, 0.1194	0.0386, 0.0990	0.0436, 0.1078	0.0566, 0.1203
R indices (all data)	0.0946, 0.2469	0.0481, 0.1230	0.0400, 0.1000	0.0588, 0.1158	0.1144, 0.1400

Table 3.3; X-ray crystallographic parameters for compounds **20-24**

3.2 1-Naphthalenesulfonate

In this section the structures of [MeGu][1-NapSO$_3$] **12**, [EtGu][1-NapSO$_3$]·H$_2$O **13**, and [DiMeGu][1-NapSO$_3$]·H$_2$O **14** are described. The structural effects of substitution on the guanidinium cation are then discussed by comparison with [Gu][1-NapSO$_3$] **II**.

[MeGu][1-NapSO$_3$] : [C(NH$_2$)$_2$(NHMe)][C$_{10}$H$_7$SO$_3$-1] 12

Asymmetric Unit

The asymmetric unit of **12** is shown in Figure 3.2 and consists of three [MeGu]$^+$ cations and three [1-NapSO$_3$]$^-$ anions.

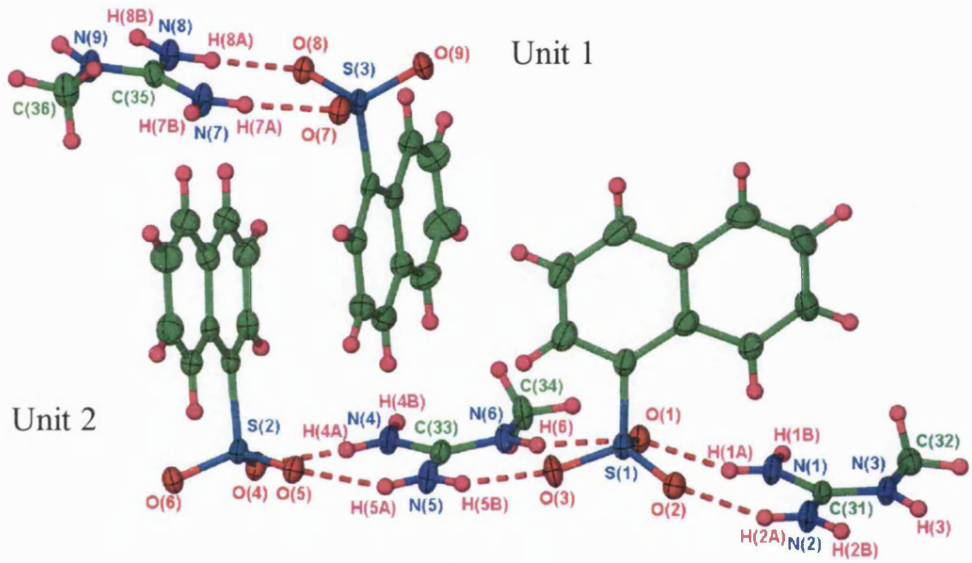

Figure 3.2; asymmetric unit of **12**. Ellipsoids are shown at 50% probability level.

There are two independent hydrogen-bonded arrays formed in the extended array and therefore these will initially be discussed separately; Unit 1 [consisting of the cation containing C(35) and anion containing S(3)] and Unit 2 [consisting of the cations containing C(33) and C(31) and the anions containing S(1) and S(2)].

Extended Structure

Unit 1

The unsubstituted cation faces and sulfonate groups of the anions form DD:AA hydrogen bonds leading to ribbons. These ribbons are linked into flat *shifted* GS sheets (θ_{IR} 179°) through hydrogen bonding incorporating the remaining N–H donor on the substituted cation

face and a sulfonate oxygen atom of a neighbouring ribbon, as shown in Figure 3.3. The naphthyl groups of the sulfonates are directed to both sides of each sheet, and the naphthyl-planes lie approximately orthogonal to the ribbons.

Unit 2

The cations and anions in Unit 2 also form ribbons through DD:AA hydrogen-bonding motifs, using the unsubstituted faces of the cations. As seen in Unit 1, these ribbons are linked into flat *shifted* GS sheets (θ_{IR} 172°) by hydrogen bonds involving the N–H donor of the substituted cation face and a sulfonate oxygen atom of a neighbouring ribbon, as shown in Figure 3.3. For details of the hydrogen bonds see Table 3.4. The naphthyl groups are directed to one side of each sheet, in contrast to Unit 1. The naphthyl planes of the sulfonates based on S(1) lie approximately parallel to the ribbons, whereas those in the anion based on S(2) are almost orthogonal. There are also edge-to-face C–H···π interactions between the naphthyl groups within and between the ribbons.

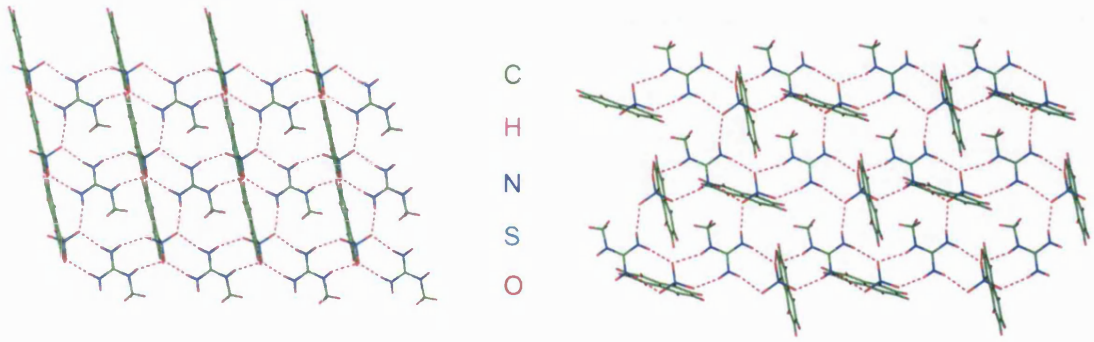

Figure 3.3 sheets formed by hydrogen bonding between the cations and anions in Unit 1 (left) and in Unit 2 (right)

Units 1 & 2 Combined

The arrays formed by Units 1 and 2 stack with interdigitating naphthyl groups, as shown in Figure 3.4. In the gross structure, the two sheets based on Unit 2 form a bilayer, sandwiching that formed by Unit 1. This arrangement is consolidated by face-to-face π···π and edge-to-face C–H···π interactions between the interdigitating naphthyl groups within the bilayer.

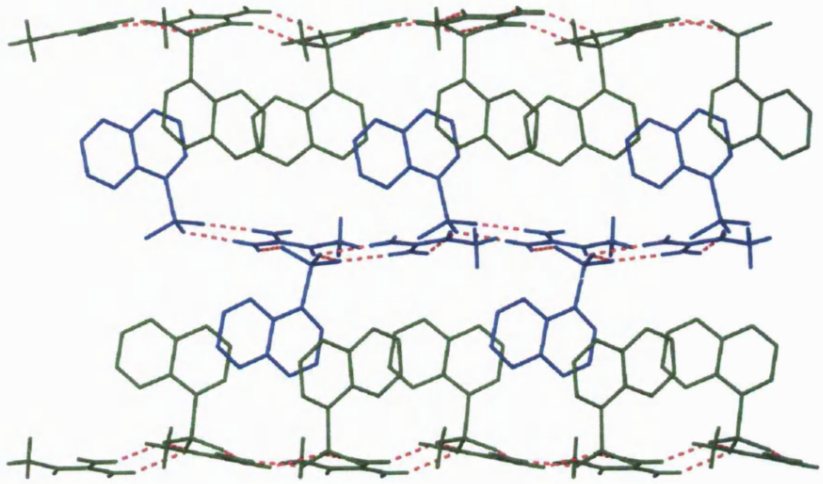

Figure 3.4; the interdigitating sheets based on Units 1 (*shown in blue*) and 2 (*shown in green*)

D–H···A	D···A /Å	H···A /Å	D–H···A /°	Symmetry operation generating D···A
N(1)–H(1A)···O(1)	2.942(4)	2.10	159	*x*, *y*, *z*
N(1)–H(1B)···O(5)	2.952(4)	2.09	166	*x*, *y*, 1+*z*
N(2)–H(2A)···O(2)	2.999(4)	2.17	157	*x*, *y*, *z*
N(2)–H(2B)···O(6)	2.932(4)	2.13	151	*x*-1, *y*, 1+*z*
N(3)–H(3)···O(4)	2.902(4)	2.11	149	*x*-1, *y*, 1+*z*
N(4)–H(4A)···O(4)	2.867(4)	2.00	169	*x*, *y*, *z*
N(4)–H(4B)···O(2)	2.960(4)	2.10	165	1+*x*, *y*, *z*
N(5)–H(5A)···O(5)	2.955(4)	2.15	152	*x*, *y*, *z*
N(5)–H(5B)···O(3)	2.882(4)	2.04	160	*x*, *y*, *z*
N(6)–H(6)···O(1)	2.999(4)	2.17	158	*x*, *y*, *z*
N(7)–H(7A)···O(7)	2.924(4)	2.05	173	*x*, *y*, *z*
N(7)–H(7B)···O(8)	3.031(4)	2.24	150	*x*-½, ½-*y*, *z*-½
N(8)–H(8A)···O(9)	2.870(4)	2.04	156	½+*x*, ½-*y*, *z*-½
N(8)–H(8B)···O(8)	2.944(4)	2.07	170	*x*, *y*, *z*
N(9)–H(9)···O(7)	2.961(4)	2.14	155	½+*x*, ½-*y*, *z*-½

Table 3.4; details of the hydrogen bonding in **12**

[EtGu][1-NapSO$_3$]·H$_2$O : [C(NH$_2$)$_2$(NHEt)][C$_{10}$H$_7$SO$_3$-1]·H$_2$O 13

Asymmetric Unit

The asymmetric unit of **13** is shown in Figure 3.5 and contains one $[EtGu]^+$ cation, one $[1\text{-}NapSO_3]^-$ anion and one molecule of H_2O.

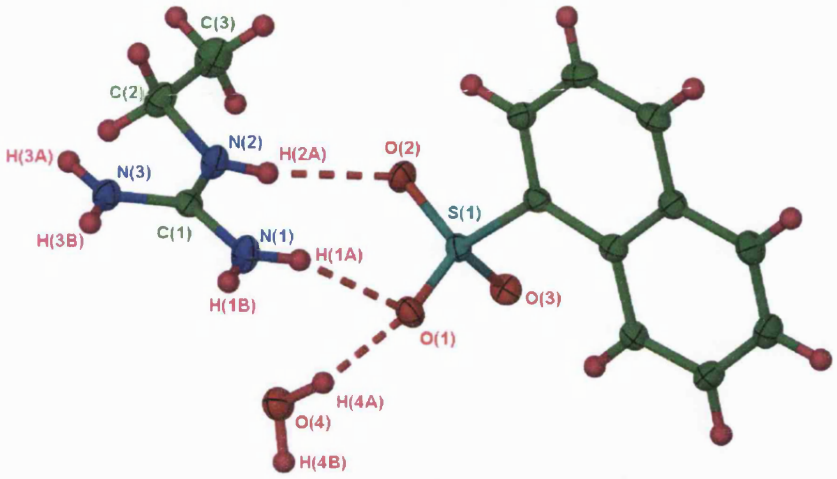

Figure 3.5; asymmetric unit in **13**. Ellipsoids are depicted at 50% probability level.

Extended Structure

The two unsubstituted cation faces form DD:AA hydrogen-bonded motifs with the sulfonate, generating ribbons. The planes of the naphthyl groups lie approximately orthogonal to the ribbons, leading to possible edge-to-face interactions between the naphthyl groups of neighbouring ribbons. The water molecules act as both hydrogen bond donors and acceptors, forming interactions with the remaining donor on the substituted cation face, as well as with a sulfonate oxygen atom of a neighbouring ribbon. These hydrogen bonds link the ribbons into sheets (Figure 3.6), which are corrugated with an inter-ribbon angle of 117°.

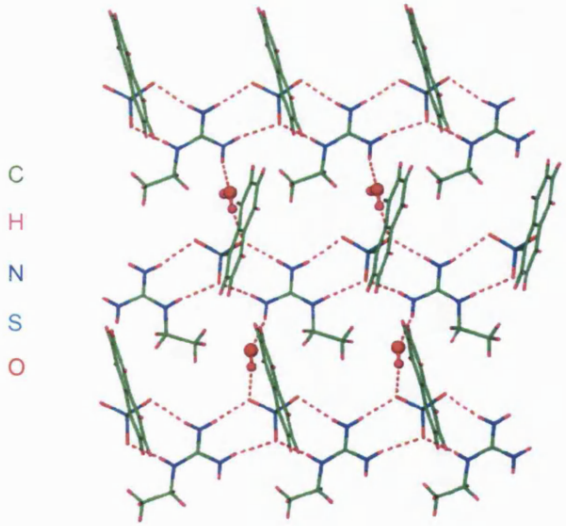

Figure 3.6; incorporation of water molecules linking the ribbons into sheets in **13**

There are also C–H···O hydrogen bonds from the methylene group of the cation in one ribbon to sulfonate oxygen atoms of a neighbouring ribbon, reinforcing the sheets. For hydrogen bond details see Table 3.5.

The sulfonate substituents are directed to one side of each sheet, forming bilayers in the extended structure. The water molecules linking the ribbons into sheets further link neighbouring bilayers to yield a three-dimensional hydrogen-bonded array. There are also face-to-face π···π interactions between the naphthyl groups of interdigitating anions.

D–H···A	D···A /Å	H···A /Å	D–H···A /°	Symmetry operation generating D···A
N(1)–H(1A)···O(1)	2.945(3)	2.10	161	*x*, *y*, *z*
N(1)–H(1B)···O(3)	2.863(3)	1.99	169	1+*x*, *y*, *z*
N(2)–H(2A)···O(2)	2.970(3)	2.10	168	*x*, *y*, *z*
N(3)–H(3A)···O(4)	2.845(3)	1.99	163	½+*x*, -*y*-½, -*z*
N(3)–H(3B)···O(2)	3.110(3)	2.28	157	1+*x*, *y*, *z*
O(4)–H(4A)···O(1)	2.831(3)	1.95	168	*x*, *y*, *z*
O(4)–H(4B)···O(3)	2.835(3)	1.96	167	2-*x*, -*y*, -*z*
C(2)–H(2C)···O(1)	3.372(3)	2.60	135	$^{5}/_{2}$-*x*, *y*-½, *z*

Table 3.5; details of the hydrogen bonding in **13**

[DiMeGu][1-NapSO$_3$]·H$_2$O : [C(NH$_2$)$_2$(NMe$_2$)][C$_{10}$H$_7$SO$_3$-1]·H$_2$O 14

Asymmetric Unit

The asymmetric unit of **14** contains one $[DiMeGu]^+$ cation, one $[1\text{-}NapSO_3]^-$ anion and a molecule of H_2O as shown in Figure 3.7.

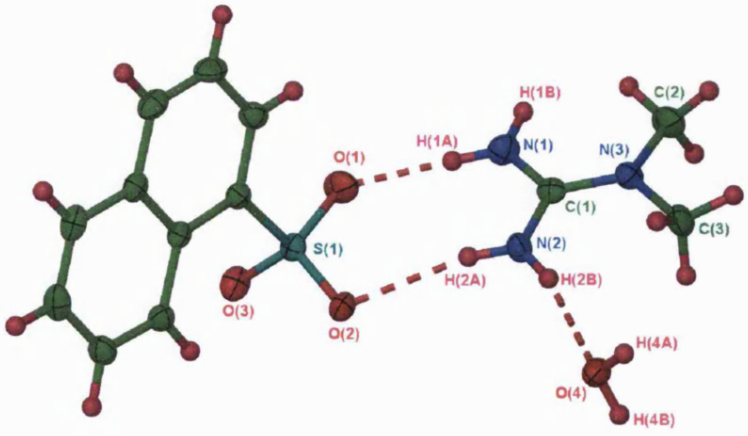

Figure 3.7; asymmetric unit of **14**. Ellipsoids are shown at 50% probability level.

Extended Structure

The unsubstituted face of the cation forms a DD:AA hydrogen-bonded motif with the sulfonate, and a single N–H···O hydrogen bond from one of the substituted cation faces links the cations and anions into chains (Figure 3.8). These chains are further linked into ribbons through C–H···O hydrogen bonds involving the methyl groups of the cation, generating the graph sets $R_2^2(9)$ and $R_4^2(8)$. As seen in [EtGu][1-NapSO$_3$]·H$_2$O **13**, the water molecules act as hydrogen bond donors and acceptors to link the ribbons into sheets (Figure 3.8) which have an inter-ribbon angle of 148°. For hydrogen bond details see Table 3.6.

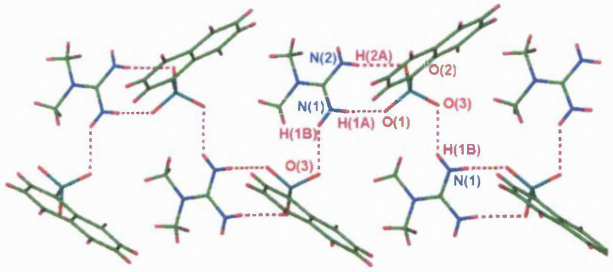

Figure 3.8; chain formed in **14**

The naphthyl groups of the sulfonates are directed to one side of each sheet, which pack to form bilayers in the gross structure. Neighbouring bilayers are linked by hydrogen bonding through the water molecules, as seen in **13**.

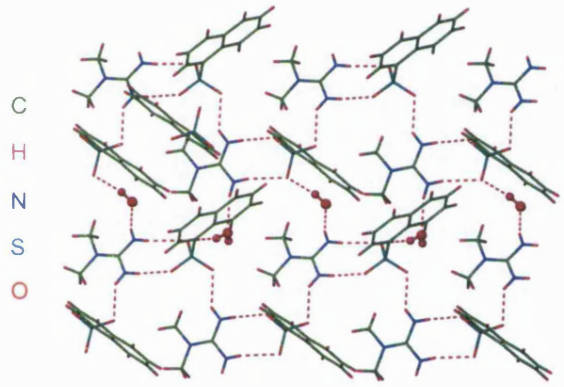

Figure 3.9; sheet formation in **14**

There are edge-to-face C–H···π interactions between the naphthyl groups of neighbouring ribbons within the same sheet. There are also edge-to-face C–H···π and face-to-face π···π interactions between the interdigitating naphthyl groups.

D–H···A	D···A /Å	H···A /Å	D–H···A /°	Symmetry operation generating D···A
N(1)–H(1A)···O(1)	2.797(2)	1.92	175	*x*, *y*, *z*
N(1)–H(1B)···O(3)	2.984(2)	2.24	141	*x*, *y*+1, *z*
N(2)–H(2A)···O(2)	3.123(2)	2.27	168	*x*-½, -*y*+½, *z*
N(2)–H(2B)···O(4)	2.979(2)	2.15	166	*x*, *y*, *z*
O(4)–H(4A)···O(3)	2.879(2)	2.06	172	-*x*, -*y*, -*z*
O(4)–H(4B)···O(2)	2.875(2)	2.07	161	*x*, *y*, *z*
C(2)–H(2C)···O(1)	3.246(2)	2.39	146	*x*, 1+*y*, *z*
C(2)–H(2E)···O(3)	3.546(2)	2.62	157	½+*x*, ½-*y*, *z*

Table 3.6; details of the hydrogen bonding in **14**

3.2.1 The structural effects of alkyl substitution in guanidinium 1-naphthalenesulfonates

As the number of hydrogen bond donors in the cation is reduced, different hydrogen-bonded arrays are observed, moving from a continuous single layer in [Gu][1-$NapSO_3$] **II**, to both single layers and bilayers in [MeGu][1-$NapSO_3$] **12**, and bilayers in both compounds [EtGu][1-$NapSO_3$]·H_2O **13** and [DiMeGu][1-$NapSO_3$]·H_2O **14**.

Compound **II** was reported by Ward *et al*[1], and contains one cation and one anion in the asymmetric unit. There are three DD:AA hydrogen-bonding motifs between the cations and anions leading to regular hexagonal hydrogen-bonded sheets, which are highly corrugated with an inter-ribbon angle of 77°. The naphthyl groups of the sulfonates all lie approximately orthogonal to the ribbons, and are directed to both sides of each sheet. Interdigitating single layers are observed in the extended structure, with face-to-face π···π interactions between naphthyl groups of interdigitating anions.

Compound **12** has three cations and anions in the asymmetric unit, forming two independent shifted GS sheets. In the sheets based on Unit 1, the naphthyl groups lie approximately orthogonal to the ribbons, and are directed to both sides of each sheet. In Unit 2 there are two independent cations and anions; the naphthyl groups of one anion lie approximately parallel to the ribbons, and those of the other anion are almost orthogonal. The naphthyl groups of each anion are directed to both sides of each sheet. In the gross structure, these two independent arrays form a sandwich bilayer consisting of three sheets; two enveloping the third as shown in Figure 3.10b. Compound **12** is the only structure reported in this thesis that forms an arrangement of this type.

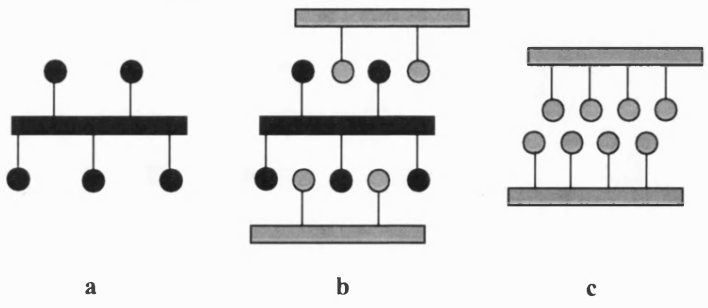

Figure 3.10; **a**) a single layer, **b**) a single layer sandwiched by a bilayer as seen in **12** and **c**) a bilayer

Compound [EtGu][1-$NapSO_3$]·H_2O **13** forms ribbons using the two unsubstituted cation faces forming DD:AA hydrogen-bonded motifs, where the naphthyl groups are directed almost orthogonal to the ribbons. The substituted face of the cation, consisting of one N–H group, links the ribbons into sheets by hydrogen bonding incorporating water molecules. The ribbons in these sheets are arranged such that a *stretched* hexagonal sheet is formed, wherein the water molecules act like a spacer between the ribbons, reducing the possible steric repulsion caused by the substitution in the cation. The naphthyl groups are directed to one side of each sheet and interdigitate with those from a neighbouring sheet forming bilayers. Neighbouring bilayers are cross-linked as a consequence of hydrogen bonding involving the water molecules.

In compound [DiMeGu][1-$NapSO_3$]·H_2O **14**, the unsubstituted cation face forms a DD:AA hydrogen-bonding motif, and an N–H group in one of the substituted cation faces forms a hydrogen bond with sulfonate oxygen atoms forming chains. Further C–H···O hydrogen bonds from the methyl groups of the cation link the chains into ribbons. Sheets are formed by means of hydrogen bonding between the water molecules and the N–H groups of one ribbon and sulfonate oxygen atoms of a neighbouring ribbon. The naphthyl groups are directed to the same side of each sheet, which interdigitate to form bilayers. As seen in **13**, neighbouring bilayers are cross-linked by hydrogen bonding involving water molecules.

The substitution of one N–H donor in the cation has resulted in the formation of shifted sheets in **12** and *stretched* hexagonal sheets incorporating water molecules in **13**. Compound **14** exhibits neither the regular hexagonal or shifted sheets; however, due to the incorporation of water into the lattice a sheet structure is observed.

Thus, overall compound **12** can be considered as an intermediate between the two different types of array that are formed between the cations and anions (single layers and bilayers) as the number of hydrogen bond donors on the cation is reduced.

3.2.2 The effects of alkyl substitution on hydrogen bond parameters in guanidinium 1-naphthelenesulfonates

The DD:AA hydrogen bond distances (N···O) in the structures **II**, **12**, **13** and **14** vary as the degree of substitution on the cation is increased. The hydrogen bond distances vary between 2.861(3)Å – 2.979(4)Å in **II**, 2.867(3)Å – 3.000(3)Å in **12**, 2.863(3)Å – 3.110(3)Å in **13** and 2.797(2)Å – 3.123(2)Å in **14**. The mean average bond distances are 2.926(4)Å in **II**, 2.931(4)Å in **12**, 2.972(3)Å in **13** and 2.960(2)Å in **14**. Compound **II** forms hexagonal sheets whereas **12** forms shifted sheets - both have similar DD:AA hydrogen bonds distances. The hydrogen bond distances in **13** and **14** are also similar, where stretched hexagonal sheets are observed in **13** and sheets are formed in **14**, with both compounds incorporating water. The DD:AA hydrogen bond distances in **13** and **14** are longer than those in **II** and **12**. This suggests that the hydrogen bonds are weaker in the compounds incorporating the -NEt and -NMe_2 substituted cations and molecules of water, compared with those containing the unsubstituted and -NMe substituted cations.

3.3 2-Naphthalenesulfonate

The structures of [MeGu][2-NapSO$_3$] **15**, [EtGu][2-NapSO$_3$] **16**, and [DiMeGu][2-NapSO$_3$] **17** are described in this section, as are the structural effects of substitution on the guanidinium cation, which are discussed and compared with [Gu][2-NapSO$_3$] **III**.

[MeGu][2-NapSO$_3$] : [C(NH$_2$)$_2$(NHMe)][C$_{10}$H$_7$SO$_3$-2] 15

Asymmetric Unit

The asymmetric unit of **15** is shown in Figure 3.11 and contains two $[MeGu]^+$ cations and two $[2\text{-}NapSO_3]^-$ anions.

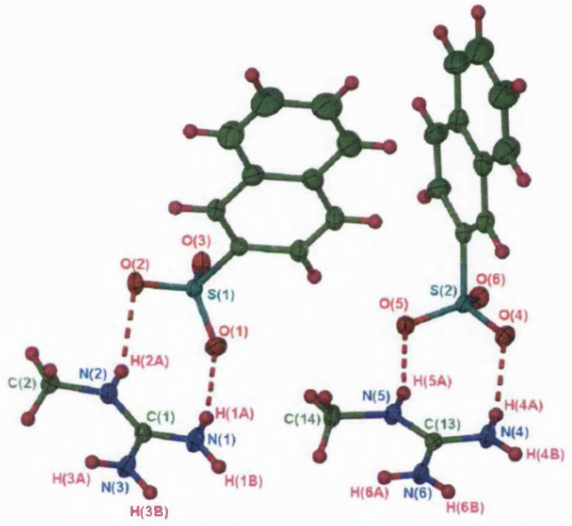

Figure 3.11; the asymmetric unit of **15**. Ellipsoids are depicted at 50% probability level.

Extended Structure

There are two unsubstituted cation faces capable of forming DD:AA hydrogen-bonded motifs with the sulfonates, and these do so giving rise to ribbons. A single ribbon incorporates both independent cations and anions of the asymmetric unit. The naphthyl groups in the anion based on S(1) lie approximately orthogonal to the ribbons, whereas those in the anion containing S(2) are almost parallel.

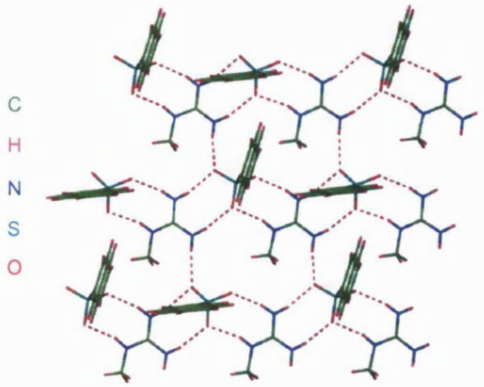

Figure 3.12; ribbons linked into a shifted GS sheet in **15**

The third face of each cation has one hydrogen bond donor, due to the substitution of a N–H group by a N–Me group, and is not involved in ribbon formation. This donor forms hydrogen bonds with the sulfonate oxygen atoms of a neighbouring ribbon, linking them into virtually flat shifted sheets (Figure 3.12), with an inter-ribbon angle of 173°. Hydrogen bond details are given in Table 3.7. The naphthyl groups are directed to the same side of each sheet, which stack forming repeating bilayers in the gross structure. There are edge-to-face C–H···π interactions between the naphthyl rings of anions in the same sheet, both within the same ribbon, and between neighbouring ribbons. There are also edge-to-face and face-to-face interactions between interdigitating naphthyl rings of neighbouring sheets.

D–H···A	D···A /Å	H···A /Å	D–H···A /°	Symmetry operation generating D···A
N(1)–H(1A)···O(1)	2.871(3)	2.03	159	*x*, *y*, *z*
N(1)–H(1B)···O(6)	3.027(3)	2.28	143	1+*x*, *y*, *z*
N(3)–H(3A)···O(3)	2.946(3)	2.09	163	1+*x*, *y*, *z*
N(3)–H(3B)···O(5)	2.941(2)	2.17	145	1+*x*, *y*, *z*
N(2)–H(2A)···O(2)	3.001(3)	2.23	148	*x*, *y*, *z*
N(4)–H(4A)···O(4)	2.882(3)	2.08	152	*x*, *y*, *z*
N(4)–H(4B)···O(3)	2.897(2)	2.04	166	*x*, *y*, *z*-1
N(5)–H(5A)···O(5)	2.867(2)	2.03	158	*x*, *y*, *z*
N(6)–H(6A)···O(6)	2.981(2)	2.11	169	1+*x*, *y*, *z*
N(6)–H(6B)···O(2)	2.979(2)	2.14	158	*x*, *y*, *z*-1

Table 3.7; details of the hydrogen bonding in **15**

[EtGu][2-NapSO$_3$] : [C(NH$_2$)$_2$(NHEt)][C$_{10}$H$_7$SO$_3$-2] 16

Asymmetric Unit

The asymmetric unit of **16** contains two $[EtGu]^+$ cations and two $[2\text{-NapSO}_3]^-$ anions as shown in Figure 3.13.

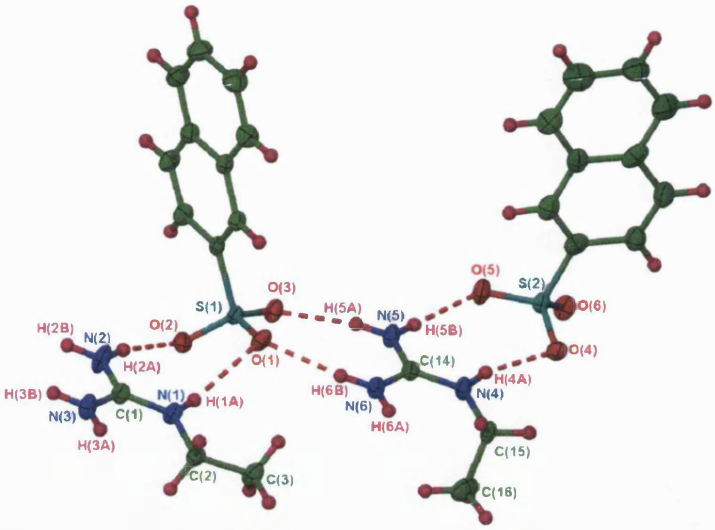

Figure 3.13; asymmetric unit of **16**. Ellipsoids are depicted at 50% probability level.

Extended Structure

The two unsubstituted faces of each cation form DD:AA hydrogen-bonded motifs with the sulfonates forming ribbons. As seen in [MeGu][2-NapSO$_3$] **15**, both independent cations and anions are incorporated into the same ribbon. The naphthyl planes of the anion based on S(1) lie almost orthogonal to the ribbons, whereas those based on S(2) are relatively parallel. The N–H group on the substituted cation face forms hydrogen bonds with the sulfonate oxygen atoms of a neighbouring ribbon linking them into shifted sheets, as shown in Figure 3.14. Details of the hydrogen bonds are given in Table 3.8.

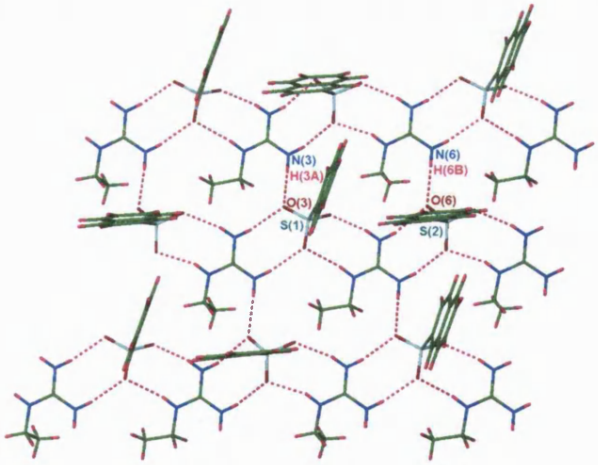

Figure 3.14; sheet formation in **16**

The naphthyl groups are orientated to the same side of each sheet, which are almost flat with an inter-ribbon angle of 177°. In the gross structure, a repeating bilayer is observed where the naphthyl groups are interdigitating. As seen in **15**, there are edge-to-face C–H···π interactions between the naphthyl rings of anions in the same sheet both within the same ribbon and between neighbouring ribbons and between the interdigitating naphthyl rings of neighbouring sheets. There are also face-to-face π···π interactions between interdigitating anions.

D–H···A	D···A /Å	H···A /Å	D–H···A /°	Symmetry operation generating D···A
N(1)–H(1A)···O(5)	3.081(3)	2.27	153	*x*-1, *y*, *z*
N(1)–H(1B)···O(1)	2.954(3)	2.08	171	*x*, *y*, *z*
N(2)–H(2A)···O(6)	2.877(4)	2.03	161	*x*-1, *y*, *z*-1
N(2)–H(2B)···O(2)	2.901(3)	2.06	159	*x*, *y*, *z*
N(3)–H(3A)···O(4)	2.900(3)	2.05	161	*x*-1, *y*, *z*-1
N(4)–H(4A)···O(2)	2.975(3)	2.21	145	*x*, *y*, *z*
N(4)–H(4B)···O(4)	2.952(3)	2.10	162	*x*, *y*, *z*
N(5)–H(5A)···O(5)	2.994(3)	2.14	164	*x*, *y*, *z*
N(5)–H(5B)···O(3)	2.887(4)	2.02	168	*x*, *y*, *z*-1
N(6)–H(6A)···O(1)	3.070(3)	2.27	152	*x*, *y*, *z*-1

Table 3.8; details of the hydrogen bonding in **16**

[DiMeGu][2-NapSO$_3$] : [C(NH$_2$)$_2$(NMe$_2$)][C$_{10}$H$_7$SO$_3$-2] 17

Asymmetric Unit

The asymmetric unit of **17** is shown in Figure 3.15 and consists of two $[DiMeGu]^+$ cations and two $[2\text{-}NapSO_3]^-$ anions.

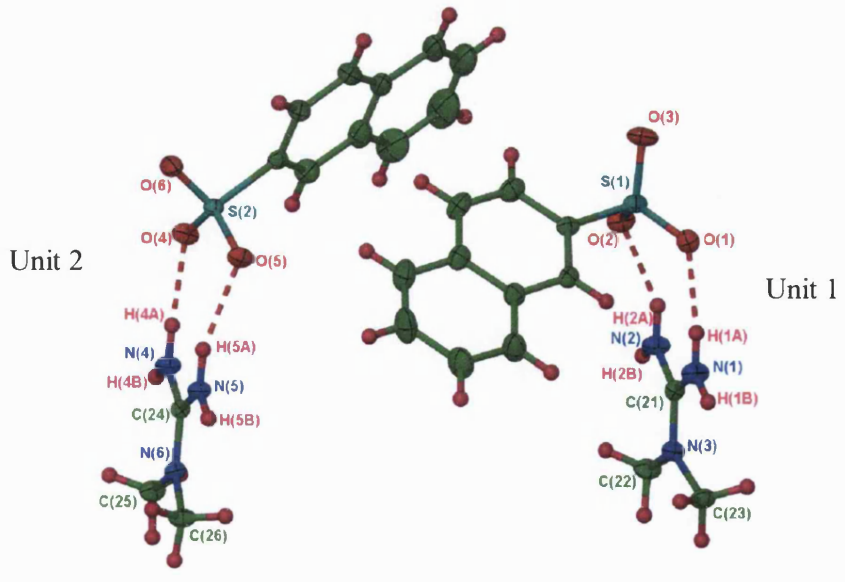

Figure 3.15; asymmetric unit of **17**. Ellipsoids are depicted at 50% probability level.

Extended Structure

Two independent sheets are observed and therefore these are initially discussed separately. These are based on Unit 1 [cation based on C(21) and anion containing S(1)] and Unit 2 [cation based on C(24) and anion containing S(2)].

Unit 1

The cation has one unsubstituted hydrogen-bonding face available, which forms DD:AA hydrogen bonds with the sulfonate generating the graph set $R_2^2(8)$. This cation-anion 'pair' forms hydrogen bonds with another Unit 1 'pair' leading to a ribbon generating the graph set $R_4^2(8)$.

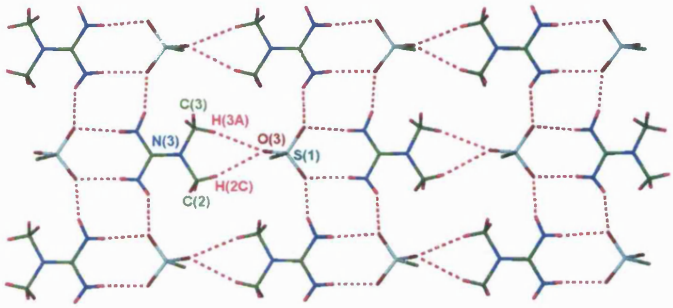

Figure 3.16; sheet formed in **17** (*part of the anion is omitted for clarity*).

All of the N–H donors are used to form this ribbon, however only two of the three sulfonate oxygen atoms are involved. The Unit 1 ribbons are linked into sheets by C–H···O hydrogen bonds between the methyl groups on the substituted cation face and a single sulfonate oxygen atom in a neighbouring ribbon (Figure 3.16) through the graph set $R_2^1(6)$. The naphthyl groups are directed to one side of each sheet, which are reasonably flat with an inter-ribbon angle of 165°.

Unit 2

A second ribbon is formed by the cation-anion pair in Unit 2 and follows the same packing pattern as that of Unit 1, forming reasonably flat sheets (θ_{IR} 167°). Hydrogen bond details are given in Table 3.9.

Units 1 and 2 combined

The sheets in Units 1 and 2 are independent of each other. The naphthyl groups in Unit 1 are directed towards each other (Figure 3.17 *left*), with edge-to-face C–H···π interactions between rings in the same ribbon. However, the naphthyl groups in Unit 2 are directed away from each other (Figure 3.17 *right*), with edge-to-face C–H···π interactions between the naphthyl rings of neighbouring ribbons. The sulfonate substituents of the Unit 1 sheet

interdigitate with those of a Unit 2 sheet forming a bilayer, where edge-to-face C–H···π and face-to-face π···π interactions exist between Unit 1 and Unit 2 naphthyl groups.

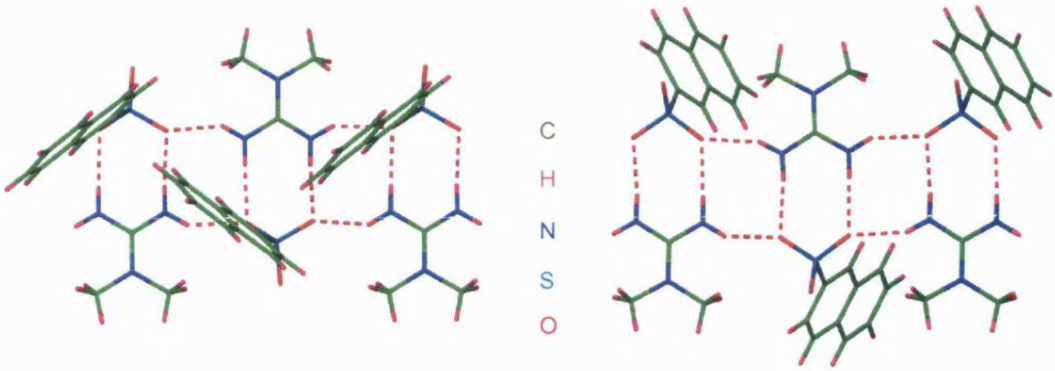

Figure 3.17; the ribbon formed in Unit 1 (left) and the ribbon formed in Unit 2 (right)

D–H···A	D···A /Å	H···A /Å	D–H···A /°	Symmetry operation generating D···A
N(1)–H(1A)···O(1)	2.903(2)	2.08	156	*x*, *y*, *z*
N(1)–H(1B)···O(2)	2.833(2)	2.04	150	*x*, -*y*+$^3/_2$, *z*-½
N(2)–H(2A)···O(2)	2.904(2)	2.03	174	*x*, *y*, *z*
N(2)–H(2B)···O(1)	2.818(2)	2.10	138	*x*, -*y*+$^3/_2$, *z*+½
N(4)–H(4A)···O(4)	2.999(2)	2.15	163	*x*, *y*, *z*
N(4)–H(4B)···O(5)	2.835(2)	2.04	150	*x*, -*y*+$^3/_2$, *z*+½
N(5)–H(5A)···O(5)	2.892(2)	2.01	177	*x*, *y*, *z*
N(5)–H(5B)···O(4)	2.837(2)	2.10	141	*x*, -*y*+$^3/_2$, *z*-½
C(22)–H(22B)···O(3)	3.241(2)	2.29	164	*x*, *y*-1, *z*
C(23)–H(23B)···O(3)	3.336(2)	2.45	151	*x*, *y*-1, *z*
C(25)–H(25B)···O(6)	3.439(2)	2.42	163	*x*, *y*-1, *z*
C(26)–H(26B)···O(6)	3.441(2)	2.51	159	*x*, *y*-1, *z*

Table 3.9; details of the hydrogen bonding in **17**

3.3.1 The structural effects of alkyl substitution in guanidinium 2-naphthalenesulfonates

The structure of [Gu][2-NapSO$_3$] **III** has been reported by Ward *et al*[1]. The asymmetric unit consists of two cations and two anions which form regular hexagonal GS sheets through DD:AA hydrogen-bonding motifs. The naphthyl groups of the anion based on S(1) lie almost orthogonal to the ribbons, whereas those based on S(2) are approximately parallel. The sheets are reasonably flat with an inter-ribbon angle of 146°. The naphthyl groups of the sulfonates are directed to the same side and interdigitate with those of a neighbouring sheet forming bilayers in the gross structure. There are edge-to-face C–H···π interactions between the naphthyl groups of the same sheet, both within the same ribbons and between neighbouring ribbons, and those of neighbouring sheets. There are also face-to-face π···π interactions between naphthyl groups of interdigitating anions.

Compounds [MeGu][2-NapSO$_3$] **15** and [EtGu][2-NapSO$_3$] **16** have two cations and anions in the asymmetric unit, and the two unsubstituted faces of each cation form DD:AA hydrogen-bonding motifs with the sulfonates leading to ribbons. The ribbons are linked into shifted sheets through hydrogen bonding between the N–H donor on the substituted cation face in one ribbon and the sulfonate oxygen atoms of a neighbouring ribbon. The naphthyl groups are directed to the same side of each sheet forming a repeating bilayer in the gross structure.

In [DiMeGu][2-NapSO$_3$] **17**, the cations and anions of Unit 1 and Unit 2 form independent sheets, involving one $R_2^2(8)$ motif from the unsubstituted cation face, two single N–H···O hydrogen bonds from the two substituted cation faces and C–H···O hydrogen bonds between the two N–Me groups of the cation and the remaining oxygen atom in the anion. In the extended structure, the naphthyl groups of the Unit 1 sheets interdigitate with those of the Unit 2 sheets forming bilayers.

The structures formed in the 2-naphthalenesulfonate series are not impacted upon significantly as the cation becomes more substituted. The compounds [Gu][2-NapSO$_3$] **III**, [MeGu][2-NapSO$_3$] **15**, [EtGu][2-NapSO$_3$] **16** and [DiMeGu][2-NapSO$_3$] **17** all exhibit interdigitating sheets leading to bilayers in the gross structure. Regular hexagonal sheets are not observed as the cation donors are substituted; instead **15** and **16** give rise to the formation

of shifted GS sheets, while **17** forms a two-dimensional array by utilising C–H···O hydrogen bonds that arise from the methyl groups of the cation.

3.3.2 The effects of alkyl substitution on hydrogen bond parameters in guanidinium 2-naphthalenesulfonates

The DD:AA hydrogen bond distances in the structures **III**, **15**, **16** and **17** are not greatly affected as the degree of substitution on the cation is increased. The hydrogen bond distances (N···O) vary between 2.863(6)Å – 3.017(6)Å in **III**, 2.867(2)Å – 3.010(3)Å in **15**, 2.877(4)Å – 3.070(3)Å in **16** and 2.892(2)Å – 2.999(2)Å in **17**. The mean DD:AA hydrogen bond distances are 2.940(6)Å, 2.933(3)Å, 2.953(4)Å and 2.925(2)Å in **III**, **15**, **16** and **17** respectively. These similar hydrogen bond distances are not unexpected, as the same DD:AA hydrogen-bonded ribbons are formed in **15** and **16**, and there are only DD:AA hydrogen bonds between each cation-anion pair in **17**.

3.4 (1S)-(+)-10-Camphorsulfonate

In this section the structures of [MeGu][10-CamphorSO$_3$] **18**, [EtGu][10-CamphorSO$_3$] **19**, and [DiMeGu][10-CamphorSO$_3$] **20** are described, as are the structural effects of substitution on the guanidinium cation. These compounds are discussed by comparison with [Gu][10-CamphorSO$_3$] **IV** which incorporates the unsubstituted guanidinium cation.

[MeGu][10-CamphorSO$_3$] : [C(NH$_2$)$_2$(NHMe)][C$_{10}$H$_{17}$OSO$_3$] 18

Asymmetric Unit

The asymmetric unit of **18** consists of two $[MeGu]^+$ cations and two $[10\text{-CamphorSO}_3]^-$ anions as shown in Figure 3.18.

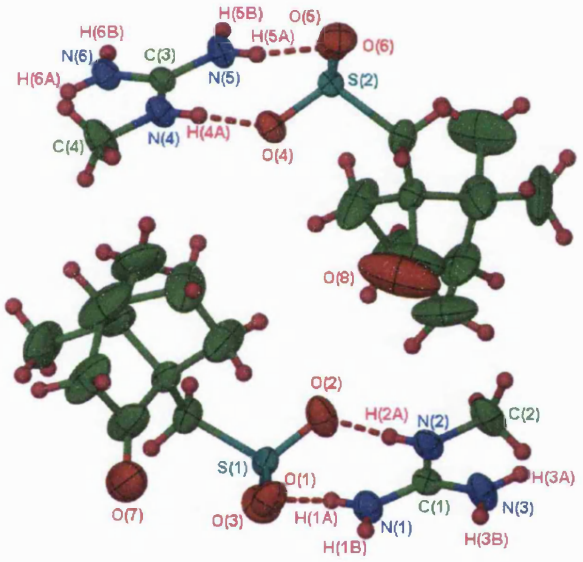

Figure 3.18; asymmetric unit of **18**. Ellipsoids are depicted at 30% probability level.

The single crystal data for **18** are presented from a 293 K data collection. Data were initially collected at 150 K and later at 240 K. It was clear that the crystals undergo a phase change on cooling, which spans a wide temperature range. The data collected for the high temperature phase, at 293 K, resulted in optimal convergence.

Extended Structure

The two independent cations and anions in the asymmetric unit both form DD:AA hydrogen bonds incorporating the two unsubstituted cation faces, giving ribbons. There is one remaining N–H donor on the substituted face of each cation, which forms hydrogen bonds with the sulfonate oxygen atoms of a neighbouring ribbon, linking them into shifted GS sheets (Figure 3.19). The camphor groups are directed to both sides of each sheet, which are corrugated with an inter-ribbon angle of 129°. The hydrogen bond details are given in Table 3.11

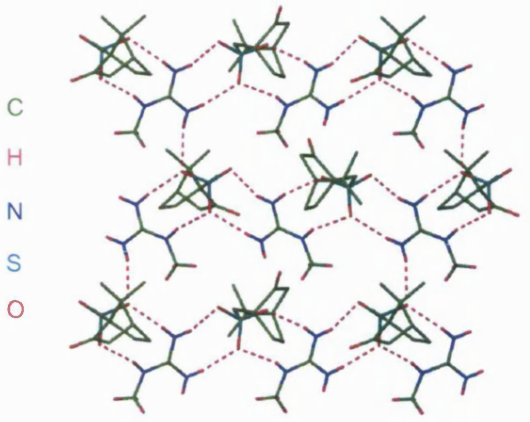

Figure 3.19; sheet formed in **18**
(*the anion hydrogen atoms have been removed for clarity*)

A continuous repeating single layer is observed in the extended array, with interdigitation between the camphor groups of neighbouring sheets (Figure 3.20). The two independent camphor groups are orientated differently to each other. The carbonyl group of one independent anion is directed almost parallel to the ribbons, whereas the corresponding functionalities of the other independent anion is directed almost orthogonally, as can be seen in Figure 3.19.

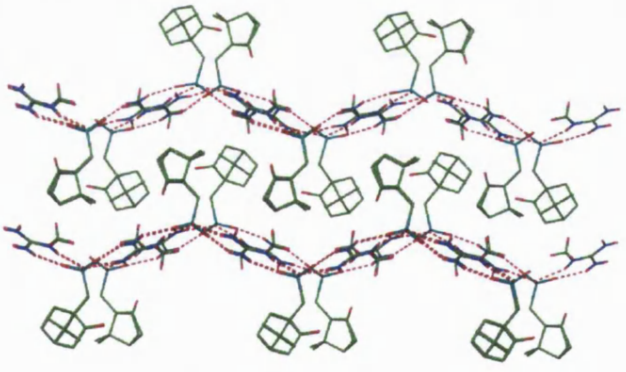

Figure 3.20; side view of sheets,
which form interdigitating single layers in **18**
(*the anion hydrogen atoms have been removed for clarity*)

The donor N(3)–H(3A) forms a hydrogen bond with sulfonate oxygen atom O(1). This donor also forms a hydrogen bond to O(7), the carbonyl oxygen atom, thus reinforcing the sheet formation. However, the latter interaction is longer and less directional, and therefore weaker than that involving the sulfonate oxygen atom. The carbonyl moiety including O(7) is also involved in weak C–H···O hydrogen bonds. The oxygen atom forms a hydrogen bond with a C–H donor of the methyl group in the cation. However, the position of the sulfonate and

hence the carbonyl groups are dictated by the GS hydrogen-bonded array, rather than being driven by C–H···O hydrogen bonds. The interatomic distances suggest that the carbonyl oxygen atom O(8) is not involved in C–H···O interactions.

D–H···A	D···A /Å	H···A /Å	D–H···A /°	Symmetry operation generating D···A
N(1)–H(1A)···O(1)	2.992(7)	2.11	155	*x*, *y*, *z*
N(1)–H(1B)···O(6)	2.897(6)	2.09	156	$-x+^{3}/_{2}$, $-y+1$, $z-½$
N(2)–H(2A)···O(2)	2.965(7)	2.16	156	*x*, *y*, *z*
N(3)–H(3A)···O(1)	3.416(6)	2.61	157	$x-½$, $-y+½$, $-z$
N(3)–H(3B)···O(4)	2.937(7)	2.08	173	$-x+^{3}/_{2}$, $-y+1$, $z-½$
N(4)–H(4A)···O(4)	2.850(5)	2.01	165	*x*, *y*, *z*
N(5)–H(5A)···O(5)	2.966(5)	2.12	166	*x*, *y*, *z*
N(5)–H(5B)···O(3)	2.835(7)	2.03	155	$-x+^{3}/_{2}$, $-y$, $z+½$
N(6)–H(6A)···O(5)	3.034(5)	2.20	163	$x+½$, $-y+½$, $-z+1$
N(6)–H(6B)···O(2)	2.984(5)	2.13	169	$-x+^{3}/_{2}$, $-y$, $z+½$
N(3)–H(3A)···O(7)$_{C=O}$	3.105(9)	2.48	130	$x-½$, $-y+½$, $-z$
C(2)–H(2E)···O(7)$_{C=O}$	3.492(9)	2.62	152	$x-½$, $-½-y$, $-z$

Table 3.11; details of the hydrogen bonding in **18**

[EtGu][10-CamphorSO$_3$] : [C(NH$_2$)$_2$(NHEt)][C$_{10}$H$_{17}$OSO$_3$] 19

Asymmetric Unit

The asymmetric unit of **19** is shown in Figure 3.21 and consists of two $[EtGu]^+$ cations and two $[10\text{-CamphorSO}_3]^-$ anions.

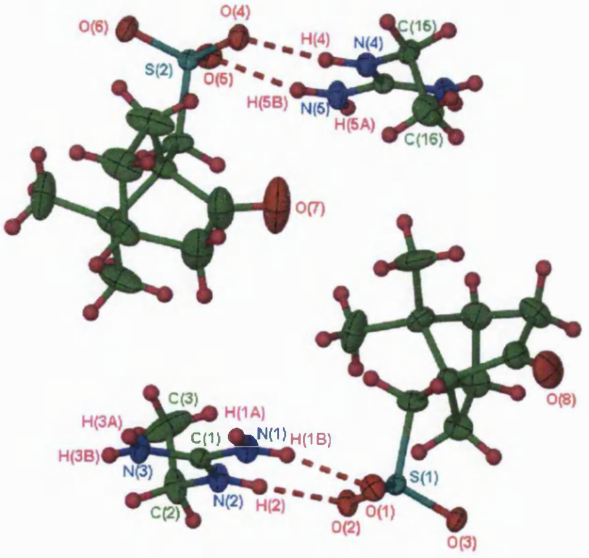

Figure 3.21; asymmetric unit of **19**. Ellipsoids are depicted at 30% probability level.

The single crystal data for **19** were ultimately collected at 240 K. Data were also collected at 150 K and 293 K, however the single crystals undergo phase changes at low temperatures and at high temperatures. Optimal convergence was observed from data collected at 240 K.

Extended Structure

The two cations and anions in the asymmetric unit form DD:AA hydrogen bonds via the two unsubstituted faces of the cation, forming ribbons. The remaining N–H donors of the substituted cation faces each form hydrogen bonds with the sulfonate oxygen atoms in a neighbouring ribbon, forming a shifted sheet (Figure 3.22). This is less corrugated than that in [MeGu][10-CamphorSO_3] **18,** as evidenced by the inter-ribbon angle of 152°. The camphor groups are directed to both sides of each sheet, which stack as repeating single layers in the gross structure, as shown in Figure 3.23. Hydrogen bond details are given in Table 3.12.

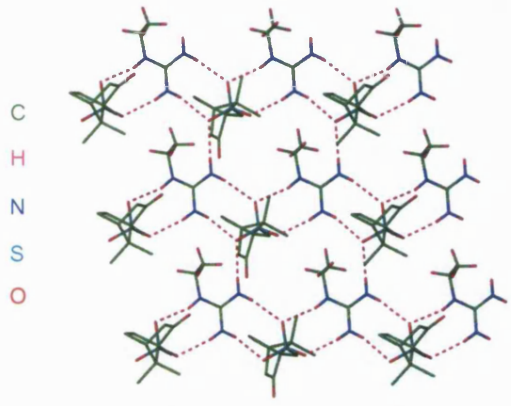

Figure 3.22; sheet formed in **19**
(*hydrogen atoms of the camphor have been removed for clarity*)

As seen in **18**, the two sulfonate camphor groups are orientated differently to each other, such that the carbonyl groups of the anions containing S(1) are directed almost orthogonal to the ribbons, whereas those in the anion containing S(2) are approximately parallel. Both of these carbonyl oxygen atoms may form weak hydrogen bonds with C–H donors. The oxygen atom O(7) forms a hydrogen bond with a methyl C–H donor from within the same ribbon.

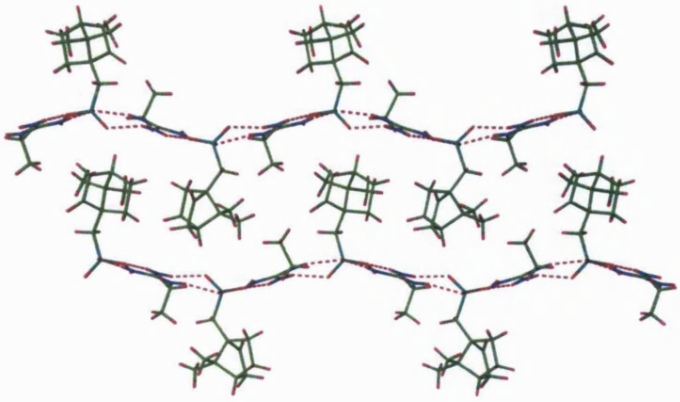

Figure 3.23; side view of sheets,
which form interdigitating single layers in **19**

The parameters suggest that the acceptor atom O(8) forms two hydrogen bonds with anion C–H donors, one from a neighbouring ribbon reinforcing the sheets, and the other from a neighbouring sheet.

D–H···A	D···A /Å	H···A /Å	D–H···A /°	Symmetry operation generating D···A
N(1)–H(1B)···O(6)	2.868(5)	2.10	168	*x*, *y*, *z*
N(1)–H(1A)···O(6)	2.947(5)	2.10	165	-*x*+2, *y*+½, -*z*
N(2)–H(2)···O(2)	2.932(4)	2.10	161	*x*, *y*, *z*
N(3)–H(3A)···O(4)	2.963(5)	2.11	165	-*x*+2, *y*+½, -*z*
N(3)–H(3B)···O(6)	3.001(5)	2.18	156	-*x*+1, *y*+½, -*z*
N(4)–H(4)···O(4)	2.917(5)	2.08	162	*x*, *y*, *z*
N(5)–H(5A)···O(3)	2.939(5)	2.09	164	-*x*+2, *y*-½, -*z*+1
N(5)–H(5B)···O(5)	2.924(5)	2.07	166	*x*, *y*, *z*
N(6)–H(6A)···O(2)	2.992(5)	2.14	166	-*x*+2, *y*-½, -*z*+1
N(6)–H(6B)···O(3)	2.999(5)	2.15	164	-*x*+3, *y*-½, -*z*+1
C(22)–H(22B)···O(8) $_{C=O}$	3.666(6)	2.92	133	*x*-1, *y*, *z*
C(23)–H(23A)···O(8) $_{C=O}$	3.645(5)	2.87	136	*x*-1, *y*, *z*
C(16)–H(16A)···O(7) $_{C=O}$	3.689(8)	2.75	163	*x*, *y*, *z*

Table 3.12; details of the hydrogen bonding in **19**

[DiMeGu][10-CamphorSO$_3$] : [C(NH$_2$)$_2$(NMe$_2$)][C$_{10}$H$_{17}$OSO$_3$] 20

Asymmetric Unit

The asymmetric unit of **20** is shown in Figure 3.24 and consists of two $[EtGu]^+$ cations and two $[10\text{-CamphorSO}_3]^-$ anions.

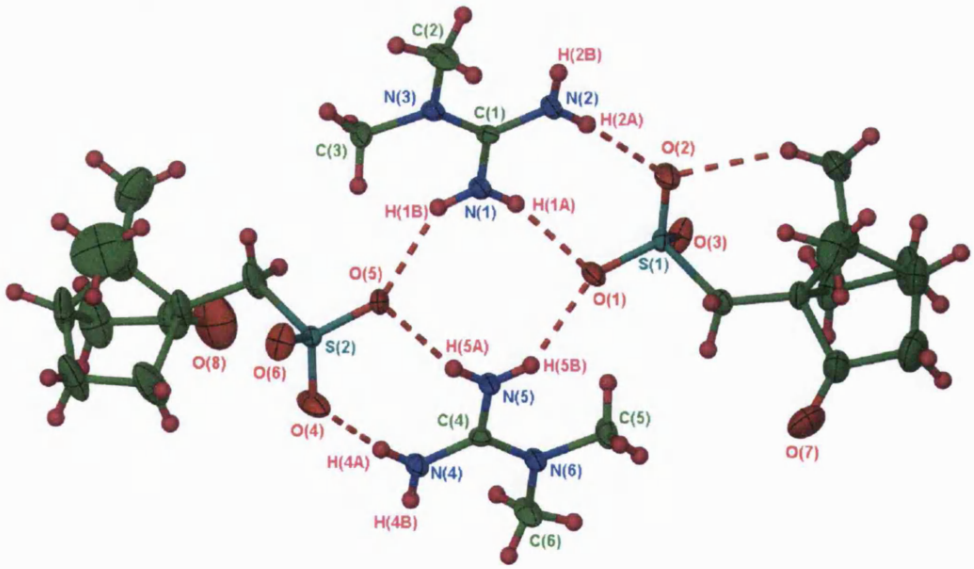

Figure 3.24; asymmetric unit of **20**. Ellipsoids are depicted at 30% probability level.

The single crystal data for **20** were collected at 240 K. Data were originally collected at 150 K where a different unit cell was noted having twice the volume of that presented here. The space group was *P*1 at 150 K, with eight cations and eight anions forming the asymmetric unit. These two structures represent different phases. The data collected for the high temperature phase resulted in satisfactory convergence whereas that for the low temperature phase was poorer, probably due to an incomplete phase change.

Extended Structure

The two independent cations and anions form DD:AA hydrogen bonds through the unsubstituted cation faces, linking them into pairs. Two of these pairs form hydrogen bonds with each other using one of the two substituted cation faces, giving the motif shown in Figure 3.24 which generates the graph set $R_4^2(8)$. These motifs are linked into sheets through hydrogen bonds using the remaining donors of the substituted cation faces, as shown in Figure 3.25. These are corrugated with an inter-ribbon angle of 119°. Details of the hydrogen bonds are given in Table 3.13.

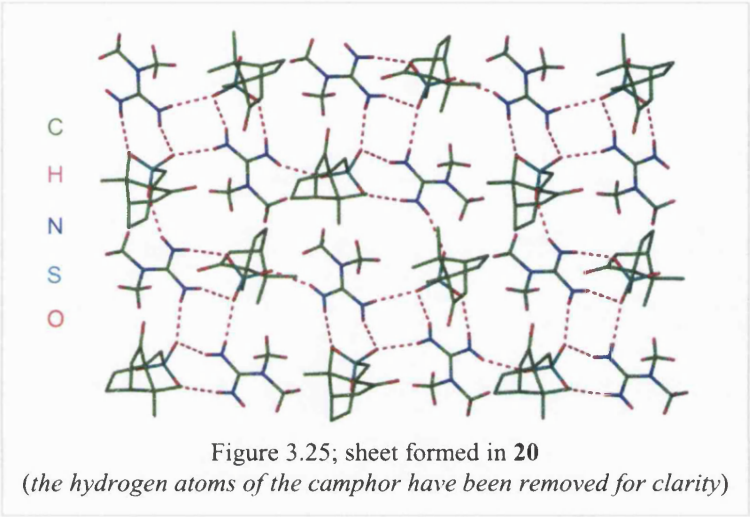

Figure 3.25; sheet formed in **20**
(*the hydrogen atoms of the camphor have been removed for clarity*)

As seen in [MeGu][10-CamSO$_3$] **18** and [EtGu][10-CamSO$_3$] **19**, the camphor groups are arranged with two different orientations almost perpendicular to each other, as can be seen in Figure 3.25. The sulfonate substituents are directed to both sides of each sheet, which stack to form interdigitating single layers in the gross structure, as shown in Figure 3.26. There also appears to be a weak C–H···O interaction involving the carbonyl moiety containing O(7) and a C–H donor of the cation based on C(1).

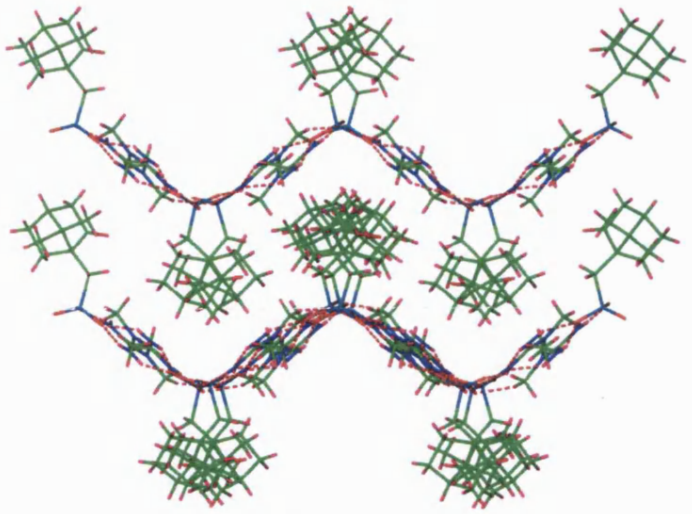

Figure 3.26; interdigitating single layers formed in **20**

D–H···A	D···A /Å	H···A /Å	D–H···A /°	Symmetry operation generating D···A
N(1)–H(1A)···O(1)	2.895(5)	2.07	158	*x*, *y*, *z*
N(1)–H(1B)···O(5)	2.870(6)	2.13	143	*x*, *y*, *z*
N(2)–H(2A)···O(2)	2.969(6)	2.10	174	*x*, *y*, *z*
N(2)–H(2B)···O(6)	2.931(6)	2.10	161	-*x*+1, -*y*-½, -*z*+1
N(4)–H(4A)···O(4)	2.851(6)	1.99	169	*x*, *y*, *z*
N(4)–H(4B)···O(3)	2.952(5)	2.14	154	-*x*+2, *y*+½, -*z*+2
N(5)–H(5A)···O(5)	2.910(5)	2.07	162	*x*, *y*, *z*
N(5)–H(5B)···O(1)	2.863(5)	2.09	148	*x*, *y*, *z*
C(3)–H(3C)···O(7)$_{C=O}$	3.446(9)	2.67	137	1+*x*, *y*, *z*

Table 3.13; details of the hydrogen bonding in **20**

3.4.1 The structural effects of alkyl substitution in guanidinium 10-camphorsulfonates

The structure of [Gu][10-CamphorSO$_3$] **IV** has been reported by Ward *et al*[1], and contains one cation and one anion in the asymmetric unit. The three cation and anion faces form DD:AA hydrogen bonds linking them into regular hexagonal GS sheets, corrugated with an inter-ribbon angle of 122°. The camphor groups of the sulfonate are directed to both sides of each sheet forming continuous interdigitating single layers in the extended structure. The carbonyl functionalities of the camphor groups all lie approximately parallel to the ribbons.

In compounds [MeGu][10-CamphorSO$_3$] **18** and [EtGu][10-CamphorSO$_3$] **19**, there are two cations and anions in the asymmetric unit that form DD:AA hydrogen bonded ribbons by means of the two unsubstituted cation faces. The substituted face of the cations has one donor, which forms a hydrogen bond to sulfonate oxygen atoms of a neighbouring ribbon, linking the ribbons into shifted GS sheets with inter-ribbon angles of 129° in **18** and 152° in **19**. The carbonyl functionalities of the camphor groups are orientated such that half are directed approximately parallel to the ribbons and the remainder are almost orthogonal, and directed to both sides of each sheet. These sheets stack forming interdigitating continuous single layers in the gross structures.

In [DiMeGu][10-CamphorSO$_3$] **20**, the cation-anion DD:AA hydrogen-bonded pairs are linked into sheets, corrugated with an inter-ribbon angle of 119°, by hydrogen bonds involving the N–H donors of the substituted cation faces. The carbonyl functionalities of the camphor groups are orientated almost perpendicular to each other. The sulfonate substituents are directed to both sides of each sheet, which interdigitate forming continuous single layers.

The (1S)-(+)-10-camphorsulfonate anion is chiral. This limits the number of possible space groups that the compounds **IV**, **18**, **19** and **20** can crystallise in to those that are non-centrosymmetric. The space group $P2_1$ is observed in the structures **IV**, **19** and **20** whereas compound **18** crystallises in the space group $P2_12_12_1$. While all of these space groups contain a 2_1 screw axis, this symmetry element does not have a common role across all structures in the generation of ribbons, sheets or the three-dimensional structure.

As seen in the 2-naphthalenesulfonate series, the substitution of the hydrogen bond donors in the cations of the 10-camphorsulfonate series does not significantly affect the gross structures. The compounds **IV**, **18**, **19** and **20** all form repeating single layers in the gross structure. In **IV** there is only one cation and one anion in the asymmetric unit that are linked into a hexagonal sheet, whereas in **18** and **19** there are two cations and anions in the asymmetric unit in order to facilitate the formation of a shifted sheet. However, it is notable that the arrangement of the ribbons in the shifted sheets in **18** and **19** are different. In **18** the ribbons are alternating in direction relative to each other, whereas in **19** the ribbons align in the same orientation (see Figure 3.27). In all cases, the camphor groups are orientated in two different directions, relative to the hydrogen-bonded array formed.

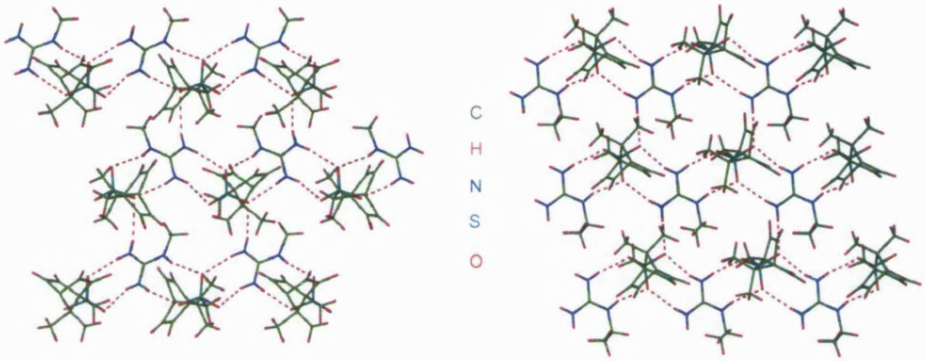

Figure 3.27; ribbons formed in [MeGu][10-CamphorSO_3] **18** (left) and in [EtGu][10-CamphorSO_3] **19** (right)

3.4.2 The effects of alkyl substitution on hydrogen bond parameters in guanidinium 10-camphorsulfonates

The DD:AA hydrogen bond distances in the structures **IV**, **18**, **19** and **20** are not greatly affected as the degree of substitution on the cation is increased. The hydrogen bond distances (N···O) vary between 2.897(3) – 2.960(3)Å in **IV**, 2.807(7) – 2.975(6)Å in **18**, 2.863(5) – 2.998(5)Å in **19** and 2.851(6) – 2.969(6)Å in **20**. The mean average hydrogen bond distances are 2.925(5)Å in **IV**, 2.928(7)Å in **18**, 2.935(5)Å in **19** and 2.904(6)Å in **20**. This consistency could be expected since the same DD:AA hydrogen bonded ribbons are formed in **18** and **19**, and there are only DD:AA hydrogen bonds between each cation-anion pair in **20**.

3.5 The overall effects of alkyl substitution in guanidinium ions when crystallised with 1-naphthalenesulfonate, 2-naphthalenesulfonate and 10-camphorsulfonate

The extended structures in the 1-naphthalenesulfonate series are significantly affected as the N–H groups of the cation are substituted. In [Gu][1-$NapSO_3$] **II** single layers are observed, in [MeGu][1-$NapSO_3$] **12** there are single layers encompassed by bilayers, and in [EtGu][1-$NapSO_3$]·H_2O **13** and [DiMeGu][1-$NapSO_3$]·H_2O **14** bilayers are observed. Compound **12** can be thought of as an intermediate between single layer and bilayer formation. As the substitution on the cation is increased, the preference for single layers is lost as bilayers are formed, suggesting that the size of the naphthalene group, the substitution of the cation and the inclusion of solvent are all potential factors that determine the three-dimensional array. This observation does not conform with Ward's assertion that the gross structure depends solely on the sulfonate substituent, as discussed in Chapter 1. However, all of the compounds studied in Ward's work contain the unsubstituted guanidinium cation and exhibit either regular hexagonal or shifted sheets.

However, there are similarities in the 1-naphthalenesulfonate structures. In all cases, the unsubstituted faces of the cation form $R_2^2(8)$ motifs via DD:AA hydrogen-bonds with the anion sulfonate groups. Regular hexagonal sheets are formed in **II**, a *stretched* hexagonal sheet with water molecules acting as spacers between the ribbons is observed in **13** and shifted sheets are formed in **12**. Compound **14** also forms sheets by the incorporation of water into the lattice.

In contrast to the 1-naphthalenesulfonate compounds, the extended structures in the 2-naphthalenesulfonate series are not significantly affected as the cation is substituted. The compounds [Gu][2-$NapSO_3$] **III**, [MeGu][2-$NapSO_3$] **15**, [EtGu][2-$NapSO_3$] **16** and [DiMeGu][2-$NapSO_3$] **17** all form bilayers in the extended array. In **III** a regular hexagonal sheet is observed, in **15** and **16** shifted sheets are formed, and in **18** there are C–H···O hydrogen bonds linking the hydrogen-bonded ribbons into sheets. The unsubstituted faces of the cations in these compounds form $R_2^2(8)$ motifs through DD:AA hydrogen-bonds with the sulfonate groups of the anions. These compounds also include two cations and two anions in the asymmetric unit, and the planes of the naphthyl rings occupy two orientations relative to the ribbons.

The extended structures in the 10-camphorsulfonate series are also not greatly affected by substitution on the cation. Structures [Gu][10-CamphorSO_3] **IV**, [MeGu][10-CamphorSO_3] **18**, [EtGu][10-CamphorSO_3] **19** and [DiMeGu][10-CamphorSO_3] **20** all contain repeating single layers in the extended array. The sulfonate substituent is too large to permit formation of bilayers, and a single layer array where the camphor groups are orientated to both sides of the sheet is more favourable. The regular hexagonal sheets are formed in **IV**, shifted sheets are observed in **18** and **19**, and sheets are formed in **20**. Compound **IV** has one cation and anion in the asymmetric unit, and consequently the camphor groups exhibit only one orientation relative to the ribbons. In contrast, compounds **18**, **19** and **20** have two cations and anions in the asymmetric unit, and the camphor groups have two orientations. As seen in the 1-naphthalenesulfonate and 2-naphthalenesulfonate series, all of the unsubstituted faces of the cation in the 10-camphorsulfonate series form $R_2^2(8)$ motifs via DD:AA hydrogen bonds with the sulfonate groups of the anions.

The C–N bond lengths in the cation and the S–O bond lengths of the anion are similar in the structures **II**, **III**, **IV**, **V** and **12**, **13**, **14**, **15**, **16**, **17**, **18**, **19** and **20**. This confirms that these bond lengths are not significantly affected as the cations and anions are varied, and is also the case for the N–C–N and O–S–O bond angles.

3.6 *N,N*-Dimethylguanidinium structures

Since the greatest differences between the structures of substituted and unsubstituted guanidinium structures have been observed with $[DiMeGu]^+$, it was of interest to expand the range of *N,N*-dimethylguanidinium sulfonate structures. A range of simple sodium sulfonates and disulfonates were therefore crystallised with $[DiMeGu]_2SO_4$. The structures of $[DiMeGu][MeSO_3]$ **21**, $[DiMeGu][PhSO_3]$ **22**, $[DiMeGu]_2[1,5\text{-}Nap(SO_3)_2]$ **23** and $[DiMeGu]_2[2,6\text{-}Nap(SO_3)_2]$ **24** are described in this section. The structural effects of substitution on the guanidinium cation are discussed by comparison with the compounds $[Gu][MeSO_3]$[1] **V**, $[Gu][PhSO_3]$[1] **VI**, $[Gu]_2[1,5\text{-}Nap(SO_3)_2]\cdot C_6H_{11}N_2$[2] **VII** and $[Gu]_2[2,6\text{-}Nap(SO_3)_2]\cdot C_{10}H_8$[3] **VIII**, which have been previously reported and incorporate the unsubstituted cation.

$[DiMeGu][MeSO_3]$: $[C(NH_2)_2(NMe_2)][CH_3SO_3]$ 21

Asymmetric Unit

The asymmetric unit of **21** is shown in Figure 3.28 and consists of one $[DiMeGu]^+$ cation and one $[MeSO_3]^-$ anion.

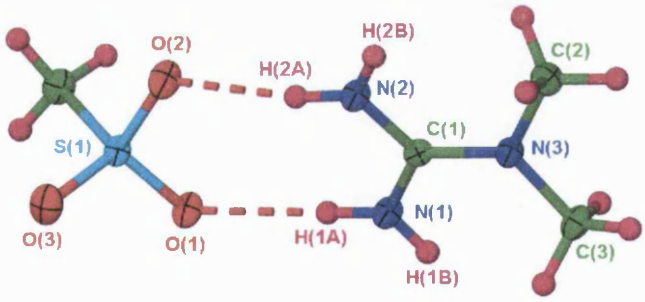

Figure 3.28; asymmetric unit of **21**. Ellipsoids are shown at 50% probability level.

Extended Structure

The unsubstituted face of the cation forms a DD:AA hydrogen-bonded motif with the anion generating the graph set $R_2^2(8)$. The substituted cation faces each form hydrogen bonds with the sulfonate group of neighbouring anions forming the graph set $R_4^2(8)$. These motifs propagate to

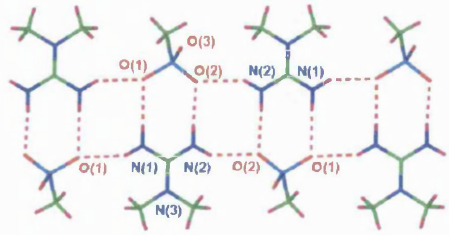

Figure 3.29; the ribbon formed in **21**

generate an infinite ribbon, as shown in Figure 3.29. Details of the hydrogen bonds are given in Table 3.14.

The sulfonate acceptor O(3) is not involved in the ribbon formation. The ribbons are slightly 'stepped', and this can be seen by looking at the N···N···O angles along the ribbon, as the angle N(1)···N(2)···O(2) is larger than that of N(2)···N(1)···O(1) (168° and 149° respectively). In the gross structure these ribbons align into layers, half of which are directed along one vector, and the remainder in another direction, with the two related by an angle of 102° (Figure 3.30). Overall, these layers pack in an alternating fashion in the lattice.

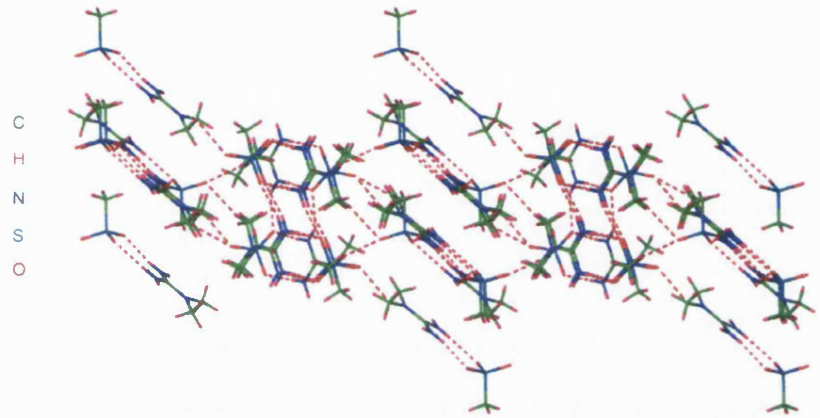

Figure 3.30; the extended array formed in **21**

The oxygen atom O(3) is involved in the formation of two C–H···O hydrogen bonds, involving a C–H donor of the methyl group of the substituted cation [C(3)–H(3C)···O(3)] and a C–H donor of the methyl group of the anion [C(4)–H(4A)···O(3)]. These hydrogen bonds cross-link the ribbons to form a three-dimensional array.

D–H···A	D···A /Å	H···A /Å	D–H···A /°	Symmetry operation generating D···A
N(1)–H(1A)···O(1)	2.945(2)	2.07	178	*x*, *y*, *z*
N(1)–H(1B)···O(1)	2.990(2)	2.30	136	-*x*+2, -*y*, -*z*+1
N(2)–H(2A)···O(2)	2.823(2)	1.95	172	*x*, *y*, *z*
N(2)–H(2B)···O(2)	2.901(2)	2.12	147	-*x*+1, -*y*+1, -*z*+1
C(3)–H(3C)···O(3)	3.280(2)	2.91	104	1+*x*, ½-*y*, *z*-½
C(4)–H(4A)···O(3)	3.428(2)	2.48	163	1-*x*, *y*-½, $^{3}/_{2}$-*z*

Table 3.14; details of the hydrogen bonding in **21**

[DiMeGu][$PhSO_3$] : [$C(NH_2)_2(NMe_2)$][$C_6H_5SO_3$] 22

Asymmetric Unit

The asymmetric unit of **22** is shown in Figure 3.31 and consists of one $[DiMeGu]^+$ cation and one $[PhSO_3]^-$ anion.

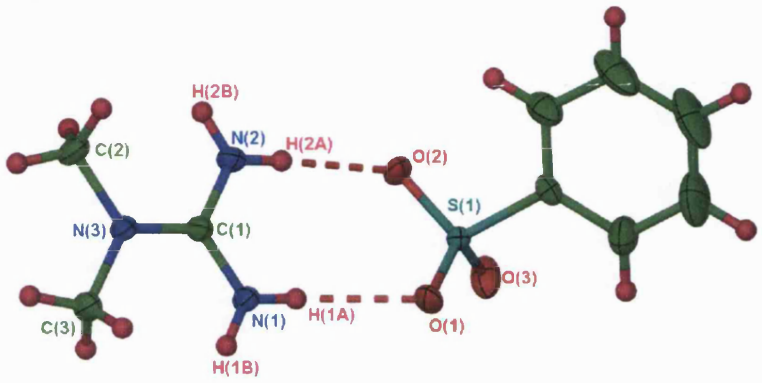

Figure 3.31; asymmetric unit of **22**. Ellipsoids are depicted at 50% probability level.

Extended Structure

The unsubstituted face of the cation forms a DD:AA hydrogen-bonded motif with the sulfonate group of the anion linking them into pairs. These cation-anion pairs are connected into ribbons by hydrogen bonds involving the substituted cation faces, forming the graph set $R_4^2(8)$, including the guanidinium N–H donors but only two of the sulfonate oxygen atoms, as shown in Figure 3.32.

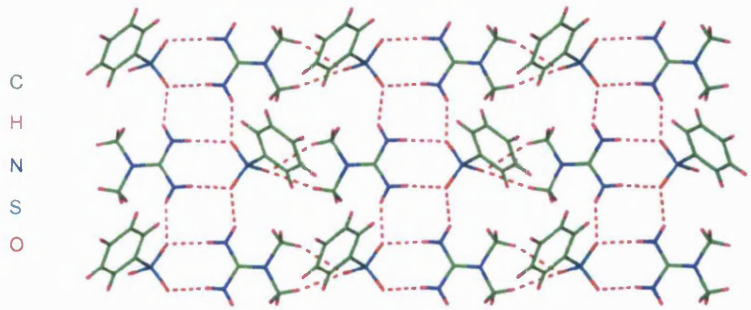

Figure 3.32; sheet formed in **22**

This ribbon is formed using the same hydrogen-bonding motifs as seen in [DiMeGu][$MeSO_3$] **21**. However, in **22** there are no C–H···O interactions between the anion and oxygen atoms of neighbouring ribbons, in contrast to **21**. Instead, the ribbons are linked into almost flat sheets (θ_{IR}162°) by C–H···O hydrogen bonds from the two Me groups of the

cation generating a $R_2^1(6)$ motif. For details of the hydrogen bonds see Table 3.15. The phenyl rings in one ribbon are involved in C–H···π interactions with those in a neighbouring ribbon. The sulfonate substituents are directed to the same side of each sheet leading to bilayers in the gross structure. There are also edge-to-face C–H···π interactions between the phenyl groups of interdigitating anions.

D–H···A	D···A /Å	H···A /Å	D–H···A /°	Symmetry operation generating D···A
N(1)–H(1A)···O(1)	2.951(2)	2.12	159	*x*, *y*, *z*
N(1)–H(1B)···O(2)	2.836(2)	2.04	150	-*x*+½, *y*, *z*+½
N(2)–H(2A)···O(2)	2.908(2)	2.03	177	*x*, *y*, *z*
N(2)–H(2B)···O(1)	2.866(2)	2.20	133	-*x*+½, *y*, *z*+½
C(2)–H(2D)···O(3)	3.288(2)	2.57	156	*x*-1, *y*, *z*
C(3)–H(3B)···O(3)	3.370(2)	2.42	163	*x*-1, *y*, *z*

Table 3.15; details of the hydrogen bonding in **22**

$[DiMeGu]_2[1,5\text{-}Nap(SO_3)_2]$: $[C(NH_2)_2(NMe_2)]_2[C_{10}H_6(1,5\text{-}SO_3)_2]$ 23

Asymmetric Unit

The asymmetric unit of **23** is shown in Figure 3.33 and contains one $[DiMeGu]^+$ cation and half of one $[1,5\text{-}Nap(SO_3)_2]^{2-}$ anion.

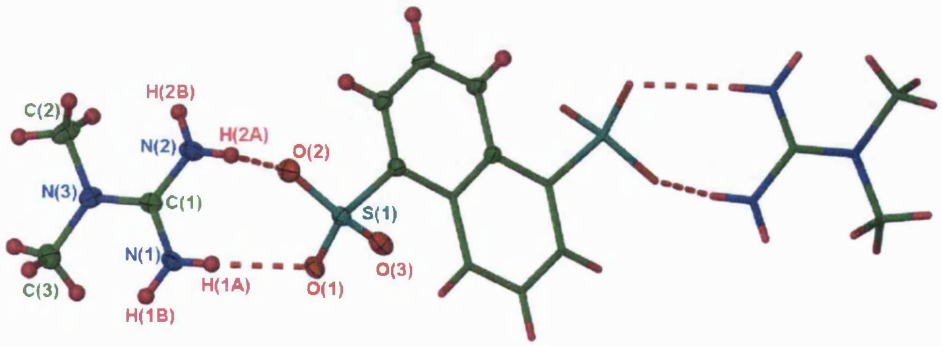

Figure 3.33; asymmetric unit of **23**. Ellipsoids are depicted at 50% probability level.
(*the asymmetric unit is denoted by ellipsoids, the stick model represents atoms generated by symmetry*)

Extended Structure

The unsubstituted face of the cation forms a DD:AA hydrogen-bonded motif with the anion. One of the substituted cation faces forms the hydrogen bond N(1)–H(1B)···O(3) with the sulfonate oxygen atom of a neighbouring anion generating a $R_4^4(12)$ motif (Figure 3.34). The remaining donor [N(2)–H(2B)] on the other substituted cation face links these motifs

into a complex sheet, as shown in Figure 3.35, in which there are no significant C–H···O hydrogen bonds.

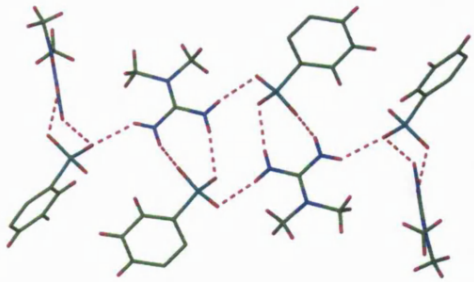

Figure 3.34; hydrogen-bonded motif in **23**

Nonetheless, all of the guanidinium N–H donors and sulfonate acceptors contribute to the hydrogen-bonding array in this structure. The sheet itself is thicker than those observed in the other structures in this chapter due to the orientation of the cations and anions, with a S···S distance of 5.5Å. For details of the hydrogen bonds see Table 3.16.

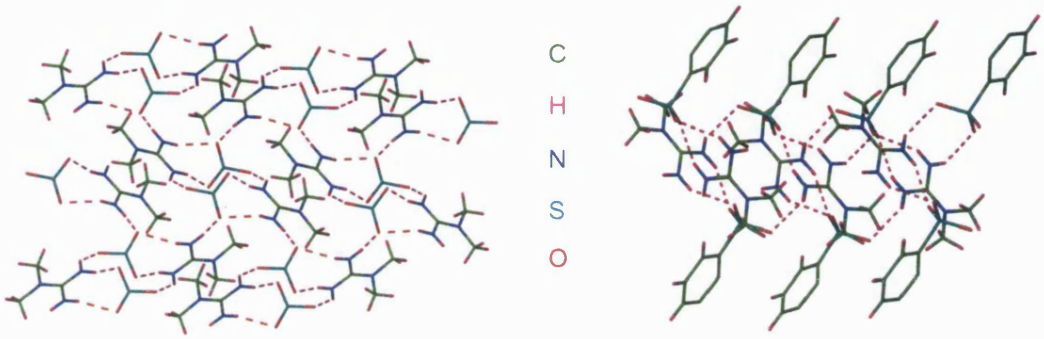

Figure 3.35; complex sheet formed in **23** (*left*) and side view (*right*)
(*part of the anion is removed for clarity*)

The sulfonate substituents are directed to both sides of each sheet, leading to the formation of a pillared brick architecture in the gross structure.

D–H···A	D···A /Å	H···A /Å	D–H···A /°	Symmetry operation generating D···A
N(1)–H(1A)···O(1)	2.910(2)	2.08	158	*x*, *y*, *z*
N(1)–H(1B)···O(2)	2.892(2)	2.16	140	-*x*, -*y*, -*z*
N(2)–H(2A)···O(3)	2.960(2)	2.18	148	*x*, *y*, *z*
N(2)–H(2B)···O(2)	2.881(2)	2.14	142	*x*, -*y*+½ , *z*-½

Table 3.16; details of the hydrogen bonding in **23**

$[DiMeGu]_2[2,6\text{-}Nap(SO_3)_2]$: $[C(NH_2)_2(NMe_2)]_2[C_{10}H_6(2,6\text{-}SO_3)_2]$ 24

Asymmetric Unit

The asymmetric unit of **24** is shown in Figure 3.36 and consists of two $[DiMeGu]^+$ cations and two independent half units of $[2,6\text{-}Nap(SO_3)_2]^{2-}$ anions.

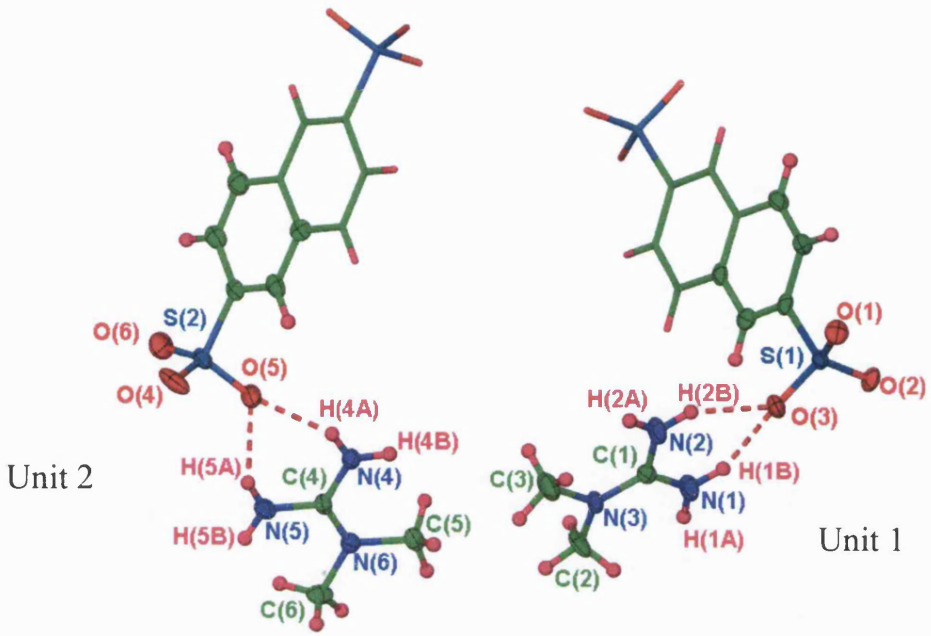

Figure 3.36; asymmetric unit of **24**. Ellipsoids are depicted at 50% probability level.
(*the asymmetric unit is denoted by ellipsoids, the stick model represents atoms generated by symmetry*)

Extended Structure

These two sets of cation-anion units are involved in different packing arrangements, so will be first described separately. Unit 1 contains the anion based on S(1) and the cation containing C(1), whereas Unit 2 consist of the anion based on S(2) and the cation based on C(4).

Unit 1

The cation and the sulfonate oxygen atoms are approximately coplanar. The unsubstituted face of the cation does not form the expected DD:AA motif, but forms a DD:A hydrogen-bonded motif generating the graph set $R_2^1(6)$ with only one oxygen atom of the sulfonate. The two N–H donors of the substituted cation faces form hydrogen bonds with neighbouring sulfonates, linking the cations and anions into hydrogen-bonded sheets, as shown in Figure 3.37.

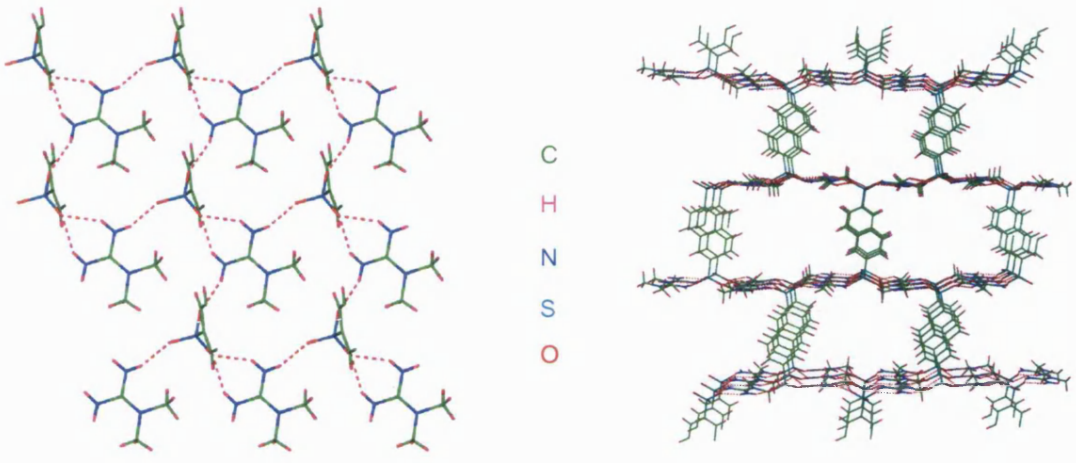

Figure 3.37; the sheet (*left*) and pillared brick array (*right*) formed in Unit 1

This sheet is reinforced by C–H···O hydrogen bonds, involving C–H donors of the cation methyl groups, and is virtually flat (θ_{IR} of 173°) with naphthyl groups directed to both sides. Neighbouring sheets are linked by the disulfonate, forming a pillared brick architecture in the gross structure, as shown in Figure 3.37.

Unit 2

The cation and sulfonate oxygen atoms are almost perpendicular, in contrast to those in Unit 1. The unsubstituted cation face forms a DD:A hydrogen-bonded motif with the sulfonate generating the graph set $R_2^1(6)$. The donors of the substituted cation faces form hydrogen bonds with neighbouring sulfonate oxygen atoms leading to the formation of parallel ribbons, as shown in Figure 3.38, which are reinforced by C–H···O interactions that utilise donors from the cation methyl groups. These ribbons are linked into a two-dimensional array via the two sulfonate groups of the anion (Figure 3.38). For details of the hydrogen bonding see Table 3.17.

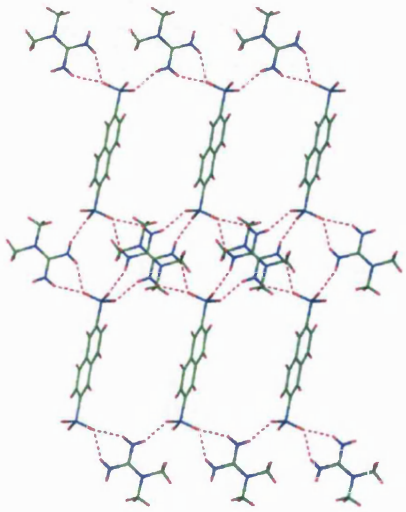

Figure 3.38; ribbon formed in Unit 2 in **24**

Units 1 and 2 Combined

The two-dimensional array of Unit 2 interpenetrates the pillared brick architecture of Unit 1, minimising the void space in the gross structure, as shown in Figure 3.39. There are no hydrogen bonds formed between these two arrays, however there are face-to-face π···π interactions between the Unit 1 and Unit 2 sulfonate naphthalene groups.

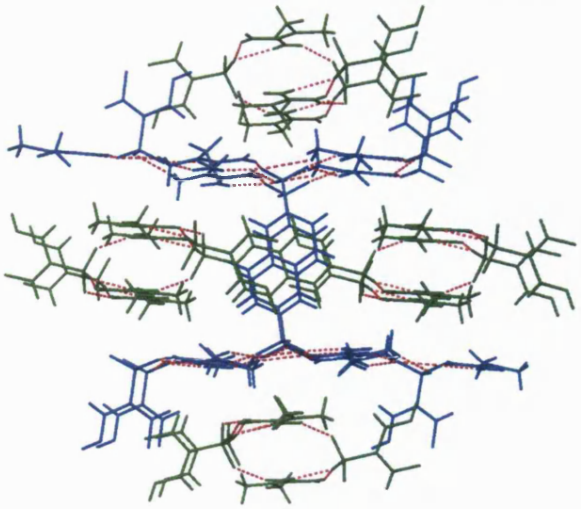

Figure 3.39; the interpenetrating lattices formed in **24** (*Unit 1 shown in blue, Unit 2 shown in green)*

D–H···A	D···A /Å	H···A /Å	D–H···A /°	Symmetry operation generating D···A
N(1)–H(1A)···O(1)	2.796(5)	2.00	151	*x*, -*y*+½, *z*+½
N(1)–H(1B)···O(3)	2.844(5)	2.05	149	*x*, *y*, *z*
N(2)–H(2A)···O(2)	2.800(5)	2.04	145	*x*-*1*, *y*, *z*
N(2)–H(2B)···O(3)	2.877(6)	2.10	147	*x*, *y*, *z*
N(4)–H(4A)···O(5)	2.891(5)	2.10	149	*x*, *y*, *z*
N(4)–H(4B)···O(4)	2.877(5)	2.05	156	*x*+1, *y*, *z*
N(5)–H(5A)···O(5)	2.923(5)	2.15	147	*x*, *y*, *z*
N(5)–H(5B)···O(6)	2.904(5)	2.09	153	-*x*-1, -*y*, -*z*+1
C(2)–H(2D)···O(2)	3.401(6)	2.44	167	*x*-1, *y*-½, ½+*z*
C(2)–H(2E)···O(1)	3.425(5)	2.54	151	*x*, *y*-½, ½+*z*

Table 3.17; details of the hydrogen bonding in **24**

3.6.1 Comparison of *N,N*-dimethylguanidinium sulfonates with their guanidinium analogues

The structures of $[Gu][MeSO_3]$[1] **V**, $[Gu][PhSO_3]$[1] **VI**, $[Gu]_2[1,5\text{-}Nap(SO_3)_2]\cdot C_6H_{11}N$[2] **VII** and $[Gu]_2[2,6\text{-}Nap(SO_3)_2]\cdot C_{10}H_8$[3] **VIII** have previously been reported by Ward *et al.*

$[Gu][MeSO_3]$ **V** has one cation and one anion in the asymmetric unit. The cations and anions form hydrogen bonds with each other through three DD:AA motifs forming the regular hexagonal GS sheet. The methyl groups of the sulfonate are directed to one side of each flat sheet (θ_{IR} 180°) and interdigitate in the gross structure generating a repeating bilayer.

The compound $[DiMeGu][MeSO_3]$ **21** also has one cation and anion in the asymmetric unit, however the repeating bilayer structure is not observed. The unsubstituted face of the cation forms a DD:AA motif with the anion. These cation-anion pairs form a ribbon through hydrogen bonding involving the single N–H donors of the two substituted cation faces. These ribbons stack with C–H···O hydrogen-bonding involving C–H donors of the methyl groups in both the cations and anions. This links the ribbons into a three-dimensional hydrogen-bonded network.

The structures observed in **V** and **21** are very different. Bilayers of hexagonal sheets are formed in **V** whereas ribbons are formed in **21** using N–H···O hydrogen bonds. In compound **21** the C–H donors of the anion methyl group compete with the C–H donors of the cation methyl groups, linking the ribbons into a three-dimensional array, which may explain why sheets are not observed.

* * *

$[Gu][PhSO_3]$ **VI** has two cations and two anions in the asymmetric unit. These form DD:AA hydrogen bonds forming the regular hexagonal GS sheets, which are reasonably flat with an inter-ribbon angle of 150°. The phenyl groups of one of the independent anions lie almost orthogonal to the ribbons, whereas those of the other independent anion are approximately parallel. The phenyl groups are directed to one side of each sheet, generating repeating interdigitating bilayers in the extended structure.

The compound [DiMeGu][$PhSO_3$] **22** has one cation and anion in the asymmetric unit. The unsubstituted cation face forms a DD:AA hydrogen-bonded motif with the sulfonate, and the substituted cations faces form single hydrogen bonds with neighbouring sulfonates generating a ribbon. Hydrogen bonds from the methyl C–H donors of the cation to a sulfonate oxygen atom link the ribbons into flat sheets. The phenyl groups are directed to one side of each sheet leading to interdigitating bilayers in the gross structure.

The structures of **VI** and **22** show similarities, even though there is only one DD:AA motif available in **22** due to the substitution in the cation. Bilayers are formed in both cases. However, the sheets in these structures are different. In **VI** the regular hexagonal sheets are formed using the three faces of the cations and anions. In compound **22**, ribbons are linked into sheets by hydrogen bonding utilising the cation C–H donors.

* * *

$[Gu]_2[1,5\text{-}Nap(SO_3)_2]\cdot C_6H_{11}N$ **VII** has one cation, half an anion and a half a molecule of hexanenitrile in the asymmetric unit. The hexanenitrile is a guest molecule and not involved in hydrogen bond formation. The cations and anions are linked by three DD:AA hydrogen bonding motifs, forming highly corrugated hexagonal GS sheets (θ_{IR} of 72°). The naphthalene groups are directed to both sides of each sheet, where the second sulfonate group in each anion forms another sheet, by DD:AA hydrogen bonds with the cations, generating a corrugated pillared brick architecture. There are pores running perpendicular to the ribbons, which are occupied by the hexanenitrile molecules.

$[DiMeGu]_2[1,5\text{-}Nap(SO_3)_2]$ **23** has one cation and half an anion in the asymmetric unit, linked by DD:AA hydrogen-bonds via the unsubstituted face of the cation. The other two substituted cation faces form single hydrogen bonds involving the N–H donors and the sulfonate oxygen atoms. This hydrogen bonding links the cations and anions into a complex sheet, where the naphthyl groups are directed to either side forming a pillared brick architecture.

The structures observed in **VII** and **23** exhibit some commonalities, even though there is only one DD:AA motif in **23**. Pillared brick architectures are formed in both compounds, with guest molecules incorporated in **VII** but no guests included in **23**. However, the sheets

formed in these structures are different. In **VII** the regular hexagonal sheets are formed, whereas in **23** a thick and complex sheet is observed.

* * *

$[Gu]_2[2,6\text{-}Nap(SO_3)_2]\cdot{}^3/_2C_{10}H_8$ **VIII** has one cation, half an anion and one and three quarters of a guest naphthalene molecule in the asymmetric unit. The cations and anions form three DD:AA hydrogen-bonding motifs linking them into hexagonal GS sheets, with an inter-ribbon angle of 133°. The naphthyl groups are directed to both sides forming a pillared brick architecture in the extended array, with pores which are occupied by naphthalene molecules.

$[DiMeGu]_2[2,6\text{-}Nap(SO_3)_2]$ **24** has two cations and two halves of the anion in the asymmetric unit that form two independent arrays. Ribbons are formed between half of the cations and anions, which are linked into a two-dimensional array via the two sulfonate groups of each anion. A pillared brick array is also observed by hydrogen bonding between the remaining cations and anions, with parallel sheets linked by the disulfonates. These two arrays interpenetrate in the gross structure minimising possible void space.

The structures observed in **VIII** and **24** show surprising similarities, considering there are no DD:AA hydrogen bonds observed in **24**. However, pillared brick arrays are observed in both compounds, although the sheets formed in these two structures are different and guest molecules are incorporated in **VIII** but not in **24**. In compound **VIII** regular hexagonal sheets are formed, while in **24** there are two packing motifs, an independent ribbon and a pillared brick architecture, which interpenetrate in the extended structure.

* * *

The compounds $[DiMeGu][PhSO_3]$ **22**, $[DiMeGu]_2[1,5\text{-}Nap(SO_3)_2]$ **23** and $[DiMeGu]_2[2,6\text{-}Nap(SO_3)_2]$ **24** form the expected bilayer and pillared brick arrays due to the size of the sulfonate substituents, even though **24** does not form DD:AA hydrogen bonds and the cations in these structures only have one DD hydrogen-bonding face. Notably, $[DiMeGu][MeSO_3]$ **21** does not form a bilayer structure, but ribbons that are further linked into a three-dimensional array through C–H···O hydrogen bonds.

Compounds [DiMeGu][2-NapSO_3] **17**, [DiMeGu][MeSO_3] **21** and [DiMeGu][PhSO_3] **22** all form similar hydrogen-bonded ribbons, where only two of the three sulfonate oxygen atoms are involved. However, a similar ribbon is not formed in [DiMeGu][1-NapSO_3]·H_2O **14**, possibly due to the inclusion of water molecules. The ribbon observed in **17**, **21** and **22** is also not formed in [DiMeGu][10-CamphorSO_3] **20** due to the steric bulk of the camphor substituent, and its expected proximity to the substituted cation if this array was observed. By contrast, in compound [DiMeGu][mTPPMS] **3** (Chapter 2, section 2.2) all of the sulfonate oxygen atoms are involved in the ribbons as shown in Figure 3.40.

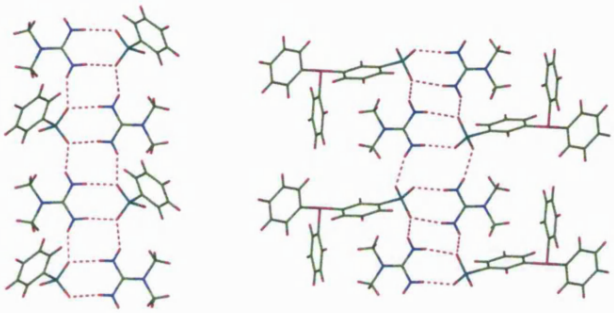

Figure 3.40; the hydrogen-bonded ribbons incorporating two sulfonate oxygen atoms (*left*) and all three sulfonate oxygen atoms (*right*).

The guanidinium-monosulfonate structures [Gu][MeSO_3] **V** and [Gu][PhSO_3] **VI** form bilayers, which is expected, as this array is most favourable when the sulfonate groups are small (ion centre-to-centre distance <4.75Å)[2]. The guanidinium-disulfonate structures [Gu]$_2$[1,5-Nap$(SO_3)_2$]·$C_6H_{11}N$ **VII** and [Gu]$_2$[2,6-Nap$(SO_3)_2$]·$^3/_2C_{10}H_8$ **VIII** both form pillared brick architectures, which is also expected as large pillars are more likely to form this type of array either with or without the inclusion of guest molecules[4]. The regular hexagonal hydrogen-bonded sheets are observed in all of these compounds, and the DD:AA hydrogen bond distances (N···O) are similar (see Table 3.18).

The dimethylguanidinium-sulfonate compounds [DiMeGu][PhSO_3] **22** and [DiMeGu]$_2$[1,5-Nap$(SO_3)_2$] **23** exhibit similar DD:AA hydrogen bond distances to each other. In contrast, in [DiMeGu][MeSO_3] **21** a decrease in the mean DD:AA hydrogen bond distance is observed (Table 3.18), suggesting an increase in hydrogen bond strength. However, the two DD:AA hydrogen bond distances in compound **21** are 2.945(2)Å and 2.828(2)Å. The latter distance is short and it is this short contact that leads to the mean hydrogen bond distance for this compound being the shortest reported in this chapter. It is unclear why this contact is so

short, as the ribbons generated in **21** are similar to those observed in **17** and **22**, which both exhibit longer hydrogen bond distances.

	V	VI	VII	VIII	21	22	23	24
N···O Å	2.893(2)-2.935(3)	2.885(6)-3.060(7)	2.914-3.033	2.881-3.027	2.823(2)-2.945(2)	2.908(2)-2.951(2)	2.910(2)-2.960(2)	–
Mean N···O Å	2.915(3)	2.939(7)	2.965	2.939	2.884(2)	2.930(2)	2.935(2)	–

Table 3.18; DD:AA hydrogen bond lengths in **V-VIII** and **21-23**

The C–N and S–O bond lengths and N–C–N and O–S–O bond angles are similar, respectively, in the structures **V-VIII** and **21-24** revealing that these parameters are unaffected by variation of the cation and anion.

3.6.2 Future Work

The reactions of MeGuCl and $[EtGu]_2SO_4$ with the sulfonates $Na[MeSO_3]$, $Na[PhSO_3]$, $Na_2[1,5\text{-}Nap(SO_3)_2]$ and $Na_2[2,6\text{-}Nap(SO_3)_2]$ did not produce single crystals from water or methanol reaction mixtures. With the exception of $[EtGu][1\text{-}NapSO_3]\cdot H_2O$ **13**, where a stretched hexagonal sheet is formed, all of the compounds in this chapter that incorporate $[MeGu]^+$ or $[EtGu]^+$ cations form hydrogen-bonded shifted sheets. Therefore, isolating these crystalline products needs to be attempted so that their structures can be compared with those reported here, and to ascertain if the shifted sheet array is maintained.

The incorporation of larger mono- and disulfonates such as $Na(1\text{-}MeC_6H_4SO_3\text{-}3)$ and Na_2(2,6-anthracenedisulfonate) into guanidinium- and substituted guanidinium-sulfonate structures requires investigation to assess if the extended array formed can be predicted, based on the results already reported (Figure 3.41). The compound $[Gu][PhSO_3]$ **V** exhibits bilayers in the gross array. The ion centre-to-centre distance in $[PhSO_3]^-$ is 4.04Å, which is smaller than the value 4.75Å used by Ward to predict single layer or bilayer formation. However, the ion centre-to-centre distance in $[1\text{-}MeC_6H_4SO_3\text{-}3]^-$ is 5.27Å. Therefore, using Ward's hypothesis, single layers would be predicted in the guanidinium-sulfonate

compounds containing this anion. The crystal structure of [Gu][1-$MeC_6H_4SO_3$-3] has been reported by Ward *et al*[5] and repeating single layers are indeed observed. It would be of interest to see if this degree of structure prediction was maintained for the substituted guanidinium analogues.

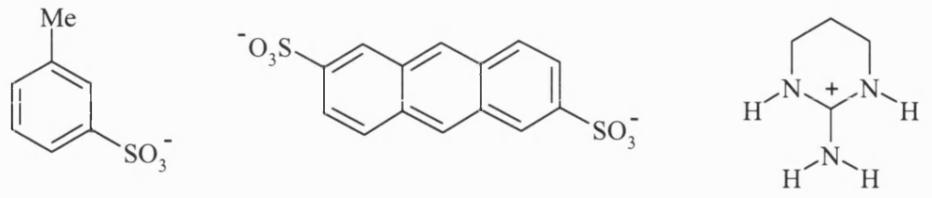

Figure 3.41; structures of [1-$MeC_6H_4SO_3$-3]$^-$ (*left*), [2,6-anthracenedisulfonate]$^-$ (*centre*) and [*N*,*N*'-methylamine-cyclo-propanamine]$^+$ (*right*)

The crystal structure of $[Gu]_2$[2,6-anthracenedisulfonate]·3anthracene has been reported by Ward *et al*[3], where regular hexagonal hydrogen-bonded sheets are linked into a pillared brick array via the disulfonate, and the anthracene molecules are guests. The compounds $[DiMeGu]_2$[1,5-$Nap(SO_3)_2$] **23** and $[DiMeGu]_2$[2,6-$Nap(SO_3)_2$] **24** also exhibit a pillared brick architecture, however the two-dimensional sheet is complex in **23** and in **24** there are two interpenetrating arrays. Therefore, a pillared brick architecture is expected when incorporating the 2,6-anthracenedisulfonate anion into substituted guanidinium-sulfonate structures, but prediction of the sheet formed is much more difficult. The compounds containing the 2,6-anthracenedisulfonate anion and substituted guanidinium cations require investigation to identify the two-dimensional array in these structures.

The impact of including more constrained substituted guanidinium cations into GS arrays, for example *N*,*N*'-methylamine-cyclo-propanamine (Figure 3.41) where the third hydrogen-bonding face of the cation is blocked by the ring, should be examined to assess the effect of this restraint on the robustness of the extended array. A ribbon consisting of DD:AA hydrogen bonds between the cations and anions would be expected. However, a two dimensional array may be less probable due to the lack of a third face containing N–H donors. However, C–H donors are available and could form C–H···O hydrogen bonds with the sulfonate oxygen atoms linking the ribbons into sheets.

3.7 Experimental

The sodium salts of 1-naphthalenesulfonic acid, $Na[C_{10}H_7SO_3\text{-}1]$, 2-naphthalenesulfonic acid, $Na[C_{10}H_7SO_3\text{-}2]$, *d*-10-camphorsulfonic acid, $Na[C_{10}H_{17}SO_4]\cdot H_2O$, methyl sulfonic acid, $Na[CH_3SO_3]$, benzenesulfonic acid, $Na[C_6H_5SO_3]$, 1,5-naphthalenedisulfonic acid, $Na_2[C_{10}H_6(1,5\text{-}SO_3)_2]\cdot xH_2O$ and 2,6-naphthalenedisulfonic acid, $Na_2[C_{10}H_6(2,6\text{-}SO_3)_2]$ were purchased from Aldrich Chemical Co. Microanalysis (C, H and N) were carried out by Mr. Alan Carver (University of Bath Microanalytical Service). It is notable that many of the microanalysis results repeatedly showed lower than anticipated percentages of carbon, hydrogen and nitrogen. This may be a consequence of the presence of impurities, or be a result of incomplete combustion.

Synthesis of [MeGu][1-NapSO$_3$] 12

A solution of $[C(NH_2)_2(NHMe)]Cl$ (0.048g, 0.43mmol) in methanol (2cm^3) was added to a solution of $Na[C_{10}H_7SO_3\text{-}1]$ (0.100g, 0.43mmol) in methanol (2cm^3) and allowed to slowly evaporate. Small colourless crystals of $[C(NH_2)_2(NHMe)][C_{10}H_7SO_3\text{-}1]$ **12** were collected. Calc for $C_{12}H_{15}N_3O_3S$: C, 51.2; H, 5.37; N, 14.9. Found: C, 44.7; H, 4.45; N, 11.1%. The microanalysis repeatedly produced poor results. However, the powder diffraction pattern of **12** shows good agreement with that simulated from single crystal data. No other crystalline product was identified after numerous single crystal analyses, suggesting that amorphous material is present as an impurity in the bulk.

Synthesis of [EtGu][1-NapSO$_3$]·H$_2$O 13

A solution of $[C(NH_2)_2(NHEt)]_2SO_4$ (0.048g, 0.43mmol) in water (2cm^3) was added to a solution of $Na[C_{10}H_7SO_3\text{-}1]$ (0.100g, 0.43mmol) in water (2cm^3) and allowed to slowly evaporate. Small colourless crystals of $[C(NH_2)_2(NHEt)][C_{10}H_7SO_3\text{-}1]\cdot H_2O$ **13** were collected. Crystals with the same cell parameters were also prepared from methanol. Calc for $C_{13}H_{19}N_3O_4S$: C, 49.8; H, 6.11; N, 13.4. Found: C, 49.2; H, 6.06; N, 13.5%.

Synthesis of [DiMeGu][1-NapSO$_3$]·H$_2$O 14

A solution of $[C(NH_2)_2(NMe_2)]_2SO_4$ (0.059g, 0.22mmol) in water (2cm^3) was added to a solution of $Na[C_{10}H_7SO_3\text{-}1]$ (0.100g, 0.43mmol) in water (2cm^3) and allowed to slowly evaporate. Small colourless crystals of $[C(NH_2)_2(NMe_2)][C_{10}H_7SO_3\text{-}1]\cdot H_2O$ **14** were collected. Crystals with the same cell parameters were also collected from methanol. Calc for $C_{13}H_{19}N_3O_4S$: C, 49.8; H, 6.11; N, 13.4. Found: C, 49.6; H, 5.7; N, 13.7%.

Synthesis of [MeGu][2-NapSO$_3$] 15

A solution of [C(NH$_2$)$_2$(NHMe)]Cl (0.048g, 0.43mmol) in water (2cm^3) was added to a solution of Na[C$_{10}$H$_7$SO$_3$-2] (0.100g, 0.43mmol) in water (2cm^3) and allowed to slowly evaporate. Small colourless crystals of [C(NH$_2$)$_2$(NHMe)][C$_{10}$H$_7$SO$_3$-2] **15** were collected. Calc for C$_{12}$H$_{15}$N$_3$O$_3$S: C, 51.2; H, 5.37; N, 14.9. Found: C, 43.9; H, 4.42; N, 12.1%. The microanalysis results are consistently poor. However, the powder pattern and the simulated powder pattern from single crystal data show good agreement. This suggests that the single crystal is representative only of the crystalline bulk material, and that an amorphous impurity is present.

Synthesis of [EtGu][2-NapSO$_3$] 16

A solution of [C(NH$_2$)$_2$(NHEt)]$_2$SO$_4$ (0.059g, 0.22mmol) in methanol (5cm^3) was added to a solution of Na[C$_{10}$H$_7$SO$_3$-2] (0.100g, 0.43mmol) in methanol (5cm^3) and allowed to slowly evaporate. Small colourless crystals of [C(NH$_2$)$_2$(NHEt)][C$_{10}$H$_7$SO$_3$-2] **16** were collected. Calc for C$_{13}$H$_{17}$N$_3$O$_3$S: C, 52.9; H, 5.80; N, 14.2. Found: C, 43.8; H, 4.87; N, 11.0%. The microanalysis results are poor indicating an impurity in the bulk material. However, a crystalline impurity cannot be identified from the powder diffraction results as the diffraction pattern observed is different to that simulated from single crystal data. It is possible that the single crystal lattice is disrupted on grinding.

Synthesis of [DiMeGu][2-NapSO$_3$] 17

A solution of [C(NH$_2$)$_2$(NMe$_2$)]$_2$SO$_4$ (0.059g, 0.22mmol) in methanol (5cm^3) was added to a solution of Na[C$_{10}$H$_7$SO$_3$-2] (0.100g, 0.43mmol) in methanol (5cm^3) and allowed to slowly evaporate. Small colourless crystals of [C(NH$_2$)$_2$(NMe$_2$)][C$_{10}$H$_7$SO$_3$-2] **17** were collected. Calc for C$_{13}$H$_{17}$N$_3$O$_3$S: C, 52.9; H, 5.80; N, 14.2. Found: C, 42.0; H, 4.81; N,11.9 %. The microanalysis results are repeatedly low, however X-ray powder diffraction results are consistent with the simulated powder pattern from the single crystal data, suggesting the presence of an amorphous impurity in the bulk material.

Synthesis of [MeGu][10-CamphorSO$_3$] 18

A solution of [C(NH$_2$)$_2$(NHMe)]Cl (0.057g, 0.52mmol) in water (2cm^3) was added to a solution of Na[C$_{10}$H$_{17}$OSO$_3$]·H$_2$O (0.130g, 0.52mmol) in water (3cm^3) and allowed to slowly evaporate. Small colourless crystals of [C(NH$_2$)$_2$(NHMe)][C$_{10}$H$_{17}$OSO$_3$] **18** were collected. Calc for C$_{12}$H$_{19}$N$_3$O$_4$S: C, 47.2; H, 7.59; N, 13.8. Found: C, 45.5; H, 7.50; N 14.2 %. There

is good agreement in the powder diffraction results and simulated powder pattern, revealing that the crystal is representative of the bulk material. However, this does not negate the possibility of an amorphous impurity in the bulk which would contribute to discrepancy in the microanalysis results.

Synthesis of [EtGu][10-CamphorSO$_3$] 19

A solution of $[C(NH_2)_2(NHEt)]_2SO_4$ (0.071g, 0.26mmol) in methanol (2cm^3) was added to a solution of $Na[C_{10}H_{17}OSO_3]\cdot H_2O$ (0.130g, 0.52mmol) in methanol (3cm^3) and allowed to slowly evaporate. Small colourless crystals of $[C(NH_2)_2(NHEt)][C_{10}H_{17}OSO_3]$ **19** were collected. Calc for $C_{13}H_{21}N_3O_4S$: C, 48.9; H, 7.89; N, 13.2. Found: C, 46.1; H, 7.50; N 12.4%. The microanalysis results are poor, suggesting the presence of an impurity in the bulk material. However, an impurity could not be identified sufficient crystals were not produced for analysis by powder diffraction. Many attempts were made to produce more crystals of **19** for this analysis, but these were unfortunately unsuccessful.

Synthesis of [DiMeGu][10-CamphorSO$_3$] 20

A solution of $[C(NH_2)_2(NMe_2)]_2SO_4$ (0.071g, 0.26mmol) in methanol (2cm^3) was added to a solution of $Na[C_{10}H_{17}OSO_3]\cdot H_2O$ (0.130g, 0.52mmol) in methanol (3cm^3) and allowed to slowly evaporate. Small colourless crystals of $[C(NH_2)_2(NMe_2)][C_{10}H_{17}OSO_3]$ **20** were collected. Calc for $C_{13}H_{17}N_3O_3S$: C, 49.5; H, 6.71; N, 13.3. Found: C, 45.3; H, 7.42; N 10.6%. Powder diffraction results confirm that the major product in the bulk material is compound **20**, however there is also evidence for $(DiMeGu)SO_4\cdot H_2O$ being present as an impurity.

Synthesis of [DiMeGu][MeSO$_3$] 21

A solution of $[C(NH_2)_2(NMe_2)]_2SO_4$ (0.057g, 0.21mmol) in methanol (5cm^3) was added to a solution of $Na[CH_3SO_3]$ (0.050g, 0.42mmol) in methanol (3cm^3) and allowed to slowly evaporate. Small colourless crystals of $[C(NH_2)_2(NMe_2)][CH_3SO_3]$ **21** were collected. Calc for $C_4H_{13}N_3O_3S$: C, 26.2; H, 7.15; N, 22.9. Found: C, 24.8; H, 6.69; N 21.0%. Additional peaks present in the powder diffraction pattern correspond to the presence of $Na[MeSO_3]$ in the bulk material.

Synthesis of [DiMeGu][$PhSO_3$] 22

A solution of $[C(NH_2)_2(NMe_2)]_2SO_4$ (0.060g, 0.22mmol) in methanol ($5cm^3$) was added to a solution of $Na[C_6H_5SO_3]$ (0.080g, 0.44mmol) in methanol ($3cm^3$) and allowed to slowly evaporate. Small colourless crystals of $[C(NH_2)_2(NMe_2)][C_6H_5SO_3]$ **22** were collected. Calc for $C_9H_{15}N_3O_3S$: C, 44.1; H, 6.16; N, 17.4. Found: C, 43.3; H, 5.86; N 15.7%. The powder diffraction pattern reveals the presence of $(DiMeGu)_2SO_4 \cdot H_2O$ in the bulk product.

Synthesis of [DiMeGu]$_2$[1,5-Nap(SO_3)$_2$] 23

A solution of $[C(NH_2)_2(NMe_2)]_2SO_4$ (0.051g, 0.19mmol) in methanol ($5cm^3$) was added to a solution of $Na_2[C_{10}H_6$1,5-$(SO_3)_2] \cdot xH_2O$ (0.060g, 0.19mmol) in methanol ($3cm^3$) and allowed to slowly evaporate. Small colourless crystals of $[C(NH_2)_2(NMe_2)]_2[C_{10}H_6$1,5-$(SO_3)_2]$ **23** were collected. Calc for $C_{16}H_{26}N_6O_6S_2$: C, 41.5; H, 5.55; N, 18.2. Found: C, 30.4; H, 5.13; N, 17.4%. The microanalysis results are poor, and the powder diffraction pattern is reproducibly different to that of the powder pattern simulated from single crystal data. No other crystalline products were identified. Thus, it is possible that an unrepresentative minor compound was analysed on the sample crystal diffractometer.

Synthesis of [DiMeGu]$_2$[2,6-Nap(SO_3)$_2$] 24

A solution of $[C(NH_2)_2(NMe_2)]_2SO_4$ (0.051g, 0.19mmol) in methanol ($5cm^3$) was added to a solution of $Na_2[C_{10}H_6$2,6-$(SO_3)_2]$ (0.060g, 0.19mmol) in methanol ($3cm^3$) and allowed to slowly evaporate. Small colourless crystals of $[C(NH_2)_2(NMe_2)]_2[C_{10}H_6$2,6-$(SO_3)_2]$ **24** were collected. Calc for $C_{16}H_{26}N_6O_6S_2$: C, 41.6; H, 5.57; N, 18.2. Found: C, 30.7; H, 5.28; N, 18.1%. The powder diffraction pattern is notably different to the simulated powder pattern, and it further reveals the presence of $(DiMeGu_2)SO_4 \cdot H_2O$ in the bulk product. It is possible that the crystal lattice is disrupted during the grinding process while preparing the powder sample, or that the single crystal analysed was not representative of the bulk.

3.8 References

[1] V. A. Russell, M. C. Etter, M. D. Ward; *J. Am. Chem. Soc.,* 1994, 1941, 116

[2] V. A .Russell, C. C. Evans, W. Li, M. D. Ward; *Science,* 1997, 575

[3] K. T. Holman, M. D. Ward; *Angew. Chem. Int. Ed.,* 2000, 1653, 39

[4] P Fagan, M. Ward. *Sci. Am.*, 1992, 28

[5] V. A. Russell, M. D. Ward; *J. Mater. Chem.*, 1997, 7, 1123

CHAPTER 4

The reactions of sulfonate dyes and guanidinium and substituted guanidinium derivatives

4.0 Introduction

Methyl orange $Na[O_3SC_6H_4N{=}NC_6H_4NMe_2]$ Na[MO][1], ethyl orange $Na[O_3SC_6H_4N{=}NC_6H_4NEt_2]$ Na[EO][1] and sodium 4-aminoazobenzene-4'-sulfonate $Na[O_3SC_6H_4N{=}NC_6H_4NH_2]$ Na[ABS][2] are azo dyes with a sulfonate group at one end of the molecule and a NR_2 group [where R=Me, Et or H] at the other (Figure 4.1).

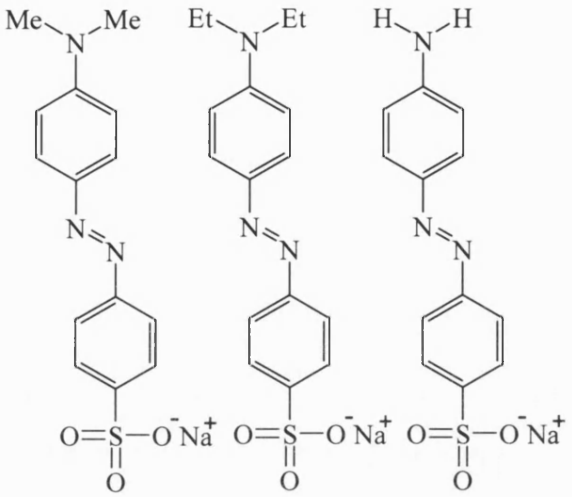

Figure 4.1; methyl orange, ethyl orange and sodium 4-aminoazobenzene-4'-sulfonate (from left to right respectively)

These dyes are best known as acid-base indicators[3]. The sulfonate dyes have been studied as part of this project to ascertain if it is possible to protonate the N=N bond of the dye whilst the anion is part of the hydrogen-bonded lattice with the guanidinium cation, without loss or with little loss of crystallinity. The azo functionality can be protonated in acidic conditions promoting a colour change. In basic conditions, this proton can be removed returning the dye to its original state, as shown in Figure 4.2.

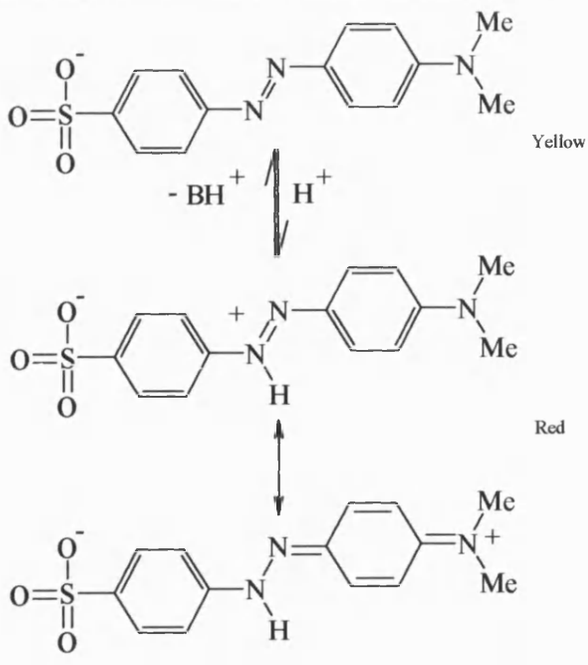

Figure 4.2; mechanism of reversible protonation of methyl orange showing the resonance structures of the protonated species (B=base)

Azo compounds have been used as sensors due to their ability to exhibit sensitive colour changes upon complexation with guest molecules, and hence have applications in analytical science[4]. Scott and co-workers have reported an azo host complex that exhibits a different colour upon inclusion of guest molecules, such as pyridine, in the solid state[5]. The structure of the host compound, 3-{4-[4-(3-hydroxy-3,3-diphenylprop-1-ynyl)phenylazo]phenyl}-1,1-diphenylprop-2-yn-1-ol (**a**), is shown in Figure 4.3.

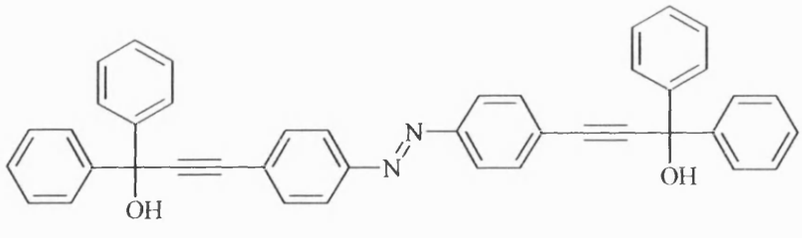

Figure 4.3; structure of 3-{4-[4-(3-hydroxy-3,3-diphenylprop-1-ynyl)phenylazo]phenyl}-1,1-diphenylprop-2-yn-1-ol, (**a**)

The host compound (**a**) is yellow, however, upon recrystallisation from the guest solvent a colour change from yellow to orange/red is observed. This colour change is observed for a number of guests that are incorporated into the host (**a**). The solid state UV spectra of these inclusion compounds reveal a red-shift in the spectra in all of the samples analysed.

It is also interesting that the same observation occurs when crystals of the host (**a**) are exposed to a guest vapour. Host (**a**) forms orange/red inclusion crystals with DMF under gas-solid reaction conditions, after exposure for 24 hours to the solvent vapour. Upon heating in the solid state, the inclusion crystal loses the guest molecules to give yellow host crystals.

Garrone and co-workers have used azo dyes to monitor the permeability of micelles in surfactant-containing MCM-41[6]. They have used mesoporous silica containing surfactant-embedded Congo Red (CR, the structure of which is shown in Figure 4.4) and assessed its porosity to $HCl_{(g)}$ and $NH_{3(g)}$.

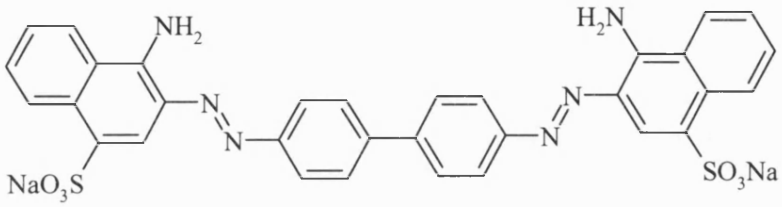

Figure 4.4; the structure of Congo Red (CR)

Accessibility of the dyes to HCl and NH_3 was studied by exposing CR-MCM-41 powder to these vapours. Exposure of CR-MCM-41 to HCl results in a colour change from red to blue, representing the presence of the protonated CR (this change in colour from red to blue is also observed in pure CR). Exposure of this protonated-CR-MCM-41 to NH_3 immediately leads to the reformation of CR-MCM-41. These results are also observed in UV-visible spectra, as shown in Figure 4.5. More than 10 protonation-deprotonation cycles were reproducibly carried out, confirming that the probable formation of ammonium chloride within the solid does not prevent the permeation of the gases used.

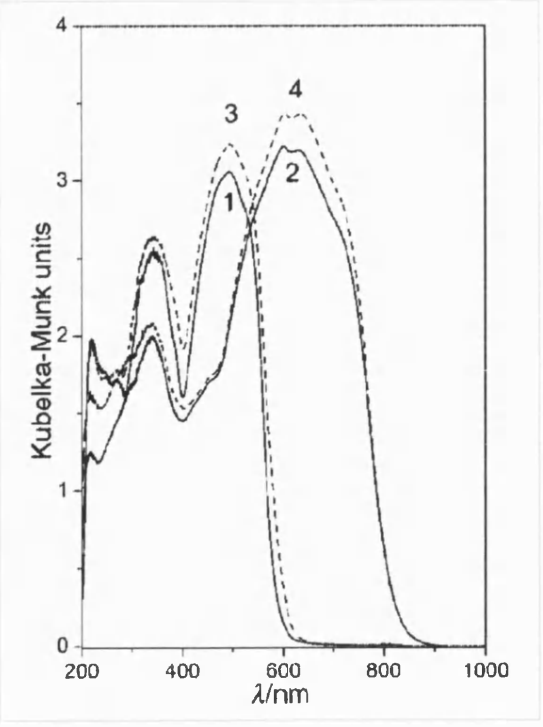

Figure 4.5;
Curve 1: CR-MCM-41
Curve 2: CR-MCM-41 + HCl
Curve 3: CR-MCM-41 + HCl followed by NH_3
Curve 4: CR-MCM-41 + HCl, then NH_3 then HCl

(Figure taken directly from B. Onida, B. Bonelli, L. Flora, F. Geobaldo, C. O.-Arean, E. Garrone, *Chem. Commun.*, 2001, 2216)

The azo dyes methyl orange, ethyl orange and sodium 4-aminoazobenzene-4'-sulfonate are functionalised with a sulfonate group, making them soluble in aqueous and alcohol solutions. This makes them ideal materials for incorporation into guanidinium-sulfonate networks. Therefore guanidinium, methylguanidinium, ethylguanidinium and *N*,*N*-dimethylguanidinium salts were crystallised with the azo dyes and the results are presented in this chapter. Also discussed are the results of reactions between these solid state compounds and gaseous HCl followed by ammonia, which were monitored by X-ray powder diffraction, diffuse reflectance UV-visible and IR spectroscopies.

4.1 Reactions of sulfonate dyes with guanidinium and substituted guanidinium cations

The guanidinium and substituted guanidinium salts were reacted in a 1:1 molar ratio with each of the sulfonate dyes. The two compounds were dissolved separately in methanol, the solutions mixed together, and the solvent mixture allowed to slowly evaporate. The same reactions were also carried out in water. In the majority of cases, crystals suitable for X-ray analysis were only observed from one of the two solvents. Where crystals were formed from both solvents, X-ray data were taken from both sets of crystals to determine whether the same products were observed. Powder precipitates that were formed in place of single crystals were subjected to microanalysis and X-ray powder diffraction and the results of the latter were compared with the simulated powder pattern from single crystal X-ray data. As a result, the following crystal structures are described in this chapter (crystallographic information is given in Tables 4.1, 4.2 and 4.3).

25: [Gu][MO] : $[C(NH_2)_3][O_3SC_6H_4N{=}NC_6H_4NMe_2]$

26: [MeGu][MO]·MeOH : $[C(NH_2)_2(NHMe)][O_3SC_6H_4N{=}NC_6H_4NMe_2]\cdot MeOH$

27: [EtGu][MO] : $[C(NH_2)_2(NHEt)][O_3SC_6H_4N{=}NC_6H_4NMe_2]$

28: [DiMeGu][MO] : $[C(NH_2)_2(NMe_2)][O_3SC_6H_4N{=}NC_6H_4NMe_2]$

29: HMO : $[O_3SC_6H_4NH{=}NC_6H_4NMe_2]$

30: [Gu][EO] : $[C(NH_2)_3][O_3SC_6H_4N{=}NC_6H_4NEt_2]$

31: [MeGu][EO]·MeOH : $[C(NH_2)_2(NHMe)][O_3SC_6H_4N{=}NC_6H_4NEt_2]\cdot MeOH$

32: [EtGu][EO] : $[C(NH_2)_2(NHEt)][O_3SC_6H_4N{=}NC_6H_4NEt_2]$

33: [DiMeGu][EO] : $[C(NH_2)_2(NMe_2)][O_3SC_6H_4N{=}NC_6H_4NEt_2]$

34: HEO·H_2O : $[O_3SC_6H_4NH{=}NC_6H_4NEt_2]\cdot{}^3/_4H_2O$

35: [Gu][ABS] : $[C(NH_2)_3][O_3SC_6H_4N{=}NC_6H_4NH_2]$

36: [MeGu][ABS] : $[C(NH_2)_2(NHMe)][O_3SC_6H_4N{=}NC_6H_4NH_2]$

37: $[EtGu]_2[ABS][NBS]\cdot 2H_2O$:

$[C(NH_2)_2(NHEt)]_2[O_3SC_6H_4N{=}NC_6H_4NH_2]\ [O_3SC_6H_4N{=}NC_6H_4NO_2]\cdot 2H_2O$

38a: [DiMeGu][ABS] : $[C(NH_2)_2(NMe_2)][O_3SC_6H_4N{=}NC_6H_4NH_2]$

38b: [DiMeGu][ABS] : $[C(NH_2)_2(NMe_2)][O_3SC_6H_4N{=}NC_6H_4NH_2]$

Crystallographic measurements for compounds **26**, **27**, **28**, **30**, **31**, **32**, **33**, **34**, **37** and **38a** were made at 150 K on a Nonius Kappa CCD diffractometer. Crystallographic measurements for compounds **25**, **29**, **35**, **36** and **38b** were made at 150 K on the Bruker SMART CCD diffractometer at Daresbury SRS Station 9·8.

Compound	**25**	**26**	**27**	**28**	**29**
Empirical formula	$C_{15}H_{20}N_6O_3S$	$C_{17}H_{26}N_6O_4S$	$C_{17}H_{24}N_6O_3S$	$C_{17}H_{24}N_6O_3S$	$C_{14}H_{15}N_3O_3S$
M	364.43	410.50	392.48	392.48	305.35
Crystal system	Monoclinic	Monoclinic	Triclinic	Orthorhombic	Monoclinic
Space group	$P2_1/c$	$P2_1/a$	P-1	$Pbca$	$P2_1$
Wavelength / Å	0.6867	0.71073	0.71073	0.71073	0.6894
a / Å	19.3867(11)	14.7160(3)	7.7640(3)	7.4080(2)	7.290(4)
b / Å	7.4234(4)	7.3400(2)	12.1950(5)	12.9640(3)	7.551(4)
c / Å	12.1792(7)	19.0810(5)	20.4040(7)	39.6160(11)	12.727(6)
α / °	90	90	80.885(3)	90	90
β / °	100.810(2)	107.1970(10)	85.359(3)	90	104.447(9)
γ / °	90	90	88.608(2)	90	90
U / Å^3	1721.67(17)	1968.90(8)	1901.11(13)	3804.61(17)	678.4(6)
Z	4	4	4	8	2
μ (Mo-Kα) / mm^{-1}	0.217	0.201	0.201	0.201	0.253
Reflections collected	11912	30524	4757	15133	4538
Independent reflections	4765	4485	4266	3470	3359
R(int)	0.0311	0.1371	0.0179	0.0486	0.0167
$R1$, w$R2$	0.0445, 0.1173	0.0512, 0.1010	0.0398, 0.0937	0.0586, 0.1029	0.0471, 0.1070
R indices (all data)	0.0542, 0.1229	0.1035, 0.1200	0.0523, 0.1012	0.1324, 0.1243	0.0617, 0.1136

Table 4.1; X-ray crystallographic parameters for compounds **25-29**

Compound	**30**	**31**	**32**	**33**	**34**
Empirical formula	$C_{17}H_{24}N_6O_3S$	$C_{19}H_{30}N_6O_4S$	$C_{19}H_{28}N_6O_3S$	$C_{19}H_{28}N_6O_3S$	$C_{16}H_{20.50}N_3O_{3.75}S$
M	392.48	438.55	420.53	420.53	346.91
Crystal system	Monoclinic	Triclinic	Orthorhombic	Monoclinic	Triclinic
Space group	$P2_1/n$	P-1	$P2_12_12_1$	$P2_1/n$	P-1
Wavelength / Å	0.71073	0.71073	0.71073	0.71073	0.71073
a / Å	7.6920(2)	7.7870(2)	7.3660(1)	8.2740(3)	8.3730(2)
b / Å	31.918(1)	14.3030(3)	7.4200(1)	9.9410(3)	9.0090(3)
c / Å	7.7980(3)	19.9880(5)	39.3020(6)	25.206(1)	11.6500(3)
α / °	90	87.132(1)	90	90	102.601(2)
β / °	95.489(2)	82.817(1)	90	96.242(1)	109.008(2)
γ / °	90	88,024(1)	90	90	97.340(2)
U / Å^3	1905.73(11)	2205.08(9)	2148.08(5)	2060.95(13)	791.81(4)
Z	4	4	4	4	2
μ (Mo-Kα) / mm^{-1}	0.201	0.184	0.183	0.191	0.230
Reflections collected	16394	29592	21523	29177	11474
Independent reflections	3919	9949	5788	4506	3536
R(int)	0.1062	0.1154	0.0350	0.1288	0.0688
$R1$, w$R2$	0.0642, 0.1118	0.0604, 0.1178	0.0371, 0.0889	0.0563, 0.1179	0.0556, 0.1219
R indices (all data)	0.1356, 0.1341	0.1425, 0.1487	0.0457, 0.0929	0.1410, 0.1480	0.0873, 0.1381

Table 4.2; X-ray crystallographic parameters for compounds **30-34**

Compound	**35**	**36**	**37**	**38a**	**38b**
Empirical formula	$C_{13}H_{16}N_6O_3S$	$C_{14}H_{18}N_6O_3S$	$C_{30}H_{42}N_{12}O_{10}S_2$	$C_{15}H_{20}N_6O_3S$	$C_{15}H_{20}N_6O_3S$
M	336.38	350.40	794.88	364.43	364.43
Crystal system	Monoclinic	Monoclinic	Monoclinic	Orthorhombic	Orthorhombic
Space group	$P2_1/c$	$P2_1/c$	$P2_1/c$	*Pbca*	$Pca2_1$
Wavelength / Å	0.6778	0.6778	0.71073	0.71073	0.6778
a / Å	7.6824(4)	8.8581(7)	21.0560(2)	11.0040(1)	10.9424(5)
b / Å	39.8135(19)	31.583(3)	7.3230(1)	9.7610(2)	15.6353(8)
c / Å	10.5148(5)	11.724(1)	23.7050(2)	31.2630(5)	9.7921(5)
α / °	90	90	90	90	90
β / °	90.351(1)	92.687(1)	95.164(1)	90	90
γ / °	90	90	90	90	90
U / Å^3	3216.0(3)	3276.4(5)	3640.31(7)	3357.96(9)	1675.31(14)
Z	8	8	4	8	4
μ (Mo-Kα) / mm^{-1}	0.226	0.224	0.219	0.222	0.223
Reflections collected	34681	7066	65940	37645	13925
Independent reflections	9588	3766	10629	4811	4918
R(int)	0.0375	0.0881	0.0575	0.0842	0.0319
*R*1, w*R*2	0.0431, .1129	0.0715, .1643	0.0522,0.1225	0.0460, 0.1156	0.0391, .0980
R indices (all data)	0.0500, .1164	0.1188, .1826	0.0800,0.1391	0.0715, 0.1282	0.0471, .1018

Table 4.3; X-ray crystallographic parameters for compounds **35-38b**

Structure determinations have been carried out using single crystal X-ray crystallography. In most cases microanalysis and X-ray powder diffraction analysis confirm that the single crystal is representative of the bulk sample (in a few examples this is not the case, see experimental section 4.6 for more details). All non-hydrogen atoms were allowed to vibrate anisotropically in the final least squares cycles. Some compounds include molecules of water from the solvent. The water hydrogen atom positions are determined from the electron density map, and the O–H bond lengths have been refined as fixed at 0.89(3)Å. All other hydrogen atoms were included at calculated positions.

4.2 Methyl orange sulfonates

$[Gu][MO] : [C(NH_2)_3][O_3SC_6H_4N{=}NC_6H_4NMe_2]$ 25

Asymmetric Unit

The asymmetric unit in **25** consists of one $[Gu]^+$ cation and one $[MO]^-$ anion as shown in Figure 4.6.

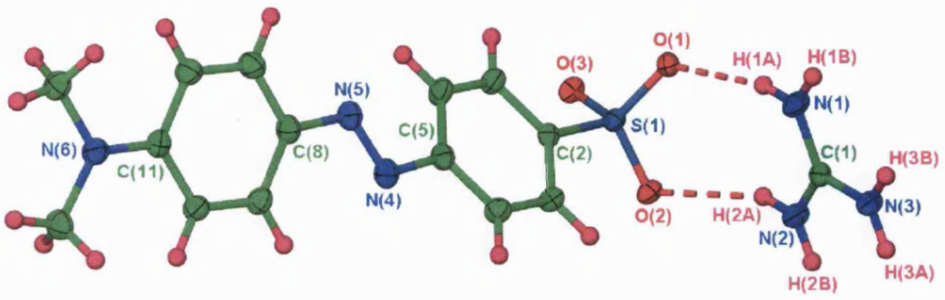

Figure 4.6; asymmetric unit of **25**. Ellipsoids are depicted at 50% probability level.

Extended Structure

The guanidinium cation has three faces, each of which is available to form DD:AA hydrogen bonds with the anion forming three $R_2^2(8)$ motifs. These hydrogen-bonding motifs link the cations and anions into regular, hexagonal hydrogen-bonded guanidinium sulfonate (GS) sheets, as shown in Figure 4.7. These sheets are virtually flat with an inter–ribbon angle of 173°. All of the hydrogen-bond donors and acceptors are used to form this sheet and details of these hydrogen bonds are given in Table 4.4. The R groups of the sulfonate are directed to one side of the sheet; half of the phenyl planes lie almost parallel to the ribbons whereas half lie nearly orthogonal to the ribbons. Neighbouring sheets in the gross structure inter-digitate to form a bilayer, shown in Figure 4.8, which repeats into the extended structure. This inter-digitation minimises the

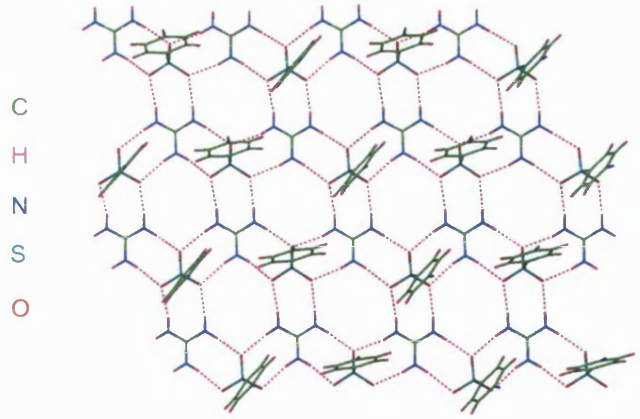

Figure 4.7; the hydrogen bonded sheet observed in **25**. The ribbons are shown horizontally on the page. (*half of each anion has been omitted for clarity*).

void space in the structure. There are no hydrogen bonds between the bilayers nor are there open channels present to incorporate any solvent or other guest molecules.

Each of the anions is twisted with an angle of 31° between the least-squares planes of the two phenyl rings. This serves to allow π···π interactions between the N=N bond of one anion and the phenyl rings of a neighbouring inter-digitated anion.

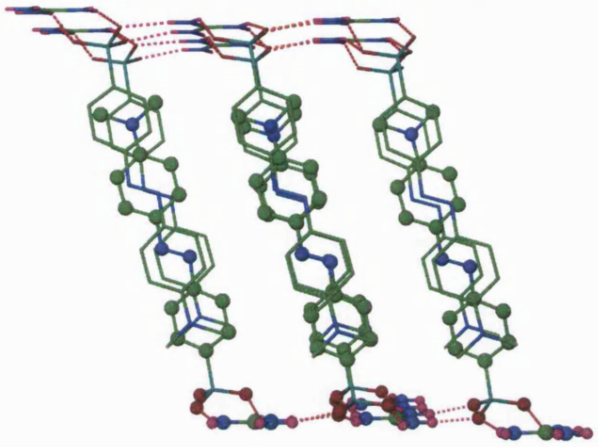

Figure 4.8; interdigitating bilayer formed in **25**
(*the hydrogen atoms on the anion have been removed for clarity*).

D–H···A	D···A /Å	H···A /Å	D–H···A / °	Symmetry operation generating D···A
N(1)–H(1A)···O(1)	2.877 (2)	2.03	163	*x, y, z*
N(1)–H(1B)···O(3)	2.873 (2)	2.03	161	*x, 1+y, z*
N(2)–H(2A)···O(2)	2.924 (2)	2.14	148	*x, y, z*
N(2)–H(2B)···O(1)	2.892 (2)	2.03	168	*x, $^{3}/_{2}$-y, ½+z*
N(3)–H(3A)···O(3)	2.885 (1)	2.03	165	*x, $^{3}/_{2}$-y, ½+z*
N(3)–H(3B)···O(2)	2.967 (2)	2.12	161	*x, 1+y, z*

Table 4.4; details of the hydrogen bonding in **25**

[MeGu][MO]·MeOH:[$C(NH_2)_2(NHMe)$][$O_3SC_6H_4N{=}NC_6H_4NMe_2$]·MeOH 26

Asymmetric Unit

The asymmetric unit in **26** consists of one $[MeGu]^+$ cation, one $[MO]^-$ anion and a molecule of methanol as shown in Figure 4.9.

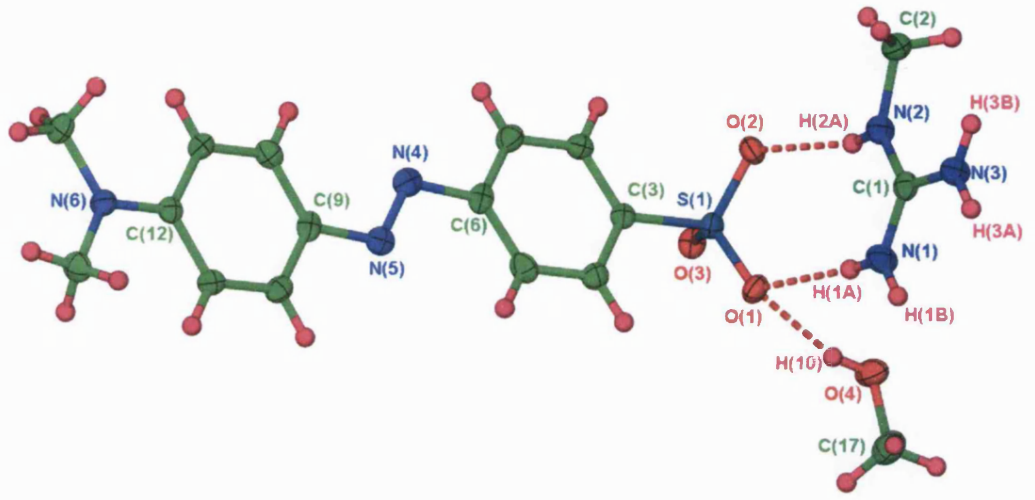

Figure 4.9; asymmetric unit in **26**. Ellipsoids are depicted at 50% probability level.

Extended Structure

Two DD:AA hydrogen-bonding motifs are formed between the unsubstituted faces of the cation and two of the sulfonate faces of the anion via graph set $R_2^2(8)$ forming ribbons, as shown in Figure 4.10. The cations and the sulfonate oxygens are approximately co-planar. One of the cation faces has lost a N–H donor due to the substitution by a N–Me group, and can no longer form DD:AA hydrogen bonds with the sulfonate. One edge of the ribbon is available to form hydrogen bonds via the N–H donor of the substituted face, while the other edge of the ribbon consists of the sulfonate acceptors.

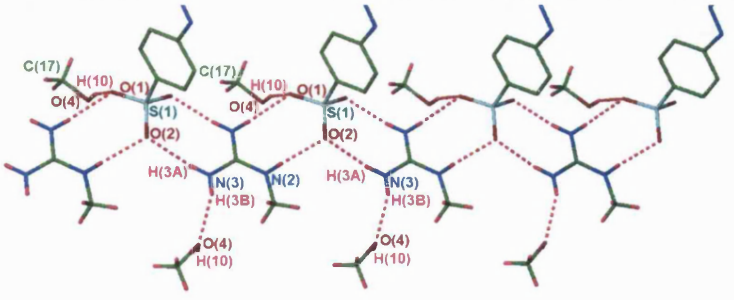

Figure 4.10; DD:AA ribbons formed in **26**
(part of the anion is removed for clarity)

The ribbons form hydrogen bonds via the single N–H donor of the substituted face of the cation to the oxygen acceptor of methanol. The O–H donor of the methanol also forms a hydrogen bond with the O(1) atom of the sulfonate. Pairs of ribbons are hydrogen-bonded together into tapes via solvent molecules acting as both hydrogen-bond donors and acceptors. The hydrogen bonds involved are detailed in Table 4.5. The tapes stack to form the repeating *pseudo*-bilayer structure shown in Figure 4.11.

There are edge-to-face C–H···π interactions between the phenyl rings of neighbouring anions. There are also face-to-face interactions between the phenyl rings of the anions of inter-digitating R groups.

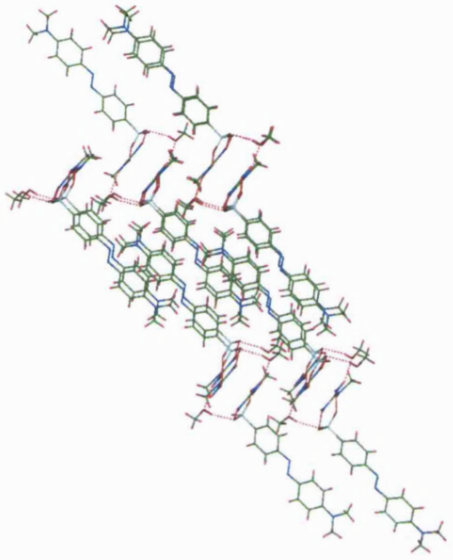

Figure 4.11; *pseudo*-bilayer formed in **26**

The phenyl rings of the anion are virtually coplanar, with an angle of only 7° between their respective least-squares planes.

D–H···A	D···A /Å	H···A /Å	D–H···A / °	Symmetry operation generating D···A
N(1)–H(1A)···O(1)	2.924 (2)	2.06	167	*x, y, z*
N(1)–H(1B)···O(3)	2.874 (2)	2.00	170	*x, y*-1, *z*
N(2)–H(2A)···O(2)	2.876 (2)	2.05	156	*x, y, z*
N(3)–H(3A)···O(2)	2.973 (3)	2.13	162	*x, y*-1, *z*
N(3)–H(3B)···O(4)	2.907 (2)	2.09	154	½-*x, y*-½, 2-*z*
O(4)–H(10)···O(1)	2.795 (2)	2.00	164	*x, y, z*

Table 4.5; details of the hydrogen bonding in **26**

[EtGu][MO] : $[C(NH_2)_2(NHEt)][O_3SC_6H_4N{=}NC_6H_4NMe_2]$ 27

Asymmetric Unit

The asymmetric unit of **27** contains two $[EtGu]^+$ cations and two $[MO]^-$ anions as shown in Figure 4.12.

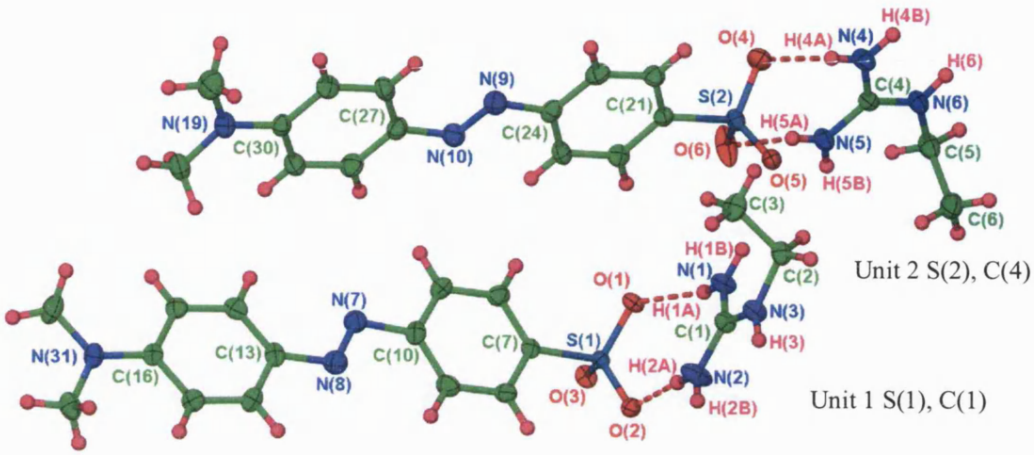

Figure 4.12; asymmetric unit of **27**. Ellipsoids are depicted at 50% probability level.

Extended Structure

These two sets of cation-anion units are involved in different packing arrangements. Therefore they are initially described here separately, labelled as Unit 1 and Unit 2, as shown in Figure 4.12.

DD:AA hydrogen-bonding motifs (graph set $R_2^2(8)$) form between the two unsubstituted faces of the Unit 1 cations and anions forming a hydrogen-bonded ribbon, where the cation and the sulfonate oxygens of the anion are approximately coplanar. The hydrogen bond donor [N(1)–H(1B)] of the substituted face of the cation is not involved in the ribbon formation and is directed away from the ribbon backbone, as shown in Figure 4.13.

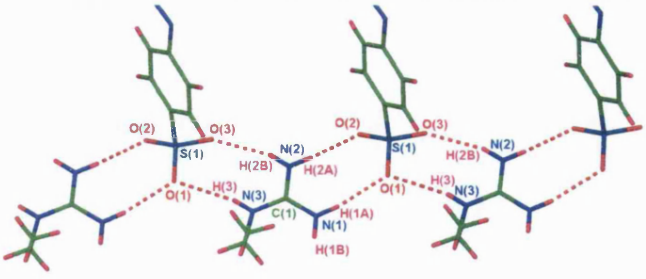

Figure 4.13; ribbon formed in **27**
(part of the anion is removed for clarity).

In Unit 2 there are $R_2^2(8)$ motifs formed between a cation-anion pair that interact via DD:AA hydrogen bonds. The cation plane is almost perpendicular to that of the sulfonate oxygens of the anion. Two of these cation-anion pairs are hydrogen-bonded into a 'dimer' via two N(6)–H(6)···O(5) hydrogen bonds, as shown in Figure 4.14.

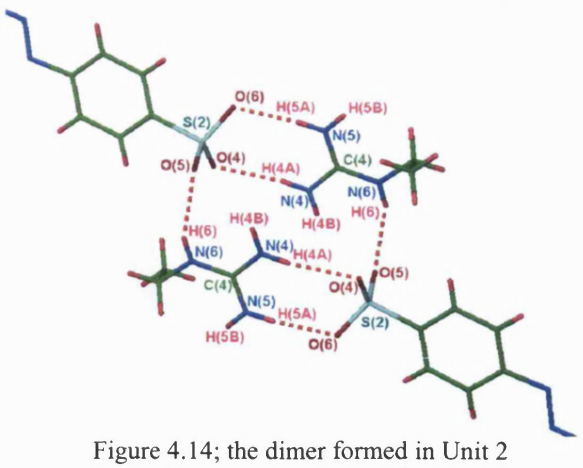

Figure 4.14; the dimer formed in Unit 2
(part of the anion is removed for clarity).

The ribbons of Unit 1 form hydrogen bonds with the dimers of Unit 2 via the hydrogen bonds N(1)–H(1B)···O(5), N(4)–(4B)···O(2) and N(5)–H(5B)···O(3) forming a complex two-dimensional sheet. For details of the hydrogen bonds formed, see Table 4.6. A hydrogen-bonded interdigitating *pseudo*-bilayer is formed in the extended structure, with the sulfonate R groups directed to both sides of each sheet, as shown in Figure 4.15.

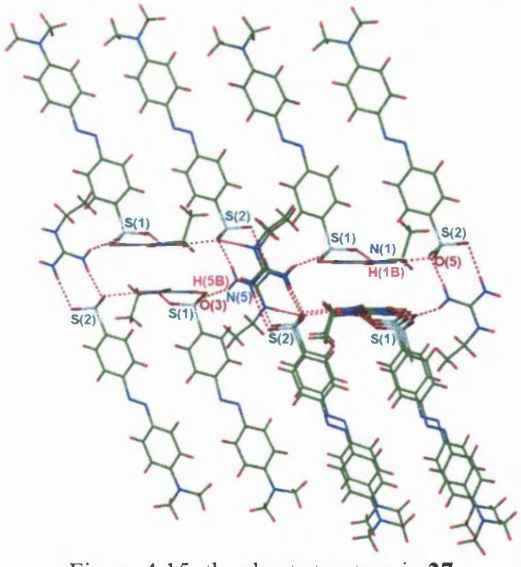

Figure 4.15; the sheet structure in **27**

There are face-to-face π···π interactions between the phenyl rings of interdigitating anions. There are also edge-to-face C–H···π interactions between the phenyl rings of the anions in one plane, and those of the interdigitating anions of the neighbouring plane.

The phenyl rings in each of the anions are almost planar, with the angles between least-squares planes of 10° in Unit 1 and 2° in Unit 2.

D–H···A	D···A /Å	H···A /Å	D–H···A / °	Symmetry operation generating D···A
N(1)–H(1A)···O(1)	2.996 (3)	2.16	163	*x*, *y*, *z*
N(1)–H(1B)···O(5)	2.960 (3)	2.11	168	*x*, *y*, *z*
N(2)–H(2A)···O(2)	2.887 (4)	2.03	175	*x*, *y*, *z*
N(2)–H(2B)···O(3)	2.982 (4)	2.18	155	*x*-1, *y*, *z*
N(3)–H(3)···O(1)	3.049 (3)	2.34	139	*x*-1, *y*, *z*
N(4)–H(4A)···O(4)	3.015 (3)	2.16	171	*x*, *y*, *z*
N(4)–H(4B)···O(2)	2.992 (3)	2.31	137	*x*, 1+*y*, *z*
N(5)–H(5A)···O(6)	2.849 (3)	2.00	170	*x*, *y*, *z*
N(5)–H(5B)···O(3)	2.880 (3)	2.01	155	1-*x*, 1-*y*, 2-*z*
N(6)–H(6)···O(5)	2.892 (3)	2.12	148	-*x*, 2-*y*, 2-*z*

Table 4.6; details of the hydrogen bonding in **27**

[DiMeGu][MO] : $[C(NH_2)_2(NMe_2)][O_3SC_6H_4N{=}NC_6H_4NMe_2]$ 28

Asymmetric Unit

The asymmetric unit in **28** contains one $[DiMeGu]^+$ cation and one $[MO]^-$ anion. There is disorder in the ratio 55:45 between the atoms C(2)-C(13), N(4) and N(5) and their counterparts C(2A)-C(13A), N(4A) and N(5A) respectively. The thermal parameters of the atoms in the phenyl rings in each disordered part were restrained to be similar. The asymmetric unit is shown in Figure 4.16.

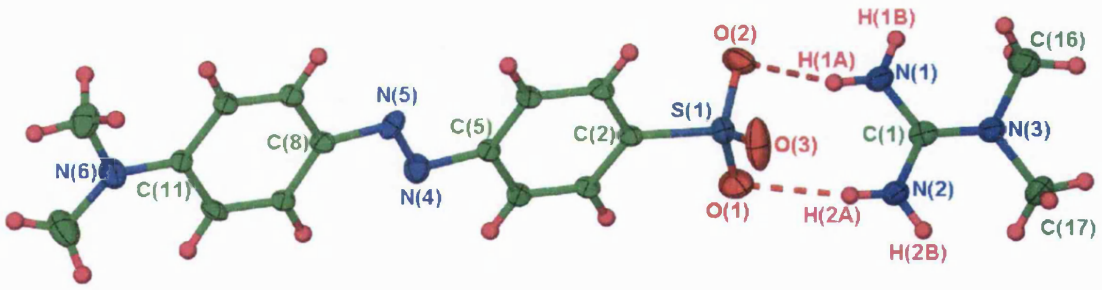

Figure 4.16; asymmetric unit of **28**. Ellipsoids are depicted at 50% probability level.
(*the disordered part of 45% occupancy is not shown for clarity*)

Extended Structure

The unsubstituted face of the cation forms DD:AA hydrogen bonds (graph set $R_2^2(8)$) with one face of the sulfonate in the anion. The cation is virtually perpendicular to the plane of the sulfonate oxygen atoms. The other faces of the cation only have one N–H donor each due to the substitution of two N–H groups by N–Me groups. The cation-anion pairs are linked together via hydrogen bonding [N(1)–H(1B)···O(3)] to form a chain (Figure 4.17). The

N(2)–H(2A) donors are not involved and are all directed to the same side of the chain, forming hydrogen bonds to O(2) of a neighbouring chain, linking the cations and anions into a sheet. The hydrogen bond details can be seen in Table 4.7. In this sheet, all the cations lie approximately perpendicular to the plane of the sheet itself (Figure 4.17). The sulfonates are directed to both sides of these sheets, forming an inter-digitating *pseudo*-bilayer, as shown in Figure 4.18.

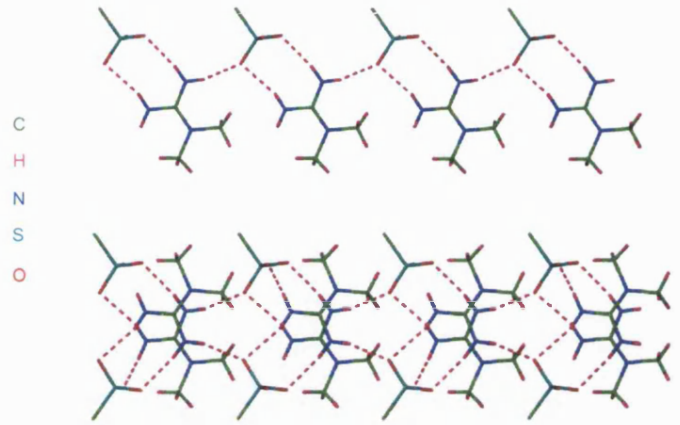

Figure 4.17; Single chain (top) and chains linked into sheets (bottom) in **28**.
(*the majority of the anion is removed for clarity*)

There are edge-to-face C–H···π interactions between the phenyl rings of neighbouring anions. There are also face-to-face π···π interactions between the phenyl rings of the anions in one plane, and those of the inter-digitating anions of the neighbouring plane. There is only a small twist of 9° between the least-squares phenyl planes in the anion.

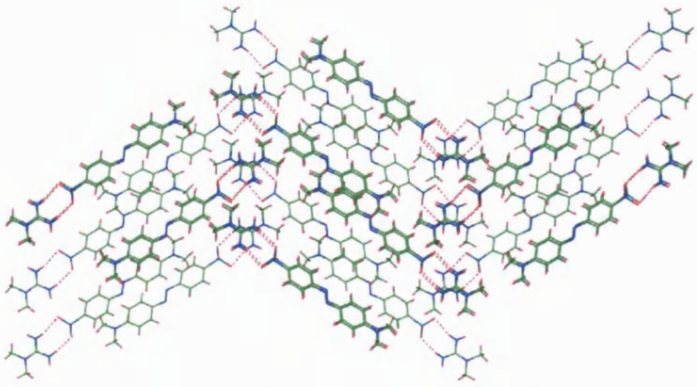

Figure 4.18; bilayer formation in **28**

D–H···A	D···A /Å	H···A /Å	D–H···A / °	Symmetry operation generating D···A
N(1)–H(1A)···O(2)	3.053(3)	2.24	154	*x, y, z*
N(1)–H(1B)···O(3)	2.830(3)	2.06	146	½+*x, y,* ½-*z*
N(2)–H(2A)···O(1)	3.025(3)	2.16	168	*x, y, z*
N(2)–H(2B)···O(2)	2.903(3)	2.04	165	½-*x, y*-½, *z*

Table 4.7; details of the hydrogen bonding in **28**

HMO : $O_3SC_6H_4NH{=}NC_6H_4NMe_2$ 29

Methyl orange and the unsubstituted guanidinium salt were each dissolved in water and mixed together. A small amount of dilute HCl was then added drop wise to the solution in an attempt to crystallise a guanidinium-sulfonate network incorporating the protonated anion as well as the Cl^- ion. Small red crystals were produced instantly, however these crystals were identified as $O_3SC_6H_4NH{=}NC_6H_4NMe_2$ **29** and do not contain the guanidinium cation or the Cl^- ion. Dissolving the methyl orange salt in H_2O and adding dilute HCl to the solution also leads to the formation of **29**.

Asymmetric Unit

The asymmetric unit of **29** contains one HMO zwitterion that has been protonated at N(1) as shown in Figure 4.19. The N(1)=N(2) bond has lengthened from 1.266(2)Å in **25** to 1.307(3)Å in **29**, consistent with the greater single bond character anticipated on the basis of the delocalised resonance form (Figure 4.2 of section 4.0).

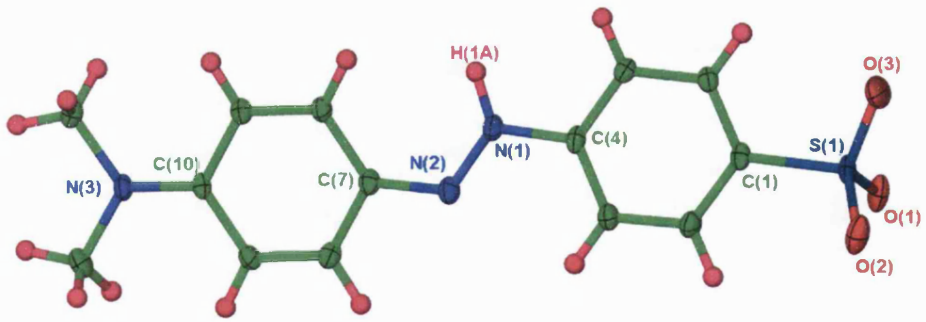

Figure 4.19; asymmetric unit in **29**. Ellipsoids are depicted at 50% probability level.

Extended Structure

The $O_3SC_6H_4NH{=}NC_6H_4NMe_2$ zwitterions interact with neighbouring zwitterions via N(1)–H(1A)···O(1) hydrogen bonds, which link the protonated azo group and one of the sulfonate oxygen atoms to form chains. The chains are further linked into a two-dimensional array via DD:AA C–H···O hydrogen bonds (graph set $R_2^2(8)$) formed between the methyl groups of one molecule and the sulfonate oxygen atoms of a neighbouring molecule, as shown in Figure 4.20. The details of the hydrogen bonds are given in Table 4.8.

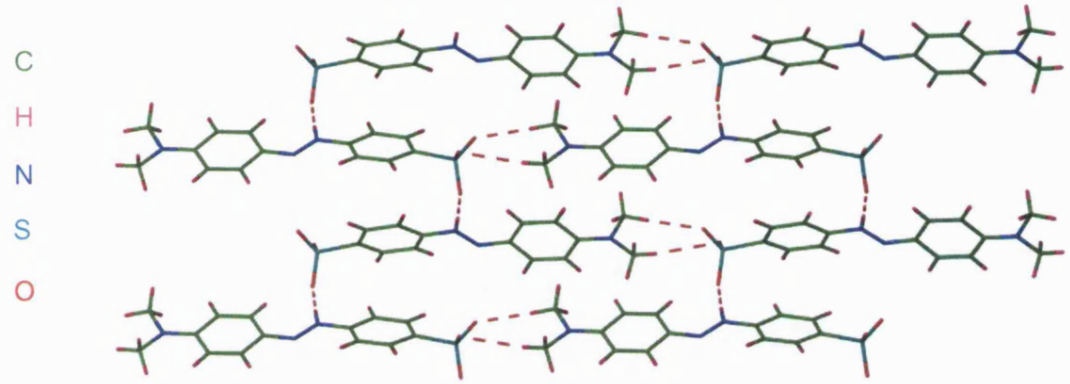

Figure 4.20; sheet formed in **29**

These two-dimensional arrays stack in the extended structure, as shown in Figure 4.21. There is a small twist of 15° between the least-squares planes of the two phenyl rings in the zwitterion, presumably to accommodate the hydrogen bond formation between the neighbouring molecules. There are also edge-to-face C–H···π interactions between the phenyl rings of neighbouring zwitterions.

Figure 4.21; two-dimensional arrays formed in **29**

The bonds N(3)–C(10) and N(2)–C(7) are shorter than N(1)–C(4) (see Figure 4.19), with bond lengths of 1.325(3), 1.331(3) and 1.407(3)Å respectively. This difference in bond length is due to the contribution of the resonance form of the zwitterion with the charge on the NMe_2 group, as shown in Figure 4.2 (section 4.0). The N–N bond is in the same plane as the C(7)–C(12) phenyl ring, whereas the C(1)–C(6) phenyl ring is twisted out of this plane.

(This suggests that the delocalisation does not extend through the phenyl rings of the zwitterion, therefore affecting the bond lengths mentioned above.)

D–H···A	D···A /Å	H···A /Å	D–H···A / °	Symmetry operation generating D···A
N(1)–H(1A)···O(1)	2.784(3)	1.82	178	1-*x*, ½+*y*, 1-*z*
C(13)–H(13B)···O(2)	3.562(4)	2.71	146	*x*-2, *y*, *z*-1
C(14)–H(14B)···O(3)	3.324(4)	2.34	179	*x*-2, *y*, *z*-1

Table 4.8; details of hydrogen bonding in **29**

4.2.1 The structural effects of alkyl substitution in guanidinium ions when crystallised with methyl orange

The hydrogen-bonding patterns observed in the structures of [Gu][MO] **25**, [MeGu][MO]·MeOH **26**, [EtGu][MO] **27** and [DiMeGu][MO] **28** are greatly affected by the level of substitution on the cation, with the hexagonal hydrogen-bonded guanidinium sulfonate sheet only observed in **25**. This consequence may seem obvious, however the reduction in dimensionality with cation substitution is not inevitable. In Chapter 2, the crystal structures of [MeGu][mTPPMS] **1** and of [EtGu][mTPPMS] **2** were shown to be remarkably similar to that of [Gu][mTPPMS] **I**, both being based on hexagonal GS sheets with a C–H···O hydrogen bond taking the place of the missing N–H···O interaction.

Even though the hydrogen-bonding motifs in structures **25-28** are different, the overall structures observed are remarkably similar. In **25** a bilayer formation is observed and in **26, 27** and **28** *pseudo*-bilayers are formed. These bilayers or *pseudo*-bilayers contain regions dominated by hydrogen bonding, separated by regions containing the organic fragment of the sulfonate. It has previously been shown[7] that bilayers are favoured when the R group is small with a width of up to 4.75Å, and these results are in line with this trend.

The hexagonal GS sheets in [Gu][MO] **25** are relatively flat with an inter-ribbon angle of 173°. Two GS sheets lie parallel to each other; the R groups of the sulfonate are directed to one side of each sheet and interdigitate, forming a bilayer.

The formation of a sheet is not observed in [MeGu][MO]·H_2O **26**. Instead, ribbons are formed via the remaining unsubstituted faces of the cations forming hydrogen bonds with the anions. Molecules of methanol, from the solvent, act as hydrogen bond donors and acceptors to form hydrogen bonds with the N–H donor of the substituted face of the cation and a vacant acceptor site of the sulfonate, linking two parallel ribbons into tapes. These tapes align into a *pseudo*-bilayer with interdigitating R groups.

Two cations and anions are observed in the asymmetric unit of [EtGu][MO] **27**, and these interact through hydrogen bonds to form a sheet. However, the regular hexagonal GS sheet formed in **25** is not observed here. Pairs of sheets are formed that are cross-linked via the

substituted cations, which are positioned approximately perpendicular to each sheet. A *pseudo*-bilayer is formed in the extended array with interdigitating R groups.

Compound [DiMeGu][MO] **28** forms chains by linking DD:AA hydrogen-bonded cation-anion pairs. These chains form further hydrogen bonds to each other linking them into two-dimensional sheets, which stack in the extended structure as *pseudo*-bilayers with interdigitating sulfonate R groups.

One obvious difference observed between the structures **25-28** is the inclusion of solvent in **26**. It may be expected that as the cation is substituted and N–H donors are lost, the inclusion of solvent could be advantageous by increasing the hydrogen-bonding groups present in the structure. However, when ethyl and *N,N*-dimethylguanidinium cations are incorporated into the structure, solvent molecules are not included. There are several explanations that could be used to rationalise this observation. It may be that crystals of **27** and **28** are formed in favour of those that may incorporate solvent molecules. It is likely that both thermodynamic and kinetic effects are responsible for the observation of the crystals that are formed.

Another major difference observed in these structures concerns the formation of sheets in **25**, **27**, and **28** but not in **26**. In **25**, the cations and sulfonate oxygens of the anion are approximately co-planar, linking into flat hexagonal sheets via hydrogen bonding. However, in **27** half of the cations are virtually perpendicular to the sulfonate oxygens, and in **28** all of the cations and sulfonate oxygens are almost perpendicular to each other. This seems to have the effect of a *wide* sheet being observed, and the formation of *pseudo*-bilayers.

Structures **26**, **27** and **28** have a small twist between the least-squares planes of the phenyl rings in the anion of up to 10°, and all have face-to-face $\pi\cdots\pi$ and edge-to-face C–H$\cdots\pi$ interactions between neighbouring anions. These observations are also different to those seen in **25**, where there is a substantial twist of 31° between the phenyl rings, and no face-to-face interactions but instead $\pi\cdots\pi$ interactions between the azo group of one anion and the phenyl ring of a neighbouring anion.

4.2.2 The effects of alkyl substitution in guanidinium ions on bond and hydrogen bond parameters when crystallised with methyl orange

The DD:AA hydrogen bond distances in the structures **25-28** lengthen as the degree of substitution on the cation is increased. The hydrogen bond distances (N···O) range from 2.885(2)Å – 2.967(2)Å in **25**, 2.875(3)Å – 2.973(3)Å in **26**, 2.849(3)Å – 3.049(3)Å in **27** and 3.025(3)Å – 3.053(3)Å in **28**. The mean average hydrogen bond distances are calculates as 2.903(2)Å in **25**, 2.912(3)Å in **26**, 2.971(4)Å in **27** and 3.039(3)Å in **28**. This suggests that the strength of the DD:AA hydrogen bonding is decreasing as the number of DD faces of the cation is reduced.

The C–N bond lengths in the cation and the S–O bond lengths of the anion are similar, respectively, in all four structures **25-28** revealing that these bond lengths are not affected as the cation is substituted. This is also the case for the N–C–N and O–S–O bond angles.

There is no obvious trend observed for the changes in length of the N=N bond as the cation donors are substituted, as shown in Table 4.9. These data also show that there is no correlation between the N=N bond length and the twist between phenyl planes in the anion.

	25	**26**	**27** (U1)	**27** (U2)	**28***
Bond lengths N=N (Å)	1.266(2)	1.260(3)	1.265(3)	1.257(4)	1.310(3) 1.206(3)
Anion twist°	31	7	10	2	9

Table 4.9; variation of N=N bond length and twist between least-squares planes of phenyl rings in the anions of structures **25-28** (**disorder present*).

However, the relative twist between the anion phenyl rings does affect the bond lengths C–N(a) and C–N(b), depicted in Figure 4.22. When there is a large twist between the phenyl rings, as seen in **25**, the bond C–N(a) is shorter than C–N(b) (Table 4.10). This is due to the N=N bond being in the same plane as the $-NMe_2$ functionalised phenyl ring, whereas the $-SO_3$ functionalised phenyl ring is not in this plane.

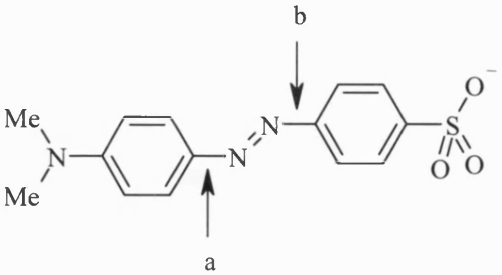

Figure 4.22; C–N bond lengths a and b

This leads to delocalisation between the $-NMe_2$ phenyl ring and N=N bond, leading to double bond character in the C–N(a) bond but not the C–N(b) bond.

When the phenyl rings are almost coplanar, there is delocalisation in the whole backbone of the anion leading to the two bonds lengths (a) and (b) being similar, as seen in **26-28**.

	25	**26**	**27** (U1)	**27** (U2)	**28***
Bond lengths (Å)					
C–N(a)	1.408(2)	1.419(3)	1.414(3)	1.418(3)	1.401(2)
C–N(b)	1.429(2)	1.437(3)	1.439(3)	1.440(3)	1.432(1)
Anion twist°	31	7	10	2	9

Table 4.10; comparison of C–N(a) and C–N(b) bond lengths in **25-28** (**disordered*)

4.2.3 HCl and NH_3 reactions of methyl orange-guanidinium sulfonates in the solid state

When single crystals of compounds [Gu][MO] **25**, [MeGu][MO]·MeOH **26**, [EtGu][MO] **27** and [DiMeGu][MO] **28** are exposed to HCl gas, a colour change is observed from orange to dark red. These red crystals were studied using single crystal X-ray techniques; however, no change in the cell dimensions was observed. This suggests that the colour change only occurs at the surface of the crystals. This was confirmed by cleaving the crystals, as the red colour was not observed on the freshly exposed surfaces, as shown in Figure 4.23. On continued exposure to HCl the crystals crumbled.

Figure 4.23; the orange centre of the cleaved crystal **25** (left) and the red surface that has been exposed to $HCl_{(g)}$ (right)

It was therefore concluded that a protonation reaction occurred at the surface of the crystals and that on continued exposure to HCl, the crystal lattice is disturbed as there is no available void space in the lattice to incorporate both H^+ and Cl^- ions. The single crystals of **25-28** were carefully ground into crystalline powders and exposed to HCl in a dessicator over a period of three days, and subsequently exposed to NH_3 for an equal period. The powders were analysed after each of the two exposures using X-ray powder diffraction, and the resultant plots are shown in Figure 4.24.

X-ray powder diffraction studies on samples of **25** exposed to HCl revealed the disappearance of the peaks associated with **25** and the appearance of a new set of peaks, demonstrating that the HCl adduct (**25a**) is crystalline. The pattern for **25a** is different to that observed for HMO **29** confirming that **25a** is $[C(NH_2)_3]Cl{\cdot}O_3SC_6H_4NH{=}NC_6H_4NMe_2$ and not simply $[C(NH_2)_3]Cl$ plus **29**. This suggests that the GS layers remain intact during the reaction.

When samples of **25a** were exposed to ammonia gas, the peaks associated with **25a** disappeared and were replaced by peaks for **25** in addition to new diffraction lines for NH_4Cl. The inter-conversion between **25** and **25a** is reversible, hence re-exposure of sample **25** to HCl regenerated **25a**, whereas re-exposure of this sample of **25a** to NH_3 reformed **25** together with more NH_4Cl. No evidence for **29** was observed in any of these reactions.

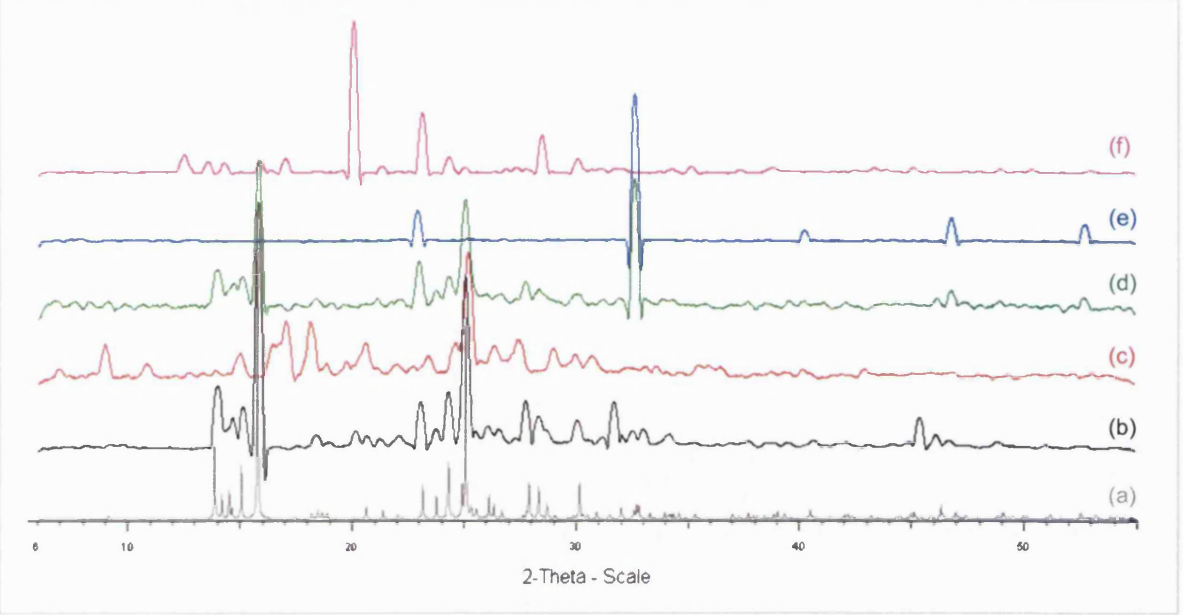

Figure 4.24; the powder diffraction studies on **25** exposed to cycles of HCl and NH_3.

(λ=1.5418Å [CuK_α])

(f) $O_3SC_6H_4NH{=}NC_6H_4NMe_2$ **29**
(e) NH_4Cl
(d) **25** plus $HCl_{(g)}$ then $NH_{3(g)}$
(c) **25** plus $HCl_{(g)}$ **(25a)**
(b) $[C(NH_2)_3][O_3SC_6H_4N{=}NC_6H_4NMe_2]$ **25**
(a) simulated powder pattern from single crystal data of $[C(NH_2)_3][O_3SC_6H_4N{=}NC_6H_4NMe_2]$ **25**

These findings are confirmed by IR and diffuse reflectance UV-visible spectroscopic studies. In the former, exposure of **25** to HCl leads to several new absorptions in the region 1650-1500cm^{-1}. Subsequent exposure (of **25a**) to NH_3 results in the loss of all of these new absorptions. The only difference between the IR spectrum of **25** and that of **25** following exposure to HCl and NH_3 is the presence of a peak at 1405cm^{-1} which can be assigned to NH_4Cl.

Diffuse reflectance spectra for **25** along with the samples exposed sequentially to HCl and NH_3 are shown in Figure 4.25. These spectra are also consistent with reformation of **25** following reaction with HCl and NH_3. The spectrum of **29** is also shown, for comparison.

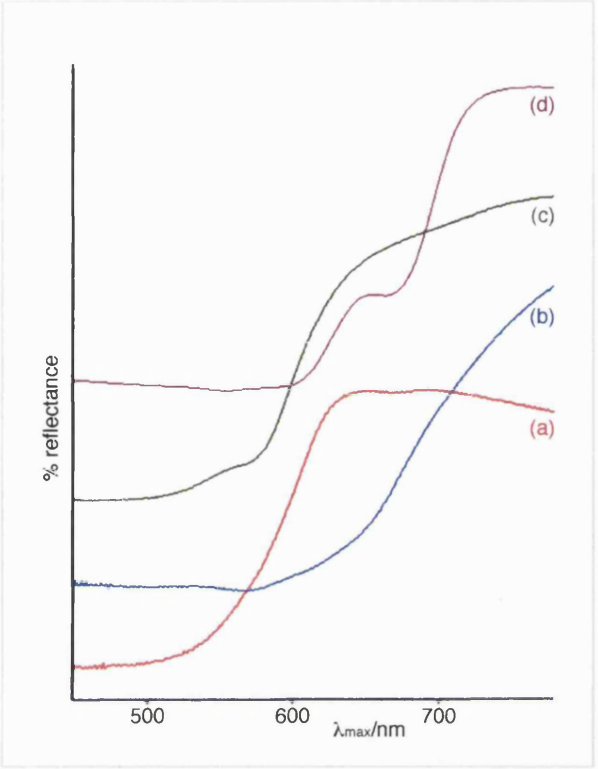

Figure 4.25; the diffuse reflectance UV-visible spectra for;

(d) **29**
(c) **25** plus HCl then NH3
(b) **25** plus HCl
(a) **25**

The X-ray powder diffraction, IR and UV-visible results, along with the single crystal data, demonstrate that the solid state reaction of **25** with $HCl_{(g)}$ proceeds in a different manner to the solution reaction of **25** with $HCl_{(aq)}$.

Similar observations were made with compounds [MeGu][MO]·MeOH **26**, [EtGu][MO] **27** and [DiMeGu][MO] **28** where partial formation of HCl adducts was observed in all cases on reaction with HCl gas. These adducts were subsequently converted back to **26-28**, respectively, on reaction with NH_3 with concomitant formation of NH_4Cl.

However, single crystals of **25-28** are unable to absorb HCl without the crystals being destroyed. This is probably due to the lack of void space in the structures, which would be required to accommodate the chloride anion. Therefore, other dye systems were studied with a view to forming crystalline compounds that might be able to accommodate guest ions while maintaining a crystalline array.

4.3 Ethyl orange sulfonates

[Gu][EO] : $[C(NH_2)_3][O_3SC_6H_4N{=}NC_6H_4NEt_2]$ 30

Asymmetric Unit

The asymmetric unit of **30** is shown in Figure 4.26 and consists of one $[Gu]^+$ cation and one $[EO]^-$ anion.

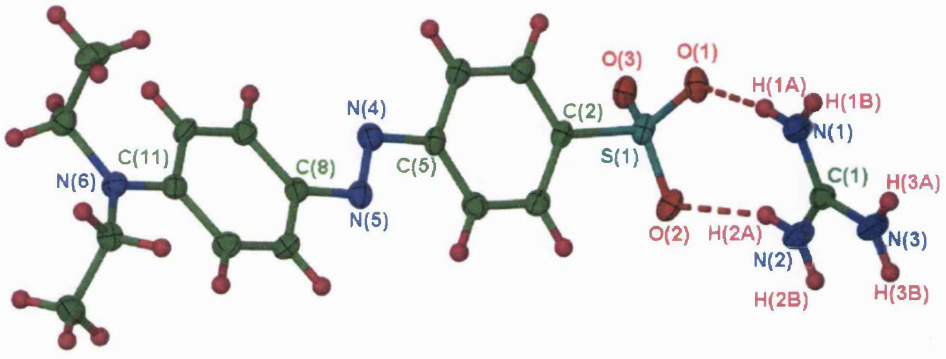

Figure 4.26; asymmetric unit of **30**. Ellipsoids are depicted at 50% probability level.

Extended Structure

The three unsubstituted faces of the cation form DD:AA hydrogen bonds with the three faces of the sulfonate via three $R_2^2(8)$ motifs, forming the regular hexagonal hydrogen-bonded GS sheet (shown in Figure 4.27). All of the N–H hydrogen bond donors and sulfonate acceptors are used to form this sheet. Hydrogen bond details are given in Table 4.11.

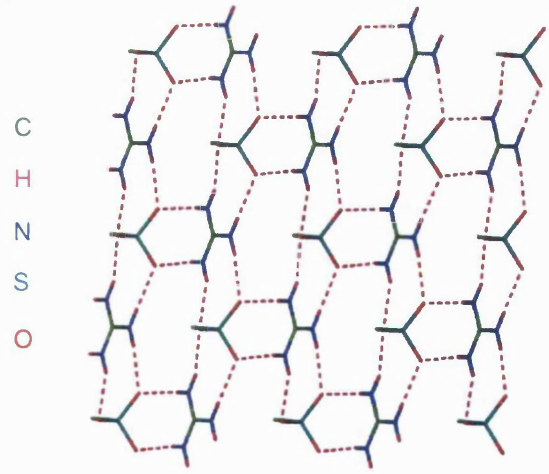

Figure 4.27; sheet formed in **30**, with the ribbons running vertically on the page.
(*most of the anion is omitted for clarity*)

The sulfonates are directed to both sides of the GS sheet as shown in Figure 4.28, in contrast to that observed in [Gu][MO] **25** where the sulfonates are directed to one side of the sheet.

The cations and sulfonate oxygen atoms of each ribbon within the sheet are approximately co-planar. However, the cations and sulfonate oxygen atoms of the anions of neighbouring ribbons within this sheet are almost perpendicular. This leads to the formation of corrugated sheets, with an inter-ribbon angle of 82°, which stack in continuous inter-digitating single layers in the extended structure.

The anions are twisted with an angle of 24° between the least-squares planes of the two phenyl rings. This allows greater π···π interactions between the N=N bond of one anion and the phenyl rings of a neighbouring anion, which is also seen in **25**.

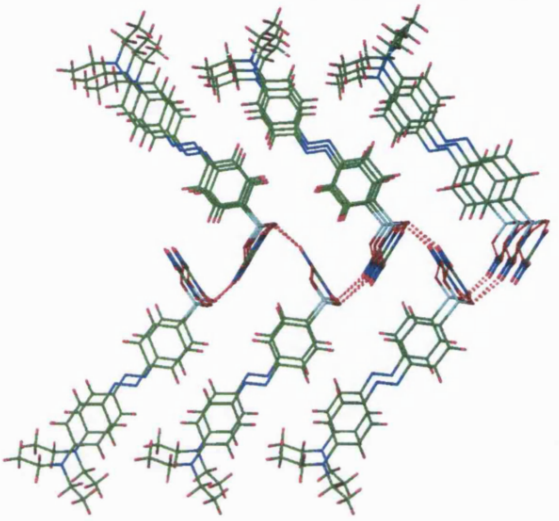

Figure 4.28; side view of sheet formed in **30**

D–H···A	D···A /Å	H···A /Å	D–H···A / °	Symmetry operation generating D···A
N(1)–H(1A)···O(1)	2.919(3)	2.06	165	*x*, *y*, *z*
N(1)–H(1B)···O(3)	2.945(3)	2.07	172	*x*, *y*, *z*-1
N(2)–H(2A)···O(2)	3.031(3)	2.19	160	*x*, *y*, *z*
N(2)–H(2B)···O(3)	2.977(3)	1.12	165	*x*-½, ½-*y*, *z*-½
N(3)–H(3B)···O(1)	2.941(3)	2.09	161	*x*-½, ½-*y*, *z*-½
N(3)–H(3A)···O(2)	3.019(3)	2.16	164	*x*, *y*, *z*-1

Table 4.11; details of the hydrogen bonding in **30**

[MeGu][EO]·MeOH : $[C(NH_2)_2(NHMe)][O_3SC_6H_4N{=}NC_6H_4NEt_2]$·MeOH 31

Asymmetric Unit

The asymmetric unit of **31** consists of two $[MeGu]^+$ cations, two $[EO]^-$ anions and two molecules of MeOH, as shown in Figure 4.29.

The azo nitrogen atoms N(4) and N(5) and the phenyl rings based on C(3)-C(8) and C(9)-C(14) are disordered in a 60:40 ratio with partial atoms N(4A), N(5A), C(3A)-C(8A) and C(9A)-C(14A) respectively. The thermal parameters of the atoms in the phenyl rings in each disordered part were restrained to be similar. Each of the phenyl rings was also constrained to being a regular hexagon.

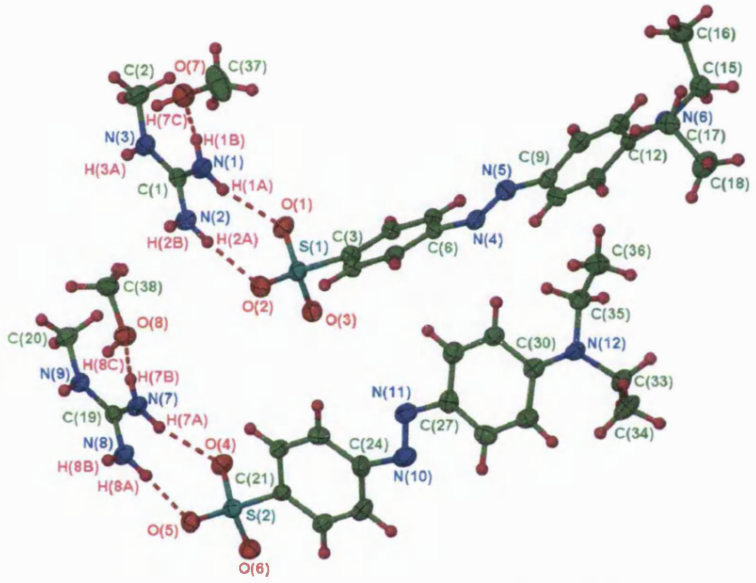

Figure 4.29; asymmetric unit of **31**. Ellipsoids are depicted at 50% probability level.
(the disordered part of 40% occupancy is not shown for clarity

Both of these cation-anion pairs form similar hydrogen-bonded arrays, therefore one pair [the anion incorporating S(1), the cation incorporating C(1) and methanol incorporating C(37)] will be described in detail.

Extended Structure

The cations and anions form ribbons through two DD:AA faces of the unsubstituted cation and the sulfonate (graph set $R_2^2(8)$). N–H···O and O–H···O hydrogen bonds involving molecules of methanol link the ribbons into tapes, as shown in Figure 4.30. All of the N–H

hydrogen bond donors and acceptors are used to form this tape. Details of the hydrogen bonds are given in Table 4.12. The sulfonate R groups are directed to both sides of the tapes, which align in the same plane forming a *pseudo*-bilayer that repeats through the extended structure.

This hydrogen-bonding arrangement is similar to that observed in the methyl orange analogue **26**, and **31** is also the only structure of the ethyl orange system that incorporates methanol from the solvent. The anions are twisted with angles between least-squares planes of the phenyl rings of 15° for the anion incorporating S(1) and 20° for that incorporating S(2).

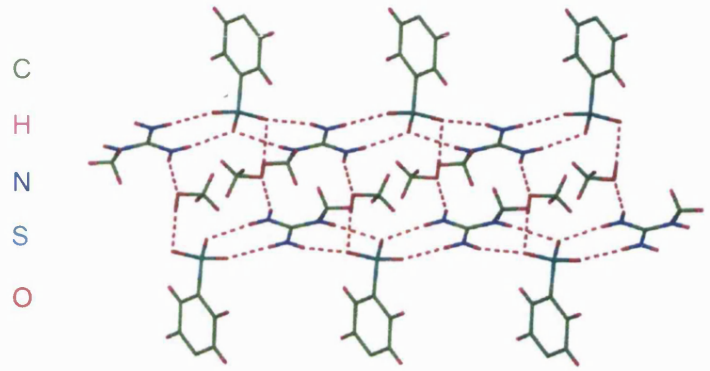

Figure 4.30; cross-linked ribbons (or tapes) formed in **31**.
(*half of the sulfonate R group has been removed for clarity*).

D–H···A	D···A /Å	H···A /Å	D–H···A / °	Symmetry operation generating D···A
N(1)–H(1B)···O(7)	2.910(3)	2.09	155	*x*, *y*, *z*
N(1)–H(1A)···O(1)	2.914(3)	2.05	167	*x*, *y*, *z*
N(2)–H(2A)···O(2)	2.890(3)	2.01	175	*x*, *y*, *z*
N(2)–H(2B)···O(3)	2.913(3)	2.07	161	*x*-1, *y*, *z*
N(3)–H(3A)···O(1)	2.998(3)	2.22	148	*x*-1, *y*, *z*
N(7)–H(7B)···O(8)	2.870(3)	2.04	157	*x*, *y*, *z*
N(7)–H(7A)···O(4)	2.988(3)	2.12	167	*x*, *y*, *z*
N(8)–H(8A)···O(5)	2.879(3)	2.01	168	*x*, *y*, *z*
N(8)–H(8B)···O(6)	2.914(3)	2.06	165	*x*-1, *y*, *z*
N(9)–H(9C)···O(4)	2.938(3)	2.12	154	*x*-1, *y*, *z*
O(7)–H(7C)···O(3)	2.824(3)	1.99	177	-*x*+1, -*y*+1, -*z*+1
O(8)–H(8C)···O(5)	2.857(3)	2.04	166	-*x*+1, -*y*+1, -*z*+1

Table 4.12; details of the hydrogen bonding in **31**

[EtGu][EO] : $[C(NH_2)_2(NHEt)][O_3SC_6H_4N{=}NC_6H_4NEt_2]$ 32

Asymmetric Unit

The asymmetric unit of **32** is shown in Figure 4.31 and consists of one $[EtGu]^+$ cation and one $[EO]^-$ anion. The azo nitrogen atoms N(4) and N(5) and the phenyl rings based on C(4)-C(9) are disordered in a 67:33 ratio with partial atoms N(4A), N(5A) and C(4A)-C(9A) respectively. It is also likely that the second phenyl ring C(10)-C(15) is disordered in a similar ratio. However, attempted modelling of this potential disorder did not improve convergence, largely because the separation between fragments is likely to be minimal.

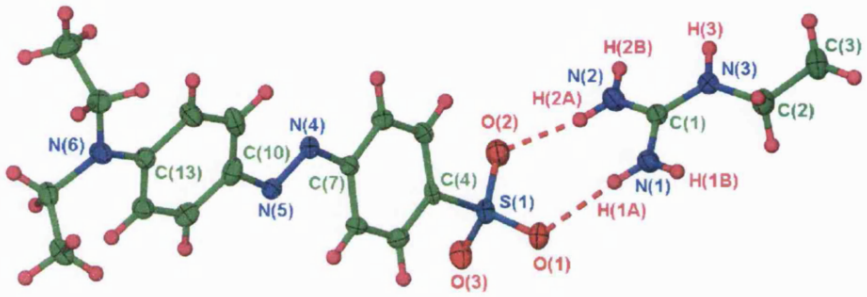

Figure 4.31; asymmetric unit in **32**. Ellipsoids are depicted at 50% probability level.
(*the disordered part of 33% occupancy is not shown for clarity*)

Extended Structure

The two unsubstituted faces of the cation form DD:AA hydrogen bonds with the sulfonate group of the anion linking them into ribbons forming $R_2^2(8)$ motifs. The N–H donor group on the substituted face of the cation forms hydrogen bonds with the sulfonate linking these ribbons into sheets (Figure 4.32). This hydrogen bonding leads to the hexagonal GS sheet, as seen in **30**, however one of the N–H···O hydrogen bonds has been replaced by a C–H···O hydrogen bond between the methylene hydrogen bond donor and the sulfonate. Details of the hydrogen bond lengths and angles are given in Table 4.13.

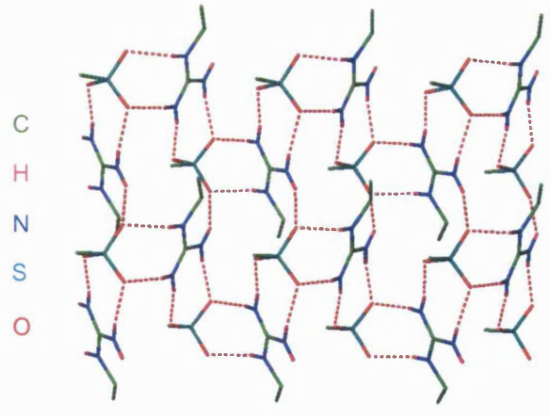

Figure 4.32; sheet formed in **32** with ribbons shown horizontally on the page
(*half of each sulfonate has been omitted for clarity*),

The sulfonates are directed to alternate sides of the GS sheet (Figure 4.33), which are highly corrugated, with an inter-ribbon angle of 71°. These sheets stack as continuous interdigitating single layers in the extended structure. There is a twist between the least-squares planes of the phenyl rings in the anion of 26°, and C–H···π interactions form between the edge of one phenyl ring and the face of a phenyl ring in a neighbouring anion.

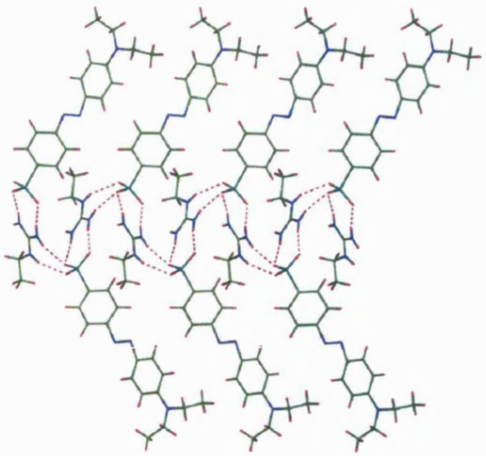

Figure 4.33; single layer in **32**

D–H···A	D···A /Å	H···A /Å	D–H···A / °	Symmetry operation generating D···A
N(1)–H(1A)···O(1)	2.987(2)	2.13	166	*x*, *y*, *z*
N(1)–H(1B)···O(3)	3.065(2)	2.32	142	*x*, *y*-1, *z*
N(2)–H(2A)···O(2)	2.834(2)	1.96	170	*x*, *y*, *z*
N(2)–H(2B)···O(1)	2.947(2)	2.09	163	½+*x*, ½-*y*, 1-*z*
N(3)–H(3)···O(3)	2.926(2)	2.11	154	½+*x*, ½-*y*, 1-*z*
C(2)–H(2D)···O(2)	3.405(2)	2.42	172	*x*, *y*-1, *z*

Table 4.13; details of the hydrogen bonding in **32**

[DiMeGu][EO] : $[C(NH_2)_2(NMe_2)][O_3SC_6H_4N{=}NC_6H_4NEt_2]$ 33

Asymmetric Unit

The asymmetric unit of **33** is shown in Figure 4.34 and consists of one $[DiMeGu]^+$ cation and one $[EO]^-$ anion.

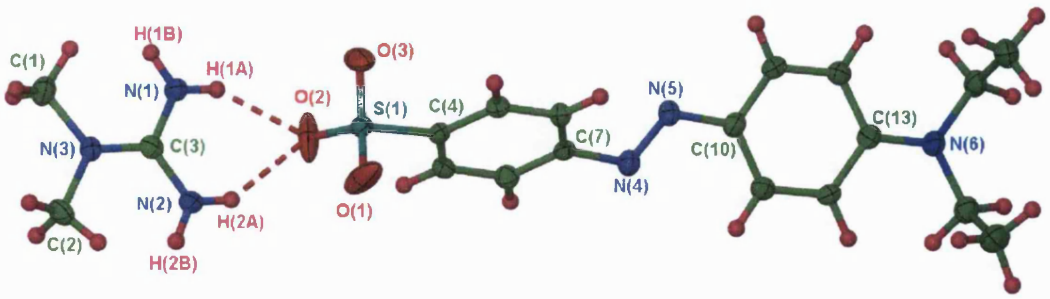

Figure 4.34; asymmetric unit in **33**. Ellipsoids are depicted at 50% probability level

Extended Structure

The unsubstituted face of the cation forms a $R_2^1(6)$ hydrogen-bonding motif with one sulfonate face of the anion instead of the $R_2^2(8)$ motif seen in previous structures involving the unsubstituted faces of the cations. The two remaining N–H donors of the substituted faces of the cation form single hydrogen bonds with sulfonate groups of neighbouring anions leading to the formation of a ribbon (graph set $R_4^4(12)$). All of the donors and acceptors are involved in the formation of these ribbons; details of the hydrogen bonds formed are given in Table 4.14. The substitution within the cation has disrupted the hydrogen-bonding faces such that sheet formation is no longer possible. The sulfonate R groups are directed to either side of this ribbon, as shown in Figure 4.35.

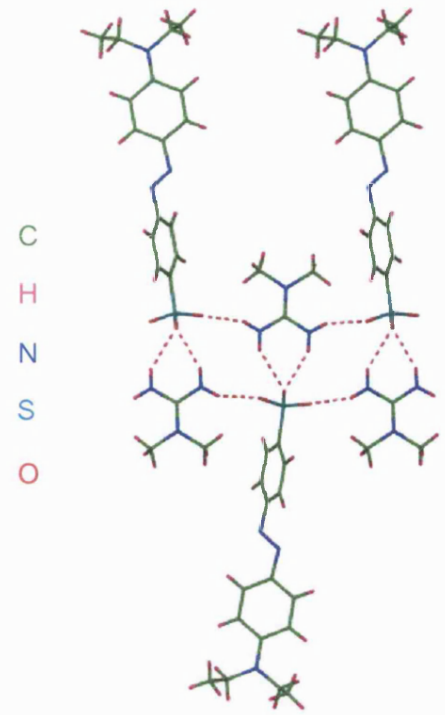

Figure 4.35; R groups directed to both sides of ribbon in **33** (*half of the sulfonate group has been removed for clarity*)

These ribbons are independent of each other, with no further hydrogen bonding between them. Further ribbons are generated by a centre of inversion proximate to N(4), leading to stacked ribbons in the extended structure. The two methyl groups of the NEt_2 of the anion are orientated in the same direction from the phenyl ring that the NEt_2 group is bonded to (see Figure 4.34). This is due to their proximity to the sulfonate groups of the neighbouring ribbon, minimising the possible void space in the structure. The anion is significantly twisted, with an angle of 58° between the least-squares planes of the phenyl rings. There are edge-to-face C–H···π interactions between the phenyl rings of neighbouring anions.

D–H···A	D···A /Å	H···A /Å	D–H···A / °	Symmetry operation generating D···A
N(1)–H(1A)···O(2)	2.135(3)	2.95	153	*x, y, z*
N(1)–H(1B)···O(1)	2.065(3)	2.84	146	*-x-½, y-½ , -z+½*
N(2)–H(2B)···O(3)	2.010(3)	2.84	156	*-x-½, y-½ , -z+½*
N(2)–H(2A)···O(2)	2.237(3)	3.02	149	*x, y, z*

Table 4.14; details of the hydrogen bonding in **33**

$HEO\cdot^{3}/_{4}H_2O$: $O_3SC_6H_4NH{=}NC_6H_4NEt_2\cdot^{3}/_{4}H_2O$ **34**

The zwitterion in **34** was prepared using the method as described for HMO **29**. However, molecules of water from the solvent have been incorporated into the structure in **34**, whereas this is not the case in **29**.

Asymmetric Unit

The asymmetric unit of **34** contains one HEO zwitterion that has been protonated at N(1) and a 0.75 molecule of water, as shown in Figure 4.36.

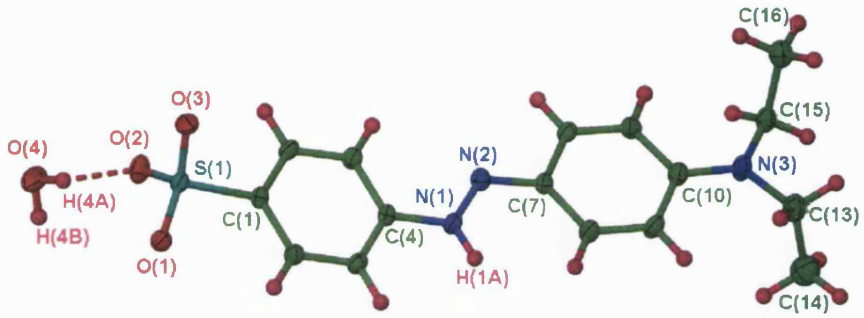

Figure 4.36; asymmetric unit in **34**. Ellipsoids are depicted at 50% probability level

The N(1)=N(2) bond has lengthened from 1.276(2)Å in **30** to 1.296(2)Å in **34** consistent with the greater single bond character anticipated on the basis of the delocalisation (Figure 4.2 of section 4.0) also seen in HMO **29**.

Extended Structure

Two zwitterions, related by a centre of inversion, form two N(1)–H(1A)···O(3) hydrogen bonds to each other via a $R_2^2(4)$ motif, ultimately linking into a chain, as shown in Figure 4.37.

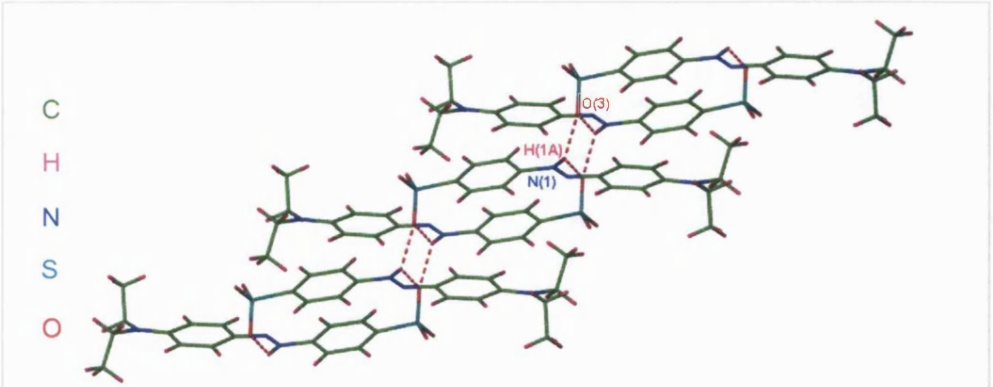

Figure 4.37; chain structure formed in **34**

The $R_2^2(4)$ motif formed between the zwitterions in **34** is rarely observed. A study of the crystallographic database showed that in all the structures containing the component functional groups (the donors and acceptors required), this motif is only observed in 1.9% of cases[8].

These chains are further linked into a two dimensional array via O–H···O hydrogen bonds, where water molecules act as donors and sulfonate oxygen atoms act as acceptors (graph set $R_4^4(12)$), as shown in Figure 4.38. These two-dimensional arrays stack in the extended structure, with no further hydrogen bonds between them. There is a small twist of 12° between the least-squares planes of the phenyl rings in the zwitterion. There are also π···π interactions between the protonated azo group and the phenyl rings of a neighbouring molecule.

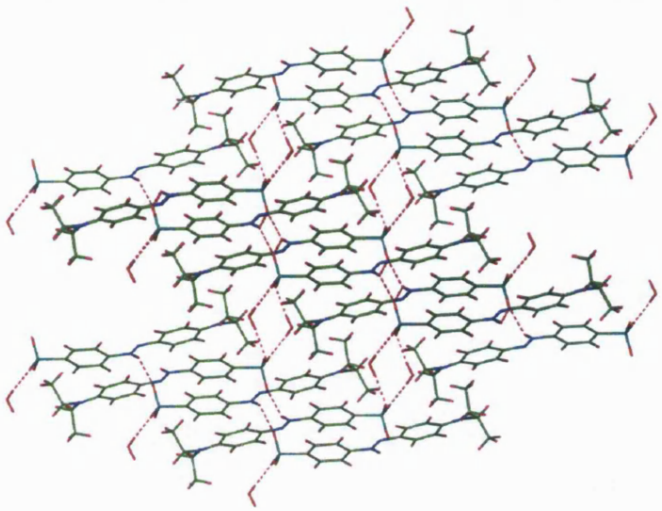

Figure 4.38; three-dimensional array in **34**

The bonds N(3)–C(10) and N(2)–C(7) are shorter than N(1)–C(4), with bond lengths of 1.337(3), 1.338(3) and 1.407(3)Å respectively (see Figure 4.36). This difference in bond length is due to the resonance form of the zwitterion, as seen in HMO (shown in Figure 4.2, section 4.0). The plane of the N=N bond is between the least-squares planes of the two phenyl rings. This suggests that the delocalisation of the positive charge on N(1) is not disrupted by the small twist between the plane of the phenyl ring C(7)-C(12) and the N(1)=N(2) bond.

D–H···A	D···A /Å	H···A /Å	D–H···A / °	Symmetry operation generating D···A
N(1)–H(1A)···O(3)	2.221(3)	2.99	146	*x*+1, *y*, *z*
N(1)–H(1A)···O(3)	2.400(3)	3.07	133	-*x*, -*y*, -*z*+1
O(4)–H(4A)···O(2)	1.984(3)	2.86	167	*x*, *y*, *z*
O(4)–H(4B)···O(1)	1.938(3)	2.82	172	-*x*-1, -*y*, -*z*

Table 4.15; details of the hydrogen bonding in **34**

4.3.1 The structural effects of alkyl substitution in guanidinium ions when crystallised with ethyl orange

The structures of [Gu][EO] **30**, [MeGu][EO]·MeOH **31**, [EtGu][EO] **32** and [DiMeGu][EO] **33** are affected differently by the substitution of the cation; with inter-digitating single layers, a *pseudo*-bilayer and independent ribbons being observed.

The crystal structure of [Gu][EO] **30** was expected to form the regular hexagonal hydrogen-bonded GS sheet, and indeed this sheet is observed. However, in contrast to [Gu][MO] **25**, the sheet in **30** is not flat but highly corrugated with an inter-ribbon angle of 82°. Also in contrast to **25**, where bilayers are observed, the R groups of the sulfonate are directed to both sides of the sheet and repeating single layers are observed with the R groups of neighbouring sheets inter-digitating. There is a twist between the phenyl rings of the anion of 24°, and $\pi\cdots\pi$ interactions are observed between the azo group of one anion and the phenyl ring of a neighbouring anion, as seen in **25**.

Compound [MeGu][EO]·MeOH **31** forms the same hydrogen-bonded array as its methyl orange analogue [MeGu][MO]·MeOH **26**, with both compounds incorporating methanol into the structure. The methanol in **31** has the same role as that in **26**, linking individual ribbons into tapes via hydrogen bonding. There are no further interactions between these tapes and they stack in the extended lattice to form a *pseudo*-bilayer. There is a higher degree of twist between the least squares planes of the phenyl rings in the anions of **31**, of 15° [the anion incorporating S(1)] and 20° [the anion incorporating S(2)], compared to that of 7° observed in **26**.

Compound [EtGu][EO] **32** forms the hexagonal GS sheet, where one N–H···O hydrogen bond has been replaced with a C–H···O hydrogen bond. The sheet is highly corrugated, with an inter-ribbon angle of 71°. The R groups are directed to either side of the sheet and, as seen in **30**, repeating single layers are observed with inter-digitating R groups. This structure is markedly different to that of its methyl orange analogue [EtGu][MO] **27**, where a *pseudo*-bilayer is observed.

In **33** independent ribbons are observed where a $R_2^1(6)$ motif is observed between the cation-anion pairs, with a further motif ($R_4^4(12)$) linking the pairs into ribbons, which stack with

edge-to-face C–H···π interactions observed between neighbouring anions. There is also a substantial twist of 58° between the least-squares planes of the phenyl rings in the anion.

In the structures of **30**, **31** and **32** the methyl groups of the ethyl orange anion are orientated in opposite directions to each other, as would be expected, as this is sterically the most favourable orientation. However, in **33** this is not the case and the ethyl groups are orientated in the same direction, due to their close proximity to a neighbouring ribbon.

4.3.2 The effects of alkyl substitution in guanidinium ions on bond and hydrogen bond parameters when crystallised with ethyl orange

The DD:AA hydrogen bond distances in the structures **30-32** decrease as the substitution on the cation is increased. The hydrogen bond distances (N···O) range from 2.919(3)Å – 3.031(3)Å, mean average 2.972(3)Å in **30**, 2.879(4)Å – 2.998(3)Å, mean average 2.929(3)Å in **31** and 2.834(2)Å – 2.987(2)Å, mean average 2.924(3)Å in **32**. This suggests that the strength of the DD:AA hydrogen-bonding is increasing as the number of DD faces in the cation is reduced.

As for the methyl orange analogues, the C–N and S–O bond lengths are similar, as are the N–C–N and O–S–O bond angles, in all four structures **30-33**, revealing that these bond lengths are not affected as the cation is substituted.

There is no trend for the changes in length of the N=N bond as the cation donors are substituted, as shown in Table 4.16, nor is there a correlation between the N=N bond length and the twist between phenyl planes in the anion.

	30	**31*** (U1)	**31** (U2)	**32***	**33**
Bond lengths N=N (Å)	1.276(3)	1.24(1) 1.30(1)	1.330(4)	1.269(3) 1.251(7)	1.270(3)
Anion twist°	24	15	20	26	58

Table 4.16; variation of bond length N=N and phenyl twists in the anions of structures **30-33** (**disordered)*

As seen in the methyl orange system, the relative twist of the anion phenyl rings affects the bond lengths C–N(a) and C–N(b) (depicted in Figure 4.22). There is a large twist between the least-squares planes of the phenyl rings in **33**, leading to the bond C–N(a) being shorter than C–N(b) (Table 4.17). Once again, the N=N bond is in the same plane as the $-NMe_2$ functionalised phenyl ring, whereas the $-SO_3$ functionalised phenyl ring is not in this plane. This leads to delocalisation in the $-NMe_2$ functionalised phenyl ring and N=N bond, hence there is double bond character in the C–N(a) bond but not the C–N(b) bond. When the phenyl rings are almost co-planar the two bonds (a) and (b) are similar, as seen in **30-32**.

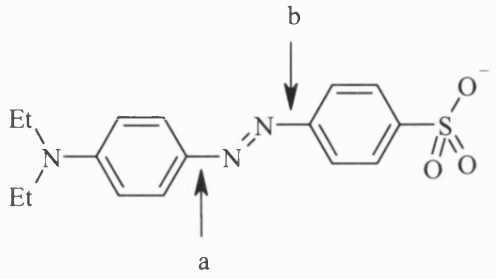

Figure 4.39; C–N bond lengths a and b

	30	**31*** (U1)	**31** (U2)	**32***	**33**
Bond lengths (Å)					
C–N(a)	1.410(3)	1.441(7) 1.425(9)	1.452(3)	1.448(3) 1.436(5)	1.412(3)
C–N(b)	1.420(3)	1.465(8) 1.39(1)	1.447(4)	1.424(3) 1.467(7)	1.441(3)
Anion twist°	24	15	20	26	58

Table 4.17; comparison of C–N (a) and C–N (b) bond lengths in **30-33** (**disordered)*

4.3.3 Comparison of structures in the zwitterions HMO 29 and $HEO\cdot^3/_4H_2O$ 34

The major difference between the structures of HMO **29** and that of $HEO\cdot^3/_4H_2O$ **34** is that in the latter, molecules of water are incorporated into the structure, whereas this does not occur in **29**. It is notable that crystals of **29** and **34** form from both water and methanol solutions. In the case of **29**, molecules of solvent are not included in the structure from either solvent system.

In **29**, the zwitterions are linked into chains via N–H···O hydrogen bonds between the protonated azo group and the sulfonate acceptors of a neighbouring zwitterion. These chains link into a two-dimensional array via C–H···O hydrogen bonds from the methyl group of the anion to a sulfonate acceptor, which in turn stack in the extended structure with evident edge-to-face C–H···π interactions. There is a small twist between the least-squares planes of the phenyl rings of 15°.

In **34**, the zwitterions are linked into chains via N–H···O hydrogen bonding between the protonated azo group and the sulfonate acceptors of a neighbouring zwitterion. These chains are linked into a two-dimensional array via O–H···O hydrogen bonds from the two donors of the water. This two-dimensional array stacks in the extended structure. As seen in **29**, there is a small twist of 12° between the phenyl rings of the zwitterion. However, in contrast to **29**, there are no C–H···π interactions present between phenyl rings of the zwitterions, but π···π interactions between the azo group of one molecule and the phenyl ring of a neighbouring molecule.

In both structures, the N(1)=N(2) bond has been lengthened, from 1.266(2)Å in **25** to 1.307(3)Å in **29**, and from 1.276(2)Å in **30** to 1.296(2)Å in **34**. This increased bond length is due to the delocalisation through the phenyl rings bonded to the NMe_2 and NEt_2 groups and the N=N bonds. This delocalisation also accounts for the N(3)–C(10) and N(2)–C(7) being shorter than N(1)–C(4) bonds in both **29** and **34** (see Figure 4.39). In **29** the N=N bond is in the same plane as the C(7)-C(12) phenyl ring, in contrast to the C(1)-C(6) phenyl ring which is twisted out of this plane by 15°. In **34** this is not the case as the N=N bond is between the two least-squares planes of the phenyl rings, which are twisted relative to each other by 12°. This suggests that the small twist between the phenyl rings in these structures does not affect the delocalisation in the two zwitterions.

4.3.4 HCl and NH_3 reactions of ethyl orange-guanidinium sulfonates in the solid state

When single crystals of compounds [Gu][EO] **30**, [MeGu][EO]·MeOH **31**, [EtGu][EO] **32** and [DiMeGu][EO] **33** are exposed to HCl gas a colour change is observed from red/orange to purple/red. On exposure, the crystals crumbled following the colour change. Therefore the single crystals of compounds **30-33** were ground into powders, exposed to HCl and NH_3 in a dessicator as described for the methyl orange series, and studied using X-ray powder diffraction. The resultant plots for **30** are shown in Figure 4.40. Interestingly, the results of these reactions are different to those observed in the methyl orange series.

X-ray powder diffraction analysis of **30** exposed to HCl revealed the disappearance of the peaks associated with **30** and the appearance of a new set of peaks; the crystalline HCl adduct **30a**. However, there are a number of peaks present in **30a** that are also observed in the zwitterion $O_3SC_6H_4NH{=}NC_6H_4NEt_2$ (powder pattern (f) in Figure 4.40) and there are also additional peaks in the powder pattern of **30a** that are present in the simulated powder pattern of GuCl (powder pattern (g) in Figure 4.40). This suggests that when ground crystals of [Gu][EO] are exposed to $HCl_{(g)}$, the lattice is broken down and the formation of HEO and GuCl is observed. There are also peaks observed in **30a** that are not observed in the powder patterns of either the zwitterion or GuCl. It is most likely that these peaks correspond to a co-crystal incorporating both the zwitterion and GuCl.

When samples of **30a** were exposed to $NH_{3(g)}$, all the peaks associated with **30a** disappeared and were replaced by peaks for **30** and NH_4Cl (as seen in the methyl orange analogues **25** and **25a**), showing that there is complete re-formation of [Gu][EO]. The inter-conversion between **30** and **30a** is reversible, thus re-exposure of this sample to HCl regenerated **30a**, and re-exposure of this sample of **30a** to NH_3 reformed **30** together with more NH_4Cl.

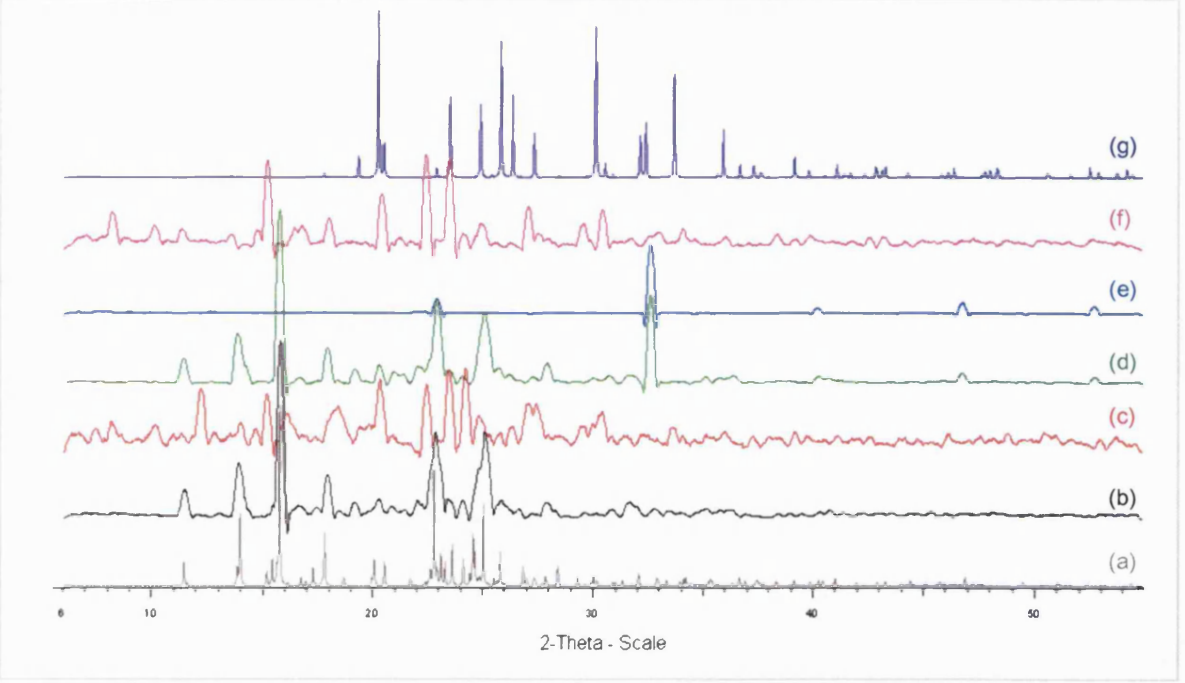

Figure 4.40; the powder diffraction studies on **30** exposed to cycles of HCl and NH_3

(λ=1.5418 [CuK_α])

(g) simulated powder pattern from single crystal data of GuCl
(f) $O_3SC_6H_4NH{=}NC_6H_4NEt_2$ **34**
(e) NH_4Cl
(d) **30** plus $HCl_{(g)}$ then $NH_{3(g)}$
(c) **30** plus $HCl_{(g)}$ (**30a**)
(b) $[C(NH_2)_3][O_3SC_6H_4N{=}NC_6H_4NEt_2]$ **30**
(a) simulated powder pattern from single crystal data of $[C(NH_2)_3][O_3SC_6H_4N{=}NC_6H_4NEt_2]$ **30**

These findings are confirmed by IR spectroscopy. The formation of **30a** leads to new absorptions in the region 1650-1500cm^{-1} that are not observed in **30**. Subsequent exposure of **30a** to NH_3 results in the loss of all of these new absorptions. The difference between the IR spectrum of **30** and that of **30a** exposed to NH_3 is a broadening of the peak at 1400cm^{-1} that can be assigned to NH_4Cl. Also confirmed is the presence of the zwitterion **34** in the spectrum of [Gu][EO] exposed to HCl (**30a**). In addition to these peaks, there are several peaks in **30a** that are not present in the spectrum of the zwitterion alone, showing there are other compounds as well as the zwitterion present in **30a**, already identified as GuCl and a possible [zwitterion][GuCl] co-crystal.

Diffuse reflectance spectra for **30** in addition to the samples having been exposed sequentially to HCl and NH_3 are shown in Figure 4.41. These spectra show that the conversion between **30** and **30a** is reversible. However, from the powder diffraction results,

similar peaks would be expected in the spectra of both **30a** and that of **34** (the zwitterion). This is not the case, as different peaks are observed in **34** to those observed in **30a**. It is unclear why these results are observed, and more detailed work is required to investigate this further.

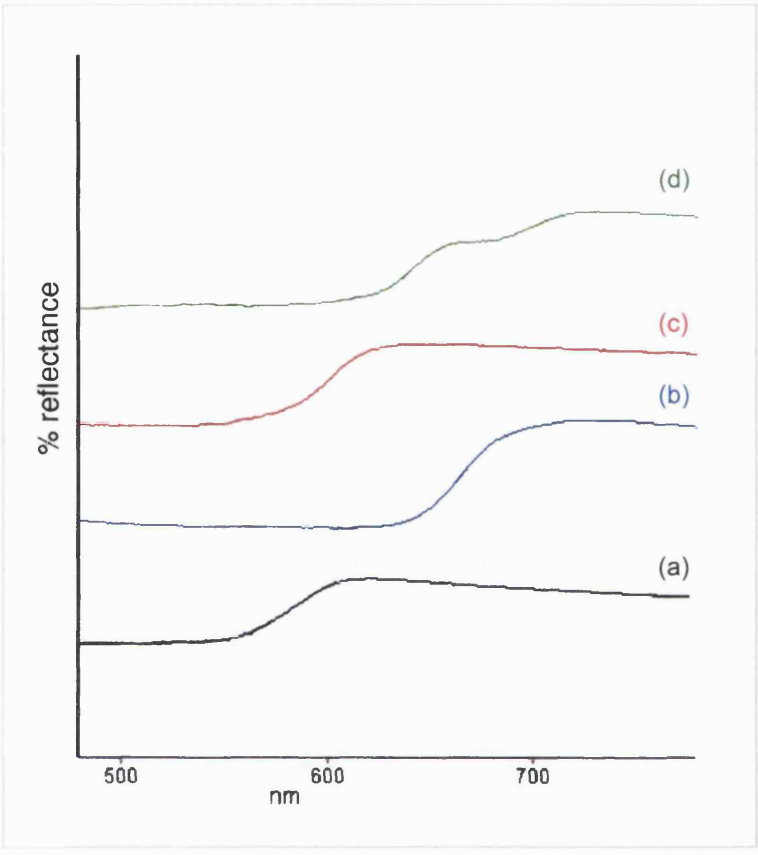

Figure 4.41; the diffuse reflectance UV-visible spectra for;

(d) **34**
(c) **30** plus HCl then NH_3
(b) **30** plus HCl (**30a**)
(a) **30**

The compounds [MeGu][EO]·MeOH **31**, [EtGu][EO] **32** and [DiMeGu][EO] **33** revealed similar behaviour to **30** where formation of the zwitterion HEO is observed when the samples are exposed to HCl. The powder patterns formed on exposure of these samples to NH_3 show that all the compounds formed in **31a**, **32a** and **33a** revert back to **31**, **32** and **33** respectively, with concomitant formation of NH_4Cl.

4.4 4-Aminoazobenzene-4'-sulfonate

[Gu][ABS] : $[C(NH_2)_3][O_3SC_6H_4N{=}NC_6H_4NH_2]$ 35

Asymmetric Unit

The asymmetric unit of **35** is shown in Figure 4.42 and consists of two $[Gu]^+$ cations and two $[ABS]^-$ anions.

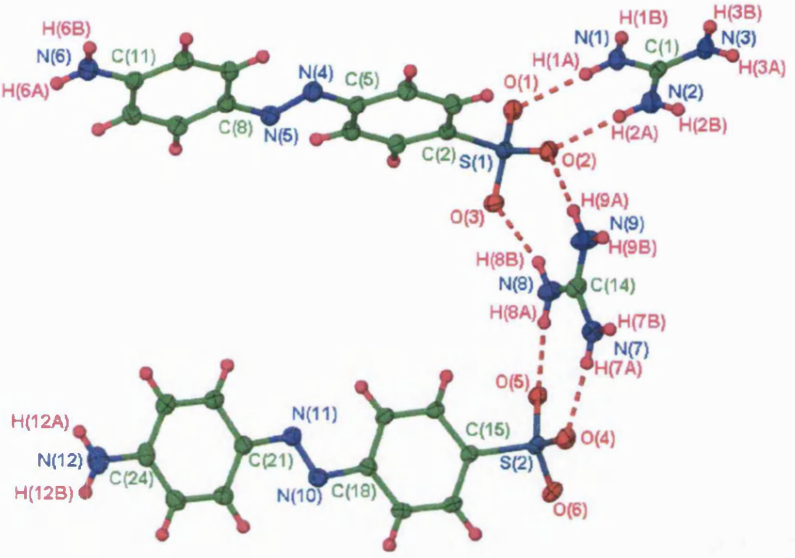

Figure 4.42; asymmetric unit of **35**. Ellipsoids are depicted at 50% probability level.

Extended Structure

The oxygen atoms of the two sulfonate groups in the anions are approximately co-planar with the cation containing C(14). However, the cation based on C(1) is not co-planar with the sulfonates, with an angle of 45° between the planes of the cation containing C(1) and the oxygens of the sulfonate containing S(1). The cation derived from C(14) forms three DD:AA $R_2^2(8)$ hydrogen-bonding motifs with two anions based on S(1) and one anion containing S(2) (Figure 4.43). This hydrogen bonding links this cation and the two anions based on S(1) into ribbons (Figure 4.43). The cation based on C(1) forms one

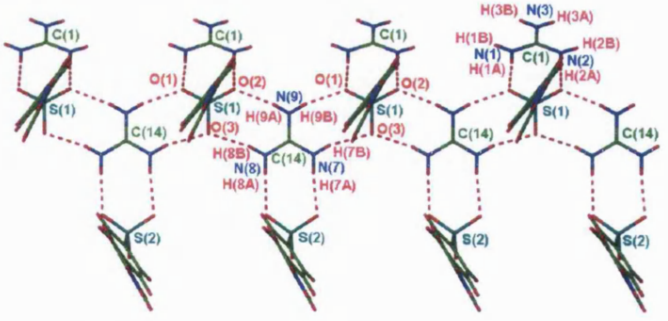

Figure 4.43; ribbon formed between cations based on C(14) and two anions (based on S(1) and S(2)) in **35**

DD:AA hydrogen-bonding motif (graph set $R_2^2(8)$) with the third face of the anion based on S(1), also shown in Figure 4.43.

Two of these ribbons lie parallel to each other, related by a centre of inversion, as shown in Figure 4.44. The R groups of the sulfonates are directed to one side of each ribbon. These ribbons are hydrogen-bonded together via the DD:AA hydrogen bonding face of the cation containing C(1) and two of the four remaining N–H donors available from the cation based on C(1) [N(1)–H(1B) and N(2)–H(2B)] which form two hydrogen bonds to the oxygen acceptor sites of two different anions containing S(2).

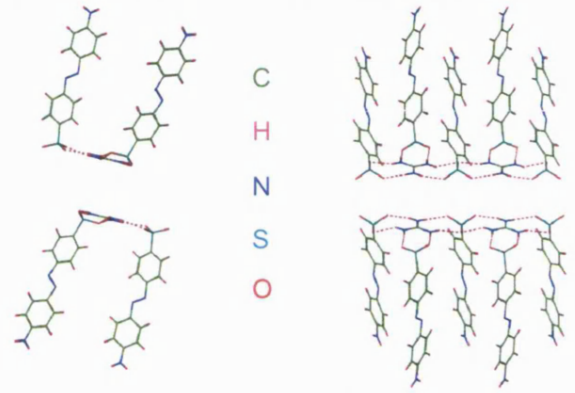

Figure 4.44; two views of the ribbon formation in **35**

The two remaining N–H donors, N(1)–H(1B) and N(2)–H(2B), link these ribbons into sheets (Figure 4.45) with the R groups of the sulfonates directed to both sides. There is further hydrogen bonding involving the NH_2 group at the opposite end of the anion. N(6)–H(6A) and N(6)–H(6B) form hydrogen bonds with O(4) and O(3) of a neighbouring sheet, respectively. However, N(12)–H(12A) and N(12)–H(12B) do not form any hydrogen bonds, and their position seems to be driven by steric constraints; there are no N···N or N···O contacts within 3.6Å. For the hydrogen bond details see Table 4.18.

In the extended structure a three-dimensional architecture is observed, similar to the pillared brick architecture observed in guanidinium disulfonate structures (section 1.3). The two anions have a small twist between the least-squares planes of the phenyl rings of 10°. There are also edge-to-face interactions between the phenyl rings of neighbouring anions.

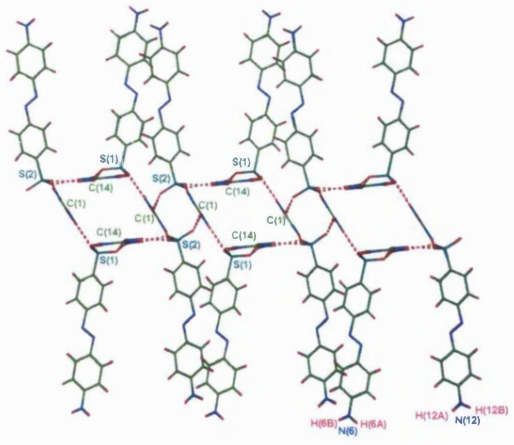

Figure 4.45; sheet formed in **35**

D–H···A	D···A /Å	H···A /Å	D–H···A / °	Symmetry operation generating D···A
N(1)–H(1A)···O(1)	2.922(2)	2.04	177	*x*, *y*, *z*
N(1)–H(1B)···O(5)	3.086(2)	2.36	140	-*x*+1, *y*-½ , *z*
N(2)–H(2A)···O(2)	2.887(2)	2.01	178	*x*, *y*, *z*
N(2)–H(2B)···O(6)	2.973(2)	2.38	125	*x*, ½-*y*, ½+*z*,
N(3)–H(3A)···O(4)	2.798(1)	1.93	169	-*x*+2, *y*-½, -*z*+$^3/_2$
N(3)–H(3B)···O(5)	2.810(1)	1.98	156	-*x*+1, *y*-½ , *z*
N(6)–H(6B)···O(3)	3.128(2)	2.31	154	*x*, -*y*+½, *z*+½
N(6)–H(6A)···O(4)	3.393(2)	2.64	144	*x*-1, *y*, *z*
N(7)–H(7A)···O(4)	2.911(2)	2.04	171	*x*, *y*, *z*
N(7)–H(7B)···O(3)	3.033(2)	2.22	154	*x*+1, -*y*+½, *z*+½
N(8)–H(8A)···O(5)	2.909(2)	2.03	175	*x*, *y*, *z*
N(9)–H(9B)···O(1)	2.875(2)	2.01	168	*x*+1, -*y*+½, *z*+½
N(9)–H(9A)···O(2)	2.871(2)	2.00	171	*x*, -*y*+½, *z*+½

Table 4.18; details of the hydrogen bonding in **35**

[MeGu][ABS] : $[C(NH_2)_2(NHMe)][O_3SC_6H_4N{=}NC_6H_4NH_2]$ 36

Asymmetric Unit

The asymmetric unit of **36** is shown in Figure 4.46 and consists of two $[MeGu]^+$ cations and two $[ABS]^-$ anions. There is possibly disorder in backbone of the anion containing S(1). However, the attempted modelling of this potential disorder did not improve convergence, largely because the separation between fragments is likely to be minimal.

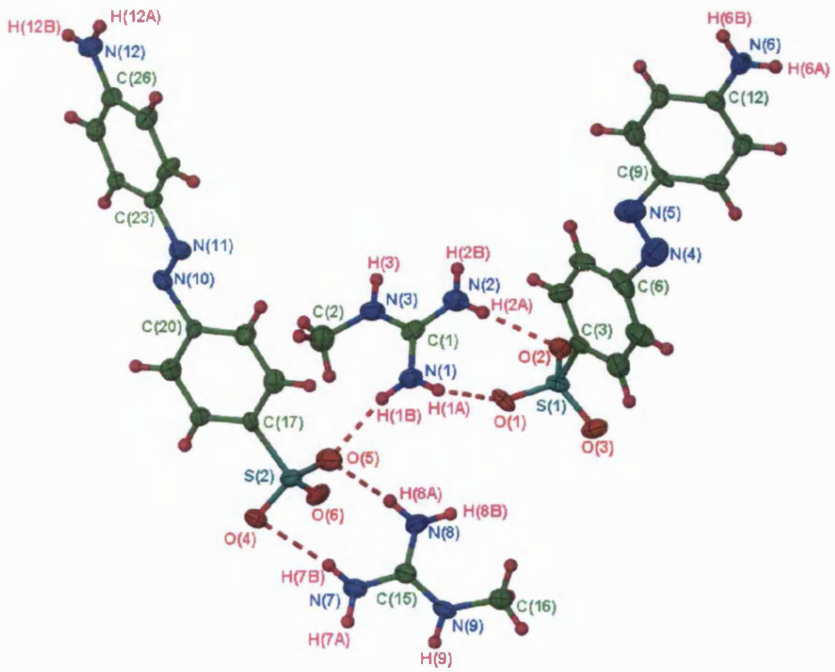

Figure 4.46; asymmetric unit in **36**. Ellipsoids are depicted at 50% probability level.

Extended Structure

Both cations and anions of the asymmetric unit are involved in ribbon formation, as shown in Figure 4.47. However, the two cations and two sulfonates fulfil different roles within the structure.

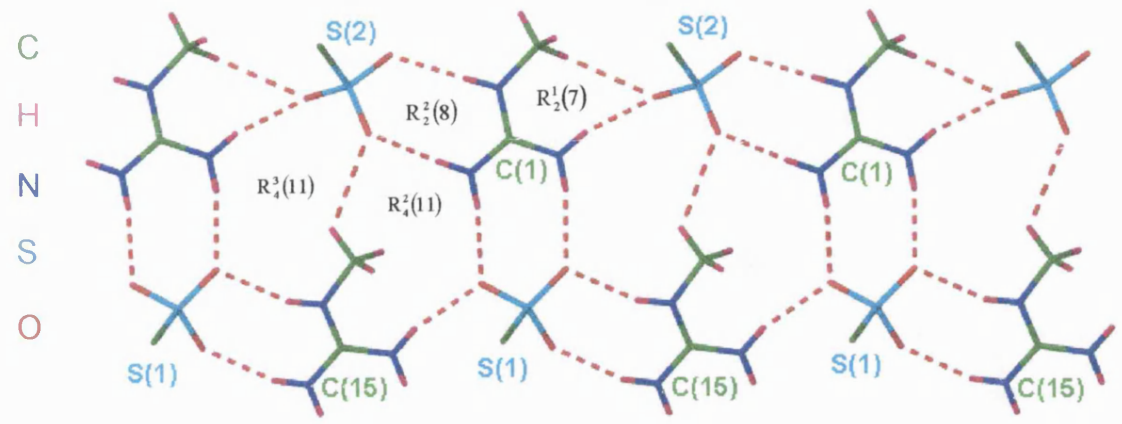

Figure 4.47; the ribbon formed in **36**

The sulfonate containing S(1) forms two DD:AA hydrogen bonds (graph set $R_2^2(8)$) with one of the unsubstituted faces of each cation. The sulfonate based on S(2) forms only one DD:AA hydrogen-bonding motif with one of the unsubstituted faces of the cation based on C(1).

The two unsubstituted faces in the cation based on C(1) form DD:AA hydrogen bonds within the ribbon. The remaining N–H donor on the substituted face, along with a C–H donor of the methyl group in this face, form single hydrogen bonds with an oxygen of the sulfonate containing S(2) via the graph set $R_2^1(7)$. However, the cation based on C(15) only forms one DD:AA hydrogen bonding motif within the ribbon. The N–H donor of the substituted face forms a single hydrogen bond to an oxygen of the sulfonate containing S(1), whereas the C–H donor of the methyl group of this face forms a hydrogen bond to an oxygen atom in the sulfonate based on S(2) via the graph sets $R_4^3(11)$ and $R_4^2(11)$. The remaining unsubstituted face is not involved in the ribbon formation.

This ribbon interacts with a second inversion related ribbon via the remaining unsubstituted face of the cation based on C(15), forming a DD:AA hydrogen-bonded motif with the available face on the sulfonate containing S(2). This hydrogen bonding links the ribbons into

a cylindrical array (shown in Figure 4.48). All the sulfonate R groups are directed away from the cylinder.

These cylindrical arrays align in the same plane, with the sulfonate R groups directed above and below this plane, as shown in Figure 4.49. There are distinct regions of hydrogen-bonded cations and anion sulfonate groups, which are separated by regions of the sulfonate R groups.

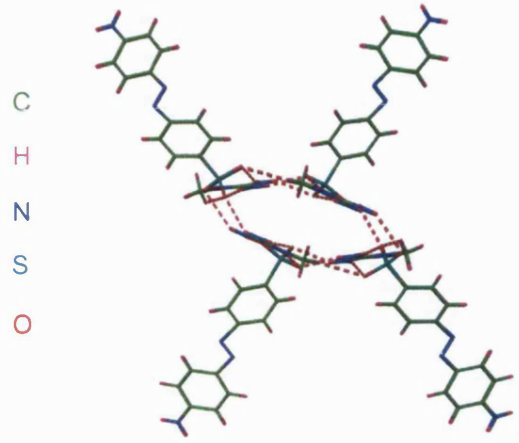

Figure 4.48; the cylindrical hydrogen-bonded array formed in **36**

The two anions each contain an amino group, and these are involved in the formation of hydrogen bonds. One N–H donor of each amino group forms a hydrogen bond to a sulfonate oxygen atom from a cylinder in the neighbouring plane, and the other N–H group of each anion forms a hydrogen bond to a nitrogen atom of the azo group in a neighbouring anion. These interactions link the hydrogen-bonded cylindrical units into a three-dimensional array, similar to the pillared brick architecture observed in guanidinium disulfonate structures. The details of the hydrogen bonds formed are given in Table 4.19.

There is a twist in the anions between the least-squares phenyl planes of 32° in the anion based on S(1) and 28° in the anion based on S(2). There are no significant π···π interactions between the phenyl rings of neighbouring anions, with the closest contact being greater than 4Å. Moreover, the phenyl rings are not orientated such that face-to-face or edge-to-face interactions are possible.

The bond lengths N(4)=N(5) and N(10)=N(11) are 1.212(8)Å and 1.279(7)Å respectively. This lengthening in the N(10)=N(11) bond length is due to the formation of a N–H···N hydrogen bond. The azo group containing N(4)=N(5) is not involved in such an interaction.

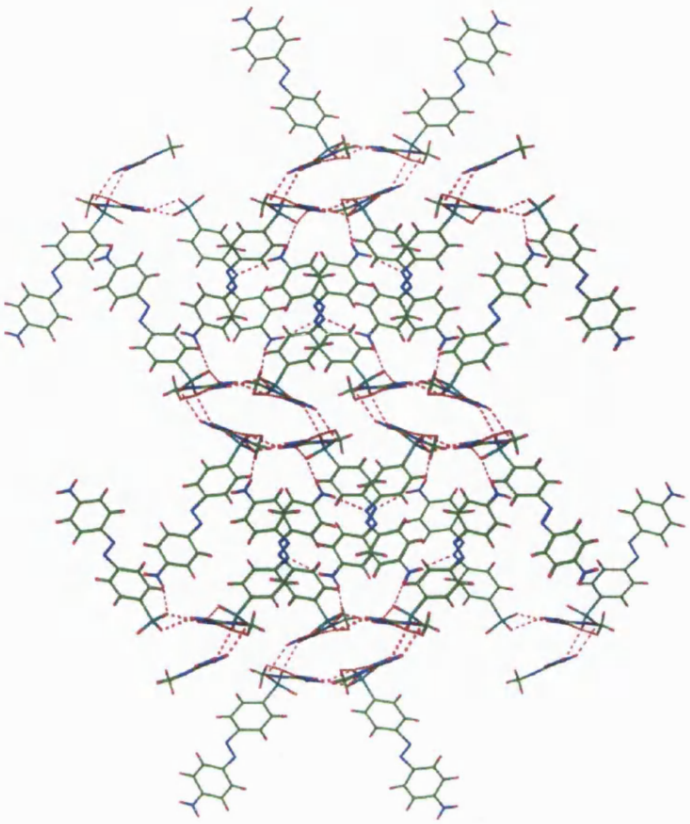

Figure 4.49; three-dimensional array formed in **36**

D–H···A	D···A /Å	H···A /Å	D–H···A / °	Symmetry operation generating D···A
N(1)–H(1A)···O(1)	2.946(2)	2.08	166	*x*, *y*, *z*
N(1)–H(1B)···O(5)	2.913(2)	2.05	165	*x*, *y*, *z*
N(2)–H(2A)···O(2)	2.934(2)	2.13	151	*x*, *y*, *z*
N(2)–H(2B)···O(6)	2.914(2)	2.08	159	*x*+1, *y*, *z*
N(3)–H(3)···O(4)	2.885(2)	2.01	175	*x*+1, *y*, *z*
N(6)–H(6A)···N(10)	3.157(2)	2.32	160	*x*+1, -*y*+$^3/_2$, *z*+$^3/_2$
N(6)–H(6B)···O(1)	3.031(2)	2.19	159	*x*+1, -*y*+$^3/_2$, *z*+½
N(7)–H(7A)···O(4)	3.196(2)	2.44	144	*x*, *y*, *z*
N(7)–H(7B)···O(3)	2.859(2)	2.01	163	-*x*-1, -*y*+1, -*z*
N(8)–H(8A)···O(5)	2.892(2)	2.18	138	*x*, *y*, *z*
N(8)–H(8B)···O(2)	2.922(2)	2.07	163	-*x*, -*y*+1, -*z*
N(9)–H(9)···O(1)	2.953(2)	2.13	155	-*x*-1, -*y*+1, -*z*
N(12)–H(12A)···O(6)	3.098(2)	2.26	160	*x*+1, -*y*+$^3/_2$, z-½
N(12)–H(12B)···N(4)	3.260(2)	2.39	169	*x*, -*y*+$^3/_2$, z-$^3/_2$
C(2)–H(2C)···O(5)	3.274(2)	2.72	124	-*x*-1, 1-*y*, -*z*
C(16)–H(16C)···O(6)	3.373(2)	2.52	134	*x*, *y*, *z*

Table 4.19; details of the hydrogen bonding in **36**

$[EtGu]_2[ABS][NBS]\cdot 2H_2O$: $[C(NH_2)_2(NHEt)]_2[O_3SC_6H_4N{=}NC_6H_4NH_2]\ [O_3SC_6H_4N{=}NC_6H_4NO_2]\cdot 2H_2O$ 37

Crystals were produced from the reaction of $(EtGu)_2SO_4$ and $Na[O_3SC_6H_4N{=}NC_6H_4NH_2]$ in water. However, a minor impurity of the anion salt was incorporated into the crystals. The single crystal X-ray data clearly showed that the NH_2 group of Na[ABS] was not present in one of the two anions in the asymmetric unit, due to the large electron density where the proton positions should have been. This electron density was modelled as a number of groups, including NO_2, which gave the best convergence. IR analysis also supports the presence of an NO_2 group, with peaks observed at 1306, 1317 and 1506cm^{-1}. Powder diffraction was not definitive in providing evidence that the single crystal is representative of the bulk material as a different powder diffraction pattern was observed compared to that from the simulated single crystal data. However, it is possible that the included water molecules are lost; leading to a different crystal lattice (also seen in $[MeGu][MO]\cdot H_2O$ **26** and $[MeGu][EO]\cdot H_2O$ **31**). Microanalysis also supports this loss of water (when calculated for the presence of an NO_2 group). Several crystals were consequently analysed, consistently producing the same cell data observed for **37**. It was therefore concluded that the impurity present is likely to be $Na[O_3SC_6H_4N{=}NC_6H_4NO_2]$ (Na[NBS]).

Asymmetric Unit

The asymmetric unit of **37** is shown in Figure 4.50 and consists of two $[EtGu]^+$ cations, one $[ABS]^-$ anion, one $[NBS]^-$ anion and two molecules of water.

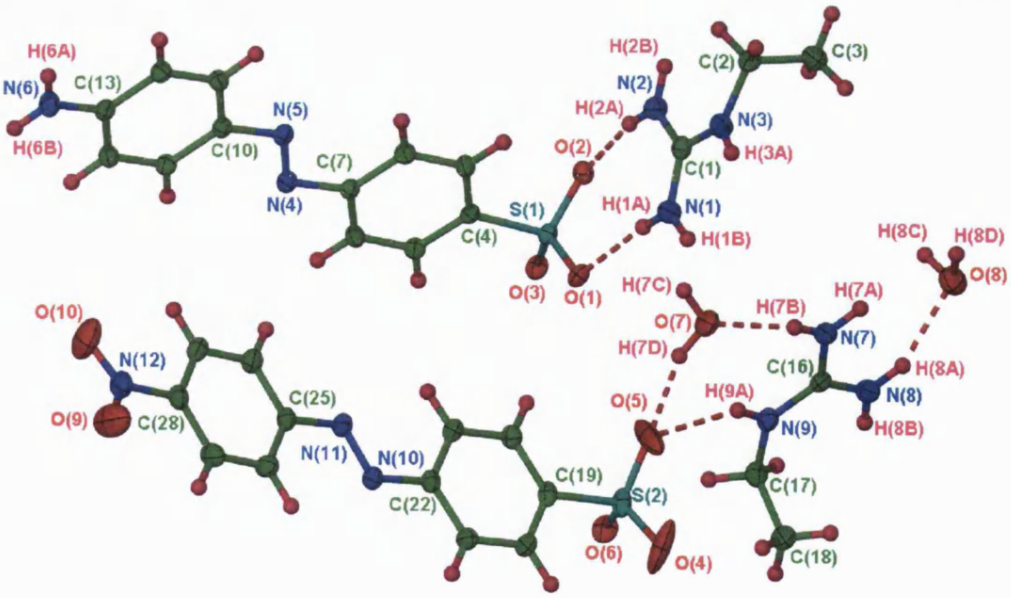

Figure 4.50; asymmetric unit in **37**. Ellipsoids are depicted at 50% probability level.

Extended Structure

The two cations and anions are involved in different packing motifs, therefore are primarily described separately as Unit 1 [the anion containing S(1) and cation containing C(1)], and Unit 2 [anion containing S(2), cation based on C(16), and both molecules of water].

Unit 1

The two unsubstituted faces of the cation form DD:AA hydrogen-bonding motifs, via the graph set $R_2^2(8)$, with the anion. This hydrogen bonding links the cations and anions into ribbons, where the cations are approximately co-planar with the oxygen atoms of the sulfonate of the anion. The hydrogen bond donor of the substituted face of the cation is not involved in the ribbon formation.

Unit 2

One N–H donor on each unsubstituted face of the cation forms a hydrogen bond to a neighbouring anion, whereas the other N–H donor forms a hydrogen bond to a water molecule. Hydrogen bonds are formed from both O–H donors of the O(8) water molecule to neighbouring sulfonate acceptors, and also by the O(7)–H(7D) donor of the O(7) water molecule to a neighbouring sulfonate acceptor. These hydrogen bonds link the cations, anions and water molecules into a complex ribbon, where the cations are approximately perpendicular to the oxygen atoms of the sulfonate group of the anions. There are no DD:AA hydrogen bonds formed via the unsubstituted faces of the cation. The hydrogen bond donor of the substituted face of the cation is not involved in the formation of this ribbon.

Units 1 and 2 combined

The two different ribbons formed based on Units 1 and 2 are shown in Figure 4.51.

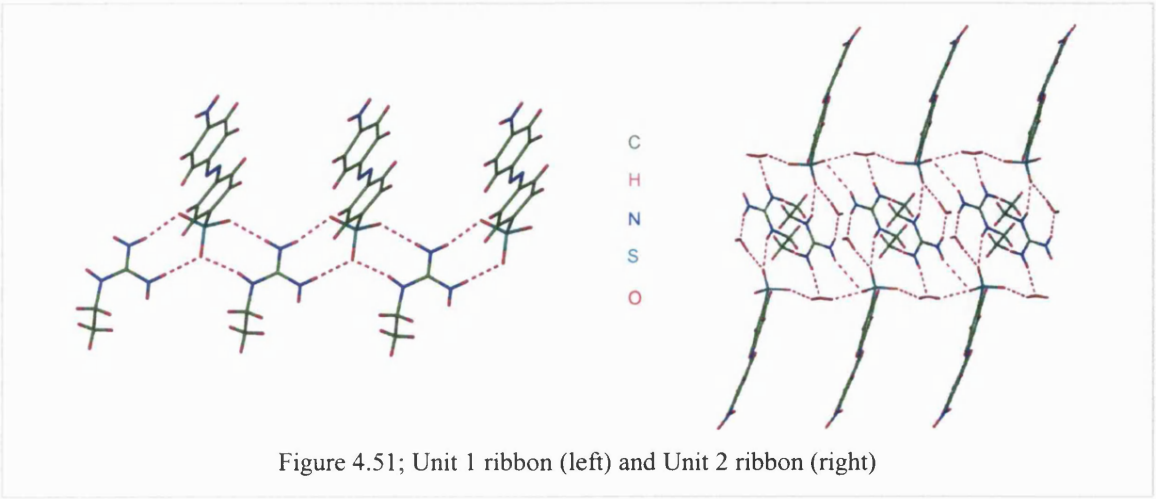

Figure 4.51; Unit 1 ribbon (left) and Unit 2 ribbon (right)

These two sets of ribbons are linked into a complex sheet, formed via hydrogen bonds involving the N–H groups of the substituted faces of the cations in each unit and oxygen atoms of the other unit [N(2)–H(2B)···O(6) and N(8)–H(8B)···O(3)]. There is also a hydrogen bond from the remaining O–H donor of the O(7) water molecule (of Unit 2) to a sulfonate acceptor group of Unit 1. The R groups of both units are directed to both sides of these sheets, as shown in Figure 4.52.

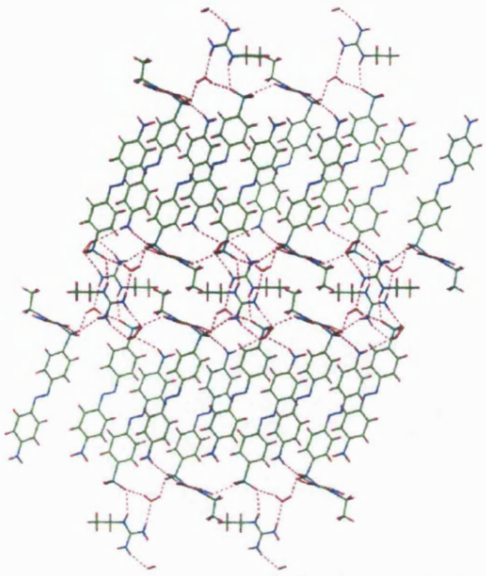

Figure 4.52; pseudo-bilayer formed in **37**

The NH_2 group of the $[ABS]^-$ anion is involved in hydrogen bond formation. One donor, N(6)–H(6B), forms a hydrogen bond to the $[ABS]^-$ oxygen atom O(1) of a neighbouring sheet, whereas the other donor N(6)–H(6A) interacts with the oxygen atom O(8) of the water molecule. These hydrogen bonds link the cations and anions into a three-dimensional hydrogen-bonded array, similar to the pillared brick motif observed when disulfonates are incorporated into GS arrays. There is also a possible hydrogen bond present between a donor of the water molecule [O(8)–H(8D)] and a N=O acceptor of the $[NBS]^-$ anion, however the N–H···O angle is substantially distorted from linearity. The hydrogen bond details are given in Table 4.20.

There are edge-to-face C–H···π interactions between the phenyl rings of the Unit 1 anions, as well as between the phenyl rings of the Unit 1 and Unit 2 anions. There is also a small twist of 7° between the least-squares planes of the phenyl rings in each anion.

D–H···A	D···A /Å	H···A /Å	D–H···A / °	Symmetry operation generating D···A
N(1)–H(1A)···O(1)	2.909(2)	2.04	169	*x*, *y*, *z*
N(1)–H(1B)···O(3)	2.966(2)	2.09	173	*x*, *y*+1, *z*
N(2)–H(2A)···O(2)	2.927(2)	2.06	169	*x*, *y*, *z*
N(2)–H(2B)···O(6)	2.967(2)	2.27	136	*x*, -*y*+½, *z*-½
N(3)–H(3A)···O(2)	2.887(2)	2.02	168	*x*, *y*+1, *z*
N(6)–H(6A)···O(8)$_w$	3.224(2)	2.39	158	*x*-1, -*y*+½, *z*-½
N(6)–H(6B)···O(1)	3.143(2)	2.29	163	-*x*, *y*-½, -*z*+½
N(7)–H(7A)···O(4)	3.528(3)	2.68	163	1-*x*, 1-*y*, 1-*z*
N(7)–H(7B)···O(7)$_w$	2.886(2)	2.03	164	*x*, *y*, *z*
N(8)–H(8A)···O(8)$_w$	2.866(2)	2.04	156	*x*, *y*, *z*
N(8)–H(8B)···O(3)	2.892(2)	2.07	155	-*x*+1, -*y*, -*z*+1
N(9)–H(9A)···O(5)	2.974(2)	2.18	150	*x*, *y*, *z*
O(7)–H(7C)···O(1)	2.927(2)	2.24	134	*x*, *y*, *z*
O(7)–H(7D)···O(5)	2.720(2)	1.87	159	*x*, *y*, *z*
O(8)–H(8C)···O(6)	3.042(2)	2.21	157	-*x*+1, -*y*, -*z*+1
O(8)–H(8D)···O(4)	2.889(3)	2.08	151	-*x*+1, -*y*+1, -*z*+1
O(8)–H(8D)···O(9)	2.894(3)	2.51	107	1+*x*, *y*, *z*

Table 4.20; details of the hydrogen bonding in **37**

[DiMeGu][ABS] : $[C(NH_2)_2(NMe_2)][O_3SC_6H_4N{=}NC_6H_4NH_2]$ 38a

The reaction of $(DiMeGu)_2SO_4$ with Na[ABS] produced crystals from solutions of methanol (**38a**) and water (**38b**), with different cell data respectively. Both compounds crystallise in orthorhombic crystal systems, however the cell volume of **38a** is twice that of **38b** a consequence of doubling along the one axis (see Table 4.3, section 4.1). However, the packing and hydrogen-bonding motifs are similar in both compounds; therefore only one structure (**38a**) is described in detail. The powder diffraction analysis of **38a** and **38b** were similar and also matched the simulated XRD traces generated from the single crystal data for both compounds.

Asymmetric Unit

The asymmetric unit of **38a** is shown in Figure 4.53 and consists of one $[DiMeGu]^+$ cation and one $[ABS]^-$ anion.

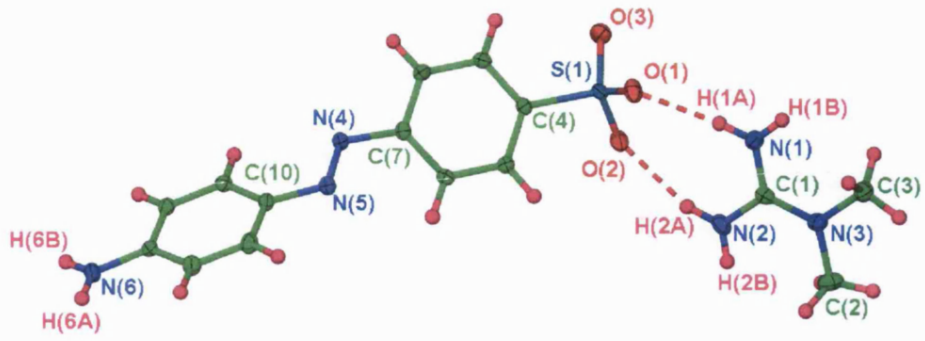

Figure 4.53; asymmetric unit in **38a**. Ellipsoids are depicted at 50% probability level.

Extended Structure

The unsubstituted face of the cation forms DD:AA hydrogen bonds with the anion via the $R_2^2(8)$ motif. The two substituted faces each have one N–H donor and form hydrogen bonds with neighbouring cation-anion pairs forming ribbons via the motif $R_4^3(10)$ (Figure 4.54). All of the donors and acceptors are employed in ribbon formation, with details of the hydrogen bond lengths and angles given in Table 4.21. The sulfonate R groups are directed to one side of each ribbon, which are aligned in the same plane forming a sheet, with C–H···O hydrogen bonds from the Me substituents of the cation of one ribbon to an oxygen atom of a neighbouring ribbon. However, these interactions are weak, as the hydrogen bond lengths are long (see section 1.1 of Chapter 1) [(C(3)–H(3B)···O(3), with C···O and H···O distances of 3.879Å and 2.94Å respectively with a C–H···O angle of 160°; and C(2)–H(2D)···O(3) with C···O and H···O distances of 4.124Å and 3.27Å with a C–H···O angle of 147°].

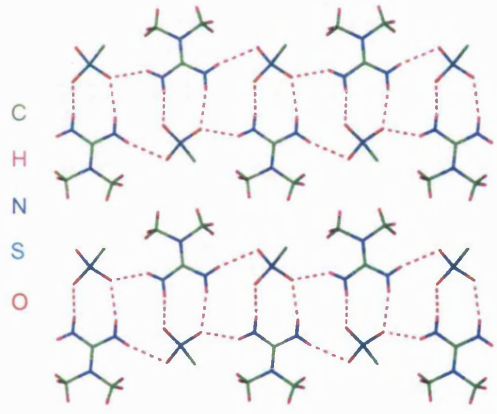

Figure 4.54; ribbons formed in **38a**
(*most of the anion is removed for clarity*)

The R groups of the sulfonates interdigitate forming bilayers in the extended structure. The NH_2 groups on the opposite end of the anion are also involved in hydrogen bonding. One N–H donor [N(6)–H(6A)] forms a hydrogen bond to O(2) of the anion in the neighbouring plane, linking the two sheets of the bilayer. The other N–H donor [N(6)–H(6B)] forms a hydrogen bond to the azo group of another anion crosslinking the anions of the bilayer (Figure 4.55). These bilayers stack in the extended structure, without further interactions between them.

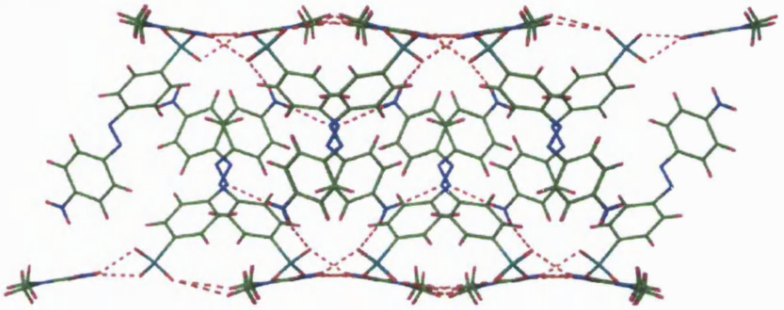

Figure 4.55; bilayer formation in **38a**

There are also edge-to-face C–H···π interactions between the phenyl rings of neighbouring anions, with a twist of 48° in the anion between the least-squares planes of the phenyl rings.

D–H···A	D···A /Å	H···A /Å	D–H···A / °	Symmetry operation generating D···A
N(1)–H(1A)···O(1)	2.938(2)	2.12	155	*x*, *y*, *z*
N(1)–H(1B)···O(2)	2.834(2)	2.06	146	$^{3}/_{2}$-*x*, ½+*y*, *z*
N(2)–H(2A)···O(2)	3.052(2)	2.20	163	*x*, *y*, *z*
N(2)–H(2B)···O(3)	3.158(2)	2.29	168	$^{3}/_{2}$-*x*, ½-*y*, *z*
N(6)–H(6A)···O(1)	3.072(2)	2.28	149	*x*-$^{1}/_{2}$, *y*-1, ½-*z*
N(6)–H(6B)···N(4)	3.068(2)	2.20	167	-*x*, *y*-½, ½-*z*

Table 4.21; details of the hydrogen bonding in **38a**

[DiMeGu][ABS] : $[C(NH_2)_2(NMe_2)][O_3SC_6H_4N{=}NC_6H_4NH_2]$ 38b

As previously mentioned, the extended structure in **38b** is similar to that in **38a**, therefore is not discussed. The asymmetric unit in **38b** is similar to that in **38a**, and is shown in Figure 4.56. The details of the hydrogen bonding are given in Table 4.22.

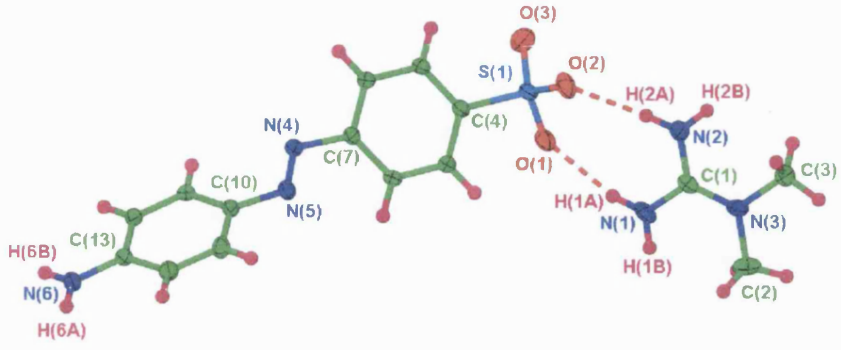

Figure 4.56; asymmetric unit in **38b**. Ellipsoids are depicted at 50% probability level.

D–H···A	D···A /Å	H···A /Å	D–H···A / °	Symmetry operation generating D···A
N(1)–H(1A)···O(1)	2.987(2)	2.12	166	x, y, z
N(1)–H(1B)···O(3)	3.327(3)	2.45	172	$-x+^{3}/_{2}, y, z-½$
N(2)–H(2A)···O(2)	2.974(2)	2.16	153	x, y, z
N(2)–H(2B)···O(1)	2.835(2)	2.07	145	$-x+^{3}/_{2}, y, z+½$
N(6)–H(6A)···O(2)	3.051(2)	2.24	152	$x+^{1}/_{2}, -y+2, z-1$
N(6)–H(6B)···N(4)	3.073(2)	2.21	166	$-x+3, -y+2, z-½$

Table 4.22; details of hydrogen bonding in **38b**

HABS : $O_3SC_6H_4NH{=}NC_6H_4NH_2$ 39

Sodium 4-aminoazobenzene-4'-sulfonate and the unsubstituted guanidinium salt were each dissolved in water and mixed together. Dilute HCl was then added drop-wise in an attempt to crystallise compound **39**, analogous to the approach used in synthesising compounds HMO **29** and HEO·H_2O **34**. Unfortunately, this compound could not be isolated as a crystalline powder or single crystals, as an emulsion was formed instantly on addition of $HCl_{(aq)}$.

4.4.1 The structural effects of alkyl substitution in guanidinium ions when crystallised with 4-aminoazobenzene-4'-sulfonate

The substitution of one N–H donor by a NMe group or NEt group does not have a profound effect on the extended structure. The compounds [Gu][ABS] **35**, [MeGu][ABS] **36** and $[EtGu]_2[ABS][NBS]\cdot 2H_2O$ **37** have two cations and anions in the asymmetric unit and form a *pseudo*-pillared brick architecture whereas [DiMeGu][ABS] **38a/b** has one cation and anion in the asymmetric unit and forms independent bilayers.

In [Gu][ABS] **35** the cations and anions form hydrogen bonds leading to pairs of ribbons that are further linked into complex sheets, with the sulfonate R groups directed to both sides of the sheets. A three-dimensional array similar to the pillared brick architecture is observed due to the amine donors of the anion forming hydrogen bonds to the sulfonate oxygen atoms of neighbouring sheets. However, the N–H donors of the anion containing S(2) are not involved in forming hydrogen bonds, and is the only example where this is observed.

In [MeGu][ABS] **36,** the cations and anions form hydrogen bonds leading to a cylindrical array, and this is the only compound of the dye series that forms this type of architecture. These one-dimensional arrays align into the same plane, though are not hydrogen-bonded into a sheet. The R groups are directed to both sides of this plane, and interdigitate in the extended structure. The NH_2 groups of both anions are involved in hydrogen bonding, with one N–H donor of each anion forming hydrogen bonds to the sulfonate oxygen atoms of the neighbouring plane. The other N–H donor of each anion forms hydrogen bonds to the azo group of a neighbouring anion cross-linking the interdigitating anions. This leads to a three-dimensional *pseudo*-pillared brick network.

In $[EtGu]_2[ABS][NBS]\cdot 2H_2O$ **37** two different anions are incorporated into the structure (ABS^- and NBS^-), as well as molecules of water from the solvent. Two different ribbons are formed, which are linked together into a sheet. One of the donors of the NH_2 group of the $[ABS]^-$ anion forms hydrogen bonds to an oxygen atom of the $[ABS]^-$ anion of a neighbouring sheet. The other N–H donor forms a hydrogen bond to the oxygen acceptor of the O(8) water molecule. These hydrogen bonds link neighbouring sheets, therefore a *pseudo*-pillared brick architecture is observed.

Structures **38a** and **38b** are polymorphs, and lead to similar hydrogen-bonded arrays. The cations and anions are hydrogen-bonded into ribbons, via a $R_2^2(8)$ and $R_4^3(10)$ motifs, which are further linked into flat sheets via C–H···O hydrogen bonds. This is in contrast to the MO analogue [DiMeGu][MO] **33** where the ribbons are formed via a $R_2^1(6)$ and $R_4^4(12)$ motif. The R groups are directed to one side of each sheet, and interdigitate with those of a neighbouring sheet leading to the formation of bilayers. The bilayers are further linked via one N–H donor of the amide forming hydrogen bonds to the sulfonate oxygen atoms of the neighbouring sheet. The anions are also cross-linked through the other N–H donor of the amide forming N–H···N hydrogen bonds to the azo group of a neighbouring anion.

The structures of these compounds are very different to those observed in the methyl and ethyl orange series due to the presence of the NH_2 group in $[ABS]^-$ anion and the hydrogen bonding these N–H donors are involved in. The structure of $[Gu][1\text{-}(NH_2)C_6H_4SO_3\text{-}3]$[9] has been reported by Ward *et al* and also shows N–H···O hydrogen bonding from the NH_2 group in the anion to the sulfonate group of a neighbouring sheet. It is also notable that in compounds **35-37** there are unsubstituted faces of the cations that do not form the expected DD:AA hydrogen bond motifs with the sulfonates, via the $R_2^2(8)$ graph set, but instead form single hydrogen bonds with the sulfonates, or with water molecules incorporated into the lattice (as in **37**).

4.4.2 The effects of alkyl substitution in guanidinium ions on bond and hydrogen bond parameters when crystallised with 4-aminoazobenzene-4'-sulfonate

The DD:AA hydrogen bond distances in the structures of **35**, **36**, **37**, **38a** and **38b** are affected differently as the degree of substitution on the cation is increased. The hydrogen bond distances (N···O) range from 2.871(2) – 3.032(2)Å in **35**, 2.859(2)Å – 3.196(2)Å in **36**, 2.887(2)Å – 2.963(2)Å in **37**, 2.938(2) – 3.052(2)Å in **38a** and 2.974(2) – 2.987(2)Å in **38b**. The mean average hydrogen bond distances in **35**, **36**, **37**, **38a** and **38b** are calculates as 2.923(2)Å, 2.947(2)Å, 2.922(2)Å, 2.995(2)Å and 2.976(2)Å respectively. This suggests that the strength of the DD:AA hydrogen bonding is affected by the structure formed, and the number of DD:AA hydrogen bonds present in the structures. In **35**, only four out of six possible DD:AA hydrogen-bonding motifs are observed. In **36**, all of the possible DD:AA hydrogen-bonding motifs possible are observed, and the hydrogen bonds are longer than those in **35**. In **37** only half of the possible DD:AA hydrogen bonds are observed, and they are shorter than those in **35**. In **38a/b** only one DD:AA motif is possible, and is observed. The hydrogen bonds in **38a** are longer than those in **35**. The range of hydrogen bond lengths in **38a** are different to those observed in **38b**; in **38b** two hydrogen bonds are similar, and fall within the range of hydrogen bonding seen in **35**.

The C–N and S–O bond lengths of the anion are similar in all structures **35-38a/b** revealing that these bond lengths are not affected as the cation is substituted. This consistency is also seen in the N–C–N and O–S–O bond angles.

All of the structures **35-38a/b** show hydrogen bonds from a portion of the anion NH_2 donor groups to the oxygen acceptor groups of an anion in a neighbouring sheet. However, only structures **36** and **38a/b** show hydrogen bonding from these NH_2 donors to the azo group of a neighbouring inter-digitated anion. In **36** both N(4)=N(5) and N(10)=N(11) are involved in hydrogen bonding with an N–H donor; the N(4)=N(5) bond is the shortest N=N bond in the $[ABS]^-$ structures. All other N=N bonds are similar, a shown in Table 4.23. The twist in the anion does not seem to have a specific effect on the N=N bond length.

	35	36	37	38a	38b
N(4)=N(5) (Å)	1.252(2)	1.212(8)	1.263(2) [ABS]	1.269(2)	1.261(2)
N(10)=N(11) (Å)	1.257(2)	1.279(7)	1.255(2) [NBS]		
Anion twist in U1°	10	32	7 [ABS]	48	50
Anion twist in U2°	10	28	7 [NBS]		

Table 4.23; variation of bond length N=N and the twist between phenyl planes in the anions of structures **35**, **36**, **37**, **38a** and **38b**.

As seen in the methyl orange and ethyl orange series, the twist between the least-squares planes of the phenyl rings in the anion affects the bond lengths C–N(a) and C–N(b) (Figure 4.57). When there is a large twist between the phenyl rings, as seen in **38a**/**b**, the bond C–N(b) is shorter than C–N(b) (Table 4.24), as the N=N bond is in the same plane as the $-NH_2$ functionalised phenyl ring, but not in the same plane as the $-SO_3$ functionalised phenyl ring. This leads to delocalisation through the amine, the azo group and the phenyl rings between them reducing the length of the C–N(a) bond. When the phenyl ring are almost co-planar, there is delocalisation through the whole backbone of the anion leading to the bonds (a) and (b) being similar, as seen in **35-37**.

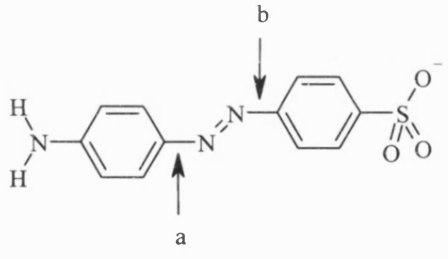

Figure 4.57; C–N bond lengths a and b

	35	36	37	38a	38b
Bond lengths (Å)					
C–N(a)	1.417(2)	1.479(9)	1.415(2) [ABS]	1.409(2)	1.409(2)
	1.414(2)	1.427(8)	1.430(2) [NO]		
C–N(b)	1.431(2)	1.52(1)	1.427(2) [ABS]	1.430(2)	1.428(2)
	1.426(2)	1.438(8)	1.436(2) [NO]		
Anion twist in U1°	10	32	7 [ABS]	48	50
Anion twist in U2°	10	28	7 [NO]		

Table 4.24; bond lengths C–N a and b in structures **35-38a**/**b**.

4.4.3 HCl and NH_3 reactions of ABS-guanidinium sulfonates in the solid state

When single crystals of [Gu][ABS] **35**, [MeGu][ABS] **36**, $[EtGu]_2[ABS][NBS]\cdot 2H_2O$ **37** and [DiMeGu][ABS] **38a/b** are exposed to HCl gas, a colour change is observed from light orange to dark orange. This colour change is not as distinct as those observed in the methyl orange and ethyl orange analogues, however the single crystals crumbled on exposure to HCl. The single crystals **35-38** were ground into a crystalline powder and exposed to HCl and NH_3, and studied using X-ray powder diffraction with the resultant plots shown in Figure 4.58.

The powder diffraction results are consistent with those observed in the methyl orange series, where the peaks observed in **35** are lost on exposure to HCl in the formation of **35a**. The peaks seen in **35** are subsequently observed on exposure of **35a** to NH_3, along with the presence of peaks confirming the formation of NH_4Cl and the loss of peaks observed in **35a**. This interconversion is also reversible. Unfortunately, neither single crystals nor a microcrystalline powder of a protonated ABS complex, analogous to HMO and HEO, could be obtained.

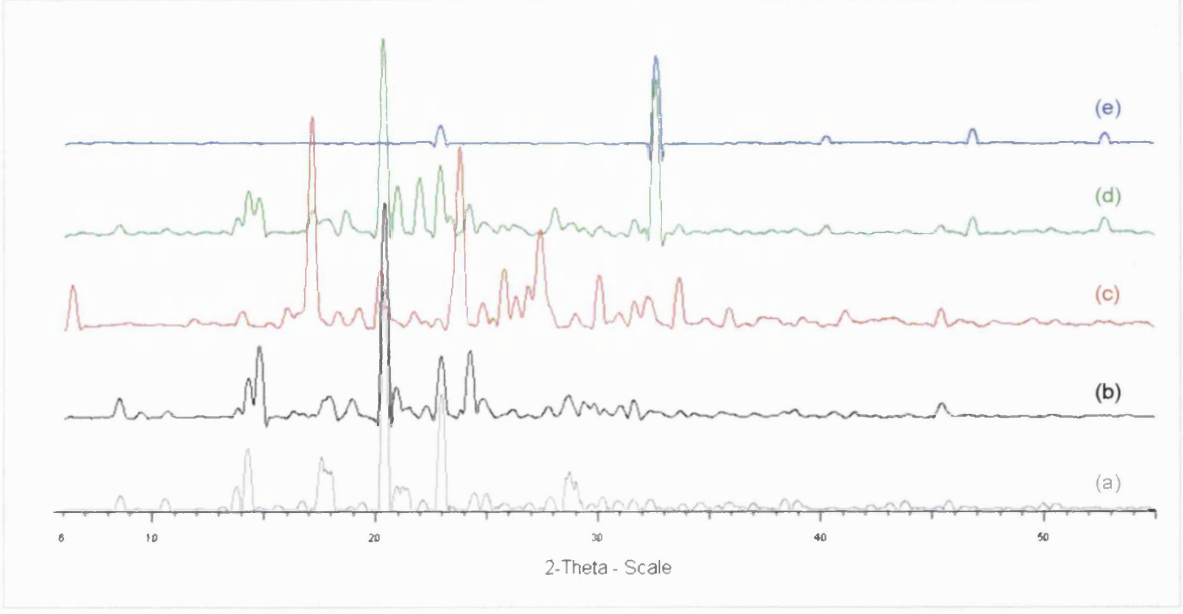

Figure 4.58; the powder diffraction studies on **35** exposed to cycles of HCl and NH_3

(λ=1.5418Å [CuK_α])

(e) NH_4Cl
(d) **35** plus $HCl_{(g)}$ then $NH_{3(g)}$
(c) **35** plus $HCl_{(g)}$ **(35a)**
(b) $[C(NH_2)_3][O_3SC_6H_4N{=}NC_6H_4NEt_2]$ **35**
(a) simulated powder diffraction pattern from single crystal data of **35**

These findings are confirmed from the IR and diffuse reflectance UV-visible spectroscopies. In the former, the formation of **35a** leads to a broadening of the peak at 1500cm^{-1} and new peaks, though weak, are observed in this region. Exposure of **35a** to NH_3 results in the loss of these new absorptions, the reformation of the peaks observed in **35** and the peak at 1500cm^{-1} returning to a sharp peak. Once again a broadening of the peak at 1400cm^{-1} is observed in the sample of **35a** exposed to NH_3, whereas this peak is sharp in **35**, and can be assigned to the presence of NH_4Cl.

Diffuse reflectance spectra for **35** as well as **35a** before and after exposure to NH_3 are shown in Figure 4.60. These spectra are also consistent with reformation of **35** following reaction with HCl and NH_3.

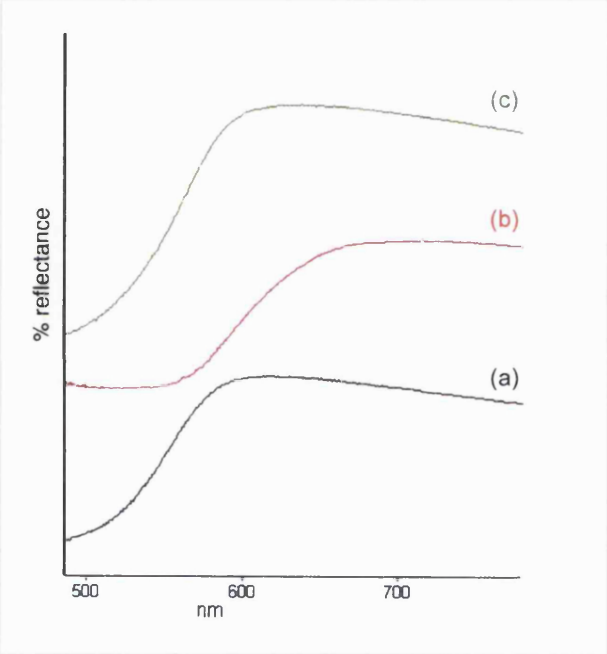

Figure 4.59; the diffuse reflectance UV-visible spectra for;

(c) **35** plus HCl then NH_3
(b) **35** plus HCl
(a) **35**

The compounds [MeGu][ABS] **36**, $[EtGu]_2[ABS][NBS]\cdot 2H_2O$ **37** and [DiMeGu][ABS] **38a/b** revealed similar observations where formation of HCl adducts were also observed when exposed to HCl gas. These adducts reverted back to **36**, **37** and **38a/b** respectively on reaction with NH_3 with concomitant formation of NH_4Cl.

4.5 The overall effects of alkyl substitution in guanidinium ions when crystallised with methyl orange, ethyl orange and 4-aminoazobenzene-4'-sulfonate

The extended structures in the methyl orange series are not significantly affected as the N–H groups of the cation are substituted. Either bilayers or *pseudo*-bilayers are observed, with sheets formed in [Gu][MO] **25** (hexagonal) [EtGu][MO] **27** and [DiMeGu][MO] **28** and tapes observed in [MeGu][MO]·MeOH **26**. In all cases, all of the unsubstituted faces of the cation form $R_2^2(8)$ motifs via DD:AA hydrogen-bonds with the sulfonate groups of the anions.

However, there is a definite effect on the extended structures in the ethyl orange system by the substitution in the cation as well as the NEt_2 group in the $[EO]^-$ anion. In [Gu][EO] **30** and [EtGu][EO] **32**, hexagonal sheets are formed (with a C–H···O hydrogen bond in the latter, in place of the missing N–H···O hydrogen bond) and single layers are observed. It was initially assumed that the NEt_2 group would be large enough to force a single layer arrangement with sulfonate R groups directed to both sides of the sheet. However, in [MeGu][EO]·MeOH **31** individual tapes are aligned into pseudo-bilayers, although this structure also incorporates solvent molecules, whereas **30** and **32** do not. [DiMeGu][EO] **33** forms independent ribbons, therefore cannot be used to further investigate the effects of the NEt_2 group in the anion. As with the methyl orange series, all of the unsubstituted cation faces form DD:AA hydrogen bonding motifs via the $R_2^2(8)$ motif.

The extended structures within the $[ABS]^-$ series are also not significantly affected by cation substitution, as similarly observed in the methyl orange series. Either a *pseudo*-pillared brick architecture (which can also be seen as an extended *pseudo*-bilayer array) or bilayers are formed. As also seen in the methyl orange series, sheets are observed in compounds [Gu][ABS] **35**, $[EtGu]_2[ABS][NBS]\cdot 2H_2O$ **37** and [DiMeGu][ABS] **38** (ABS analogues of **25**, **27** and **28**), whereas in [MeGu][ABS] **36** a cylindrical array is formed. However, in contrast to the methyl orange series, not all of the unsubstituted faces of the cation are involved in DD:AA hydrogen bonds and no hexagonal sheets are observed. In **35**, the N–H donors of two faces of one of the cations in the asymmetric unit forms four single hydrogen bonds. In **37**, two donors of the unsubstituted face of one cation form a $R_3^2(8)$ motif with a molecule of water, and the other unsubstituted face of the same cation forms two single

hydrogen bonds. It is also notable that the animo groups present in the $[ABS]^-$ anion are involved in hydrogen bond formation, resulting in more complex three-dimensional hydrogen-bonding patterns, relative to those observed in the methyl orange or ethyl orange series.

A bilayer array is expected when the width of ion centre-to-centre distance of the R group is smaller than 4.75Å (as discussed in Chapter 1)[7]. The width of the R groups in $[MO]^-$ and $[ABS]^-$ is the distance between opposite hydrogen atoms of the phenyl rings, and is measured as 4.06Å for both $[MO]^-$ and $[ABS]^-$ anions. This is significantly less than 4.75Å confirming that bilayer arrays are favoured. Therefore the differing NR_2 groups in $[MO]^-$ and $[ABS]^-$ anions are not significant enough to cause a different arrangement of the R groups. However, the widest group in $[EO]^-$ is the NEt_2 group, with a maximum possible distance of 5.83Å between the most extreme hydrogen atoms of this functionality. This suggests that bilayers are no longer likely and that single layers should be expected. As mentioned earlier, single layers are indeed observed in [Gu][EO] **30** and [Et][Gu] **32**, however bilayers are formed in [MeGu][EO]·MeOH **31**. This indicates that in the ethyl orange series, the width of the R group, the substitution of the cation and possibly the inclusion of solvent are all factors in determining whether single layers or bilayers are observed.

These azo dye compounds also react differently when the crystalline powders are exposed to cycles of HCl and ammonia gas. The methyl orange compounds **25-28** and those of the $[ABS]^-$ series **35-38** all form a [guanidinium salt][zwitterion] co-crystal after exposure to $HCl_{(g)}$, suggesting the GS layers of the original crystalline compounds (before exposure) remain intact. However, in the ethyl orange compounds **30-33** it appears that the GS layers are disrupted as the formation of the individual zwitterion and guanidinium salt are observed, along with a minor product, possibly the [guanidinium salt][zwitterion] co-crystal. These different reactivities cannot be explained by analysis of the extended structure formed, as [MeGu][MO]·MeOH **26** and [MeGu][EO]·MeOH **31** both form the same bilayer array, though they react differently on exposure to $HCl_{(g)}$. Thus it seems possible that the small difference in the anion (NMe_2, NEt_2 and NH_2 groups in $[MO]^-$, $[EO]^-$ and $[ABS]^-$ respectively) is the primary contributor to these observations. However, the new compounds formed when the original $[MO]^-$, $[EO]^-$ and $[ABS]^-$ compounds are exposed to HCl, are all

converted back to the original species when exposed to NH_3, along with the formation of NH_4Cl.

4.5.1 Future Work

It has been demonstrated that the $[MO]^-$ and $[ABS]^-$ anions can undergo a chemical reaction whilst retaining the hydrogen-bonded array that incorporates a guanidinium or substituted guanidinium cation. These results are only observed in the powdered samples as the single crystals crumble on continued exposure to $HCl_{(g)}$. It could be anticipated that larger functional groups on the anion, for example $N(CH_2CH_2CH_3)_2$, could create more space in the crystal structure to allow the inclusion of H^+ and Cl^- ions while maintaining the crystalline array. Also, the use of a disulfonated azo dye would be expected to form a pillared brick array, where pores may be inherent to the structure, allowing the movement of ions through them.

4.6 Experimental

Methyl orange, $Na[O_3SC_6H_4N{=}NC_6H_4NMe_2]$ (85%) and ethyl orange, $Na[O_3SC_6H_4N{=}NC_6H_4NEt_2]$ (90%) were purchased from Aldrich Chemical Co. Sodium 4-aminoazobenzene-4'-sulfonate, $Na[O_3SC_6H_4N{=}NC_6H_4NH_2]$ (90%) was purchased from Lancaster. The water and methanol solutions of $Na[O_3SC_6H_4N{=}NC_6H_4NMe_2]$, $Na[O_3SC_6H_4N{=}NC_6H_4NEt_2]$ and $Na[O_3SC_6H_4N{=}NC_6H_4NH_2]$ were filtered prior to use to remove insoluble impurities. Microanalysis (C, H and N) was carried out by Mr. Alan Carver (University of Bath Technical Support). It is notable that some of the microanalysis results repeatedly showed lower than anticipated percentages of carbon, hydrogen and nitrogen. This may be the result of the presence of amorphous impurities or crystalline salts, or be a consequence of incomplete combustion. Solid-state Infrared spectra were recorded on a Nicolet Nexus FT-IR spectrometer by using KBr disks. Solid-state UV-Visible spectra were recorded on a Perkin-Elmer Lambda 35 UV/VIS Spectrometer.

Synthesis of [Gu][MO] 25

A solution of $[C(NH_2)_3]Cl$ (0.030g, 0.31 mmol) in water ($1cm^3$) was added to a solution of $Na[O_3SC_6H_4N{=}NC_6H_4NMe_2]$ (0.103g, 0.27mmol) in water ($10cm^3$) and allowed to slowly evaporate, yielding a powder after two days. Recrystallisation from water gave small orange crystals of $[C(NH_2)_3][O_3SC_6H_4N{=}NC_6H_4NMe_2]$ **25**. Calc for $C_{15}H_{20}N_6O_3S$: C, 49.4; H, 5.53; N, 23.1. Found: C, 49.2; H, 5.23; N, 22.2%.

Synthesis of [McGu][MO]·MeOH 26

A solution of $[C(NH_2)_2(NHMe)]Cl$ (0.034g, 0.31mmol) in methanol ($1cm^3$) was added to a solution of $Na[O_3SC_6H_4N{=}NC_6H_4NMe_2]$ (0.103g, 0.27 mmol) in methanol ($10cm^3$) and allowed to slowly evaporate. Small orange crystals of $[C(NH_2)_2(NHMe)][O_3SC_6H_4N{=}NC_6H_4NMe_2]\cdot MeOH$ **26** were collected after approximately two weeks. Calc for $C_{16}H_{22}N_6O_3S$ (no solvent molecule): C, 50.8; H, 5.86; N, 22.2. Found: C, 50.5; H, 5.86; N, 22.2%.

Synthesis of [EtGu][MO] 27

A solution of $[C(NH_2)_2(NHEt)]_2SO_4$ (0.043g, 0.16mmol) in methanol ($5cm^3$) was added to a solution of $Na[O_3SC_6H_4N{=}NC_6H_4NMe_2]$ (0.103g, 0.27 mmol) in methanol ($10cm^3$) and allowed to slowly evaporate. Small orange crystals of $[C(NH_2)_2(NHEt)][O_3SC_6H_4N{=}NC_6H_4NMe_2]$ **27** were collected after approximately two weeks. Calc for $C_{17}H_{24}N_6O_3S$: C, 52.0; H, 6.16; N, 21.4. Found: C, 51.3; H, 6.06; N, 21.4%.

Synthesis of [DiMeGu][MO] 28

A solution of $[C(NH_2)_2(NMe_2)]_2SO_4$ (0.043g, 0.16mmol) in methanol ($5cm^3$) was added to a solution of $Na[O_3SC_6H_4N{=}NC_6H_4NMe_2]$ (0.103g, 0.27 mmol) in methanol ($10cm^3$) and allowed to slowly evaporate. Small orange crystals of $[C(NH_2)_2(NMe)][O_3SC_6H_4N{=}NC_6H_4NMe_2]$ **28** were collected after approximately two weeks. Calc for $C_{17}H_{24}N_6O_3S$: C, 52.0; H, 6.16; N, 21.4. Found: C, 51.9 H, 6.12; N, 21.4%.

Synthesis of HMO 29

Hydrochloric acid (32%, $0.5cm^3$) was added to a solution of $Na[O_3SC_6H_4N{=}NC_6H_4NMe_2]$ (0.100g, 0.36 mmol) in methanol ($10cm^3$). Small red crystals of $O_3SC_6H_4NH{=}NC_6H_4NMe_2$ **29** formed instantly. Calc for $C_{14}H_{15}N_3O_3S$: C, 55.1; H, 4.95; N, 13.8. Found: C, 54.5; H, 4.99; N, 13.8%.

Synthesis of [Gu][EO] 30

A solution of $[C(NH_2)_3]Cl$ (0.028g, 0.29mmol) in methanol (1cm^3) was added to a solution of $Na[O_3SC_6H_4N{=}NC_6H_4NEt_2]$ (0.103g, 0.26mmol) in methanol (10cm^3) and the mixture allowed to slowly evaporate. Small orange crystals of $[C(NH_2)_3][O_3SC_6H_4N{=}NC_6H_4NEt_2]$ **30** were collected after approximately one week. Calc for $C_{17}H_{24}N_6O_3S$: C, 52.0; H, 6.13; N, 21.4. Found: C, 51.5; H, 6.04; N, 21.1 %.

Synthesis of [MeGu][EO]·MeOH 31

A solution of $[C(NH_2)_2(NHMe)]Cl$ (0.032g, 0.29mmol) in methanol (1cm^3) was added to a solution of $Na[O_3SC_6H_4N{=}NC_6H_4NEt_2]$ (0.103g, 0.26mmol) in methanol (10cm^3) and allowed to slowly evaporate. Small orange crystals of $[C(NH_2)_2(NHMe)][O_3SC_6H_4N{=}NC_6H_4NEt_2]$·MeOH **31** were collected after approximately one week. Calc for $C_{18}H_{26}N_6O_3S$ (no solvent molecules): C, 50.0; H, 6.89; N, 19.2. Found: C, 50.0; H, 6.16; N, 19.7%.

Synthesis of [EtGu][EO] 32

A solution of $[C(NH_2)_2(NHEt)]_2SO_4$ (0.039g, 0.14mmol) in methanol (5cm^3) was added to a solution of $Na[O_3SC_6H_4N{=}NC_6H_4NEt_2]$ (0.103g, 0.26mmol) in methanol (10cm^3) and the mixture allowed to slowly evaporate. Small orange crystals of $[C(NH_2)_2(NHEt)][O_3SC_6H_4N{=}NC_6H_4NEt_2]$ **32** were collected after approximately one week. Calc for $C_{19}H_{28}N_6O_3S$: C, 54.3; H, 6.71; N, 20.0. Found: C, 53.0; H, 6.77; N, 19.3%.

Synthesis of [DiMeGu][EO] 33

A solution of $[C(NH_2)_2(NHMe_2)]_2SO_4$ (0.039g, 0.14mmol) in methanol (5cm^3) was added to a solution of $Na[O_3SC_6H_4N{=}NC_6H_4NEt_2]$ (0.103g, 0.26mmol) in methanol (10cm^3) and and the mixture allowed to slowly evaporate. Small orange crystals of $[C(NH_2)_2(NHMe_2)][O_3SC_6H_4N{=}NC_6H_4NEt_2]$ **33** were collected after approximately one week. Calc for $C_{19}H_{28}N_6O_3S$: C, 54.3; H, 6.71; N, 20.0. Found: C, 52.3; H, 6.62; N, 19.8%.

Synthesis of HEO·$^3/_4H_2O$ 34

Hydrochloric acid (32%, 0.5cm^3) was added to a solution of $Na[O_3SC_6H_4N{=}NC_6H_4NEt_2]$ (0.100g, 0.25mmol) in methanol (10cm^3). Small red crystals of $O_3SC_6H_4NH{=}NC_6H_4NEt_2{\cdot}{}^3/_4H_2O$ **34** formed after one day. A crystal with the same cell parameters was also formed from water. Calc for $C_{16}H_{20.5}N_3O_{3.75}S$: C, 55.3; H, 5.96; N, 12.1.

Unsubstituted guanidinium and substituted guanidinium derivatives

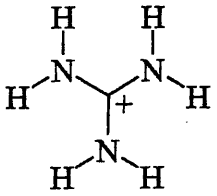

Guanidinium
$[Gu]^+$

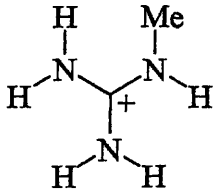

Methylguanidinium
$[MeGu]^+$

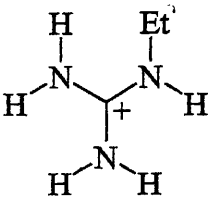

Ethylguanidinium
$[EtGu]^+$

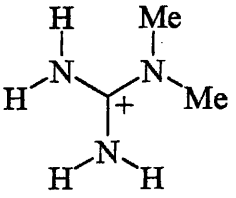

N,N-Dimethylguanidinium
$[DiMeGu]^+$

Found: C, 54.1; H, 5.81; N, 11.7%. [There is better agreement in the microanalysis when calculated for a whole molecule of water; calc for $C_{16}H_{21}N_3O_4S$: C, 54.7; H, 6.02; N, 12.0. Found: C, 54.1; H, 5.81; N, 11.7%.]

Synthesis of [Gu][ABS] 35

A solution of $[C(NH_2)_3]Cl$ (0.033g, 0.35mmol) in methanol ($1cm^3$) was added to a solution of $Na[O_3SC_6H_4N{=}NC_6H_4NH_2]$ (0.103g, 0.31mmol) in methanol ($10cm^3$) and allowed to slowly evaporate. Small orange crystals of $[C(NH_2)_3][O_3SC_6H_4N{=}NC_6H_4NH_2]$ **35** were collected after approximately one week. Calc for $C_{13}H_{16}N_6O_3S$: C, 46.4; H, 4.79; N, 25.0. Found: C, 43.9; H, 4.41; N, 21.5%. The CHN analysis is poor, however this result is repeatable. The powder diffraction pattern and the simulated powder pattern from single crystal data are the same, providing evidence that the single crystal is representative of the bulk sample.

Synthesis of [MeGu][ABS] 36

A solution of $[C(NH_2)_2(NHMe)]Cl$ (0.038g, 0.35mmol) in methanol ($1cm^3$) was added to a solution of $Na[O_3SC_6H_4N{=}NC_6H_4NH_2]$ (0.103g, 0.31mmol) in methanol ($10cm^3$) and allowed to slowly evaporate. Small orange crystals of $[C(NH_2)_2(NHMe)][O_3SC_6H_4N{=}NC_6H_4NH_2]$ **36** were collected after approximately one week. Calc for $C_{14}H_{18}N_6O_3S$: C, 48.0; H, 5.18; N, 24.0. Found: C, 41.0; H, 4.39; N, 19.4%. The CHN analysis is poor, however this result is repeatable. The powder diffraction pattern reveals extra peaks to those observed in the simulated pattern derived from single crystal data, indicating that the bulk sample contains a minor impurity. However, no other crystalline products have been isolated and characterised despite several attempts.

Synthesis of $[EtGu]_2[ABS][NBS]\cdot 2H_2O$ 37

A solution of $[C(NH_2)_2(NHEt)]_2SO_4$ (0.047g, 0.17mmol) in water ($5cm^3$) was added to a solution of $Na[O_3SC_6H_4N{=}NC_6H_4NH_2]$ (0.103g, 0.31mmol) in water ($10cm^3$) and allowed to slowly evaporate. Small orange crystals of $[C(NH_2)_2(NHEt)]_2[O_3SC_6H_4N{=}NC_6H_4NH_2][O_3SC_6H_4N{=}NC_6H_4NO_2]\cdot 2H_2O$ **37** were collected after approximately one week. Calc for $C_{30}H_{42}N_{12}O_{10}S_2$: C, 45.3; H, 5.33; N, 21.2. Calc for $C_{30}H_{38}N_{12}O_8S_2$ ($-2H_2O$): C, 47.5; H, 5.05; N, 22.2. Found: C, 47.5; H, 5.37; N, 22.9%. The CHN result calculated with the loss of solvent shows the best agreement to the observed result. Also, the powder diffraction pattern

collected from ground crystals of **37** is different to that observed for the simulated pattern, possibly reflecting the loss of solvent from the complex. These results are also reproducible.

Synthesis of [DiMeGu][ABS] 38a

A solution of $[C(NH_2)_2(NHMe_2)]_2SO_4$ (0.047g, 0.17mmol) in methanol ($5cm^3$) was added to a solution of $Na[O_3SC_6H_4N{=}NC_6H_4NH_2]$ (0.103g, 0.31mmol) in methanol ($10cm^3$) and allowed to slowly evaporate. Small orange crystals of $[C(NH_2)_2(NHMe_2)][O_3SC_6H_4N{=}NC_6H_4NH_2]$ **38** were collected after approximately one week. Calc for $C_{15}H_{20}N_6O_3S$: C, 49.4; H, 5.53; N, 23.1. Found: C, 46.2; H, 5.18; N, 21.2%. The CHN analysis is poor, however this result is repeatable. The powder diffraction pattern and the simulated pattern from single crystal data are the same showing the single crystal is representative of the bulk sample.

Synthesis of [DiMeGu][ABS] 38b

A solution of $[C(NH_2)_2(NHMe_2)]_2SO_4$ (0.047g, 0.17mmol) in water ($5cm^3$) was added to a solution of $Na[O_3SC_6H_4N{=}NC_6H_4NH_2]$ (0.103g, 0.31mmol) in water ($10cm^3$) and allowed to slowly evaporate. Small orange crystals of $[C(NH_2)_2(NHMe_2)][O_3SC_6H_4N{=}NC_6H_4NH_2]$ **38** were collected after approximately one week. Calc for $C_{15}H_{20}N_6O_3S$: C, 49.4; H, 5.53; N, 23.1. Found: C, 46.9; H, 5.30; N, 21.8%. The CHN analysis is poor, however this result is reproducible. The powder diffraction pattern of the ground crystals and the simulated pattern derived from the single crystal data are the same, therefore the single crystal is representative of the bulk material.

4.7 References

[1] Aldrich Chemical Co.

[2] Lancaster

[3] D. A. Skoog, *Analytical Chemistry an Introduction*, Saunders, 2003

[4] J. L. Scott, A. P. Downie, M. Asami, K. Tanaka, *CrystEngComm.*, 2002, 4(96), 580

[5] K. Tanaka, M. Asami, J. L. Scott, *New J. Chem.*, 2002, 26, 378

[6] B. Onida, B. Bonelli, L. Flora, F. Geobaldo, C. O.-Arean, E. Garrone, *Chem. Commun.*, 2001, 2216

[7] V. A. Russell, M. C. Etter, M. D. Ward, *J. Am. Chem. Soc.*, 1994, 114, 1941

[8] F. H. Allen, W. D. S. Motherwell, P. R. Raithby, G. P. Shields, R. Taylor, *New J. Chem.*, 1999, 25

[9] V. A. Russell, M. C. Etter, M. D. Ward, *Chem. Mater.*, 1994, 1206

APPENDIX 1

Numbering scheme
for compounds 1 to 38
[Fold out]

1: [MeGu][mTPPMS] : $[C(NH_2)_2(NHMe)][PPh_2C_6H_4SO_3\text{-}3]$

2: [EtGu][mTPPMS] : $[C(NH_2)_2(NHEt)][PPh_2C_6H_4SO_3\text{-}3]$

3: [DiMeGu][mTPPMS] : $[C(NH_2)_2(NMe_2)][PPh_2C_6H_4SO_3\text{-}3]$

6: [EtGu][mTPPMSO] : $[C(NH_2)_2(NHEt)][OPPh_2C_6H_4SO_3\text{-}3]$

7: [DiMeGu][mTPPMSO]·H_2O : $[C(NH_2)_2(NMe_2)][OPPh_2C_6H_4SO_3\text{-}3]\cdot H_2O$

8: $[Gu]_2[IrCl(CO)(mTPPMS)_2]$: $[C(NH_2)_3]_2\{trans\text{-}[IrCl(CO)(PPh_2C_6H_4SO_3\text{-}3)_2]\}$

9: $[MeGu]_2[IrCl(CO)(mTPPMS)_2]\cdot{}^3/_8H_2O$: $[C(NH_2)_2(NHMe)]_2\{trans\text{-}[IrCl(CO)(PPh_2C_6H_4SO_3\text{-}3)_2]\}\cdot{}^3/_8H_2O$

12: [MeGu][1-$NapSO_3$] : $[C(NH_2)_2(NHMe)][C_{10}H_7\text{-}1\text{-}SO_3]$

13: [EtGu][1-$NapSO_3$]·H_2O : $[C(NH_2)_2(NHEt)][C_{10}H_7\text{-}1\text{-}SO_3]\cdot H_2O$

14: [DiMeGu][1-$NapSO_3$]·H_2O : $[C(NH_2)_2(NMe_2)][C_{10}H_7\text{-}1\text{-}SO_3]\cdot H_2O$

15: [MeGu][2-$NapSO_3$] : $[C(NH_2)_2(NHMe)]$ $[C_{10}H_7\text{-}2\text{-}SO_3]$

16: [EtGu][2-$NapSO_3$] : $[C(NH_2)_2(NHEt)][C_{10}H_7\text{-}2\text{-}SO_3]$

17: [DiMeGu][2-$NapSO_3$] : $[C(NH_2)_2(NMe_2)][C_{10}H_7\text{-}2\text{-}SO_3]$

18: [MeGu][10-CamphorSO_3] : $[C(NH_2)_2(NHMe)][C_{10}H_{17}OSO_3]$

19: [EtGu][10-CamphorSO_3] : $[C(NH_2)_2(NHEt)][C_{10}H_{17}OSO_3]$

20: [DiMeGu][10-CamphorSO_3] : $[C(NH_2)_2(NMe_2)][C_{10}H_{17}OSO_3]$

21: [DiMeGu][$MeSO_3$] : $[C(NH_2)_2(NMe_2)][CH_3SO_3]$

22: [DiMeGu][$PhSO_3$] : $[C(NH_2)_2(NMe_2)][C_6H_5SO_3]$

23: $[DiMeGu]_2[1,5\text{-}Nap(SO_3)_2]$: $[C(NH_2)_2(NMe_2)]_2[C_{10}H_6(1,5\text{-}SO_3)_2]$

24: $[DiMeGu]_2[2,6\text{-}Nap(SO_3)_2]$: $[C(NH_2)_2(NMe_2)]_2[C_{10}H_6(2,6\text{-}SO_3)_2]$

25: [Gu][MO] : $[C(NH_2)_3][O_3SC_6H_4N{=}NC_6H_4NMe_2]$

26: [MeGu][MO]·MeOH : $[C(NH_2)_2(NHMe)][O_3SC_6H_4N{=}NC_6H_4NMe_2]\cdot MeOH$

27: [EtGu][MO] : $[C(NH_2)_2(NHEt)][O_3SC_6H_4N{=}NC_6H_4NMe_2]$

28: [DiMeGu][MO] : $[C(NH_2)_2(NMe_2)][O_3SC_6H_4N{=}NC_6H_4NMe_2]$

29: HMO : $[O_3SC_6H_4NH{=}NC_6H_4NMe_2]$

30: [Gu][EO] : $[C(NH_2)_3][O_3SC_6H_4N{=}NC_6H_4NEt_2]$

31: [MeGu][EO]·MeOH : $[C(NH_2)_2(NHMe)][O_3SC_6H_4N{=}NC_6H_4NEt_2]\cdot MeOH$

32: [EtGu][EO] : $[C(NH_2)_2(NHEt)][O_3SC_6H_4N{=}NC_6H_4NEt_2]$

33: [DiMeGu][EO] : $[C(NH_2)_2(NMe_2)][O_3SC_6H_4N{=}NC_6H_4NEt_2]$

34: HEO·$^3/_4H_2O$: $[O_3SC_6H_4NH{=}NC_6H_4NEt_2]\cdot{}^3/_4H_2O$

35: [Gu][ABS] : $[C(NH_2)_3][O_3SC_6H_4N{=}NC_6H_4NH_2]$

36: [MeGu][ABS] : $[C(NH_2)_2(NHMe)][O_3SC_6H_4N{=}NC_6H_4NH_2]$

37: $[EtGu]_2[ABS][NBS]\cdot 2H_2O$: $C(NH_2)_2(NHEt)]_2[O_3SC_6H_4N{=}NC_6H_4NH_2][O_3SC_6H_4N{=}NC_6H_4NO_2]\cdot 2H_2O$

38a: [DiMeGu][ABS] : $[C(NH_2)_2(NMe_2)][O_3SC_6H_4N{=}NC_6H_4NH_2]$

38b: [DiMeGu][ABS] : $[C(NH_2)_2(NMe_2)][O_3SC_6H_4N{=}NC_6H_4NH_2]$

APPENDIX 2

Schematics of the mono- and disulfonates used in this thesis

[Fold out]

Mono- and disulfonates

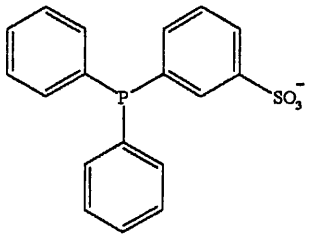

Triphenylphosphine-monosulfonate

[mTPPMS]$^-$

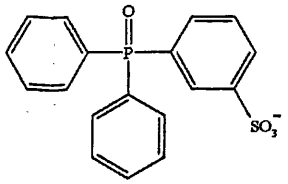

Triphenylphosphine-monosulfonate oxide

[mTPPMSO]$^-$

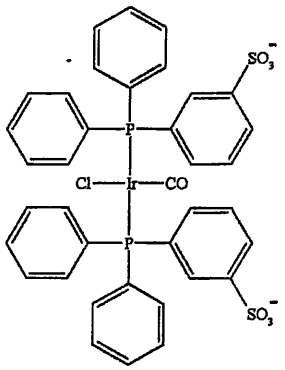

Monosulfonated-Vaska's compound

$[IrCl(CO)(mTPPMS)_2]^{2-}$

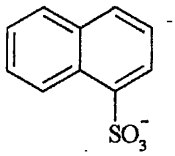

1-Naphthalenesulfonate

$[1\text{-}NapSO_3]^-$

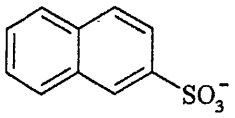

2-Naphthalenesulfonate

$[2\text{-}NapSO_3]^-$

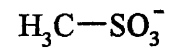

methylsulfonate

$[MeSO_3]^-$

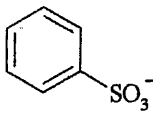

phenylsulfonate

$[PhSO_3]^-$

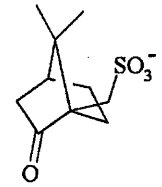

10-camphorsulfonate

$[10\text{-}CamphorSO_3]^-$

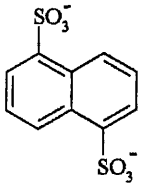

1,5-Naphthalenedisulfonate

$[1,5\text{-}Nap(SO_3)_2]^{2-}$

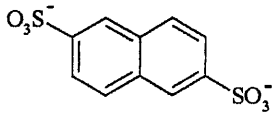

2,6-Naphthalenedisulfonate

$[2,6\text{-}Nap(SO_3)_2]^{2-}$

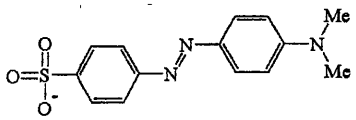

Methyl orange

$[MO]^-$

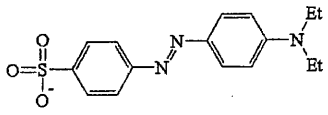

Ethyl orange

$[EO]^-$

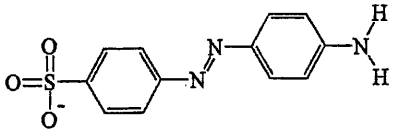

4-aminoazobenzene-4'-sulfonate

$[ABS]^-$

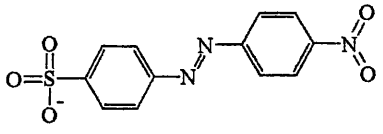

4-nitroazobenzene-4'-sulfonate

$[NBS]^-$

APPENDIX 3

Schematics of the guanidinium and substituted guanidinium derivatives used in this thesis
[Fold out]

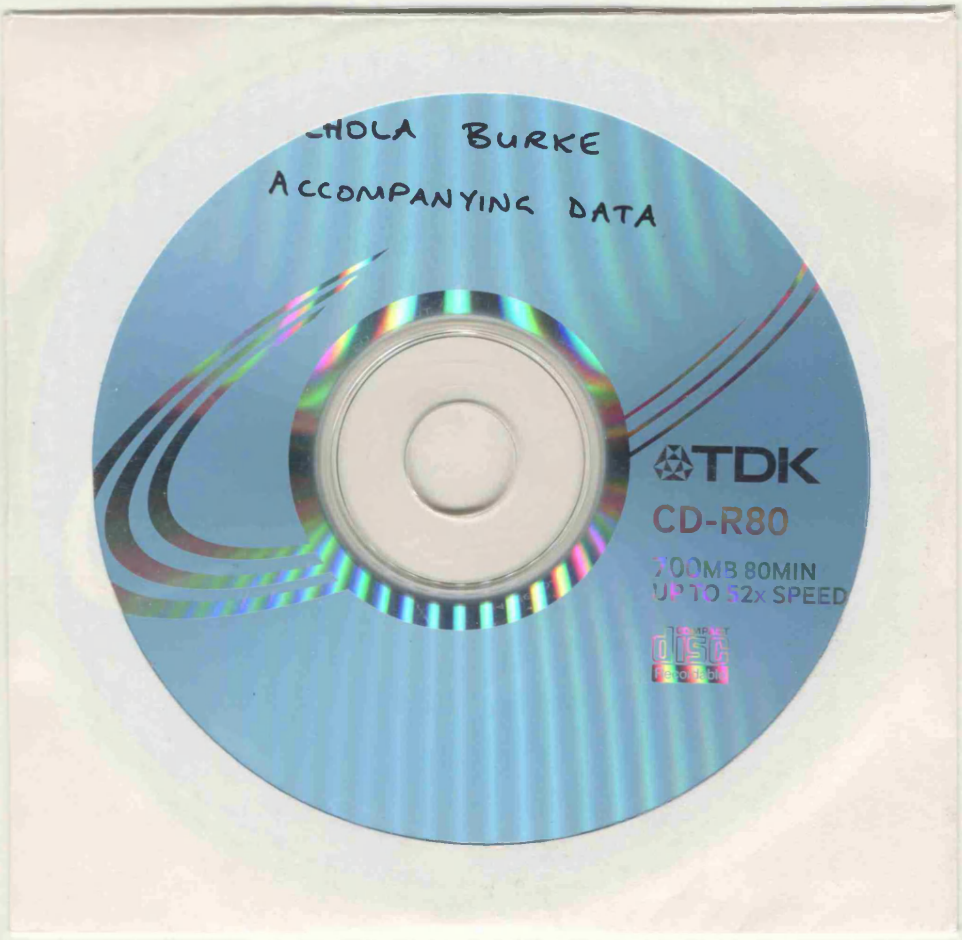
CHOLA BURKE
ACCOMPANYING DATA
TDK
CD-R80
700MB 80MIN
UP TO 52x SPEED